ORGANISATION EUROPÉENNE POUR LA RECHERCHE NUCLÉAIRE

CERN EUROPEAN ORGANIZATION FOR NUCLEAR RESEARCH

THE PHYSICS INTERESTS OF

A 10 TeV PROTON SYNCHROTRON,

400×400 GeV^2 PROTON STORAGE RINGS,

AND ELECTRON-PROTON STORAGE RINGS

Edited by

L. Camilleri

G E N E V A

1976

ABSTRACT

This report consists of a collection of documents produced by two Study Groups, one on a multi-TeV Proton Synchrotron and the other on 400×400 GeV^2 Proton Storage Rings. In both studies the reactions of interest in the weak, electromagnetic and strong interactions are discussed. The technical feasibility of the relevant experiments is investigated by attempting, in each case, the design of an experimental set-up. Event rates are estimated using currently prevailing theoretical models and by extrapolation of results at present accelerators. In addition to the work of the two Study Groups, a section on the physics interests and technical problems of ep Storage Rings is included.

FOREWORD

In the spring of 1974 two Study Groups were formed to investigate the physics that could be studied with a 10 TeV Proton Synchrotron (SSPS) and 400×400 GeV^2 Proton Storage Rings (SISR). The members of the Study Groups produced several documents on the various aspects of high-energy physics that could be investigated with these two types of machine. These documents were discussed at meetings of the Study Groups but only circulated among their members.

About a year after the two Groups ended their work it was thought useful, in view of frequent inquiries for copies of the reports, to collect the various documents into a single CERN report. This could also be used, for instance, as a starting point for further studies. Of course, during that year, several outstanding discoveries (J/ψ, dilepton events in neutrino interactions, μe coincidences in e$^+$e$^-$ collisions, etc.) took place and somewhat changed the emphasis of high-energy physics research. The documents included here, although recently updated by their authors, would perhaps have stressed the study of these phenomena more than they do, had they been written at the end of 1975.

Part A of this report is a collection of the updated documents produced by the SSPS Group. Part B is a similar collection for the SISR study. It will be noticed that, as opposed to the SSPS where no actual synchrotron design was used, the SISR Group based its studies on a tentative 400 GeV Storage Rings design using conventional magnets. This was necessary because of the very tight relationship between machine and experiments at storage rings. In actual fact in the past year superconducting storage rings have been found preferable. In order for this report to be as up to date as possible it is a description of this latter design that is included here. The conclusions of the physics reports remain unchanged as the energy, the luminosity, and the space available to experiments at intersection regions are essentially the same in the two designs. Part B also includes a document discussing the technical feasibility of storing antiprotons in one of the present ISR rings (here too the original contribution has been replaced by a more recent one) and a document discussing the physics interest of p̄p storage rings.

Finally, although ep storage rings were not included in the work of the Study Groups, it was thought useful to include in this report a section, Part C, dealing with such storage rings. Both the physics interest and the technical problems of ep machines are covered in this section.

CONTENTS

P A R T   A

STUDY OF A MULTI-TeV PROTON SYNCHROTRON

SECTION I   INTRODUCTION

SECTION II   PHYSICS OUTLOOK
                 1 HADRON INTERACTIONS
                 2 WEAK AND ELECTROMAGNETIC INTERACTIONS

SECTION III   HADRON BEAMS AND EXPERIMENTS
                 1 NOTES ON ASPECTS OF HADRONIC EXPERIMENTS WITH A 10 TeV PROTON SYNCHROTRON
                 2 HIGH p_T STUDY
                 3 PARTICLE IDENTIFICATION ABOVE 400 GeV/c
                 4 THE ROLE OF TOTAL ABSORPTION SHOWER COUNTERS WITH PARTICLES IN THE TeV RANGE
                 5 NOTES ON MANY-BODY HADRONIC REACTIONS WITH A 10 TeV PROTON ACCELERATOR

SECTION IV   NEUTRINO EXPERIMENTS
                 1 NEUTRINO EXPERIMENTS AT THE MULTI-TeV ACCELERATOR

INTRODUCTION

W.J. Willis

CERN, Geneva, Switzerland

This Part contains the first version of a study of the physics program and experimental techniques for a multi-TeV accelerator, here called SSPS. The membership of the Study Group is given at the end of this Introduction. The whole Group met on four occasions, and there were a number of meetings of a few members to discuss particular topics. We have decided to present as our report a number of papers signed by individual members.

This is the first such study, as far as we know, and as the jump from familiar energies is very large, new concepts often seemed called for when analysing a possible experiment. Thus we feel that the ideas presented here are capable of much further development.

Specific considerations relating to the accelerator complex were not part of the scope of this study, nor was there a given parameter set. Our members who were knowledgeable in this area concluded that we should assume that the accelerator would be a conventional slow-pulsing synchrotron with a good duty cycle and intensity of more than 10^{12} protons per second. Further, there did not seem to be any clear technical limit to the energy in the range below 10 TeV, assuming the availability of superconducting magnets of high quality. The limits defined by cost and site not being given or easy to estimate, we decided to explore the probable physics results and the problems of experimental technique in the range up to 10 TeV, to discover if there are considerations which might fix the energy of the machine.

Accordingly, Section II of this Part contains a discussion of the considerations for higher energies based on known or anticipated physics. These are open to the inevitable objection that the discoveries of the greatest importance are those which were not anticipated. Nevertheless, in circumstances where some choices are to be made, these arguments seem to allow us to make meaningful suggestions. In particular, we formed the opinion that the project would be more likely to be justifiable if the energy was fixed above 5 TeV, rather than in the region of 1 or 2 TeV, despite the resulting size. This opinion was based on the physics considerations reviewed in report II.2.

The following sections describe our studies of the technical problems in carrying out the experiments. Here it might be thought that one would have found that problems arise for which no solution is at hand with present or foreseeable techniques. This seems to be wrong: rather it has been possible to turn our attention to showing that *the work can be done with equipment which does not scale up in size or cost as fast as the accelerator.* We feel that this might prove to be a crucial point if such a project were ever examined from the point of view of economic feasibility.

Membership of the
Study Group on a Multi-TeV Accelerator

M. Albrow
W. Hardt
M. Jacob
C.H. Llewellyn Smith

D.R.O. Morrison
D. Perkins
C. Rubbia
D. Treille
A.M. Wetherell
W.J. Willis (convener)
E.J.N. Wilson

II.1 HADRON INTERACTIONS

M. Jacob

CERN, Geneva, Switzerland

FOREWORD

The purpose of this Section is to discuss in general terms the interest of a new proton accelerator (SSPS) with laboratory energy extending up to 10^4 GeV (10 TeV), and comparing its capabilities with those which could be expected from 2 × 400 GeV Proton Storage Rings (SISR). We do this from the point of view of the strong interactions alone, since in all other cases the advantages of the former option are overwhelming.

Indeed this is an energy range in which we cannot yet expect interactions which are usually referred to as weak to compete in any general sense with those which are globally referred to as strong. Only hadronic interactions will therefore be considered and assumed to correspond to what could be but the naive extrapolation of what is known at present.

The centre-of-mass energy range for the two schemes would then be (considering a proton target) 33 to 136 GeV and up to 800 GeV, respectively. When discussing hadronic processes the corresponding gain in rapidity may be highly relevant -- the effective rapidity interval will thus extend up to 9.8 units in the first case and up to 13.4 units in the second case. A 400 GeV machine corresponds to an interval of 6.7 units, while the ISR at top energy ($\sqrt{s}$ = 62 GeV) corresponds to 8.2 units. The respective gains thus achieved are worth being graphically displayed. The picture obtained is the following:

PS — 3.8

SPS — 6.7

ISR — 8.2

S(SPS) — 9.8

S(ISR) — 13.4
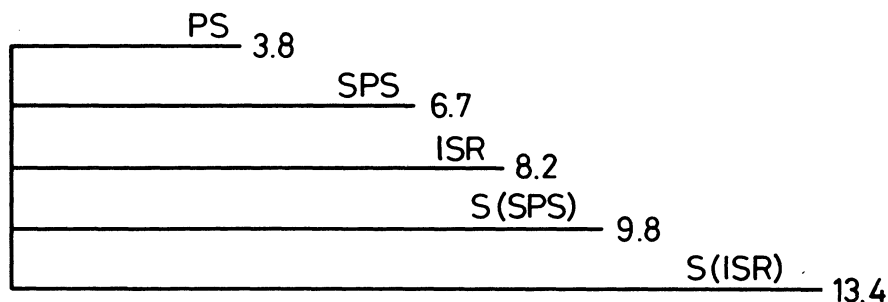
From the point of view of rapidity, the relative power of an S(ISR) with respect to an S(SPS) is not dramatically different from what we encountered at each of the previous steps. However, if the ISR goes 1.5 units only beyond the SPS, the S(ISR) would go 3.6 units beyond what would be reached at the S(SPS). We may nevertheless try, whenever necessary, to compare the respective merits of the two possible instruments in terms of what we know about the present respective capabilities of the ISR on the one hand and of Fermilab on the other. At present we have no threshold to gamble upon. This comparison therefore seems to be the only way to proceed. Indeed, the only threshold which one may consider is W production in the framework of present-day gauge theories. The S(SPS) considered here would already offer quite enough energy for that. As far as quarks are concerned, no specific threshold appears to be worth reaching at present. We are left with the straightforward extrapolation of our present knowledge, which leads us to expect that, generally speaking, log s

rather than $\sqrt{s}$ is setting the scale for changes. For typical hadronic processes the accessible rapidity range appears therefore as more relevant than the actual energy range, any hoped-for surprise not withstanding.

An extra gain in energy may therefore not appear to be as interesting as it may *a priori* sound. There are, however, some processes which show important variations in yields over the ISR energy range. This is particularly the case for large p_T phenomena. In fact, the larger the p_T, the more the observed yields rise with energy. For such processes, an energy as high as possible may therefore appear as the right thing to get. Nevertheless, we have reasons to expect that, within any particular class of phenomena, only vanishingly small cross-sections will still show rapid variations at extremely high energies. Within our present knowledge, there is again a limit to what a possible extra increase in energy can bring.

It should be clear that a large gain in energy is extremely interesting. Its value may, however, be challenged if it implies a great loss in versatility. This is the key question in our present comparison.

We may therefore proceed as follows. Within a general introduction we first attempt to itemize the important discoveries made so far with the ISR, going from PS energies to ISR energies. We then try to assess whether or not these discoveries could have all been made at Fermilab, had the machine started earlier. We come up with a positive answer. We then analyse the respective power of Fermilab (SPS) on the one hand, and of the ISR on the other to further explore and actually understand these new phenomena. Our conclusion is that both are needed and that one or the other could be better at tackling some specific questions. In the long range, however, the SPS prevails. In so doing we also analyse the impact which research at the ISR had on the hadron program at Fermilab (SPS). It was instrumental in giving it its present momentum and -- let us say it -- its present highly topical interest. This analysis then leads us to some general conclusions.

1. HADRON RESEARCH AT THE ISR

ISR results have already been widely reviewed and discussed. We may, then, merely itemize here what appears to correspond to the key improvements in our knowledge of hadronic interactions. They are the following.

1.1 The rising cross-section

Our past understanding of hadronic interactions gave an important role to a relatively simple and asymptotic behaviour which could have been practically reached at not too high energies. The relevant domain could have corresponded to $\sqrt{s} \gg m_p$ for which the ISR energy range was expected to be highly sufficient. We now know that asymptotia is but an elusive concept. The proton-proton total cross-section rises by an important amount over the ISR energy range and, what appears to be even more important, there is no indication that it may saturate at a conceivable machine energy. Every fact at hand points to the contrary. Certainly the K^+p total cross-section rises significantly over the Serpukhov energy range and the combined analysis of the behaviour of $\sigma_{tot}(K^+p)$ and $\sigma_{tot}(K^-p)$ points to a rise of the diffractive component which should *a priori* be a general fact. Nevertheless, such an effect could well have been but a transition behaviour towards a rather rapidly reached

asymptotic value. We now know that this is not the case. This is a very important point, one that is of fundamental importance in our theoretical approach to hadronic reactions.

1.2 Scaling

The theoretical framework in which constant asymptotic cross-sections were expected as the most simple option does lead, however, to an approximate understanding of hadronic processes which found support in many ways because of its predictive value. It would, then, have been a serious setback if the prediction of scaling properties for inclusive distributions would not have been supported by experiment, at least to the accuracy level where total cross-sections can be considered as energy independent. The confirmation of scaling properties, and this over the tremendous energy range which the ISR allowed us to reach, therefore constitutes a very important discovery. Although approach to a scaling limit had already been hinted at by experiments at PS energy, nevertheless, it was only after its successful probe at ISR energies that it appeared as a solid and prominent fact. Furthermore, if pion distributions scale relatively rapidly with increasing energy, it requires ISR energies to see that inclusive distributions for heavy secondaries such as K^- or $\bar{p}$ are also essentially reaching scaling limits. Such a universality of scaling is even more important than the rapid approach to scaling which pion distributions show.

1.3 Short-range order

Our previous analysis of hadron interactions gave a prominent role to hadron excitation and decay, the most explicit case being that of resonance formation. This has dominated hadron research at PS energies and therefore over a complete decade.

It could, however, be expected that the dynamics of hadron production could have more to do with local properties of each specific region of the allowed phase space than with what could actually occur to either one of the incident particles. This is particularly the case for secondary particles which are slow in the centre-of-mass system and therefore far away in phase space from either one of the colliding particles. The fact that there are many such particles produced in very high energy collisions, and that their (as a matter of fact important) correlations depend mainly on whether they are nearby or far away from each other in phase space, is an important discovery to be credited to the ISR. It turns out that the convenient range against which one should check whether two secondary particles are close by or far away in phase space is 2 units of rapidity. This alone indicates why such an effect could not be demonstrated by PS energy data, since there the accessible rapidity interval is hardly greater than what is associated with the obvious beam and target fragmentation. With 8 units of rapidity covered, the ISR could straight away produce evidence for predominantly short-range correlations in rapidity among the many produced pions. This is what is usually referred to as short-range order and interpreted in terms of clustering effects.

1.4 Diffractive excitation

A particular type of production process clearly stands out owing to properties which make it similar in many ways to elastic (diffraction) scattering. It was already known from research at PS energies that hadronic resonances with quantum numbers identical to those of an initial particle could be produced in such a way, that is with low-momentum transfer, no exchange of quantum numbers, and an energy dependence similar to that of elastic scattering.

The separation of such a process from other contributions is possible in practice only if the fraction of the total energy taken up by one final (quasi-elastically scattered) particle is large enough. This, therefore, implies very high incident energies if one wishes to study large excitation energies. An important discovery made at the ISR was that such a production mechanism is quite important (20 to 25% of all inelastic processes), and that the diffractive excitation spectrum extends much beyond the prominent low-mass resonances to reach very high excitation energies.

1.5 Large transverse momentum phenomena

It is well known that the overwhelming majority of secondary particles is produced with low values of the transverse momentum, namely $p_T \approx 0.35$ GeV/c. It is also well known that a structure in the transverse momentum distribution at large p_T could, provided it shows up at all, most generally arise from a very small distance structure within the colliding particles, thus seen in a direction which is not modified by the Lorentz contraction. Irrespective of the previously mentioned (exponential) cut-off at low p_T, the observation of a 4 GeV/c p_T secondary is flatly forbidden by energy conservation at PS energies.

Another and very important discovery at the ISR was finding that the number of particles produced at large p_T is great enough to indicate a marked structure in the corresponding distribution. Its interpretation in terms of finer, harder, structural components within the colliding particles, along similar lines to those followed for the analysis of deep inelastic electron scattering, has so far not met with any objection. At present this is probably the most topical facet of hadron physics. Leptons have eventually been found among large p_T secondaries with a production yield with respect to hadrons which is remarkably constant (10^{-4} for e^-/π^-). The origin of these leptons is raising highly challenging questions. None of the hadron mechanisms can fully account for the observed yields and p_T distributions.

Concluding, we have listed five important discoveries to be put to the credit of the ISR. All of them required the big step in energy which was thus made to go much beyond the PS or even the Serpukhov energy ranges. They will probably correspond, in due course, to such progress as the discovery of a large number of prominent hadronic resonances, which was the major finding in hadron physics at PS energies and which led to Unitary Symmetry and Regge regularities. They could all be made within a relatively short time.

2. COULD FERMILAB (SPS) HAVE DONE IT?

The obvious advantage of the ISR over Fermilab (SPS) is to extend the centre-of-mass energy range from 30 to 60 GeV. The obvious drawbacks of the ISR, as compared to Fermilab (SPS), are the following (we consider hadron physics only):

a) great difficulties in reaching very low momentum transfers where a large fraction of certain cross-sections is to be found;

b) poor momentum resolution when precision measurements would be needed (determination of a missing mass, for instance);

c) low luminosity when one wishes to study a rare process (probability lower than 10^{-3}, say);

d) inaccessibility of the actual reaction vertex;

e) lack of variety in the types of reaction which can be studied.

The last drawback is actually by far the more serious one.

We may now come back to the five important discoveries already made thanks to the ISR, and discuss whether or not Fermilab (SPS) energies would have been enough with the help of the improvements corresponding to the five points just itemized.

a) The total cross-section. It seems that high-precision measurements on $\sigma_{tot}(pp)$ up to 400 GeV should have been enough to indicate that the proton-proton cross-section was definitely not approaching a constant. In this case, information on the behaviour of other cross-sections (and in particular $\bar{p}p$ and K^+p) would have helped (and as a matter of fact did help) in concluding that a whole new phenomenon was occurring. [To the extent that the study of σ_{tot} is connected to that of very small-angle elastic scattering, point (a) is a major difficulty at the ISR. Point (e) is the major drawback to further studies at the ISR.]

b) Scaling and short-range order. A step forward to 6.7 units of rapidity (as compared to 4) already shows the emergence of a central plateau and of short-range order. Going up to 8.2 units of rapidity helps, but it seems that the new phenomena which are occurring could have been already well ascertained from 400 GeV data. This is also enough of an energy for the approach to scaling to be seen even for heavy secondary particles. Points (d) and (e) are here serious drawbacks to going further at the ISR.

c) Diffraction excitation. The special and important role of diffractive excitation as well as the existence of high-mass excitation could have been inferred from 400 GeV data alone. In this case points (a), (b), and (e) have compensated to a large extent for the lower energy limitation. The special c.m. geometry of the ISR, together with the gain in energy, may however be an asset for the study of processes referred to as double Pomeron exchange, which are of key importance.

d) Large transverse momentum phenomena. They could also have been found at Fermilab and they would probably have also emerged from a search for leptons. Indeed the large p_T yield for leptons was found at the same time at Fermilab and at the ISR. In this case points (c) and (e) and to some extent (d) compensate somewhat for the limited energy range. However, the rapid rise with energy of the pertinent cross-section (an order of magnitude over the ISR energy range) is a strong point in favour of the ISR.

Concluding, in all five cases it is good to have the extra information which can be obtained when working with equivalent energies up to 2000 GeV. It should be acknowledged, however, that information at 400 GeV would have been enough in all cases to conclude that something new was happening and to infer its key properties. As a parenthesis in this discussion it remains to point out that the present momentum of the experimental research program on hadronic interactions at Fermilab (SPS) energies owes a very great deal to these ISR results. It can be said that the main interest in the study of total cross-sections, the real part of the forward amplitude, wide-angle correlations, diffractive excitation, large p_T yields and associated multiplicities, which at present constitute the hard core of the Fermilab and SPS hadron physics programs, would only now start emerging from the first Fermilab results.

3. WHAT IS NEXT

One may first start from these few new topics, consider how to proceed at present and, from this, try to guess at what could happen in the more distant future. It is clear that

there are questions for which the ISR is now the unique instrument, or for which it is very important to go from 400 to 2000 GeV. This is in particular the case for the study of elastic scattering and, to a lesser extent, for quasi-elastic diffractive excitation. This is also the case, *and very strongly so*, for many questions which have to do with large p_T phenomena and lepton yields. The relevant cross-sections still show important variations with energies and therefore change much over the ISR energy range. It is of paramount importance to explore and understand these properties, and Fermilab (SPS) may be too limited in energy for that. This is finally the case for those processes for which high energy could be the key element because of some hitherto unknown threshold. More exotic objects not withstanding, the most conventional of these topics is high-mass lepton pair formation and, more recently, charmed particle search. Thus to date there are "several stones worth turning" at ISR energies. Altogether this should represent an extremely lively research program for a few years to come. One should also not exclude competition with Fermilab in domains where Fermilab could eventually come up with finer results. Having 1.5 more units of rapidity should help, in particular, in the further study of correlations.

It remains to say that if, in order to explore further and understand what the research at the ISR had already uncovered, one would now have to choose between the ISR and the SPS, the latter should win. It seems that the advantages associated with points (a) to (e) altogether should prevail over further explorations in the 400-2000 GeV domain.

From the point of view of the search for new particles, one may so far be disappointed by research at the ISR. The huge gain in centre-of-mass energy did not yield so far what could have been hoped for. We now understand that it comes from the fact that only a small fraction of the incident particle energy is available in practice for particle production. Cross-sections may be non-zero but get too small to be detected with present techniques. This is very different from what happens in an e^+e^- machine where all the centre-of-mass energy is to be found in the intermediate one-photon state. In this respect a 30 GeV ISR may not be more *efficient* than a 3 GeV e^+e^- storage ring. Production of large-mass lepton pairs should give very interesting clues as to what actually occurs.

Our conclusions at this stage are that, even in the perspective of hadron physics alone, an instrument of the Fermilab (SPS) type would have already been practically as successful as the ISR for the discovery of the new phenomena which did show up, and that it would appear to be a better one for their further exploration. However, the success of the ISR, as far as only new discoveries in physics are concerned (that is technological achievements notwithstanding) is overwhelming. It actually gave its present interest to the hadron research program at 400 GeV. But whereas a 400 GeV machine is enough to provide evidence for all new features of hadron physics which have been discovered, *this would not have been the case* with a 100 GeV machine.

Using the ISR-Fermilab situation described above to compare in a tentative way a 10 TeV SSPS to a 400 GeV SISR, one may say that, as far as hadron physics alone is concerned, an SSPS should be considered as preferable. However, we are comparing instruments of very different costs and one should certainly expect to collect many new interesting results with an SISR, and this in a *relatively shorter* time and at a *relatively lower* cost.

II.2 THEORETICAL REMARKS ON WEAK AND ELECTROMAGNETIC
INTERACTIONS AT MULTI-TeV ENERGIES

C.H. Llewellyn Smith

Dept. of Theoretical Physics, Univ. of Oxford, Oxford, UK

1. INTRODUCTION

This note contains some theoretical remarks about the possibility of studying weak and electromagnetic interactions using secondary beams derived from a conventional accelerator with energy $\leq$ 10 TeV. Many of the processes considered could also be studied using an ep colliding beam machine[*]. I have tried to present the results in such a way that the reader can compare the conventional and colliding beam machines for a given physics goal (making his own weighting for the ease of doing the experiment and the costs).

The general features of the strong interactions are already known up to ISR energies; the case for going to higher energies is therefore probably as clear now as it will be in a few years' time. For the weak and electromagnetic interactions, however, the situation is quite different. Very little is known about electromagnetic interactions for momentum transfers above 15 GeV^2, and neutrino experiments in the multi-GeV range are still in their infancy. Therefore it would be ridiculous to set out now a detailed promotion for going to multi-TeV energies, since many of the questions we could pose, such as "Does scaling persist at higher energies?", may well be answered by experiments at FNAL or the SPS. However, many other questions may not be answered; for example, if the intermediate vector boson really has a mass of 80 GeV, it will be hard to discover without going to higher energies. Furthermore, it seems obvious that forthcoming experiments will, as always in the past, raise as many questions as they answer.

It seems that there will be an excellent case for going to higher energies and that it is worth while to study whether it will be possible to do useful experiments in the multi-TeV range. Not knowing exactly what the case will be, however, the best we can do is ask whether such experiments can shed light on the question of interest now -- bearing in mind that the focus of attention is likely to change and that the enormous extrapolations we shall be forced to make are likely to prove grossly misleading. There are several questions on which we are on firmer ground:

  i) The question of the intermediate vector boson (W) already alluded to above. Current theoretical thinking suggests that the mass is of order 80 GeV; if this thinking survives the next few years, it is obvious that the quest for the W will be a (perhaps *the*) major goal for new machines. We would obviously like to construct a machine which is more or less guaranteed to discover the W if the mass is less than 100 GeV.

---

[*] This is a revised version of a note circulated among the SSPS Study Group in August 1974. As a result of the preliminary studies undertaken then, Bjorn Wiik and I decided, for reasons discussed in the conclusions to this paper, that further work was needed on the potentialities of very high energy ep colliding beam systems. Some of this work has been incorporated in the present paper.

We are now preparing a report[1] on our work which should be available shortly.

ii) Questions which become amenable to study purely on account of the higher energy available. Examples are the following:

a) The study of neutral current effects in inelastic eN or μN scattering; since the weak-electromagnetic interference term is expected to be of the order of

$$10^{-4} \, Q^2 \; (\text{in GeV}^2) \; ,$$

relative to the purely electromagnetic cross-section, such experiments will probably be marginal at SPS or FNAL energies but could be easy in the multi-TeV range.

b) πe or Ke scattering. For a beam of energy E, $s = 2 \, m_e E = E$ (in TeV) GeV^2. Thus a 6 TeV pion beam hitting a stationary electron is equivalent to firing the SLAC electron beam (20 GeV) at a pion target! However, the centre-of-mass energy for a particle incident at 2, 5, or 10 TeV is only equal to the c.m. energy for a 0.75, 2, or 4.5 GeV electron, respectively, incident on a proton. Thus, while the possibility of studying these processes is interesting, it will certainly not be a major goal.

c) The study of $\gamma\pi$, γK, or $\gamma\gamma$ interactions for real photons (or virtual photons in the $\gamma\gamma$ case) using the "generalized Primakoff effect":
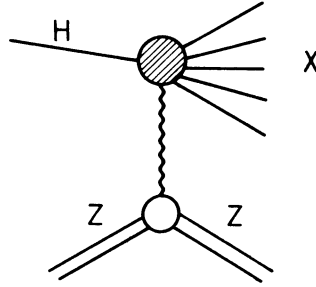
At high energies the minimum momentum transfer is given by

$$\sqrt{-t_{min}} = \frac{M_X^2 - M_H^2}{2E_H} \; .$$

In order for the process to be coherent, and gain the essential "enhancement" factor Z^2/A, we must have $\sqrt{-t_{min}} \lesssim 1/R$, where $R \simeq 1.2 \, A^{1/3}$ fm is the nuclear radius which characterizes the fall-off of the nuclear form factor. Thus for incident energy E (GeV), such experiments might be possible up to $M_X \sim 0.3 \, \sqrt{E}$ (GeV) or, in other words, up to the same centre-of-mass energy as for a photon beam of energy 0.05 E on a proton target. Thus, if such experiments are possible with multi-TeV beams, they can explore $\gamma\pi$ and γK scattering at "equivalent" multi-GeV energies.

d) The exploration of the rapidity distribution in "virtual photon" scattering:
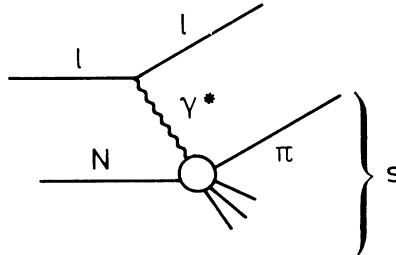
This provides an opportunity to study the effect of varying the mass of one of the incident particles. Hence it can be used to probe basic concepts such as the short-range order picture, which is invoked to explain ISR data. Is this picture true, in which case the influence of changing q^2 on $\langle p_T \rangle$, particle composition, etc., would not extend outside the photon fragmentation region, or is there a much richer structure?

For example, some theorists imagine a distribution:
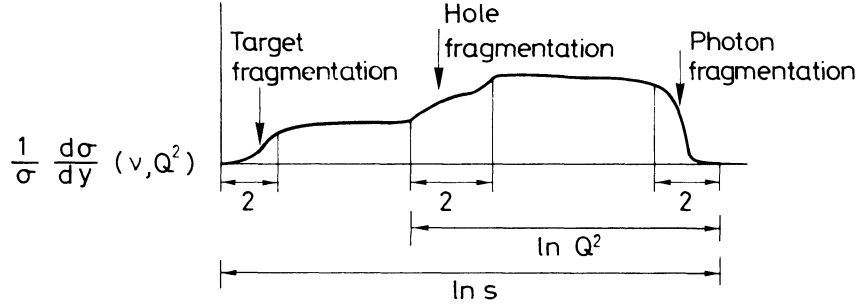
To test such ideas we would clearly like to be able to vary $\log Q^2$ by at least 6 in a region where at least 10 units of rapidity are available. This requires a lepton-nucleon centre-of-mass energy $\sqrt{s} \sim 100$. This is just in the range of a 10 TeV machine.

2. PRACTICAL REMARKS

To guide our thinking and to facilitate comparison with colliding beam machines, we must have some rough idea of what luminosities might be achieved. Deriving parent π's and K's from the primary beam of energy E_p with a fixed $\Delta p/p = \Delta x/x$, the number of parents at given x will be independent of energy (to the approximation that Feynman scaling holds). Thus, if we scaled the length of the decay path linearly with E_p, the flux of ν's and μ's would be the same as at lower energies. With a fixed decay path the flux varies as E^{-1} so, if the neutrino cross-section continues to rise linearly, the neutrino event rate would be independent of energy. Rubbia[2] has considered the design of a neutrino beam and estimates that with detectors of the same order of magnitude as those envisaged for the SPS it should be possible to achieve a luminosity of the order of 2×10^{34} cm^{-2} sec^{-1}, some (30%?) of the neutrinos (from K decay) having about 0.7 of the primary proton energy E_p and the rest (from π decay) having 0.35 E_p.

Similarly, Treille estimates[3] that with a 50 m H_2 (iron) target, muon luminosities of the order of 4×10^{33} cm^{-2} sec^{-1} (4×10^{35} cm^{-2} sec^{-1}) might be achieved for $E_\mu \sim \frac{1}{2}E_p$. Treille also estimates that a broad spectrum of photons might be obtained with integrated photon luminosities of the order of 6×10^{31} cm^{-2} sec^{-1} for $E_\gamma > 0.2\ E_p$.

Study groups on ep storage rings tend to assume a luminosity L of 10^{32} cm^{-2} sec^{-1}. This gives an equivalent photon luminosity:

$$\mathcal{L}\ \frac{\Delta \bar{E}_\gamma}{\bar{E}_\gamma} \approx \frac{2\alpha}{\pi} \ln\left(\frac{\bar{E}_e}{m_e}\right)\left[\frac{1 + \left(1 - \frac{\bar{E}_\gamma}{\bar{E}_e}\right)^2}{2}\right]\frac{\Delta \bar{E}_\gamma}{\bar{E}_\gamma} \times 10^{32}\ \text{cm}^{-2}\ \text{sec}^{-1}$$

$$\approx 5 \times 10^{29} \ln\left(\frac{\bar{E}_e}{m_e}\right)\left[\frac{1 + \left(1 - \frac{\bar{E}_\gamma}{\bar{E}_e}\right)^2}{2}\right]\frac{\Delta \bar{E}_\gamma}{\bar{E}_\gamma}\ \text{cm}^{-2}\ \text{sec}^{-1}\ ,$$

where $\bar{E}_\gamma$ and $\bar{E}_e$ are the equivalent lab. energy of the photon and electron. Thus at PEP energies (15 GeV electrons and 70 GeV protons), integrating over scattered electron energies from 1 to 14 GeV ($\bar{E}_\gamma$ from 1.96 TeV to 140 GeV), the photon luminosity is about 14% of L; with a suitable tagging device the integrated luminosity was estimated to be about 1% of L [4].

A *last vital practical point* is that the counting rates below assume 100% acceptance; to make a realistic assessment of a hypothetical machine, it is essential to take account of the acceptances which can be obtained and make an investigation of experimental problems which may be encountered. [In addition we say nothing about radiative corrections; they are a serious problem for interpreting neutrino experiments, when these corrections cannot be subtracted reliably and may be $\sim$ 50% in some regions at multi-TeV energies, but for μ/e scattering they are no more of a problem than at multi-GeV energies[5], although they are much bigger since some terms grow like log E.]

3. COUNTING RATES[*]

We now consider counting rates for some interesting processes.

3.1 Deep inelastic: $\mu N \to \mu + \ldots$, $\nu N \to \mu + \ldots$, $eN \to \nu + \ldots$

We assume that scaling continues to hold with zero cross-section for longitudinal W's and photons and for right-handed W's. With $M_W = \infty$, the cross-sections will be:

$$\frac{d\sigma^{\mu N \to \mu + \ldots}}{dxdy} = \frac{4\pi\alpha^2}{s} \frac{F_2^{eN}(x)}{x^2 y^2} \left(1 - y + \frac{y^2}{2}\right)$$

$$\frac{d\sigma^{\nu N \to \mu + \ldots}}{dxdy} = \frac{G^2 s}{2\pi} F_2^{\nu N}(x)$$

$$\frac{d\sigma^{\bar\nu N \to \bar\mu + \ldots}}{dxdy} = \frac{G^2 s}{2\pi} F_2^{\nu N}(x)(1 - y)^2$$

$$\frac{d\sigma^{\bar e p \to \nu + \ldots}}{dxdy} = \frac{G^2 s}{4\pi} F_2^{\nu N}(x)$$

where, in standard notation,

$$y = \frac{2q \cdot p}{s} , \qquad x = \frac{Q^2}{2q \cdot p} .$$

For a nuclear target $[(p + n)/2]$ we take

$$F_2^{eN} = 1.3 \, f(x) ,$$

$$F_2^{\nu N} = \frac{18}{5} F_2^{eN}$$

---

[*] Further and more refined calculations of the counting rates for $\mu N \to \mu + \ldots$, $ep \to \nu + \ldots$, and weak-electromagnetic interference effects will be presented in Ref. 1.

per nucleon, with

$$f(x) = \sqrt{x} \ (1-x)^3 \quad x > 0.2$$
$$= 0.229 \qquad x < 0.2 \ .$$

For ep colliding beams (or hydrogen targets) we guess

$$F_2^{ep} \approx 1.44 \ f(x) \ ,$$

and for the weak cross-section

$$\frac{d\sigma^{e^- p \to \nu}}{dxdy} \approx \frac{2}{3} \ \frac{d\sigma^{\nu N \to \mu}}{dxdy}$$

$$\frac{d\sigma^{e^+ p \to \bar{\nu}}}{dxdy} \approx \frac{1}{3} \ \frac{d\sigma^{\bar{\nu} N \to \bar{\mu}}}{dxdy}$$

for unpolarized beams.

In Figs. 1 and 2 we show how events would be distributed over the x,y plane with these cross-sections. These relative distributions are of course energy-independent if scaling holds. The absolute rates are given by

$$\sigma^{\mu N \to \mu}(x,y > 0.01) = \frac{7.18 \times 10^{-28}}{s \ (GeV^2)} \ cm^2$$

$$= \frac{3.82 \times 10^{-28}}{E_{lab}^{\mu} \ (GeV)} \ cm^2 \ ,$$

$$\sigma^{\nu N \to \mu} = 0.40 \ s \ (GeV^2) \times 10^{-38} \ cm^2$$

$$= 0.75 \ E_{lab}^{\nu} \ (GeV) \times 10^{-38} \ cm^2 \ .$$

Assuming a luminosity of 10^{34} cm^{-2} sec^{-1}, these cross-sections would yield the following number of events per day:

	Beam energy (TeV)				
	1	2.5	5	7.5	10
$\mu N \to \mu$ events with x,y > 0.1	3.3×10^8	1.3×10^8	6.6×10^7	4.4×10^7	3.3×10^7
$\nu N \to \mu$ events	6.5×10^3	1.6×10^4	3.2×10^4	4.9×10^4	6.5×10^4

1.13 × 10³	23	6.5	2.8	1.6
2.41 × 10⁴	499	138	60	33
1.74 × 10⁵	3.59 × 10³	995	432	239
1.07 × 10⁶	2.21 × 10⁴	6.13 × 10³	2.66 × 10³	1.47 × 10³
4.73 × 10⁷	9.79 × 10⁵	2.71 × 10⁵	1.18 × 10⁵	6.51 × 10⁴
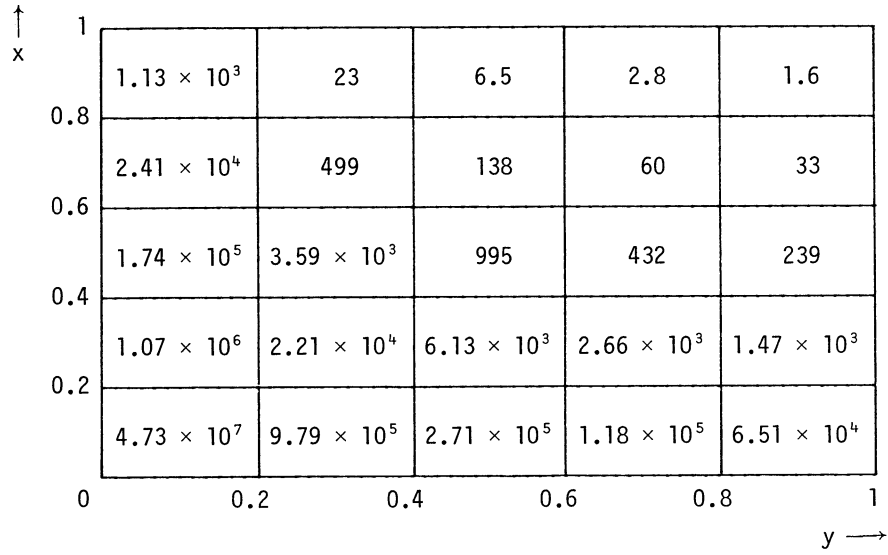
Fig. 1 Possible distribution of 5×10^7 events with x,y > 0.01 in the process $\mu N \to \mu + \ldots$. This number is roughly what might be obtained (for x,y > 0.01) in a day's running with $E_\mu = 5$ TeV and $\mathcal{L} = 10^{34}$ cm^{-2} sec^{-1} (the model in the text would give 6.6×10^7 events). The numbers in the bins with x < 0.2 or y < 0.2 and the total number are dominated by the choice of cut-off.

35	35	35	35	35
462	462	462	462	462
1693	1693	1693	1693	1693
3504	3504	3504	3504	3504
4308	4308	4308	4308	4308
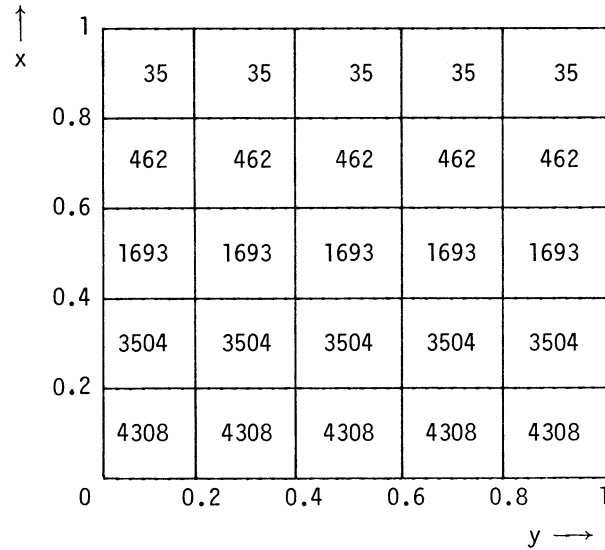
Fig. 2 Possible distribution of 5×10^4 events in the process $\nu N \to \mu + \ldots$. This number is very roughly what might be obtained in a day's running with $E_\nu = 5$ TeV and $\mathcal{L} = 10^{34}$ cm^{-2} sec^{-1} (the model in the text would give 3.24×10^4 events).

These total numbers are not of primary interest (in the electromagnetic case they are essentially determined by the cut-off in x and y). We are mainly interested in the number of events at large x and y or, better, large Q^2 [Q^2 = xys] since it is presumably Q^2 which determines the importance of scale-breaking effects as well as the importance of the W propagator in the weak case. If scaling holds, the cross-section for Q^2 greater than a certain minimum Q_0^2 itself scales thus:

$$\sigma_{\mu N}(s, Q^2>Q_0^2) = \frac{2.60 \times 10^{-31}}{s \ (GeV^2)} \ K_{\mu N} \ (Q_0^2/s) \ cm^2 \ ,$$

$$\sigma_{\nu N}(s, Q^2>Q_0^2) = 0.80 \times s \ (GeV^2) \times 10^{-38} \ Q_{\nu N} \ (Q_0^2/s) \ cm^2 \ ,$$

where (assuming $\sigma_L = 0$ and a flat y-distribution in neutrino scattering)

$$K_{\mu N}(\alpha) = \iint\limits_{Q^2>\alpha s} \frac{dxdy}{x^2y^2} \left(1 - y + \frac{y^2}{2}\right) F_2^{\mu N}(x) \ , \qquad Q_{\nu N}(\alpha) = \iint\limits_{Q^2>\alpha s} dx \ dy \ F_2^{\nu N}(x) \ .$$

The functions K and Q obtained using the simple model for the structure functions presented above are plotted in Figs. 3 and 4, which allow us to construct $\sigma(s, Q^2>Q_0^2)$ for all Q^2 and s.
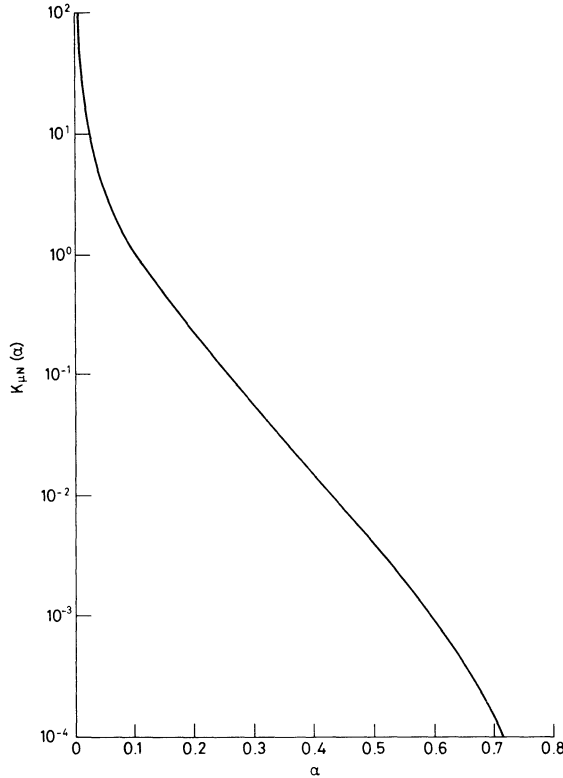
Fig. 3 The function $K_{\mu N}(\alpha)$ defined in the text, according to the simple model presented there.
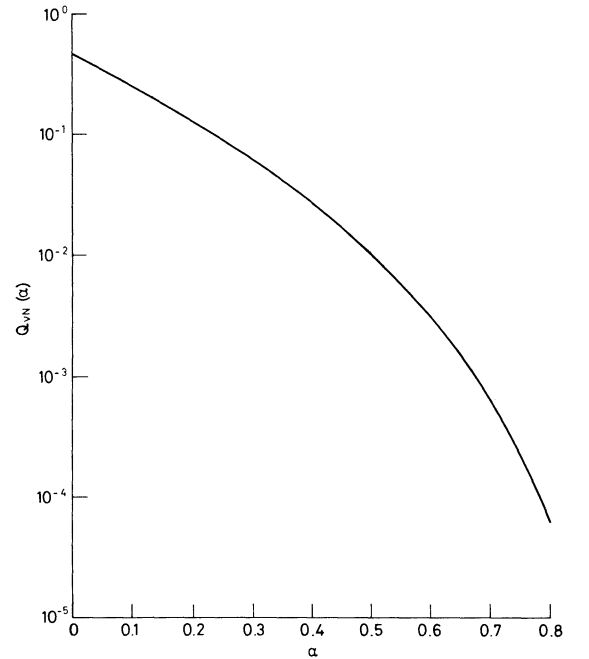
Fig. 4 The function $Q_{\nu N}(\alpha)$, defined in the text, according to the simple model presented there.

These results can be used in an instructive way to determine the luminosity required to get at least N events per day for any given s and $Q^2 > Q_0^2$. Writing the luminosity $\mathcal{L} = \ell \times 10^{32}$ cm^{-2} sec^{-1} we find

$$\ell \geq \frac{N \times s \ (GeV^2)}{2.26 \times 10^6 \times K_{\mu N} \ (Q_0^2/s)}$$

in the electromagnetic case and

$$\ell \geq \frac{N \times 14.5}{s \ (GeV^2) \times Q_{\nu N} \ (Q_0^2/s)}$$

in the weak case. In Fig. 5 we show the luminosity required to get 10 events per day with $Q^2 > Q_0^2$ for various values of Q_0^2 as a function of s. This curve shows dramatically the choice between using large luminosity or large s to reach a given Q^2 (in the electromagnetic case the events with $Q^2 > Q_0^2$ have $\langle Q^2 \rangle \approx \langle Q_0^2 \rangle$, while in the weak case Q^2's are spread between Q_0^2 and s, assuming $M_W = \infty$, so large s has an advantage). Another way to display these results is to plot Q_0^2 above which there are ten events/day as a function of s for different luminosities. This is done in Figs. 6 and 7. Armed with Figs. 3 and 4 the reader can construct whatever other N, $\mathcal{L}$, s plots he requires.

What Q^2 range would we like to reach with the next generation of machines? My feeling is that we would like to extend the Q^2 range accessible at FNAL and SPS by a factor of 10 or more, i.e. to several thousand GeV^2. This is hard to substantiate, but the following arguments might be given.

1) Small violations of scaling have been reported in experiments at FNAL. According to current theoretical thinking, it is important to determine whether this scale breaking is characterized by powers of ln Q^2 or powers of Q^2. Choosing two forms which decrease by 20% from $Q^2 = 5$ to $Q^2 = 30$ GeV, we see that an enormous Q^2 range is needed to distinguish them:

Q^2	5	15	30	50	100	500	2000	10^4
$\left(\dfrac{\ln s}{\ln Q^2}\right)^{0.298}$	1	0.86	0.80	0.77	0.73	0.67	0.63	0.59
$\left(\dfrac{5}{Q^2}\right)^{0.125}$	1	0.87	0.80	0.75	0.69	0.56	0.47	0.39

2) If $M_W = 80$ GeV, we need $Q^2 = 2650$ GeV^2 to produce a 50% change in the weak cross-section due to the propagator. (To demonstrate that a propagator is responsible we would need a big change, whose Q^2 dependence could be determined, in a range where the electromagnetic structure functions could also be measured.)

To determine how to reach such values of Q^2, we need to weight the cross-sections above with an acceptance (which will presumably only have a severe effect in the case of a muon beam derived from an accelerator). To reach, for example, Q^2's of the order of 2500, it would seem that muon/neutrino beams of the order of 2.5 TeV, and hence an accelerator of about 4 TeV, would be needed. Alternatively an ep colliding beam machine with s $\geq$ 10,000 GeV^2 might cover the same range (s = 10,000 GeV^2 corresponds, for example, to 25 GeV e$^-$ $\times$ 100 GeV p).
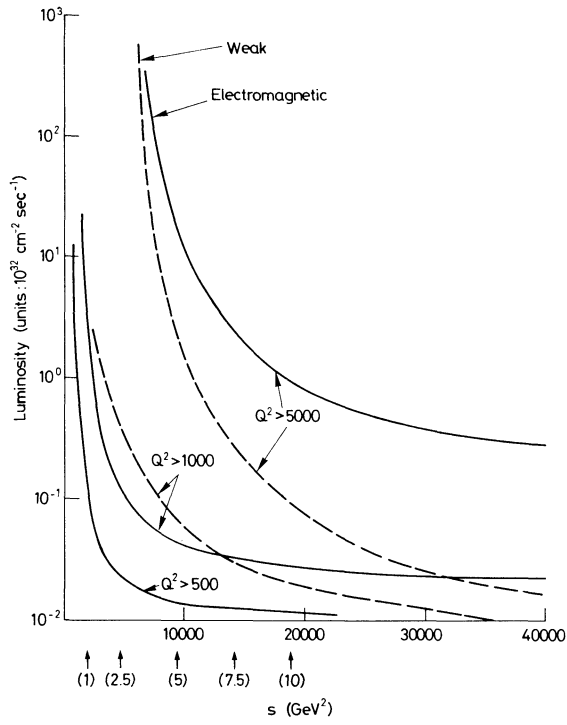
Fig. 5

Luminosity (in units of 10^{32} cm^{-2} sec^{-1}) needed to get 10 events per day above a specified value of Q^2 for

$\nu N \to \mu + \dots :$ — — — —

$\mu N \to \mu + \dots :$ ————————

as a function of s (the numbers in brackets on the x-axis indicate the beam energy in TeV for a fixed target machine). $M_W = \infty$ and exact Bjorken scaling are assumed.
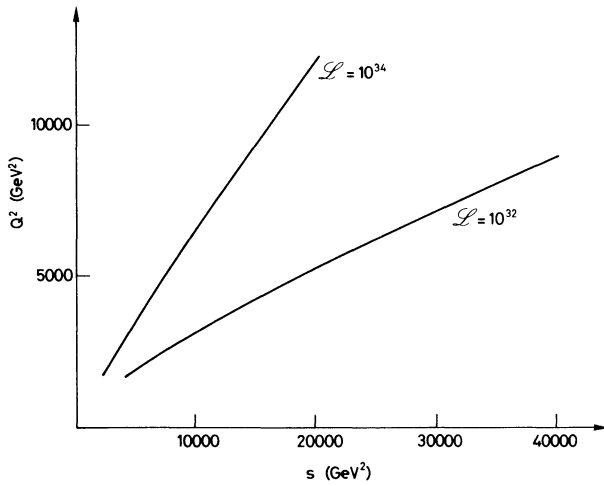
Fig. 6 The value of Q^2 above which 10 events per day for $\mu N \to \mu + \dots$ would be expected (according to the assumptions in Figs. 3 to 5) for two values of the luminosity $\mathcal{L}$ in cm^{-2} sec^{-1}.
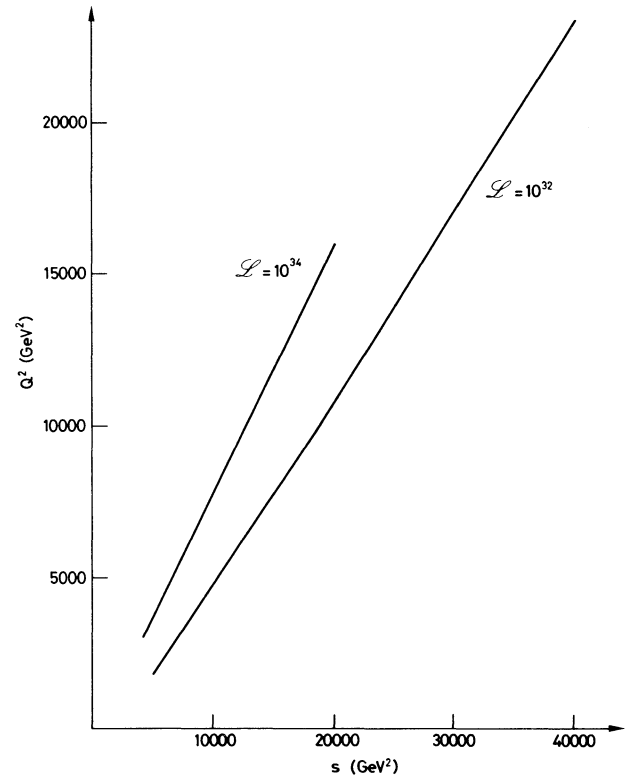
Fig. 7 As for Fig. 6 but for $\nu N \to \mu + \dots$.

3.2 W/Z production

The cross-sections for

$$\sigma(\nu Fe \to \mu^- W^+ + \ldots)/\text{nucleon} \qquad\qquad (A)$$

and

$$\sigma(^e_\mu p \to W + \ldots) \qquad\qquad (B)$$

are plotted in Fig. 8 [6]. In case (A) the effects of Fermi motion and the Pauli principle have been neglected, so the cross-sections may be wrong by a factor of 2 or so, i.e. the quantity plotted is actually

$$\frac{\sigma^{\nu n} + \sigma^{\nu p}}{2} + \frac{\sigma^{\nu Fe}_{\text{coherent}}}{56} \quad .$$

However, σ_{coherent} is actually of negligible importance at these energies except in the case $M_W = 25$ GeV, when it becomes appreciable for $E_\nu \sim 4$ TeV and dominates for $E_\nu \gtrsim 6$ TeV. In case (B) an unpolarized beam was assumed; the cross-sections for energies above 10 TeV were obtained from results calculated for lower energies and masses using the empirical observation that to a good approximation the cross-section depends only on s/M_W^2 in this case (there does not seem to be any such simple scaling law for the case of incident neutrinos where a different diagram dominates). In both cases the "anomalous moment" for the W appropriate for a gauge theory was assumed, which seems the only reasonable choice.
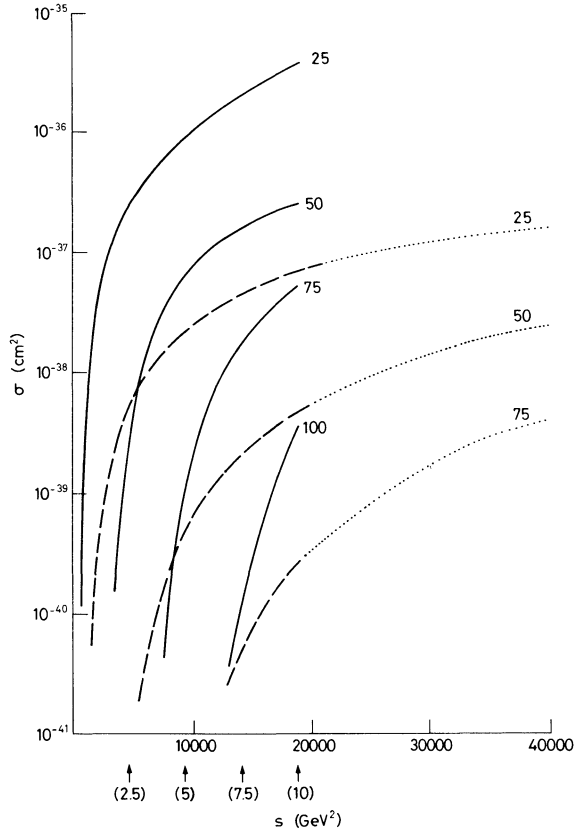
Fig. 8

Cross-sections (per nucleon) for W production on iron (Ref. 6), according to assumptions discussed in the text, for various values of M_W (noted, in GeV, next to the appropriate curves):

$\nu N \to W + \ldots$: ————————

$\mu N \to W + \ldots$: — — — — —

The dotted curves are extrapolations of $\mu N \to W + \ldots$ based on the observation that the cross-section depends only on s/M_W^2. (The numbers in brackets on the x-axis denote the beam energy in TeV for a fixed target machine.)

Note that $\sigma^A \gg \sigma^B$. This is easily understood because in one diagram:
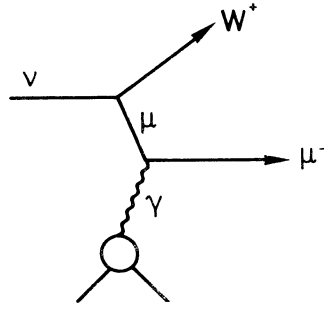
the virtual muon can have a small invariant mass; in all other cases the intermediate particle has a large invariant mass. Note further that $\sigma(\mu^- N \to W^- \nu + \ldots)$ is zero (in the approximation $m_\mu = 0$) for right-handed μ^-'s or left-handed μ^+'s, so this process is greatly suppressed with a μ beam derived from π and K decay[7]. The conclusion is well known: with an accelerator, neutrino experiments are best suited for W production. Therefore we should compare process (B) with storage ring luminosities to process (A) with accelerators. It is clear that with $\mathcal{L} = 10^{32}$ cm^{-2} sec^{-1} it would be very hard to discover a W with mass much above 25 GeV, even with an equivalent lab. energy of tens of TeV available. However, with a 7 TeV neutrino beam (from a 10 TeV proton beam -- the upper limit set for this study) and $\mathcal{L} \sim 10^{35}$ cm^{-2} sec^{-1}, it might be possible to get to $M_W \sim 70$ GeV.

This depends on finding a signature. This has been widely discussed in the literature, so we only give a brief summary here:

i) If $\Gamma(W \to \text{leptons})/\Gamma(W \to \text{hadrons}) = B$ is of the order of 1, the large p_T muon gives a clear signature (theoretical ideas about the value of B are discussed in the section on proton-proton collisions below).

ii) If $B \ll 1$, the events look like ordinary deep inelastic $\nu A \to \mu^- + \ldots$ events, but they populate the region near $x = 0$, $y = 1$ in a characteristic way which may provide a signature.

We now consider Z production in the process:
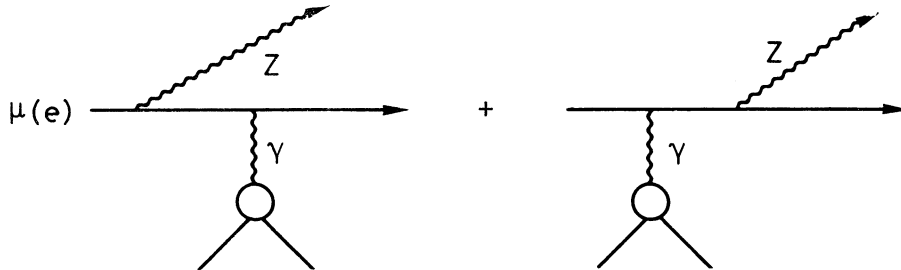
This is kinematically analogous to $\nu A \to W \mu + \ldots$ (the analogy is exact for the dominant diagram). With a coupling of the Z to the muon

$$\bar{\psi}\gamma_\lambda (g_V - g_A \gamma_5) \psi Z^\lambda$$

and

$$g_V^2 = g_A^2 = \frac{1}{\sqrt{2}} G M_Z^2 \ .$$

The cross-section satisfies

$$\sigma(\nu A \to \mu Z + \ldots) \simeq \frac{1}{2} \sigma(\nu A \to \mu W + \ldots) \ .$$

This is good to the order of 10% [8]; the factor $\frac{1}{2}$ comes from the average over polarization in the initial state in the muon case, assuming an unpolarized beam. In general, for an unpolarized beam

$$\sigma(^{\mu}_{e}A \to {}^{\mu}_{e}Z + \ldots) = \frac{g_V^2 + g_A^2}{2\sqrt{2} \ GM_Z^2} \ \sigma(\nu A \to \mu W + \ldots) \ .$$

Assuming some form of lepton-hadron universality, the neutral current cross-section observed at CERN and FNAL is proportional to

$$\frac{g_{V,A}^2}{M_Z^2} \ ,$$

so the factor $(g_V^2 + g_A^2)/2\sqrt{2} \ GM_Z^2 \equiv X$ will generally be much the same in all models which can fit the data, independent of M_Z. We take the Weinberg-Salam model, as an example, in which

$$g_V = e \left(\frac{4 \ \sin^2 \ \theta_W - 1}{2 \ \sin \ 2\theta_W} \right) \ (\approx 0.27 \ e)$$

$$g_A = \frac{e}{2 \ \sin \ 2\theta_W} \ (\approx 0.52 \ e) \qquad\qquad M_Z = \frac{73 \ \text{GeV}}{|\sin \ 2\theta_W|} \ (\approx 75 \ \text{GeV}) \ .$$

The numbers in brackets correspond to $\sin^2 \ \theta_W = 0.38$ -- a reasonable number according to existing data; they give:

$$X \approx 0.19 \ .$$

It will therefore be very hard to discover the Weinberg-Salam Z by production in ep storage rings, but it might just be possible with a 7 TeV muon beam (if the leptonic decays are reasonably abundant -- see below). However, M_Z could be much less than allowed in this model (although $X \sim 0.2$ is perhaps a reasonable model-independent estimate as discussed above).

What about the signature? If

$$B^Z = \frac{\Gamma(Z \to \mu\bar{\mu}) + \Gamma(Z \to e\bar{e})}{\Gamma(Z \to \text{hadrons})}$$

is of the order of 1, the events should be very striking. However, if $B^Z \ll 1$, there is no good signature; the events give an "anomaly" in $\mu N \to \mu + \ldots$ near $x \sim 0$, $y \approx 1$, but the electromagnetic cross-section is large in this region and it is not appreciable.

3.3 Neutral currents

The exploration of neutral currents in neutrino reactions will obviously continue to be of great interest; the estimates of counting rates for charged currents above apply with an appropriate reduction factor:

$$\frac{\sigma(\nu N \to \nu + \ldots)}{\sigma(\nu N \to \mu + \ldots)} \sim 0.2 ? \qquad \frac{\sigma(\bar\nu N \to \bar\nu + \ldots)}{\sigma(\bar\nu N \to \mu + \ldots)} \sim 0.4 ?$$

and a different (but as yet unknown) y distribution.

Here we focus on the possibility of detecting neutral current effects in μ or e scattering:
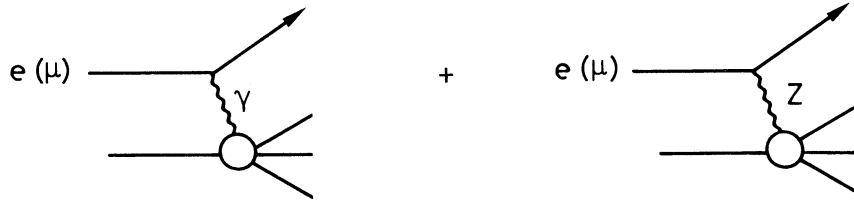
We expect that, roughly, the second amplitude should be of the order of

$$\frac{GQ^2}{e^2} \frac{1}{1 + \frac{Q^2}{M_Z^2}} \approx \frac{10^{-4} \; Q^2 (\mathrm{GeV})^2}{1 + \frac{Q^2}{M_Z^2}}$$

times the first (this expectation is borne out in models). With a 7 TeV muon beam we can, in principle, reach Q^2's at which the two terms are comparable (provided M_Z is not too small!).

What are the signatures for the Z contribution?

i) The cross-sections for left- and right-handed leptons (or antileptons) should be different:

$$d\sigma_{\mu^- L} \neq d\sigma_{\mu^- R}$$

$$d\sigma_{\mu^+ L} \neq d\sigma_{\mu^+ R} \; .$$

This parity-violating effect is an unequivocal signal of the weak interaction.

ii) The cross-sections for $\mu^-(e^-)$ and $\mu^+(e^+)$ become different (the interaction violates C as well as P). This effect can also arise from two-photon effects which, however, are expected to vary logarithmically with Q^2 rather than linearly as expected here.

iii) The weak e.m. interference violates the "inelastic Rosenbluth formula" in a well-defined way (by adding a "W_3-like" term), unlike two-photon effects, but this may be hard to check.

iv) The weak contribution gives an apparent scaling violation with a characteristic Q^2 dependence (although in principle, without doing the Rosenbluth or parity test, this cannot be separated from other sources of scaling violation).

As an example we give the result obtained for the e.m. plus interference term in a simple parton model[9]:

$$\frac{d\sigma_\eta}{dxdy} = \left(\frac{d\sigma}{dxdy}\right)_{1\gamma} \left\{ 1 + \frac{\sqrt{2}\ G\ Q^2\ M_Z^2\ g_\eta}{e^2(Q^2 + M_Z^2)} \left[A + \frac{\xi_\eta\ B\ y[1 - (y/2)]}{1 - y + (y^2/2)} \right] \right\}$$

where g_η and ξ_η depend on the projectile. Thus:

	Polarization	g_η	ξ_η
μ^-	L	g_L	+1
μ^-	R	g_R	-1
μ^+	R	g_L	-1
μ^+	L	g_R	+1

In the Weinberg-Salam model the constants A, B, g_L, and g_R are given by:

$$A^{proton} = \frac{\sqrt{2}\ (12\ \sin^2 \theta_W - 5)}{6}\ , \quad B^{proton} = - \frac{5\sqrt{2}}{6}$$

$$A^{neutron} = \sqrt{2}\ (2\ \sin^2 \theta_W - 1)\ , \quad B^{neutron} = - \sqrt{2}$$

$$g_L = \sqrt{2}\ (-1 + 2\ \sin^2 \theta_W)$$

$$g_R = 2\ \sqrt{2}\ \sin^2 \theta_W$$

$$M_Z = \frac{73\ GeV}{|\sin 2\theta_W|}\ .$$

Using $\sin^2 \theta_W = 0.38$ we obtain for a proton target

$$\frac{d\sigma}{dxdy} = \left(\frac{d\sigma}{dxdy}\right)_{em} \left\{ 1 + g_\eta \left[\frac{Q^2}{Q^2 + (75)^2}\right] \left[-0.10 - 1.16\ \xi_\eta\ f(y)\right] \right\} ,$$

with

$$f(y) = \frac{y\ [1 - (y/2)]}{1 - y + (y^2/2)}$$

$$g_R = 1.07$$

$$g_L = -0.34\ .$$

To determine the Q^2 needed to detect this effect would require a careful analysis of fluxes for beams of different polarizations and charges, etc. It would seem that an accelerator with several TeV or an ep machine with s $\gtrsim$ 10,000 would be needed to be confident of success. (It would need $e^{\pm}p$ and longitudinal polarization to be fully convincing with an ep machine.)

A final note of caution. The electromagnetic cross-section may turn out to be very much smaller than expected assuming scaling; in this case even very large asymmetries at large Q^2 will be hard to see.

3.4 Heavy lepton production

All the remarks which have been made about heavy lepton production at FNAL and the SPS apply also at higher energies. For "gauge-type" heavy leptons which couple to ν_μ with the same strength as μ^- there are good signatures (apparent violation of lepton number conservation laws; apparent neutral currents with a peculiar x,y distribution):

$$\nu A \to M^+ + \dots$$

$$\quad\quad\quad \longrightarrow \mu^+ \nu_\mu \nu_\mu$$

$$\quad\quad\quad \longrightarrow e^+ \nu_e \nu_\mu$$

$$\quad\quad\quad \longrightarrow \nu_\mu + \text{hadrons}$$

A model calculation[10] of the cross-section is shown in Fig. 9, from which it seems that it should be possible to set mass limits in the 50 GeV range with a multi-TeV machine.
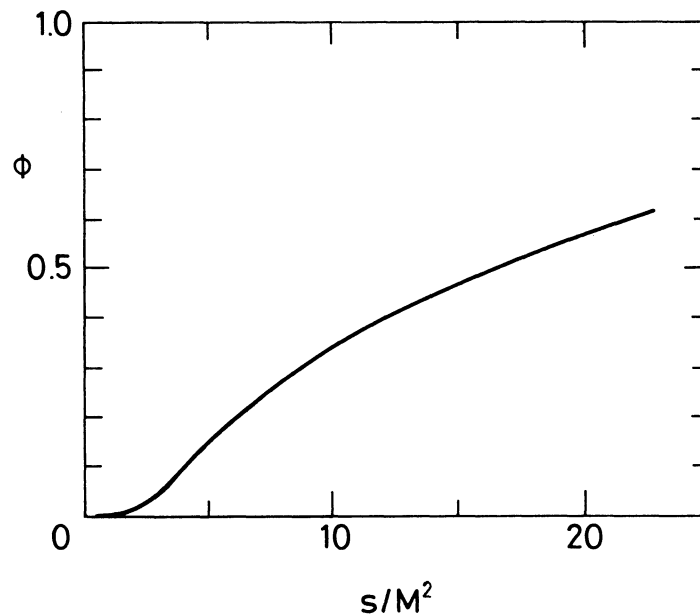
Fig. 9 Model-dependent calculation of

$$\Phi = \frac{\sigma(\nu A \to M^+ + \dots)}{\sigma(\nu A \to \mu^- + \dots)}$$

as a function of s/M_M^2, where M is a heavy lepton.

Heavy leptons can be photoproduced in the Coulomb field of the target:
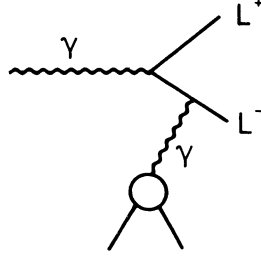
The cross-section for photoproduction from a proton (including elastic and inelastic scattering) is shown in Fig. 10 [11]. [For $E_\gamma > 2$ TeV the cross-section has been constructed from properly calculated values using the empirical observation that it scales as $\sigma \sim 1/M_L^2 \ f(s/M_L^2)$ to a reasonable approximation.] The minimum value of $|t|$ transferred to the nucleus in this reaction is given by

$$|t|_{min} \approx \frac{4M_L^4}{\left(E_\gamma^{lab}\right)^2} .$$

When the square root of this quantity is less than or of the order of the inverse of the nuclear radius, a large factor ($\sim Z^2$ for sufficiently big energies) can be gained by using
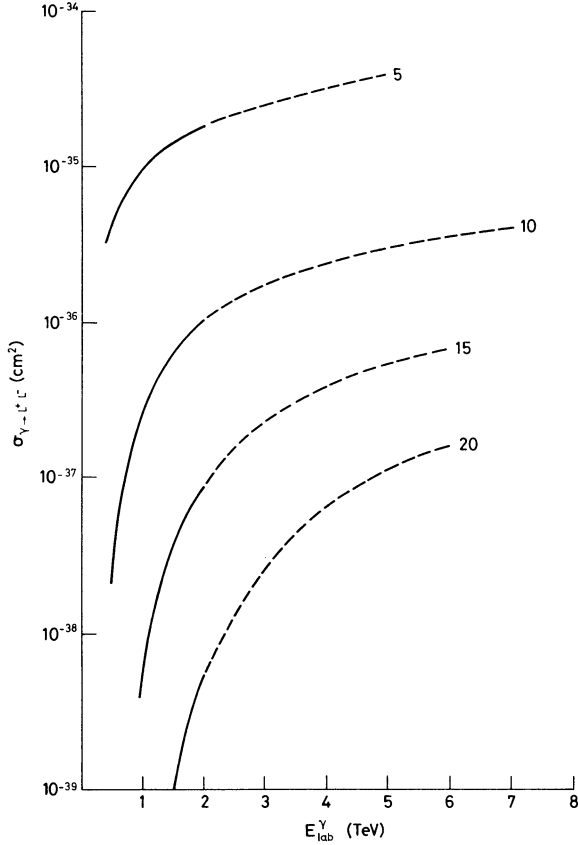
Fig. 10 Cross-sections for photon production off protons of heavy lepton pairs of various masses (Ref. 11) (the lepton masses in GeV are marked against the curves). The dotted curves are extrapolations from calculated results using the empirical observation that $\sigma \sim (1/M_L^2) f(s/M_L^2)$.

a nuclear target which recoils coherently. For a beryllium target, for example, coherent production begins to dominate at roughly the following energies:

M_L (GeV)	5	10	15
Photon energy (GeV)	700	2700	6000

[An estimate of this sort works quite well for lower energies and masses for which the coherent process has been calculated[11].]

Presumably, heavy leptons of 10 GeV or less will be discovered in a few years time in e^+e^- experiments at PETRA and PEP if they exist. For higher masses the coherent process is not important at the energies under study. It would therefore seem from Fig. 10 that future multi-TeV accelerators and ep machines will not compete with e^+e^- machines as a means of producing heavy leptons.

3.5 Photoproduction

3.5.1 With photon beams

Typical cross-sections are expected to be:

$$\sigma_{tot}(\gamma p) \approx 120 \ \mu b$$

$$\sigma(\gamma p \to pp) \sim 12 \ \mu b$$

$$\sigma(\gamma p \to \gamma p) \sim 0.1 \ \mu b$$

$$\sigma(\gamma p \to \pi^+ n) \overset{?}{\sim} \frac{20 \ \mu b}{E_\gamma^2} \ .$$

It seems that decent counting rates can be obtained for all except the last process with a multi-TeV machine or ep colliding beams.

Furthermore, photoproduction should prove to be a copious source of J/ψ's or similar objects of higher mass.

3.5.2 By the Primakoff effect

We already discussed this briefly above. In more detail for
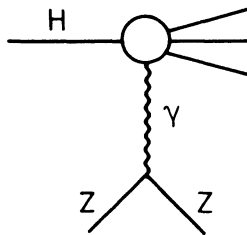
the cross-section can be written

$$\frac{d\sigma}{d^3p} = \frac{\alpha Z}{4\pi} \frac{1}{p_L^3} \sigma_{tot}(\gamma H)(\sin^2 \theta)^2 \ ,$$

where p and θ are the lab. momentum and angle of the recoiling nucleus. A counter at a fixed angle would see $d\sigma \sim dp/p$ -- a typical and sure sign of the Coulomb effect. The cross-sections are substantial and the interest obvious [see Stodolsky[12] for more detail, references, etc.]. The questions which need to be studied are practical; would such experiments be possible [the momentum of the recoiling nucleus can be very small: $(M_X^2 - M_H^2)/2E_H$]?

3.6 Dimuons

In the original draft of this report there was a brief discussion of the trident processes

$$\nu Z \rightarrow \mu e \nu Z$$
$$\nu Z \rightarrow \mu \mu \nu Z$$
$$\mu N \rightarrow \mu \bar{\mu} \mu + \dots \ ,$$

which can occur in the Coulomb field of the target nucleus. Since then, however, "direct" dimuon production by neutrinos has been observed at a very much greater rate (of the order of 1% of the total cross-section). This illustrates the fact that we are probing the unknown and suggests a question for future machines: are there tri-, quadri-, etc., muon processes at high energies?

4. WEAK AND ELECTROMAGNETIC INTERACTIONS IN PROTON COLLISIONS

The Study Group on proton-proton storage rings has reported on weak interactions[13,14]. Here I wish to present some additional estimates and comment on the suggestion, which is sometimes made, that proton-proton storage rings will inevitably prove to be a fruitful source of information about weak and electromagnetic interactions (the magic phrase "unitarity limit" is invoked to support this contention). This seems to me to be a dangerous assumption; it might happen but we have no right to expect it at present. In fact:

1) In the valence quark approximation, the parton model gives

$$\sigma(pp)_{weak} = \frac{G^2 s}{\pi} \frac{\pi\sigma^{\nu p}}{G^2 s} \frac{\pi\sigma^{\nu n}}{G^2 s}$$

for the weak contribution to hadronic processes. Assuming $\sigma^{\nu n} \simeq 2\sigma^{\nu p}$ this gives

$$\sigma(pp)_{weak} = 2.3 \times 10^{-39} \times s \ (GeV^2) \ cm^2 \ ,$$

which is about $1.5 \times 10^{-33} \ cm^2$ for 400 GeV $\times$ 400 GeV storage rings. Although this is very small, it might dominate at very large p_T. The results of model calculations[15] for the production of hadrons at large p_T, based on weak quark-quark scattering followed by quark $\rightarrow$ $\rightarrow$ hadron fragmentation, are compared to an extrapolation of the strong contribution from

ISR data[16] in Figs. 11 and 12. At the largest storage ring energies considered, the weak interaction takes over from the expected (?) strong contribution in a cross-section region which might be accessible. However, the observation of such behaviour would not necessarily prove that weak interactions were at work [unless the beams could be longitudinally polar-ized[13]] and its presence or absence would be hard to interpret without tests of Bjorken scaling at comparable energies. In addition, the naïve extrapolation of the strong cross-section may be much too small and it may dominate completely.

Although it is very interesting that it might prove possible to observe this weak contribution, it would seem unlikely that its observation would lead to fundamental informa-tion about the weak interactions. The appeal to the unitarity limit in this context is fallacious. There is no unitarity limit on the total weak cross-section -- only on partial wave cross-sections [e.g. $\sigma(\nu e \to \nu e)$ projected on the s-wave which happens to be the total cross-section in the Fermi theory -- but not if there is a W]. It is true that in the parton model used above, the parton-parton amplitude violates unitarity at parton-parton centre-of-mass energy of about 2×320 GeV (for appropriately polarized partons) if $M_W = \infty$. However, since typical partons carry a small fraction of the proton's momentum this limit is hard to reach. Furthermore, the "unitarity crisis" is likely to be avoided by some mechanism
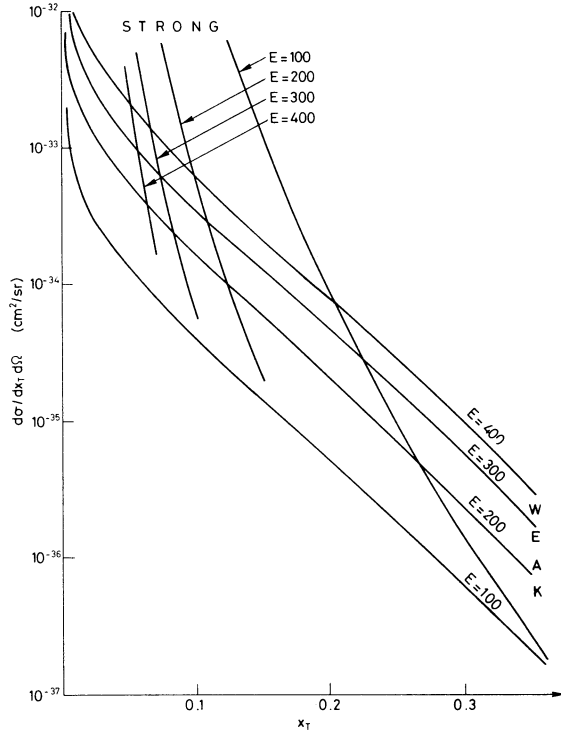
Fig. 11 Model results for the weak contribu-tion to pp $\to$ hadrons + ... at 90° as a function of
$x_T = p_T(\text{hadron})/[p_T(\text{hadron})]_{max}$
for various ISR beam energies (Ref. 15)(i.e. the label E = 400 means 400 GeV × 400 GeV). An esti-mate of the strong contribution based on an extrapolation of ISR data is also shown. $M_W = \infty$ is as-sumed here.
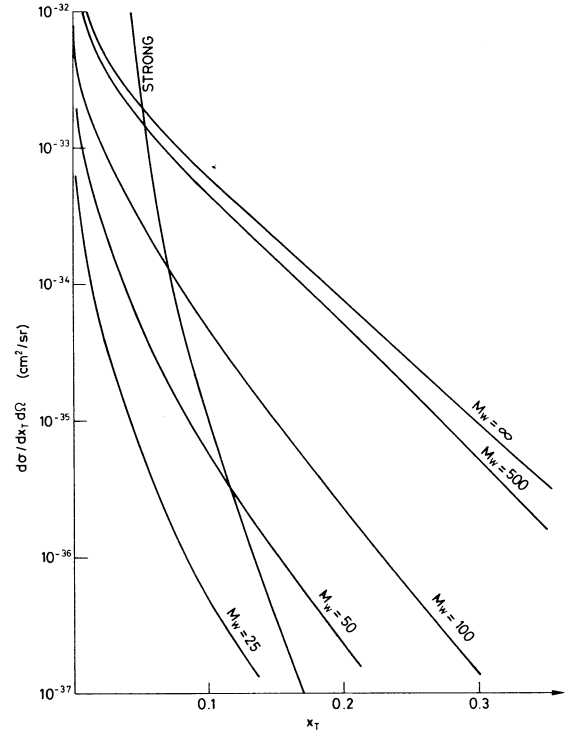
Fig. 12 The same as Fig. 11 for the case of 400 GeV × 400 GeV storage rings for various values of M_W (Ref. 15).

which reduces the parton-parton cross-section below the Fermi theory value (e.g. W exchange) rather than some striking new phenomenon.

2)   It has been suggested that fundamental information can be gleaned from studying

$$pp \rightarrow \bar{\mu}\mu + \dots$$

and

$$pp \rightarrow \mu\nu + \dots$$
$$\rightarrow e\nu + \dots \quad .$$

The cross-section estimates which give reasonable rates for these processes rely heavily on scaling laws which could be totally fallacious. If these scaling laws are correct, proton-proton storage rings may provide a unique way to produce large mass W's and Z's (see item 3 below). However, the "continuum" production of dileptons seems more likely to shed light on the nucleon's structure than on the basic nature of weak and electromagnetic inter-actions (in the parton model, parton-antiparton annihilation is involved at an average centre-of-mass energy well below the total centre-of-mass energy, since antipartons presumably carry only a small fraction of the nucleon's momentum).

3)   If the Drell-Yan scaling law for dimuon production is correct, very high energy proton collisions will provide the only way to find the W and Z bosons if their masses are of the order of 100 GeV or more (in the absence of neutrino beams of order 10 TeV or more). This assertion is independent of the origin of the scaling law and depends only on the assumption of CVC to connect the weak and electromagnetic cross-sections. Therefore *tests of the scaling law are of paramount importance to guide thinking about future storage rings and accelerators.* Scaling gives:

$$\sigma(pp \rightarrow W \dots) = \frac{\sqrt{2} \; g_W^2}{M_W^2} \; f\left(\frac{M_W^2}{s}\right) = G_F \; f\left(\frac{M_W^2}{s}\right)$$

$$\left.\frac{d\sigma}{dQ^2}\right|_{pp \rightarrow \mu\bar{\mu}+\dots} = \left(\frac{1}{Q^2}\right)^2 g\left(\frac{Q^2}{s}\right) \quad .$$

Neglecting the isoscalar contribution to the electromagnetic process, using CVC, and assuming $\sigma_{\text{vector}} = \sigma_{\text{axial-vector}}$, yields[17)]

$$\sigma(pp \rightarrow W + \dots) = \frac{0.16 \; \tau^{3/2}}{M_p^2} \left[s^{3/2} \left.\frac{d\sigma}{d\sqrt{Q^2}}\right|_{pp \rightarrow \mu\bar{\mu}} \right]$$

for an isoscalar target, where $\tau = Q^2/s$ and

$$s^{3/2} \; \frac{d\sigma}{d\sqrt{Q^2}} = F(\tau) \quad .$$

We have used the model calculation of Altarelli et al.[18] for F(τ) (which is not in disagreement with existing data) from which we have calculated values of $\sigma_{pp \to W}$ which are displayed in Fig. 13. (Unfortunately the result is very sensitive to the form of the antiparton distribution assumed for $M_W^2 \geq 0.1s$.)
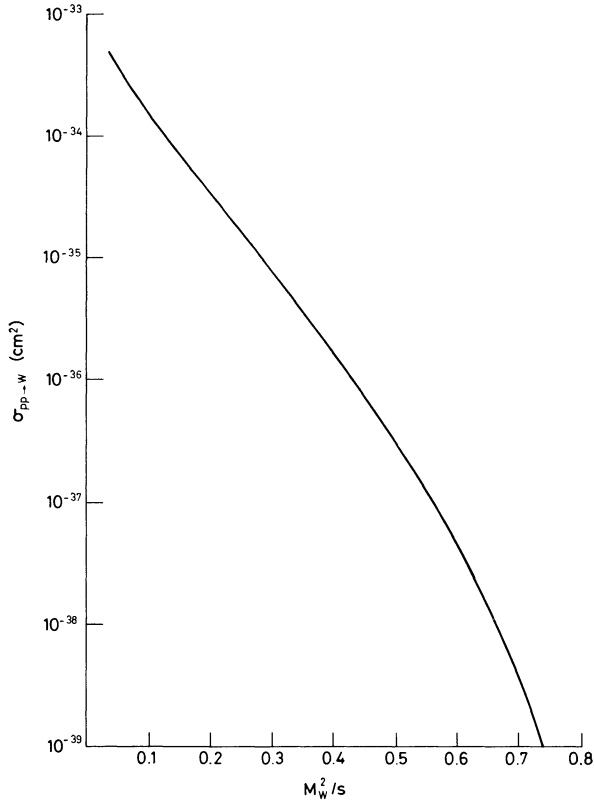
Fig. 13 W production cross-sections in pp collisions as a function of M_W^2/s assuming Drell-Yan scaling and the model of Altarelli et al. for μ pair production (Ref. 18). A factor of $1/3$ has been included by virtue of the assumption that quarks have three colours.

The signature for these events is a very sharp peak in the inclusive μ or e cross-sections at $p_T = M_W/2$, which would be easy to detect in the absence of background. The cross-section must be reduced by the branching ratio which is at present a matter for speculation; if the scaling ideas currently believed to apply to $\bar{e}e$ annihilation are valid,

$$\frac{\Gamma(W \to \mu\nu)}{\Gamma(W \to all)} = \frac{1}{No.\ of\ weak\ interaction\ doublets} .$$

Present thinking suggests $\frac{1}{4}$ or less for this number (the doublets being $\nu_e e$, $\nu_\mu \mu$, pn_c, and $p'\lambda_c$).

The cross-section and branching ratio for the Z^0 are much more model-dependent but presumably $\sigma(pp \to Z^0 + ...) \simeq \sigma(pp \to W + ...)$ with a branching ratio similar to that of the W. The signature here is a large peak in the dimuon invariant mass spectrum.

It is clear that if Fig. 13 and these branching ratio estimates are even approximately correct, accelerators might be capable of finding W's with masses up to at least $0.85\sqrt{s}$, and storage rings might discover W's with masses up to about $0.6\sqrt{s}$ as far as rates are concerned. The only problem is background. The cross-section for μ's and e's produced in the chain

$$pp \to W/Z$$
$$\qquad \downarrow$$
$$\qquad \hookrightarrow \mu/e + ...$$

has a very sharp peak at $p_T = M_W/2$ [19]. A cursory estimate of the $\pi/K \to e, \mu$ background based on Figs. 11 and 12 suggests that it will not be a serious problem (the π's and K's having a long lifetime at the relevant energies). Camilleri[14] has made the necessary detailed investigation of this point (but he did not include the contribution from the weak production of π's and K's which is the dominant contribution at large energies for large M_W according to Fig. 12!). The upshot is that a 5 TeV accelerator might discover W's up to about 85 GeV, a 10 TeV accelerator up to 120 GeV, 100 × 100 GeV storage rings up to 120 GeV, and 400 × 400 GeV rings up to 500 GeV! However, this conclusion depends entirely on an untested scaling law and on an extrapolation of π and K yields to estimate background which may be quite wrong.

5. CONCLUSIONS

The calculations presented in this paper should be considered in conjunction with the other papers in this study and folded with realistic ideas of acceptance and experimental feasibility before drawing definite conclusions[*]. Tentatively, however, it would seem to me that:

i) a multi-TeV accelerator of energy 5 TeV or more could undoubtedly provide a wealth of exciting new information about weak and electromagnetic interactions. Barring unexpected new thresholds, etc. (of which there has been no hint from the ISR), it would seem that at least 5 TeV is needed:

   a) to explore the scaling phenomenon and probe the nucleon's structure at a significantly deeper level;

   b) to explore weak electromagnetic interference in muon scattering at a significant level;

   c) to discover the intermediate boson in neutrino or proton collisions if present ideas about its mass are correct.

ii) High-energy proton storage rings might discover W's and Z's with masses as high as half the centre-of-mass energy, or more. However, this assertion relies on an untried scaling law, tests of which are eagerly awaited. Otherwise proton-proton collisions cannot be relied on as a source of new information about weak and electromagnetic interactions.

iii) As shown, for example, in Figs. 5 to 7, the Q^2 range which can be explored in muon and neutrino experiments with very large accelerators ($\gtrsim$ 5 TeV, say) can also be explored in very large ep storage rings (s $\gtrsim$ 30,000 GeV^2, say), the gain in energy compensating for the much lower luminosity in this case. However, the calculations presented here confirm Wiik's conclusion[20] that, in order to be sure of making a significant advance, higher ep energies than could be produced in a superconducting system accommodated in the existing ISR tunnel (s $\lesssim$ 6,000 GeV^2) would be required.

iv) Unless some new method of accelerating particles is discovered, it is hard to imagine the construction of an accelerator with energy of 5 TeV or more in the near future.

---

[*] Furthermore the impact on multi-TeV experiments of the "New Physics" associated with J/ψ, etc., should be carefully considered once its significance has become clear. I have not attempted this while revising this paper which was written in August 1974.

However, apart from the fact that it is not a good machine for producing W's and Z's, an ep colliding beam machine of, say, 25 GeV × 400 GeV (s = 40,000 GeV^2) could make similar contributions to the study of weak and electromagnetic interactions; in addition, it would be an excellent tool for the investigation of the seemingly hadronic physics of photoproduction. These arguments led Bjorn Wiik and myself to undertake further studies of very large ep colliding beam systems. Our report will be available shortly[1]. The preliminary conclusion is that a large e$^-$p system, to which an e$^+$ and a second proton ring could be added later, seems to be a very attractive possibility.

Acknowledgements

Some of the conclusions derived from an enjoyable collaboration with Bjorn Wiik (Ref. 1) have been incorporated in this paper. I am grateful to Roger Cashmore for reading the manuscript.

* * *

REFERENCES

1) C.H. Llewellyn Smith and B.H. Wiik, A report on physics with very high energy ep storage rings, in preparation.

2) C. Rubbia, Neutrino experiments at the multi-TeV accelerator, this report, Part A, paper IV.1.

3) D. Treille, Appendix to this paper.

4) Particle physics with positron-electron-proton colliding beams, Report SLAC 146/LBL 750 (1972).

5) L. Mo, Radiative corrections to e-p colliding beam experiments, NAL 1973 Summer Study, Vol. 2, p. 125.

6) R.W. Brown and J. Smith, Phys. Rev. D 3, 207 (1971); and cross-sections for higher energies kindly supplied by J. Smith (private communication).

7) See, for example, R.W. Brown, A.K. Mann and J. Smith, Phys. Rev. Letters 25, 257 (1970).

8) R.N. Brown, L.B. Gordon and K.O. Mikaelian, Phys. Rev. Letters 33, 1119 (1972).

9) C.H. Llewellyn Smith and D.V. Nanopoulos, Nuclear Phys. B78, 205 (1974), and Erratum, Nuclear Phys. B83, 544 (1974). The sign of the interference term is wrong in Eq. (38) of this paper.

10) J.D. Bjorken and C.H. Llewellyn Smith, Phys. Rev. D 7, 887 (1973).

11) K.J. Kim and Y.S. Tsai, SLAC-PUB 1105 (1972).

12) L. Stodolsky, J. Phys. 35, C2, 87 (1974).

13) N. Cabibbo, Production of lepton pairs in proton-proton collisions at very high energies, this report, Part B, paper II.5.

14) L. Camilleri, Lepton production at the SISR, this report, Part B, paper II.6.

15) K.H. Craig, Nuclear Phys. B (in press).

16) C. Jarlskog, Invited paper, Proc. 17th Internat. Conf. on High-Energy Physics, London, 1974 (Science Research Council, Chilton, 1974), p. V-3.

17) L.M. Lederman and B.G. Pope, Phys. Rev. Letters 27, 765 (1971).

18) C. Altarelli, N. Cabibbo, L. Maiani and R. Petronzio, Nuclear Phys. B92, 413 (1975).

19) Details may be deduced from R.L. Jaffe and J. Primack, Nuclear Phys. B61, 317 (1973).

20) B.H. Wiik, Should an electron ring be added to a pp colliding beams facility at CERN?, this report, Part C, paper 3.

EXAMPLE OF LEPTON BEAMS AT A MULTI-TeV SYNCHROTRON

D. Treille

CERN, Geneva, Switzerland

μ BEAM

10^{13} incident protons $\rightarrow$ $\sim 3.3 \times 10^{12}$ interacting efficiently 3 cycles/min.
The design below is scaled from that of R. Clifft and N. Doble, CERN/SPSC/74-12.

Description: First stage $\lesssim$ 500 m, supra, to accept and select parents:

$$\left(\frac{\Delta p}{p}\right)_\pi \simeq \left(\frac{\Delta x}{x}\right) \simeq \pm 10\% \ .$$

By adding focusing elements, one can slightly improve the acceptance (which is already $\sim$ 50% in the SPS design).

FODO   same elements as now, 12.5 times more spacing, 7 km of length; acceptance $\sim$ 1, so intensity $\sim$ proportional to the length chosen.

Back end $\lesssim$ 1 km, mostly supra, to select μ's:

$$\left(\frac{\Delta p}{p}\right)_\mu \simeq \left(\frac{\Delta x}{x}\right)_\mu \simeq \pm 6\% \ .$$

Total length $\lesssim$ 8-9 km.

Approximately same p_T and x ranges as now are accepted.

Flux: From 5 TeV protons and $(\Delta p/p)_\mu = \pm 6\%$ assuming that $x \, d\sigma/dxdp_T^2$ is independent of s

p_μ (TeV)	3.5	2.5	1.5
μ^+ intensity	$\sim 4.5 \times 10^7$	4×10^8	10^9
μ^- intensity	$\sim 10^7$	$\sim 10^8$	$\sim 5 \times 10^8$

If the primary analysis of parents is skipped, gain of $\sim$ 2 in flux at 1.5 TeV. Hagedorn-Ranft values used here seem to be high by a factor of 2 at FNAL energies.

Luminosity at 2.5 TeV (μ^+, 10^{13} protons, 3 pulses/min)

- on 50 m H_2 $\sim 4 \times 10^{33}$ cm^{-2} sec^{-1}
- on 50 m iron $\sim 4 \times 10^{35}$ cm^{-2} sec^{-1}

(compared to $\sim 10^{32}$ cm^{-2} sec^{-1} for ep rings).

e-γ BEAM

- Simply a stage of momentum analysis and recombination 200-300 m supra.
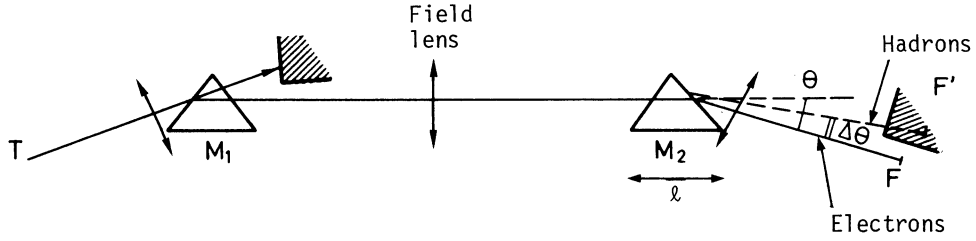
$\Delta\theta/\theta \simeq (\Delta p/p)_{synch}$ in one set of magnets (they are supposed to be identical);

$$(\Delta p/p)_{synch} \simeq 1.2 \times 10^{-6} \ p \ (GeV) \ \ell \ (m) \ B^2 \ (T) \ .$$

With $\sim$ 6 mrad of bending (20 m × 2 tesla for 2 TeV) one gets $(\Delta p/p)_{synch} \sim 20\%$ (or 40% if one chooses 10 m × 4 tesla).
The spatial separation at the recombined focus F is quite sufficient
($\sim$ 6 cm if the distance M_2F is 50 m, with 2 tesla in the magnets).
The dispersion of electrons due to fluctuations in the process of radiation may be large: perhaps some type of field lens in F can be used.

- Assuming $\Delta p/p \simeq \pm5\%$, $0°$ production, same p_T accepted as in Ref. 1 below
  (i.e. $\Delta\theta$ accept. $\simeq$ 0.1 mrad, while they had $\sim$ 1 mrad), 10^{13} incident protons at 5 TeV (see their figure at 500 GeV), a gain of 2 because of direct electron production (they had a two-step beam), we would get $\sim$ 4 × 10^8 e/pulse at 2 TeV.
  The purity is certainly sufficient for a photon beam. We consider here a broadband γ beam.

- With 10% radiation length as a radiator and a hydrogen target of 1 m one gets, for γ above 1 TeV, a luminosity of $\sim$ 6 × 10^{31} cm^{-2} sec^{-1}. This may be compared with an effective luminosity of dE_γ/E_γ × 5 × 10^{29} cm^{-2} sec^{-1} quoted for EPIC.

1) Z. Guiragossian et al., NAL Proposal 192-193 and NIM No. 173.

III.1 NOTES ON ASPECTS OF HADRONIC EXPERIMENTS
WITH A 10 TeV PROTON SYNCHROTRON

A.M. Wetherell

CERN, Geneva, Switzerland

1. INTRODUCTION

The following is an outline of some considerations of physics and technical problems contained in the list for study by the hadronic interactions section of the group.

2. BEAMS

2.1 Particle fluxes

For orientation, Table 1 gives some 0° particle yields, estimated by scaling. The primary beam momentum is 10 TeV/c, the secondary particles are 5 TeV/c, i.e. x = 0.5.

Table 1

Particle yields at 10 TeV SSPS

Particle	Invariant cross-section $(cm^2/sr \ GeV^2)$	Yield
p	2×10^{-26}	1.3×10^8
π^+	5×10^{-27}	3.1×10^7
π^-	3×10^{-27}	1.9×10^7
K^+	6×10^{-28}	3.8×10^6
K^-	8×10^{-29}	5.0×10^5
$\bar{p}$	7×10^{-30}	4.4×10^4
Σ^-	4×10^{-28}	2.5×10^6
Ξ^-	4×10^{-29}	2.5×10^5

Yield is particles/10^{-8} sr/1% momentum bite for 10^{11} protons interacting. (A 1% momentum bite is of course 50 GeV/c!)

The fluxes are high and it would appear that particle yields do not in general cause experimental limitations for most of hadronic physics.

2.2 Beam composition

Selective absorption has been used at FNAL to enrich beams. For example, an 18 m long water filter has been used on a 50 GeV/c beam to turn 95% protons + 5% pions into 58% protons + + 22% pions. Estimates indicate that a 40 m deuterium filter could improve particle ratios as follows: $\pi^+/p \sim 100$, $K^+/\pi^+ \sim 8$, $K^-/\pi^- \sim 4$. This idea would be useful at TeV energies and merits further consideration.

2.3 Hyperons

It is interesting to note the decay lengths of the common hyperons. Table 2 is for 5 TeV/c.

Table 2

Decay length of 5 TeV/c hyperons

Particle	Mass (GeV)	$\gamma c\tau$ (m)
Σ^+	1.19	101
Σ^-	1.20	185
Ξ^-	1.32	190
Ω^-	1.67	117
Λ	1.12	335

The decay lengths even at this extremely high momentum are not so long as to make experimentation straightforward.

2.4 Magnets

A superconducting magnet, 5 m long and producing 5 T, would appear to be a useful module. This gives a 1.5 mrad bend at 5 TeV, i.e. 15 cm deflection at 100 m.

2.5 Beam lengths

The present $\simeq$ 0.5 TeV machines are $\simeq$ 2 km in diameter. Scaling by a factor of 20, a warm iron machine of 10 TeV would be 40 km in diameter; a superconducting machine might be 2-3 times less, say $\sim$ 16 km diameter. Beams might be expected to grow in length in some fashion; however, it appears that "simple" beams may be accommodated in spaces of no more than about 2 km length.

2.6 Particle identification

It is assumed that transition radiation (TR) detectors will be the main device for use at TeV energies. The space occupied along beam lines will be negligible. Hyperon identification, e.g. Σ^--Ξ^-, may be difficult; probably identification by decay is the best method.

3. TOTAL CROSS-SECTION MEASUREMENTS

A conventional good geometry transmission experiment for the total cross-section of hadrons on protons measures the loss of particles within an angular cone defined approximately by 10^{-2} GeV^2 $\lesssim$ $|t|$ $\lesssim$ 10^{-1} GeV^2. An extrapolation to $|t|$ = 0 yields the total cross-section after some well-known manipulations. At a momentum of 5 TeV/c the angular range of interest extends between 1/50 and 3/50 mrad, corresponding to transverse displacements of 10 mm and 30 mm, respectively, at a distance of 500 m from a target. A multiwire proportional chamber system with spatial resolution of 0.5-1 mm would then be adequate for mapping the particle distribution in enough bins. The layout would consist of $\sim$ 1 km of beam preparation, starting from an EPB target; 500 m of space for beam definition with TR detectors for identification

and 500 m of drift space behind the target for mapping of the transmitted particles would suffice. The experiment would be a straightforward extension of those performed by Lindenbaum and collaborators 10 years ago.

A simple extension to hyperons is not so clear, noting problems for identifying the particles adequately and the rather short decay lengths. High resolution detectors, with spatial resolution of 50-100 μ would certainly be a basic part of a design. As noted previously, hyperon decay may be a more useful approach although both possibilities may be considered.

4. ELASTIC SCATTERING MEASUREMENTS

4.1 Coulomb region

The measurement of scattering in the Coulomb region is of considerable interest in that the determination of ρ, the ratio of real to imaginary parts of the forward scattering amplitude, provides a "long arm"[1] on the behaviour of σ_{tot} (see Fig. 1 for pp). While an
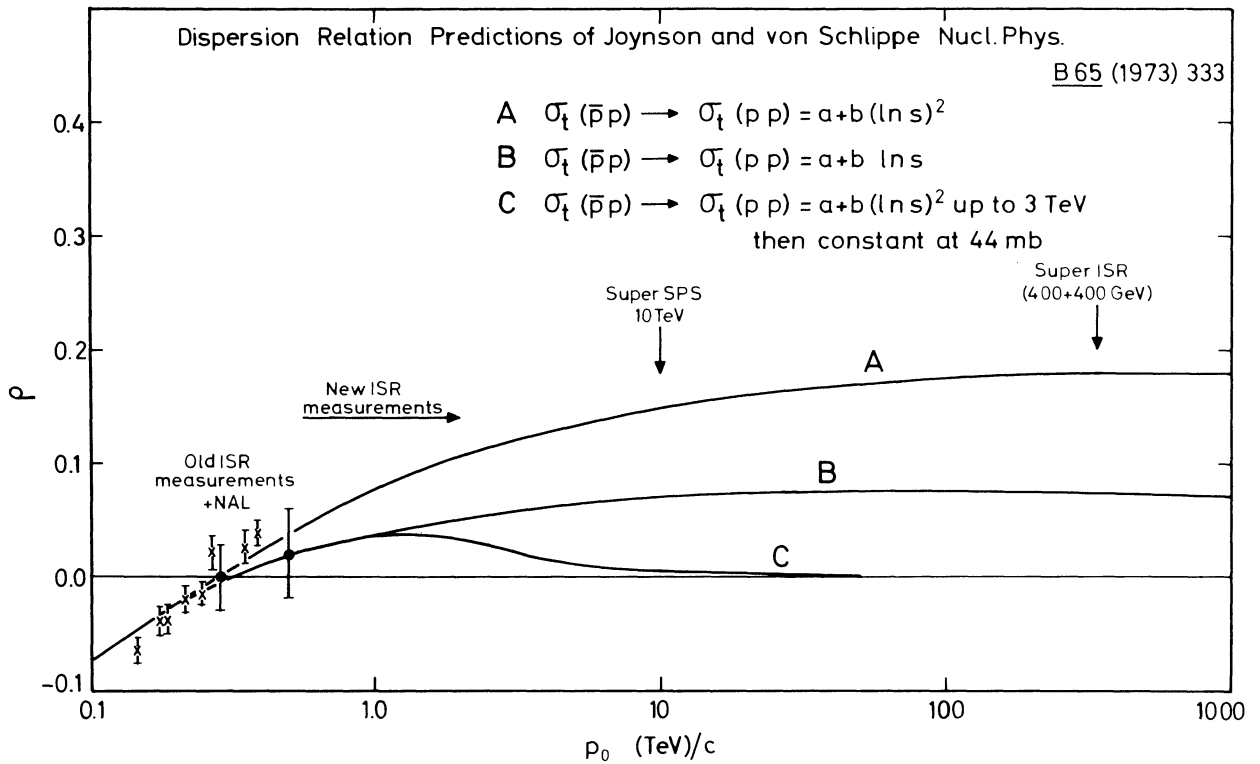
Fig. 1

extension of the Serpukhov and FNAL gas jet experiments, involving detection of the recoil proton, appears still valid at SSPS energies, the possibilities of such measurements for π-p or K-p appear very unclear.

4.2 Diffraction peak

Defining the diffraction cone as the part of the angular distribution lying within $|t| \lesssim 1$ GeV^2, then the forward particles fall inside $\simeq \frac{1}{5}$ mrad (or 10 cm transverse displacement over 500 m). A simple layout, similar to that for the σ_{tot} experiment, but involving a weak magnetic field near the target to analyse recoils ($T_{recoil} = |t|/2M$) and several of our modular magnets for the forward particle, would do the job. However, a coaxial geometry would be more elegant.

4.3 Large momentum transfer

Scattering for large $|t|$, i.e. $\sim$ several GeV^2, will be discussed together with the layout for production processes at large p_T.

5. SCATTERING OF HADRONS ON ELECTRONS

Elastic scattering of very energetic hadrons (π, K, hyperons) on atomic electrons would provide data on the hadronic form factors similar to those provided by the electron machines for the proton structure. So far energies have been too low to provide reasonable experiments as

$$s \simeq 2\, m_e\, E_{hadron} \ .$$

However, for $E_{hadron} = 5$ TeV,

$$s \simeq 5 \text{ GeV}^2 \ , \quad \sqrt{s} \simeq 2.2 \text{ GeV} \ .$$

For π-e scattering this is equivalent to a 17 GeV electron beam incident on a stationary pion and therefore looks interesting (à la SLAC).

It is even more stimulating to consider *inelastic* π-e scattering, as in fact one could enter into a "deep inelastic" region in order to begin to explore the structure functions for the pion for comparison with those for the proton. The inelastic final states available appear very interesting indeed.

6. MUON-ELECTRON INELASTIC SCATTERING

The remarks made above about π-e inelastic scattering, in particular the kinematics, show that μ-e inelastic studies could give a new dimension to electromagnetic and lepton physics.

*   *   *

REFERENCE

1) W. Bartel and A.N. Diddens, CERN NP Internal Report 73-4 (May 1973).
   D.W. Joynson and W. von Schlippe, Nuclear Phys. B65, 333 (1973).

III.2 POSSIBLE EXPERIMENTAL CONFIGURATION FOR HIGH p_T STUDIES

M. Albrow

Rutherford High-Energy Laboratory, Didcot, Berks, UK.

Without a detailed design study, we wish merely to suggest a possible experimental layout which may be considered as forming a facility for the study of high p_T processes. This solution is neither unique nor necessarily optimum. It presupposes that magnetic analysis of at least the high p_T particle is required, and for preference magnetic analysis over as much solid angle as possible, with nearly 2π azimuthal acceptance.

We suggest a superconducting, axially symmetric toroidal magnet as the major element (see Fig. 1). The current flow is along two coaxial cylinders of radii $\sim$ 20 cm and $\sim$ 80 cm, the circuit being completed with radial "spokes" which result in losses to the azimuthal acceptance. The field at radius r is given by

$$B \text{ (tesla)} = \frac{2 \times 10^{-7} \text{ I (A)}}{\text{r (m)}} ,$$

where I is the total current along the cylindrical conductor. The magnet is positioned on rails downstream of the target at a distance L which depends on the incident momentum such that particles produced at x = 0 have r $\sim$ 0.5 m, thus

$$L = 0.5 \text{ m} \times \sqrt{\frac{p}{2m_p}} = 0.365 \text{ m} \quad \sqrt{p(GeV/c)} .$$

L varies between 11.5 m at 1 TeV/c and 36.5 m at 10 TeV/c. At high p_T the magnet aperture covers -0.2 < x < +0.2 for all incident momenta. As

$$B\ell \text{ (Tm)} = 3.3 \ \Delta p_T \text{ (GeV/c)}$$

we consider a toroid of total length ℓ = 10 m, which bends particles of p_T = 5 GeV/c back parallel to the axis. Then B at 0.5 m must be 1.67 T, and B at 0.2 m (on the surface of the inner conductor) is $\sim$ 4.2 T. The total current along the central conductor is $\sim$ 4.2 $\times$ 10^6 A.
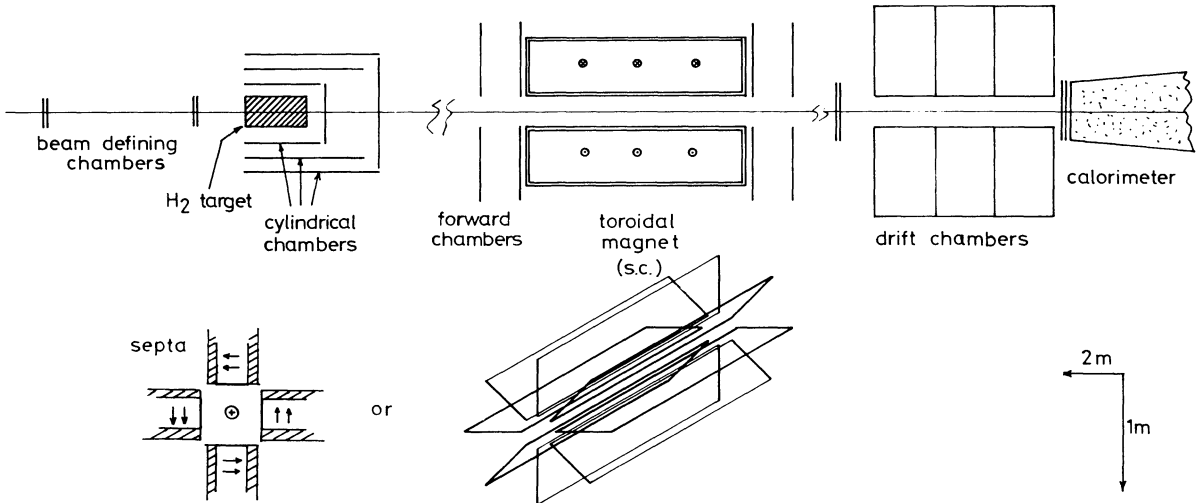
Fig. 1 Suggested experimental set-up for the study of high p_T processes at the SSPS.

Positional information on the tracks is provided by planes of MWPCs (or drift chambers) before and after the magnet. We consider that a resolution in transverse momentum of $\Delta p_T/p_T < 1\%$ is necessary (note that the invariant cross-section changes by $\sim 10\%$ over this interval of p_T), and can be achieved with $< 0.5\%$ measurements on both momentum and angle. This should be relatively straightforward with chambers of precision < 0.5 mm. Tracking through a field map would be essential.

The target is surrounded by cylindrical chambers to observe at least the event configuration in the backward hemisphere.

Identification of the particles that traverse the magnet is a problem which is not resolved clearly at the present time. The important range of momenta to be considered is ~ 100-1000 GeV/c. Transition radiation detectors are a possibility, and if they can be satisfactorily developed would require relatively little space (a few metres).

The jet of particles in the projectile fragmentation region traverses the field-free cylinder inside the toroid. Two possibilities present themselves for a more detailed study of this "jet": a calorimeter, or a magnetic spectrometer. Provided a calorimeter could withstand the major proportion of the incident beam flux, it would provide "bulk" information such as the total energy of the forward jet. We could also envisage using it as an energy loss trigger to select "central" events where a large fraction of the energy of the incident particle goes into particle production. A magnetic spectrometer, on the other hand, would have pattern recognition problems due to the high multiplicity confined to the very small angular cone in the forward direction (frequently ~ 10 charged particles in ~ 10 mrad cone). Such detailed information on the particles in the fragmentation region is probably unnecessary for an experiment on physics at high p_T.

If the above superconducting toroid proved to be technically not feasible, an alternative would be to consider a number of septum magnets placed in a circular array around the beam line, thus "approximating" the toroid. The resulting loss in solid angle would be a disadvantage, but the arrangement would have more flexibility and the field could be made essentially uniform in each magnet, which would reduce tracking problems.

High p_T experiments have the advantage of not requiring exceptionally long experimental areas; 100-200 m would seem adequate unless a forward magnetic spectrometer would be desirable (apart from incident beam definition).

III.3 PARTICLE IDENTIFICATION ABOVE 400 GeV/c

W.J. Willis

CERN, Geneva, Switzerland

The energy range below the limit fixed above can be handled with Čerenkov counters. Although the angular acceptance is rather small as the limit is approached, it is sufficient to allow the construction of focusing spectrometers with particle identification.

Above this limit, a new approach seems called for. Among methods which do not destroy the particle, transition radiation and synchrotron radiation seem to offer the most promise. Here we deal only with the former, which seems to have wider applications.

In the dimensionless form of Artru et al.[1], the radiation from a singly charged particle penetrating a foil of thickness t and plasma frequency ω_0 is

$$\frac{dW}{d\omega}(\gamma,\omega) = \frac{2\alpha}{\pi} G(\Gamma,\nu) \ ,$$

where

$$\omega/2\pi = \text{radiated photon frequency}$$
$$\gamma = E/m \text{ of particle}$$
$$\Gamma = \gamma/\Gamma_0$$
$$\Gamma_0 = \omega_0 \ t/2$$
$$\nu = \omega/(\omega_0\Gamma_0)$$
$$\omega_0 = \sqrt{n_e} \ e^2/m_e$$
$$n_e = \text{electron density} \ .$$

The function G is shown in Fig. 1. The oscillatory behaviour is due to interference of the radiation from the two surfaces of the foil. The radiation emerging from a number of foils is strongly affected by the X-ray absorption properties of the foil material. The energy dependence of the absorption of a given material (of fairly low atomic number) is shown in Fig. 2. Below a certain photon energy ω_k, the absorption is dominated by photo-electric transitions, and varies as ω^{-3}, while at higher energies it is dominated by the Compton effect, which decreases linearly. Since the γ threshold is determined by ω_k, it is usually best to work at the lowest possible energy. The absorption then eliminates low-energy photons and leaves the peak near $\nu = 1/3$. It can be seen from Fig. 1 that $\Gamma = 1$ is a kind of threshold in γ, and it follows that

$$\nu \simeq 1/3 = 2\omega_k/(\omega_0^2 t)$$
$$t = 6\omega_k/\omega_0^2$$
$$\Gamma_0 = \gamma_{threshold} = 3\omega_k/\omega_0$$
$$= 2500 \text{ for } CH_2$$
$$= 1800 \text{ for lithium}$$
$$= 1750 \text{ for diamond}$$
$$= 1000 \text{ for solid } H_2, \text{ etc.}$$

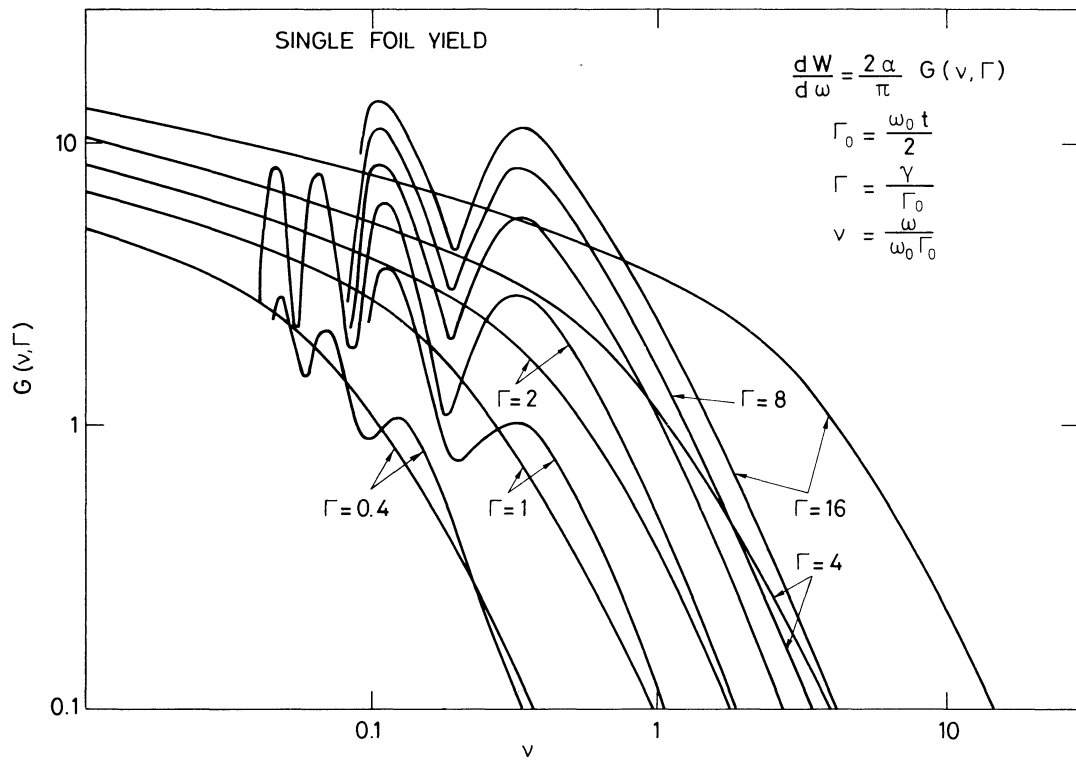**Fig. 1** The function G, entering the formula for the transition radiation of a particle penetrating a foil of thickness t, as a function of ν.
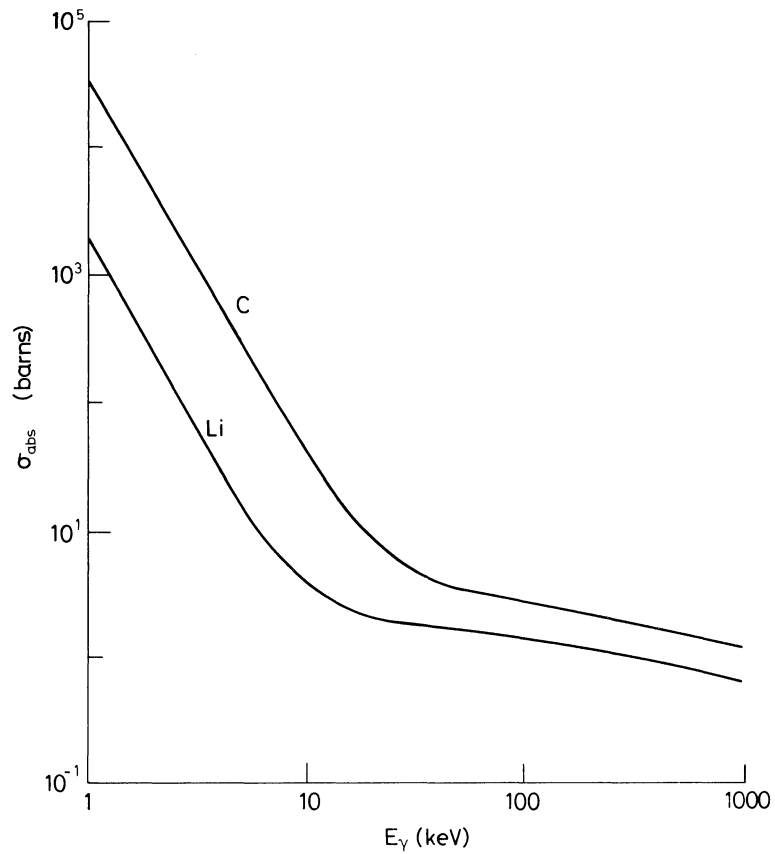

Fig. 2 Absorption cross-sections for photons in Li and C as functions of the photon energy.

Also, the number of photons radiated is

$$N \propto 1/\omega_k$$

while the energy radiated is independent of ω_k, for $\Gamma = 1$ always. If, as seems to be the case, we can detect single photons, there is some advantage in choosing the lowest available Z for the foil material. Another facet of the situation becomes evident when we consider the manner in which the radiation is to be detected. The simplest is to follow the radiator with a detector, say a proportional chamber, which is sufficiently thick to absorb all of the radiation -- or rather, most of it, since the particle itself will deposit ionization loss in the detector proportional to its thickness. The detector will be made of a material of higher Z, and will be on the photoelectric portion of the curve with a cubic slope. The signal from transition radiation with respect to the background from ionization loss will vary with the inverse cube of the Z of the foil material. This fact, as well as the larger number of photons, makes it imperative to use the lowest possible Z for the foil material. These considerations have been verified by experiment[2], as shown in Fig. 3.

The radiation from a single interface is emitted at angles with respect to the particle direction of approximately $1/\gamma$. This suggests that the angle of the radiation should be measured to determine γ. In fact, the interference between the radiation from the two surfaces of the foils comprising a real radiator, together with the absorption which eliminates low-energy photons, essentially fixes the angle of the radiation near $1/\gamma_{threshold}$ and deprives us of this attractive possibility. However, the finite angle of emission can be used with a sufficient flight path to achieve spatial separation of the transition radiation photons and the ionization of the particle track. For a separation of 10 mm, a drift path of 30 m or more would be required. Since more than one radiator detector assembly will be needed, as discussed below, the length required may be more than is allowed by solid-angle considerations in the case of identification of secondary beam particles. The use of finely divided silicon detectors would reduce this distance to a few metres. In any case, the length needed will no doubt be available in the case of identification of beam particles. Even in this case, the advantage of radiators of the lowest possible Z will probably be important, since even these tend to give no more than a few photons: a particle of $\gamma = 5000$ in an optimized lithium radiator is predicted to give about six photons.

Of course a magnetic bend between the radiator and the detector can be used to give the spatial separation sought, but substantial bending power is needed to give much reduction in the length required.

As always when using threshold detectors, the momentum range of a given system is limited if separation between pions, kaons, and protons is required. For example, the threshold for pions might be set at 450 GeV, then kaons would start to count at around 1.6 TeV and protons at around 3 TeV. In fact, the threshold is not truly sharp, and consequently it would be necessary to demand the detection of, say, four or more photons to be sure that the particle was indeed above "threshold". Then to ensure good efficiency for the wanted particle, there should be a total of about 10 photons, and two or three radiators will be required. This suffices for pions, or if antiprotons are wanted, the same array can be used as a veto above 1.6 TeV. If kaons are desired, two arrays are needed, one with a high threshold so that only pions are counted.
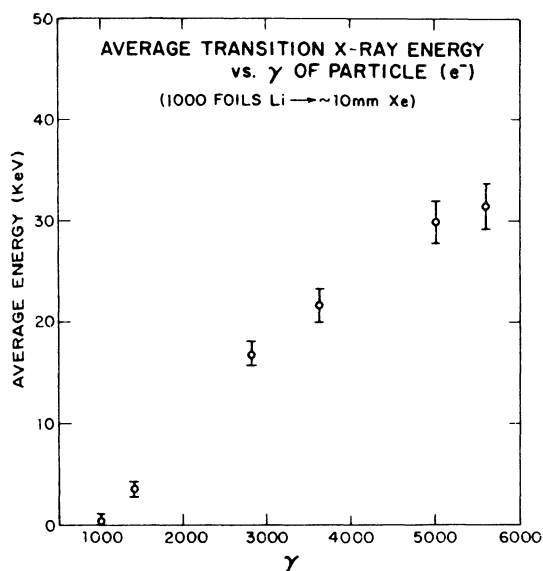
Fig. 3a Average transition X-ray energy de-
posited in the chamber. The error
bar for each point includes the un-
certainty in the energy scale cali-
bration.
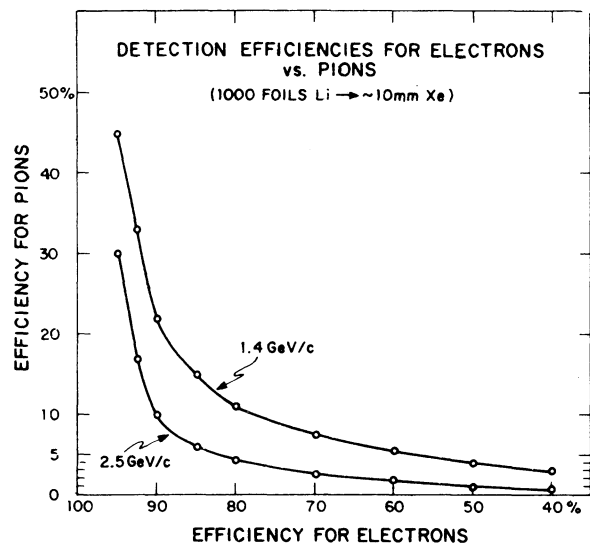
Fig. 3b Electron-pion discrimination at 1.4
and 2.5 GeV/c. Pion contamination
(expressed by the efficiency for
pions) is plotted against various
discriminating thresholds which also
determine the efficiency for elec-
trons. (The electron contamination
contained in the pion spectrum was
subtracted.)
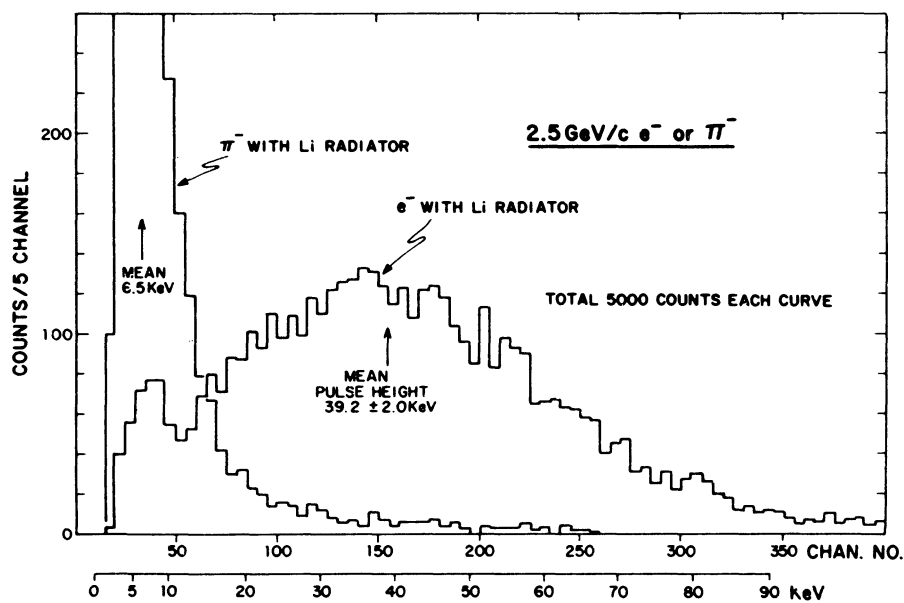
Fig. 3c Pulse-height spectra for e⁻ or π⁻ taken with a single detector
configuration, at 2.5 GeV/c. The spectrum for e⁻ with Li re-
presents the signal due to transition X-rays, background radia-
tion, and ionization loss, while the other does not contain the
transition X-rays. The pion data contain an electron contami-
nation of 0.5%.

The question of the best way to increase the threshold above the natural value then arises. The simplest way is to increase the thickness of the foils and detect more energetic photons. Somewhat better results can be obtained by artificially reducing the density of the foils by altering the structure while continuing to use low-Z materials. This avoids the introduction of too much matter from the point of view of nuclear interactions, for example. Eventually, gas cells would be used as the "foils". In fact, as γ approaches 10^5, the use of synchrotron radiation becomes more attractive, as in the case of electron identification at energies of the order of 100 GeV.

A few words on technical details may be appropriate. If we are identifying particles in a beam of a few centimetres diameter, there are no serious technical problems. The radiators can be made of lithium or beryllium foils at modest expense, and the detectors can be proportional chambers filled with xenon gas, about 15 mm thick, or possibly a silicon detector.

If the identification of particles of several masses over a large area and over a wide range of momenta in the presence of large multiplicity per event and high rates is required, we know that a solution is apt to be expensive. This is a task that has hardly been done at PS energies, and we know that it will be more difficult at SPS energies. In fact I believe it might be substantially easier at energies of a few TeV, but it involves some technical problems. Large radiators have to be built out of low-Z materials. The detectors of the low-energy photons must have good pulse-height uniformity and thin windows over large areas. A number of these systems must be mounted in series to detect different particles. One such system has been built, demonstrating that these problems can be solved[3].

The conclusion may be stated this way: we may safely assert that the identification of beam particles and secondary particles may be achieved in the TeV range with levels of effort comparable to those required with the present generation of accelerators.

* * *

REFERENCES

1) X. Artru, G. Yodh and G. Mennessier, Report CERN-TH.1992 (1975), to be published.
   See also G.M. Garibian, Transition radiation, Yerevan Physical Institute, Scientific
   Report 27 (1973).

2) J. Fischer, S. Iwata, V. Radeka, C.L. Wang and W.J. Willis, Phys. Letters 49B, 393
   (1974), Nuclear Instrum. Methods 127, 525 (1975).

3) Brookhaven-CERN-Syracuse-Yale Collaboration, Status Report of R806T Experiment,
   CERN/ISRC/75-31 (1975).

III.4 THE ROLE OF TOTAL ABSORPTION SHOWER COUNTERS
WITH PARTICLES IN THE TeV RANGE

W.J. Willis

CERN, Geneva, Switzerland

When considering methods of measurement for particles in the TeV range, it is natural
to suppose that the total absorption shower counter, or calorimeter, will play an important
role. Whereas the length of a magnetic system for measurement of momentum must increase
linearly, the size of a calorimeter must increase only logarithmically with particle energy.
Furthermore, the increase in the number of interactions and the number of particles in the
shower makes it clear that the fluctuations which contribute to the limitations on energy
resolution in the calorimeter must make a smaller relative contribution.

The exact law by which the resolution improves as the energy goes up is not obvious.
Aside from technical limitations, there seem to be two sources of fluctuation which affect
the energy resolution. One is the sort of fluctuation which occurs with particles in the
portions of the shower which are more or less well developed: sampling fluctuations, lost
neutrinos, etc. These must depend on the number of track segments, and thus this contribu-
tion must fall as the inverse root of the energy of the initial particles. However, all
calorimeters built until very recently have a somewhat different response to showers which
contain only electromagnetic particles and those which (in the limit) contain only hadrons
and are therefore rich in nuclear stars. This effect is illustrated in the curve for iron
in Fig. 1. In the latter category, there is an energy price to be paid in nuclear binding
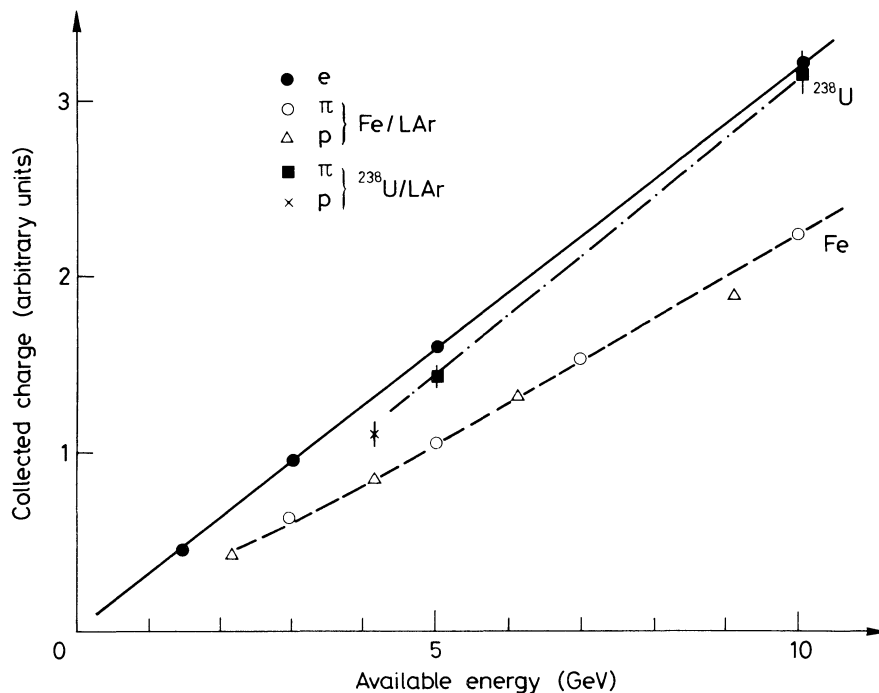
Fig. 1 The response of an iron-plate and of a uranium-plate calorimeter for different
types of particles, as a function of the available energy.

energy and other related effects. It is the first, or first few, collisions which determine the character of the shower, either rich or poor in neutral pions, and this difference in character combined with the difference in response described above leads to a fluctuation in the observed signal and the corresponding energy. These fluctuations decrease with energy rather slowly. First, the increasing multiplicity reduces the fluctuation, but the multiplicity increases only logarithmically. Also, increasing numbers of subsequent generations of interactions are sufficiently energetic to be able to create π^0's and this gives rise to an increasingly electromagnetic character to the shower, which reduces the scale of the effect, but detailed calculations have shown that this effect increases only logarithmically also.

Since these effects dominate the resolution in the best calorimeters already at present energies, it is clear that they are a serious threat to the hoped-for improvements at higher energies. One solution to this problem has recently been found[1]. In a calorimeter made with plates of ^{238}U, it is found that the deposit of visible energy due to fission correlated with energy loss to hadrons compensates for the nuclear binding effects, as shown in Fig. 1. This leads to an improvement in energy resolution, as shown in Fig. 2. The resolution extrapolates to values of a few percent for energies of several hundred GeV.

At this energy, the required depth of the absorber would be between eight and twelve interaction lengths, and the radius required would remain at about one interaction length. The latter value must be considered in more detail, since the separation between adjacent showers will often be one of the most severe design limits. Of course, if it is not required to measure the energy of each particle, but only the total energy of a cluster, the size required may be quite modest, equal to the solid angle covered plus two interaction lengths in diameter. This would often be the case for a detector for the forward cone, for example for an energy loss trigger. However, if each particle is to have a separate measurement
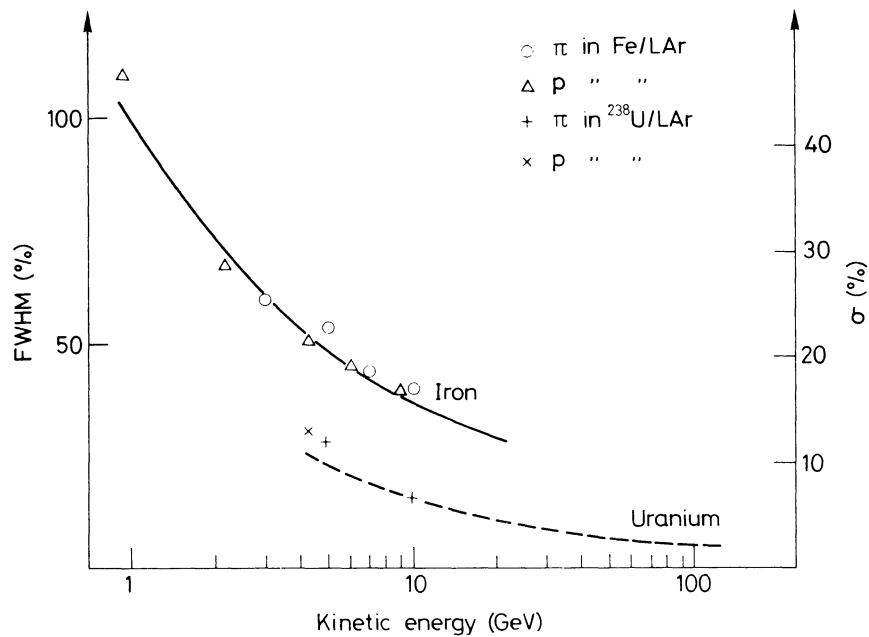
Fig. 2   Energy resolution for pions and protons in an iron-plate calorimeter and in a uranium-plate calorimeter as a function of the kinetic energy.

of its energy, there must be about one interaction length between their trajectories where they enter the calorimeter, and this can lead to long flight paths and large detectors if large solid angles are to be covered. We seem to find that the use of uranium plates is cost-effective in this case, since the interaction length in the over-all structure can then be about 10 cm. The accuracy with which the trajectory of a particle can be located could be very good if the instrumentation were justified. The error could be as small as a few millimetres.

The rate capability of these devices is fundamentally limited by the "noise" of neutrons which builds up owing to the high-energy interactions. Usually we want the detector to cover a large dynamic range, 100:1 or more, and we have to beware of the "neutron noise" tail of a high-energy particle distorting the measurement of a subsequent low-energy one. The characteristic lifetime of such neutrons in a dense block of matter is of the order of 20-40 nsec, so that the detector is clean at rates up to about 20 MHz, if there is no technical limit.

On the other hand, such a detector can be used at "large" angles to the beam to look for rare events characterized by a large energy release, in the presence of a high background of tracks of low energy. A numerical example[2] shows that many low-energy tracks per resolution time may be allowed without spoiling the measurements of the rare events. By allowing the use of very high beam intensities, up to 10^9 Hz, this technique might sometimes allow the performance of otherwise impossible experiments.

We believe the technical realization of such a device will consist of metal plates of steel or uranium, 5-10 mm thick, in a configuration suited to the spatial resolution required. The configuration will consist of strips if high spatial resolution is required. Gaps of about 3 mm between the plates will be provided for read-out. This will be either by means of scintillator or ion collection in a suitable liquid, or possibly gas. If, as is probable, the plates are uranium, the length in the beam direction will be about 1 m.

Two examples of set-ups using this technique are described. The first is a detector intended to detect the particles in the forward cone, for example in conjunction with the toroidal magnetic spectrometer described by Albrow in Section III.2 of this report. The forward cone as defined by that spectrometer (for about 5 TeV) has a half-angle of about 5 mrad. We design the calorimeter to cover this solid angle, as shown in Fig. 3. We assume that it is necessary to make distinct energy measurements on each forward particle, and therefore provide for angular resolution of 0.5 mrad. For example, this corresponds to 250 MeV/c transverse momentum for a 500 GeV/c particle. The resolution elements, which might be hexagonal in this case, are 5 cm wide with a drift path of 200 m, subtending 0.25 mrad. The detector is about 2 m in diameter, and weighs about 80 tons. The drift distance is long enough for nuclear interactions in air to be objectionable, so it is provided with a large vacuum pipe. A hadron shield blocks those particles which are bent by the spectrometer into the solid angle of the calorimeter. Transition radiators provide identification of particle mass, as described in another section of this report. These and the target may be moved to place the toroidal spectrometer at different angles in the centre of mass.

This set-up can be used with beam rates up to a few megahertz. This can be increased somewhat if the beam is focused into a small hole a few centimetres in diameter in the centre of the calorimeter, to eliminate the detection of particles which do not interact in the

Transition
radiators
and vacuum

Toroidal magnet
spectrometer

0.5 m

50 m

Calorimeter
plate array
10 int. lengths
5 cm resolution elements

Target

Beam

Wire
planes 1,2,3

Shield

Wire
planes 4,5

Vacuum
pipe

Wire
plane 6

0   100   200 m
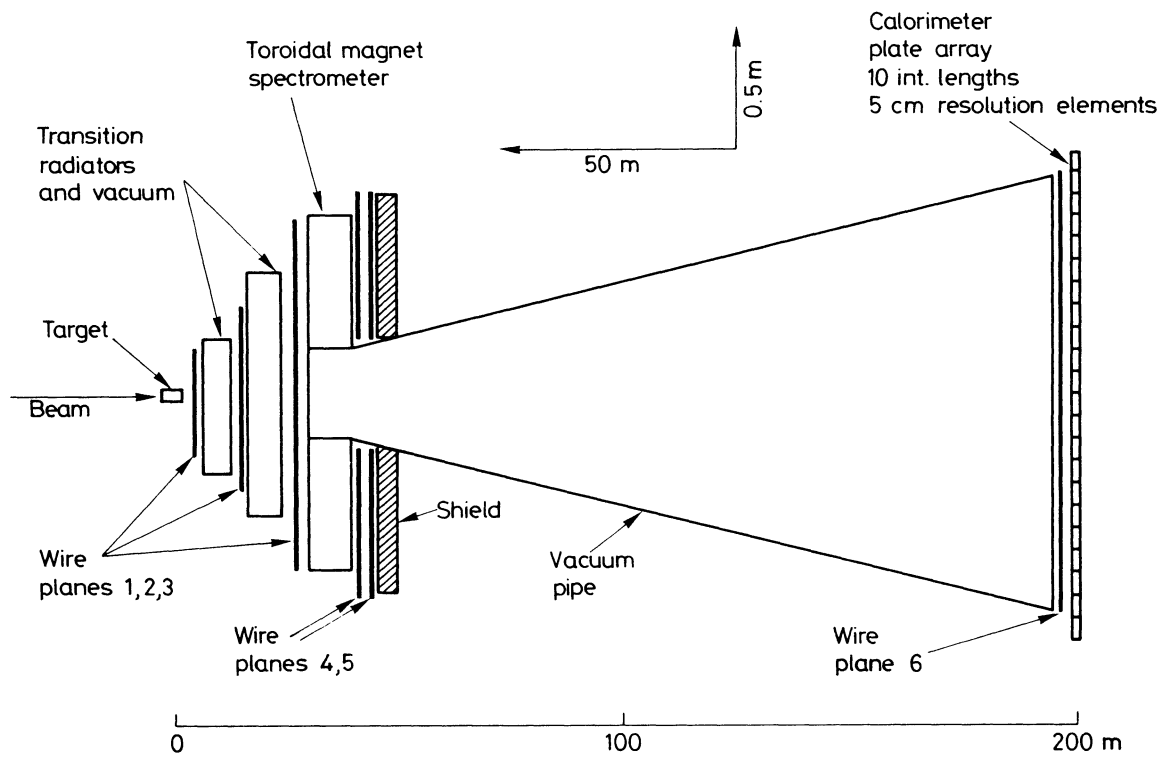
Fig. 3 Set-up for the detection of particles in the forward cone using calorimeters

Transition
radiators

Calorimeters
5 cm resolution
elements

0.5 m

50 m

Target

Beam

Wire
planes

Vacuum
pipe

Wire plane
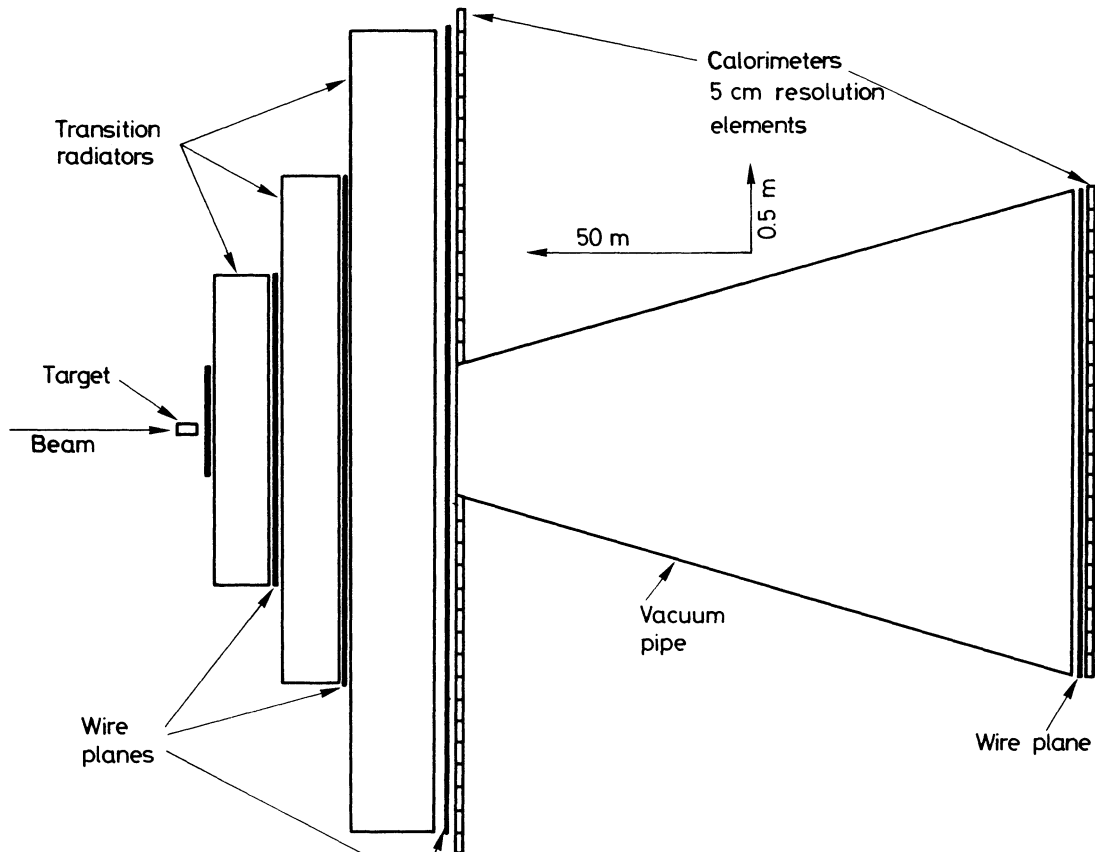
Fig. 4 Set-up for the detection of particles of large transverse momentum using calorimeters

target. The calorimeter can be used in an energy loss trigger for selecting events with large momentum transfer in an unbiased way.

The arrangement shown in Fig. 4 uses only calorimeters to study large transverse momentum events. It has a forward detector similar to that used in the previous case, and a wide-angle detector consisting of a calorimeter in the form of an annulus about 4 m in diameter, weighing about 300 tons. It has a drift distance of 60 m and an angular resolution of about 1.7 mrad. This is once more to allow measurement of the energy of each particle in closely correlated clusters.

Of course, calorimeters are sure to play an important role in experiments with incident electrons, muons, and neutrinos, and these applications are covered in the sections describing the special arrangements for those experiments.

*   *   *

REFERENCES

1) C.W. Fabjan, W. Struczinski, W.J. Willis, C. Kourkoumelis, A. Lankford and P. Rehak, Phys. Letters 60B, 105 (1976).

2) W.J. Willis and V. Radeka, Nuclear Instrum. Methods 120, 221 (1974).

III.5 NOTES ON MANY-BODY HADRONIC REACTIONS
WITH A 10 TeV PROTON ACCELERATOR

D.R.O. Morrison
CERN, Geneva, Switzerland

1. INTRODUCTION

In this paper the advantages and interest of studying many-body hadron-hadron reactions with a 2 to 10 TeV accelerator are first discussed. Some comments on the requirements and possible layout of experiments are given.

2. PHYSICS INTEREST

For a study of hadron-hadron reactions the great advantage of a 2 to 10 TeV proton synchrotron, compared to a proton storage ring of 30 to 70 GeV, is that strong secondary beams of $\pi^{\pm}$, $K^{\pm}$, $\bar{p}$, n, $\bar{n}$, Σ^{-}, etc., can be produced. In other words, the beam particle instead of always being a proton can be varied considerably, and many predictions, e.g. of the quark model, can be tested.

A further advantage is that the interacting system is no longer symmetric as in pp collisions. This permits a study to be made of effects due to fragmentation, in particular the effects of one incident particle in the opposite hemisphere. It is known from the ISR results that such effects exist (e.g. at 90° the proton cross-section is greater than the antiproton one, and the π^{+} cross-section is higher than the π^{-} at higher p_T values), but the magnitude and extent of the influence of an incident particle into the opposite hemisphere cannot be measured in a reaction symmetrical about 90°.

The basic nature of the reaction mechanism is not known. It is still possible to defend the belief that all emitted particles are fragments of the incident particle, though it is easier to understand the present results in a picture in which some emitted particles are fragments and some are from a central production process. Studying only pp collisions, there is probably insufficient information to evaluate the fraction of fragments, but if the incident particle is varied, the additional information may allow this problem to be solved.

An associated problem is that of the production of heavy particles, e.g. $\bar{\Lambda}$. Are they produced as fragments or do they come mainly from central production? By varying the incident particle, e.g. K^{-} and K^{+}, decisive data may be obtained.

Similarly, important indications as to the nature of the reaction mechanism may be obtained by studying the correlations between pairs of produced particles -- the pair being related by the need to balance quantum numbers, e.g. $\Lambda\bar{\Lambda}$, $p\bar{p}$, $K^{+}K^{-}$. Some possible mechanisms are sketched below:
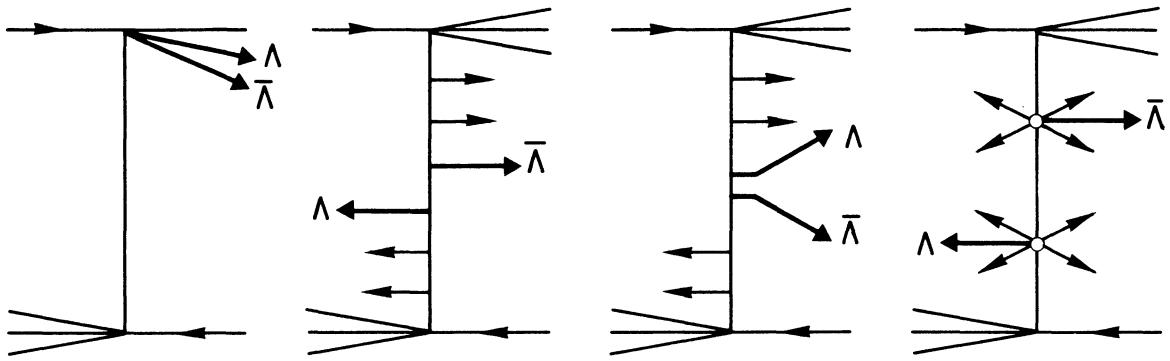
Diffraction dissociation is an important process with a cross-section comparable to that of elastic scattering. Much of the detailed information on diffraction dissociation has come from πp interactions (and been confirmed in Kp interactions). It would be exceedingly interesting to extend this work to pion diffraction into 5π, 7π, 9π, ...

The hypotheses of scaling in the central region and of limiting fragmentation have not yet been decisively studied. To obtain information in asymmetric reactions, e.g. πp, as well as symmetric reactions such as pp, would be very useful. It may be mentioned here that our hope is to study "asymptotic" effects. There appears to be a number of phenomena -- such as approach to scaling, Reggeon exchange in elastic scattering -- which are important at lower energies, but whose contribution becomes less serious above ≈ 100 GeV/c. Thus if we wish to have an extensive range of energy to study "asymptotic" physics, it is necessary to have beams of more than 1 TeV.

3. EXPERIMENTAL MEASUREMENT

In studying many-body reactions, the ideal is to be able to study each reaction channel separately, i.e. exclusive measurements. These can then be combined to give inclusive and other results. This requires a very large and complicated spectrometer. While it is essential to build such an apparatus, it has generally been found in the past that such complicated pieces of equipment are slow to come into full operation. Hence we would suggest the necessity for providing also simpler experiments: a) single-arm spectrometers to measure inclusive processes, and b) double-arm spectrometers to measure also correlations. This would imply several (≳ 3) hadronic beam lines.

Considering now the question of a spectrometer, the problem is to measure for each emitted particle the three quantities, i) direction, ii) momentum, iii) mass. The problem of measuring mass is at the present time very difficult -- Čerenkov counters would need to be very long, although transition radiation detectors offer some hope.

The problem of measuring direction and momentum is particularly severe for high-energy particles emitted forwards which will form a very narrow jet; for example, a 4 TeV particle with a typical transverse momentum of 400 MeV/c will be emitted at an angle of 1/10 mrad. The only hope of separating such a particle is to place the detectors at a large distance; for example, at 0.5 km distance the deflection would be 50 mm, which would be adequate with MWPCs measuring to 1 or 2 mm. With beam lines of ≈ 2 km length, it is not unexpected that the experiment should extend over 0.5 km. However, instead of having one long experimental hall, we would suggest three halls. The first hall containing the target would have a vertex

detector and would measure low-energy particles. The third hall would be at ≈ 0.5 km from the target and would measure the forward jet with strong (superconducting) magnets and drift or multiwire chambers plus some system to measure mass. A second hall would be needed to measure intermediate momentum particles
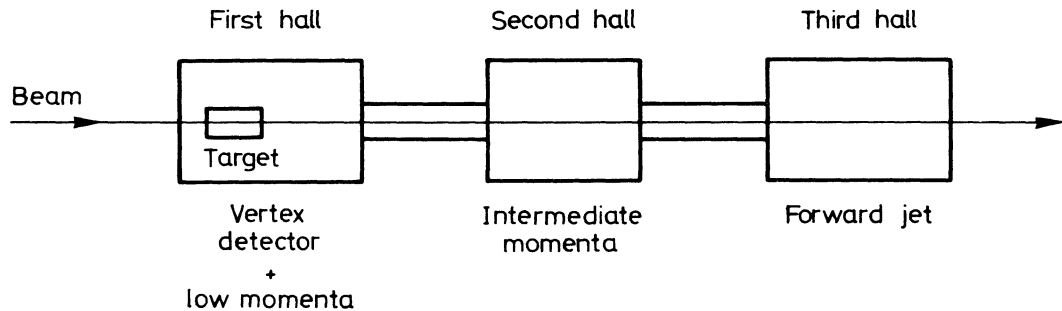
A vertex detector using counters with fast response time as well as good spatial resolution would be ideal, but at present such a system appears not to exist. A rapid cycling bubble chamber has the resolution, but is very slow so that it can only deal with major reaction processes with moderate cross-section ($\gtrsim 1$ μb). Hence at present, it would appear advantageous to plan on having two vertex detectors, one a rapid cycling bubble chamber and the other a counter system. Starting some preliminary work now in developing new vertex systems would be invaluable.

4. CONCLUSIONS

It is very interesting to perform experiments on many-body hadronic reactions using beams of different incoming particles. Such experiments may help to distinguish between different views of the mechanism of high-energy reactions. Some of the experiments are reasonably simple, but complete analysis of events using a spectrometer is difficult, although not impossible.

IV.1   NEUTRINO EXPERIMENTS AT THE MULTI-TeV ACCELERATOR

C. Rubbia

CERN, Geneva, Switzerland

We consider briefly the feasibility of a neutrino experiment with the multi-TeV acceler-
ator (SSPS). We shall assume that the main physics interest is concentrated on the neutrinos
with the highest energy.

1.   CHOICE OF THE DETECTOR

The most suitable type of detector appears to be a massive electronic set-up. The
classic bubble chamber (of BEBC type) is no longer adequate for the highest energy events.
For instance at 4 TeV, 90° in the centre of mass transforms back to the laboratory system
to $\sim$ 1.4°. Therefore particle jets are too narrow to be separated out. Also the momentum
resolution is largely insufficient, since a 1 TeV particle would have in a 33 kG field a
curvature radius of $\sim$ 1 km corresponding to a sagitta of 500 μ over a 2 m track. Hence, at
least at the present status of the art, we are oriented towards a calorimeter-muon spectro-
meter system. The energy resolution of a steel-scintillator calorimeter is quite good.
Extrapolations, according to $E^{-\frac{1}{2}}$ law, from the results of Engler et al.[1] obtained with 2 cm
plates would give:

Table 1

Energy resolution of a steel-scintillator calorimeter
as a function of incident hadron energy

E_{hadron} (TeV)	0.5	1	1.5	2	3	4
$\Delta E/E$ (%)	2.4	1.7	1.4	1.2	1.0	0.86

For 10. cm plates the resolution is expected to be $\sim$ two times worse. The containment
volume is not made larger than that required at SPS energies, since it is expected to grow
like $\log E_{hadron}$.

The detection of the muon has to be effective up to angles as large as 5° (see Fig. 1),
since for a given pair of scaling variables x,y the muon angle varies proportionally to $E_\nu^{-\frac{1}{2}}$
(in contrast to the dependence E^{-1}, which is expected in the case of strong interaction pro-
cesses with strong interaction scaling). The sagitta of a 3 TeV muon through 20 m of steel
magnetized to 2 T is 1.6 cm, which can be adequately measured with drift chambers. For a
reconstruction error $\Delta s \sim 0.2$ mm, the main contribution to the error $\Delta p_\mu/p_\mu$ comes from the
multiple Coulomb scattering (i.e. $\Delta p/p \sim 4\%$).

We shall estimate rates for a detector made of a calorimeter weighing $\sim 10^3$ tons, fol-
lowed by a muon spectrometer of adequate size (Fig. 2).
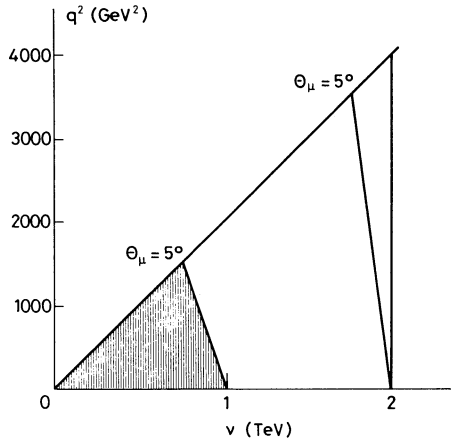
Fig. 1 Regions of q^2-ν plot to which a detector effective up to muon angles of 5° is sensitive for different neutrino energies.

$$\frac{\Delta E_h}{E_h} \approx 2-3\%$$

$$\frac{\Delta P_\mu}{P_\mu} \approx 5\%$$
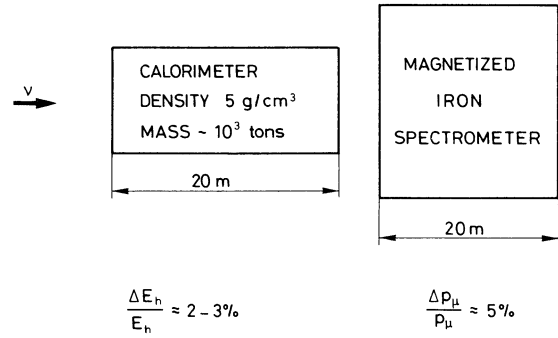
Fig. 2 Example of a possible multi-TeV neutrino facility

2. THE NEUTRINO BEAM

The neutrino beam can be of conventional design, except for the problem of the high-energy muons. The penetration depth of a 5 TeV muon is ∿ 10 km of earth. Obviously brute force absorption is probably no longer acceptable and instead one has to use magnetic deflection. Since the primary detector is an electronic experiment, one could design a sign-selected beam of the dichromatic type, essentially as a joint ν-μ facility. The products of the multi-TeV interactions (Fig. 3) are momentum-selected underground, and only particles of a given sign are brought to the decay channel. At the end of the decay channel
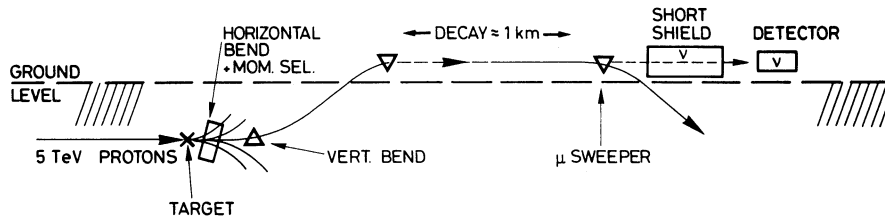
Fig. 3 Multi-TeV neutrino beam layout

a second deflection stage, probably made of magnetized iron, deflects charged particles, again underground. Determination of the energy of the neutrinos requires a fantastic accuracy in the determination of the production angle (Fig. 4).

Fluxes have been evaluated on measurements of π^+ and K^+ production on beryllium at 24 GeV, scaled to the multi-TeV range[2] (Fig. 5). The decay path has been arbitrarily set to 1 km length. Assuming that the neutrino cross-sections still rise linearly with energy in our energy range, we can give the following rough event estimates (Table 2).

CHARGED BEAM ENERGY = 2.75 TeV
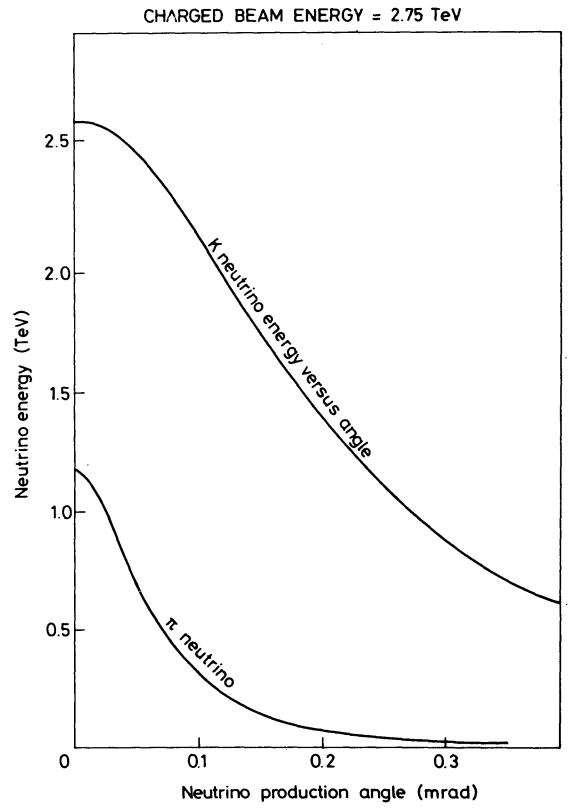
Fig. 4 Energy of the neutrinos from π and K
decays as a function of their production
angle

$E_p = 4$ TeV

DECAY DATA = 1 km

$\pi^+ \rightarrow \mu^+ + \nu$

$K^+ \rightarrow \mu^+ \nu$
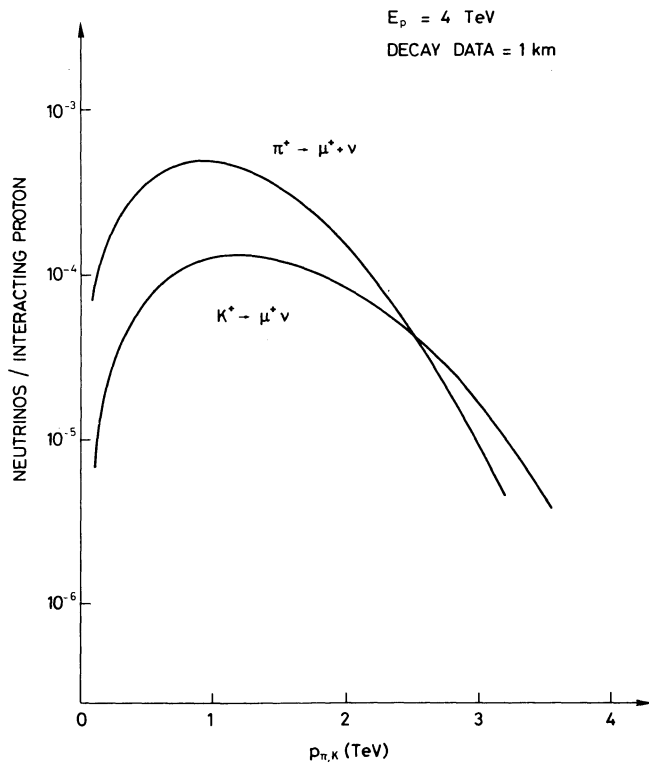
Fig. 5a Estimate of the flux of neutrinos from π
and K decays as a function of the π^+ and
K^+ momenta assuming a primary proton
energy of 4 TeV and a decay path of 1 km
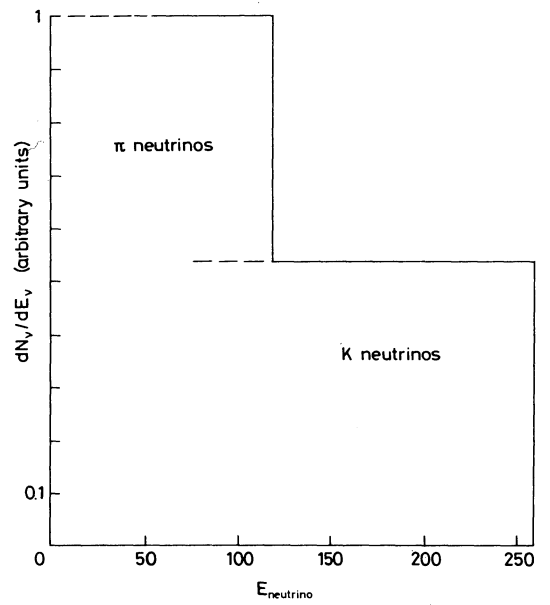
Fig. 5b Energy spectrum of neutrinos

Table 2

Rates are for 10^{12} protons of a narrow beam
with $\Delta p/p$ = 8.5% and 10^3 tons of detector
$\left[\sigma_\nu = 0.8 \times 10^{-35} \; E_\nu \; (\text{TeV})\right]$

	E_0 = 2 TeV	E_0 = 2.75 TeV
$E_\nu > E_0/2$	0.60	0.27
$E_\nu < E_0/2$	0.65	0.24

It appears possible to perform decent experiments up to energies of order 3/4 of the initial proton energy.

3. CONCLUSIONS

A straightforward extrapolation of the experimental set-ups used today at FNAL and planned for the SPS gives acceptable electronic detectors for the multi-TeV machine. On the contrary, conventional bubble chambers do not appear to be too well suited for studies of the highest energy neutrinos. The neutrino beam can only be realized provided the muon background is deflected away rather than absorbed. The typical luminosity of an experiment with a 10^3 ton target is of 2×10^{34} cm^{-2} for 10^{12} protons and $E_\nu \geq 0.35 \; E_{proton}$.

* * *

REFERENCES

1) J. Engler, W. Flauger, B. Gibbard, F. Mönnig, K. Runge and H. Schopper, Nuclear Instrum. Methods 106, 189 (1973).

2) J. Ranft, CERN Library program W129.

INTRODUCTION

L. Di Lella

CERN, Geneva, Switzerland

A Study Group to review the physics interest of proton storage rings in the region of several hundred GeV (SISR) was set up in March, 1974, with the purpose of helping the Study Group on Long-Term Plans in considering possible future long-range developments of experimental facilities at CERN.

The following persons participated to the Study Group: N. Cabibbo, L. Camilleri, P. Darriulat, A.N. Diddens, L. Di Lella (also acting as convener), K. Johnsen, E. Keil, E. Lohrmann, G. Matthiae, B. Montague, J.C. Sens, J. Steinberger and B. Zotter.

Most of the subjects of current interest in the field of physics with colliding proton beams received attention. These include elastic scattering, measurements of the total cross-section, multiple production, and production of high transverse momentum leptons and hadrons. In all these cases, the feasibility of the relevant experiments was studied by attempting a practical design of an experimental set-up.

Since the experiments are closely connected with the machine in the case of storage rings, it was necessary for most of the reports to take into account a list of storage ring parameters. A machine consisting of two 400 GeV proton rings, with a maximum luminosity of 10^{33} cm^{-2} sec^{-1}, was used in this study. Such a machine corresponds to one of the models which are at present under study in the ISR Department, and its preliminary specifications are described in report II.1. It was necessary to work in close contact with the machine experts, in order to try to resolve the sometimes conflicting requirements between machine design and physics experiments, and between physics experiments themselves.

The problems related to the measurement of the machine luminosity were also studied (see reports II.3 and II.4). It was found that the luminosity can be determined with a precision comparable to that achieved at the present ISR.

Reports II.5 through II.9 contain the results of the studies performed on the physics subjects mentioned above. However, it is worth while to stress here the main conclusions reached so far.

1) Proton storage rings with a total centre-of-mass energy of $\sim$ 800 GeV and a luminosity around 10^{33} cm^{-2} sec^{-1} are particularly well suited for the study of electromagnetic and weak interactions, by observing the production of leptons and lepton pairs. Cross-sections for the reactions pp $\rightarrow$ $\mu^+\mu^-$ + anything, and pp $\rightarrow$ $\mu\nu$ + anything can be conservatively estimated using current theoretical models (see report II.5), and a relatively simple experimental apparatus is discussed in report II.6. Rates as high as $\sim$ 2 muons/hour are expected from the reaction pp $\rightarrow$ $\mu\nu$ + anything, with the invariant mass of the $\mu\nu$ system in excess of 300 GeV, in the presence of very low background. At this value, the weak interaction cross-section reaches the unitarity limit, whose effects could therefore be studied. On the other hand, if a W$^\pm$ boson exists, much higher single-muon rates would result, at muon momenta around 0.5 M_W. As an example, for M_W = 100 GeV/c^2, approximately 200 muons/hour would be detected in the momentum interval between 40 and 60 GeV/c. These events would create a bump on the

continuum, with a signal-to-noise ratio of ~ 100 to 1. A fundamental discovery in this field is, therefore, almost unavoidable.

2)   The yield of high transverse momentum hadrons was estimated by a reasonable extrapolation of ISR results (see report II.7). At luminosities of 10^{33} cm^{-2} sec^{-1}, secondary pions with p_T above 40 GeV/c can be observed at a rate of ~ 1/hour. The study of these events, under conditions almost free from kinematics constraints (since $p_T \ll \sqrt{s}/2$), should help in understanding the mechanism responsible for this type of collisions. In particular, it may become possible to answer the question of whether these events result from scattering of hard, point-like constituents of the protons.

3)   Measurements of the pp total cross-section appear feasible, with precisions comparable to those achieved at the ISR (see report II.8). In view of the huge range of $\sqrt{s}$ values available, it becomes possible to obtain a precise determination of the energy dependence of σ_{tot}. Fits to the ISR data predict values of σ_{tot} between 65 and 75 mb at $\sqrt{s} = 800$ GeV.

4)   Particle production will benefit greatly from the range of $\sqrt{s}$ values offered by the machine, and from the large interval of rapidity ($y \approx \pm 9$ at $\sqrt{s} = 800$ GeV). The study of diffractive dissociation at $\sqrt{s} = 800$ GeV is particularly interesting, since states of very high mass (up to ~ 200 GeV/c^2) can be coherently excited in the collisions. Experiments to study these phenomena appear quite feasible (see report II.9).

In addition to the topics listed above, some members of the Study Group, in collaboration with U. Amaldi and A. Minten, studied the experimental possibilities of $p\bar{p}$ colliding beams at present ISR energies. The methods to fill one of the two ISR rings with $\bar{p}$ from the SPS, as well as estimates of the luminosity, are described in report II.10. A discussion of the physics program which could be carried out with this facility is contained in report II.11. The main conclusion here is that, because of the low luminosity foreseen ($L \lesssim 10^{26}$ cm^{-2} sec^{-1}), only studies of $p\bar{p}$ interactions with cross-sections larger than a few percent of the total cross-section can be performed.

II.1 POSSIBLE FUTURE STORAGE RINGS AT CERN

Large Storage Rings (LSR) Working Group, ISR Division,
CERN, Geneva, Switzerland

1. INTRODUCTION

Colliding proton beams have successfully entered the field of elementary particle physics through the CERN Intersecting Storage Rings (ISR), and it has been natural for CERN to start studying proton storage ring projects for higher energies than that of the present ISR.

Experience with the ISR together with studies at several laboratories in the world have in fact shown the feasibility of building colliding beam pp devices up to the highest energies of accelerators in existence or under construction, and such a facility could be constructed in connection with the SPS at CERN.

A spectrum of possible pp projects can be envisaged, from a superconducting magnet ISR conversion giving about 100 GeV in each ring, to a set of accelerating storage rings that might give up to 1000 GeV in each ring. It has been natural to choose for the start of the study of new large storage rings (SISR)[*] an energy equal to the maximum energy of the SPS, as a representative example. This falls somewhat in the middle of the range of possibilities mentioned above, but may nevertheless be in the upper range of realistic possibilities.

Two approaches can be considered, namely:

A)   400 GeV rings using normal iron magnets,

B)   400 GeV rings using superconducting magnets.

A preliminary study of model A [1] has demonstrated that large storage rings with normal magnets and good performance can actually be built. In order to achieve a luminosity of 10^{33} cm^{-2} sec^{-1} in a short interaction length of not more than 1 m, as desired by the experimentalists, 7 A of circulating protons will be necessary.

The study has, however, also demonstrated the main drawbacks of such a project: the uncomfortably large circumference needed and the very high power consumption ($\sim$ 120 MW). Adding to this the somewhat higher performance potentiality of a superconducting device and/or the possibility of reduced cost (although little is known about cost yet), we have drawn the conclusion that the study of model B should have priority, and the study effort has recently been guided correspondingly. At the time the study group on 400 GeV colliding-beam physics was convened, the only design of an SISR available was one closely resembling the one described in Ref. 1. The SISR version described in this report is, however, the superconducting version which was later found to be preferable. But the conclusions of the study group remain unchanged, as the machine parameters that affect the physics (luminosity and field-free space around intersection regions) are virtually identical in the two versions.

---

[*]   Although it has been decided to refer to these new large storage rings as SISR in this report, several documents, in particular those of the ISR division at CERN, refer to them as LSR.

2. MACHINE LATTICE

The circumference of the machine is made up of two contributions: the normal lattice, which occupies the greater part, and the colliding beam insertions which occupy the rest. Consequently, the largest contributions to single-beam space-charge phenomena come from the normal lattice, while the beam-beam space-charge (and high-energy physics) phenomena occur only in the insertions. It has therefore been convenient for the preliminary analysis to consider these two contributions separately.

Experience with the ISR has shown that the betatron tunes (Q-values) have to be controlled with rather high precision if one is to avoid enhanced beam decay rates due to non-linear resonances in the stacked beam. This imposes many tight tolerances on such a machine. In particular, the design of the machine must ensure that the image-dominated incoherent tune-shift is below the acceptable limit, and that the circulating beam is transversely stabilized by the small Q-spread available. These requirements can be met by choosing a sufficiently large aperture over most of the circumference of the machine. This is in fact the determining factor in the choice of aperture of a large-radius storage ring. A large machine aperture further helps to reduce the beam-induced gas desorption vacuum problems.

A formalism which takes these space-charge phenomena into account and leads to the physical parameters of a machine was described by Keil at the 9th International Conference on High-Energy Accelerators held in May 1974. A set of parameters for a superconducting machine arrived at in this manner is shown in Table 1.

Table 1

Parameter list for large storage rings

Maximum momentum	400 GeV/c
Maximum bending field	4 T
Circumference	6130 m
Average radius of normal lattice	617 m
Stored current	7 A
Stored energy in beam	57 MJ
Vacuum chamber aperture radius	25 mm
Betatron wave number	36.25
Period length	40.4 m
Quadrupole length	1.6 m
Bending magnet length	3.7 m
Number of periods	96
Half-period arrangement	$\frac{1}{2}$FBBB$\frac{1}{2}$D

3. TYPES OF INTERACTION REGIONS

For given energy and stacked current, the maximum design luminosity of an interaction region is limited mainly by two factors, namely the non-linear electromagnetic beam-beam interaction, and the maximum acceptable values of betatron function in the neighbouring quadrupoles. The first is fundamental but not well quantified, and the second is limited by chromaticity and tolerances. Both factors lead to a situation in which a compromise must be made between luminosity and field-free space around the interaction region.

One is therefore led to consider a machine with several types of interaction regions, each designed to be suitable for a particular class of experiment. So far, three types of interaction regions have been considered at CERN; a high-luminosity low-β region, a general-purpose interaction region with plenty of unencumbered space, and a high-β region with special optics for measurements of very small scattering angles. Parameters of examples of such interaction regions are summarized in Table 2.

Table 2

Performance estimates for three model-insertions

	Low-β	General-purpose	High-β
Luminosity (cm^{-2} sec^{-1})	1.0×10^{33}	2×10^{31}	5×10^{30}
β_v^* (m)	1.0	14	400
β_h^* (m)	6.0	40	300
β_v max $\}$ β_h max	550	490	460
Crossing angle (mrad)	2.6	19.4	19.4
Field-free half-length (m)	5	80	18
Total length of insertion (m)	230	320	280

The above data are for:

Stacked current I = 7 A

Normalized emittance $\varepsilon = 30\pi \times 10^{-6}$ rad m (both planes)

Energy 400 GeV (γ = 426.3)

Layout and size of experimental halls around these interaction regions have also been studied a little, in particular by a study group in Autumn 1974. Figure 1 shows a possible arrangement for the low-β region, with a dome around the crossing point and two tunnels to be used for the detection of very high momentum particles at 90°. Figure 2 shows a possible layout for the general-purpose region, again with a dome to accommodate the very large amount of equipment to be used in such a region. There is no tunnel at 90°, but the machine tunnel has been widened to facilitate the analysis of particles coming at small angles. The high-β region would look rather similar, except that the dome is not so high.
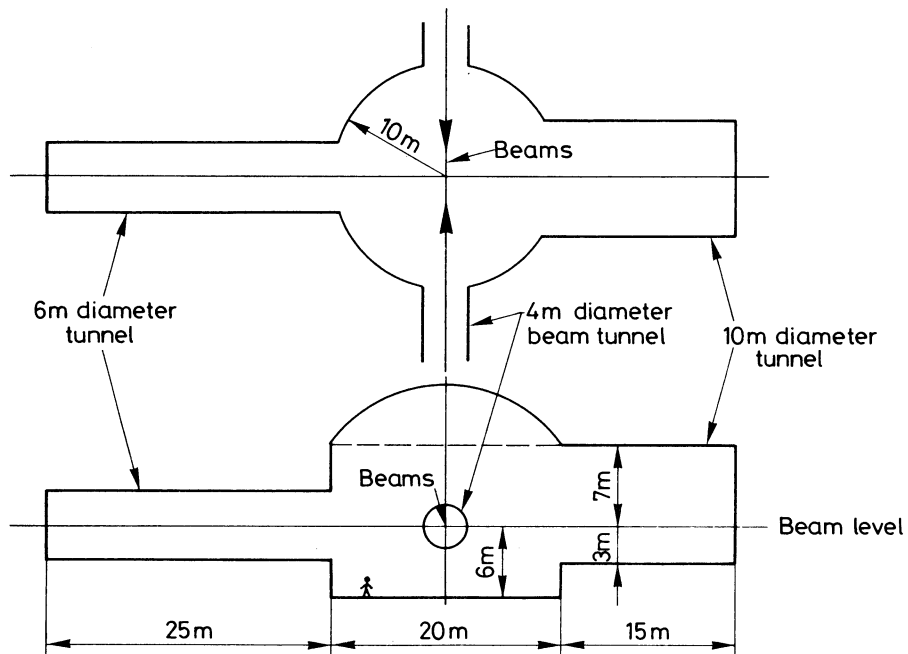
Fig. 1 Experimental hall for a low-β (high-luminosity) insertion
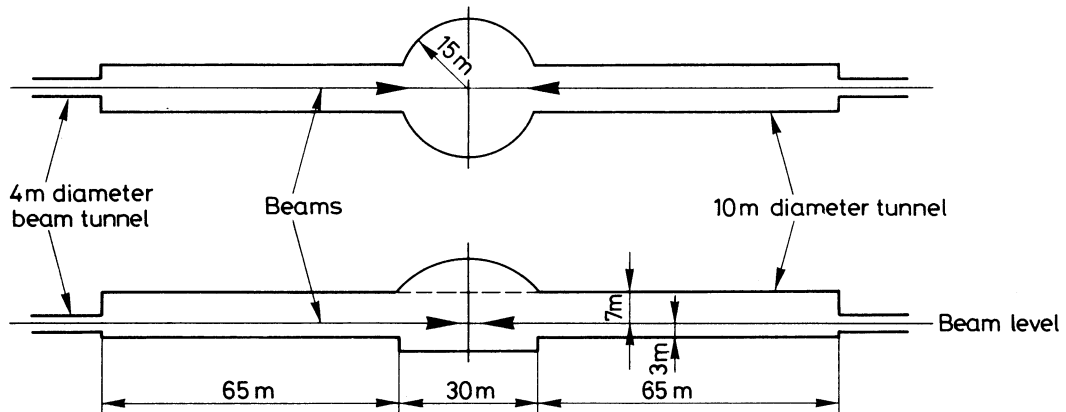
Fig. 2 Experimental hall for a general-purpose insertion

4. NUMBER OF INSERTIONS

The number of insertions is determined by the scale and scope of the physics program which the storage rings are supposed to support. In addition, special insertions will be required for injection and beam dumping. It seems likely that a minimum of six interaction regions will be required for physics experimentation, i.e. two of each of the three different types listed in Table 2.

A racetrack configuration with grouped interaction regions has been chosen. Figure 3 shows a possible layout for a superconducting machine assumed to be located about 60 m underground. Preliminary studies of underground experimental areas are encouraging but further studies are needed. In the model considered at present, the injection and dumping insertions would be in the arcs of the racetrack configuration.
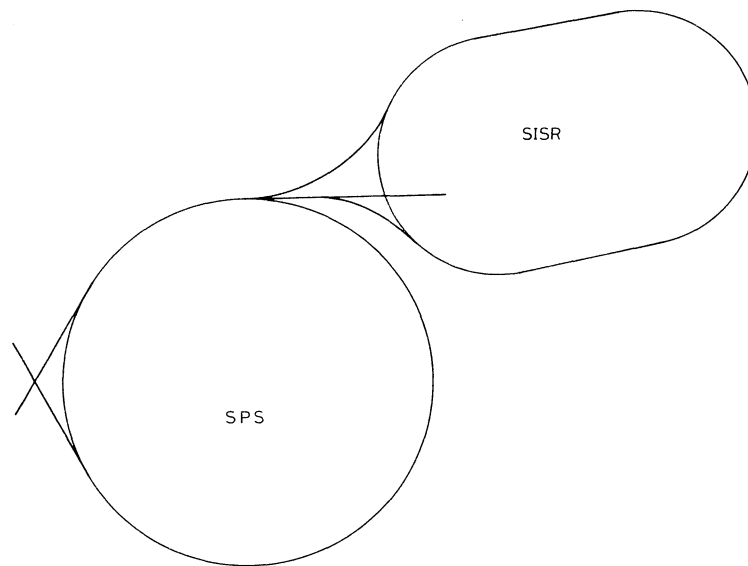
Fig. 3 Possible layout of 400 GeV storage rings

5. ANTIPROTONS IN ONE OF THE RINGS

The method would be first to fill one of the SISR rings with 400 GeV protons, say to 7 A. These protons are ejected and made to hit an antiproton-producing target from which 14 GeV antiprotons are guided towards the SPS, injected, and accelerated in this machine and then stacked in the other SISR ring. The process is repeated until the available aperture is filled, giving an $\bar{p}$ circulating beam of about 2 mA. When this beam collides with the proton beam in the other ring, one might reach a luminosity of 10^{28} cm^{-2} sec^{-1} to 10^{29} cm^{-2} sec^{-1}. The filling time works out to be uncomfortably long, about two days, and operational considerations may therefore restrict the luminosity to, say, an order of magnitude less. The main extra equipment would be ejection/injection devices, a target complex, and an additional beam transport channel between the SISR and the SPS.

6. CONCLUDING REMARKS

As mentioned already in the introduction, what has been presented here should only be taken as an illustration of the possibilities; and other possibilities do exist, both less ambitious ones as well as more ambitious ones. Discussions and studies over the next few years will, hopefully, throw more light on the elements that will determine in which direction we should go, and at which speed.

*   *   *

REFERENCE

1) b. Autin, D. Blechschmidt, A.A. Garren, K. Johnsen, E. Keil, B.W. Montague, J.C. Schnuriger, C. Zettler and B.W. Zotter, 400 GeV Large Storage Rings with conventional magnets, CERN/ISR-LTD/75-45 (1975).

II.2 GEOMETRIES FOR A SUPERCONDUCTING
STORAGE RING IN THE ISR TUNNEL

D.A. Swenson [*)]

CERN, Geneva, Switzerland

1. INTRODUCTION

With the prospect of higher-energy proton beams from the SPS, it is appropriate to consider the possibility of extending the energy range of the colliding beam physics now in progress at the ISR. One alternative which provides a significant step in the collision energies at an intermediate cost is to replace the ISR with a pair of superconducting storage rings (SSR) housed in the ISR tunnel and using many of its basic facilities and services (buildings, shielding, cranes, power, water).

The selection of a geometry for such rings must strike a balance between two conflicting requirements, namely that of making the radius of the curved sections as large as possible to increase the energy storage capability, and, at the same time, leaving some long straight sections free of bending magnets to accommodate experiments, while remaining within the confines of the ISR tunnel[1]. The radii of the present ISR tunnel and rings are:

Outer radius of tunnel	157.5 m
Outer radius of rings	154.3 m
Radius of intersection	148.6 m
Inner radius of rings	145.5 m
Inner radius of tunnel	142.6 m

In the following, it is assumed that the two rings required for colliding beams lie close to each other, being separated either horizontally or vertically by a constant distance of one metre or less. The close, constant spacing of the rings lends itself to the design of pairs of magnets which serve both rings, but which are fabricated as single units housed in single cryostats. Long straight sections are spaced periodically around the circumference, where the perturbations are introduced to bring the beams into collision at small angles.

2. RING GEOMETRIES

The first-order geometrical constraints can be studied by considering both rings to be of the same simple geometry, namely a smooth closed curve of S identical curved sections of radius R, and S identical straight sections of length L. The radius R of the curved section of the orbit is related to the maximum radius $\bar{R}$ of the orbit, the straight section length L, and the superperiod S by

$$R = \bar{R} - \frac{L}{2 \sin \frac{\pi}{S}} .$$

The difference between the maximum and minimum radii of the orbit is:

$$\Delta R = (\bar{R} - R) \left(1 - \cos \frac{\pi}{S}\right) .$$

Table 1 gives some values of R and ΔR for $\bar{R}$ = 155 m over a range of values for L and S.

Table 1

Values of R and ΔR, as defined in the text,
as a function of L and S

		L = 20	L = 30	L = 40	L = 50	L = 60
S = 2	R = ΔR =	145.0 10.0	140.0 15.0	135.0 20.0	130.0 25.0	125.0 30.0
S = 3	R = ΔR =	143.5 5.8	137.7 8.6	132.0 11.5	126.2 14.4	120.4 17.3
S = 4	R = ΔR =	140.9 4.1	133.8 6.2	126.7 8.3	119.6 10.4	112.6 12.4
S = 5	R = ΔR =	138.0 3.3	129.5 4.9	121.0 6.5	112.5 8.1	104.0 9.7
S = 6	R = ΔR =	135.0 2.7	125.0 4.0	115.0 5.4	105.0 6.7	95.0 8.0
S = 7	R = ΔR =	132.0 2.3	120.4 3.4	108.9 4.6	97.4 5.7	85.9 6.9
S = 8	R = ΔR =	128.8 2.0	115.8 3.0	102.7 4.0	89.6 5.0	76.5 6.0

The upper right region of this table represents geometries which are unsuitable because of large ΔR (largest practical values of $\Delta R \simeq$ 10 m). The desire for the largest R for a given L forces us up in this table (down in S) to the limit $\Delta R \simeq$ 10 m. In the region of L = 30-50 m, this implies an S of 3 or 4.

For S = 3, both the limit of three interaction regions and the limit of 30 m per straight section seem uncomfortably small. When the details of the horizontal orbit separators are considered, odd values of S have the strong disadvantage that the two rings cannot have the same symmetry, and it even seems unlikely that they could have the same circumference.

A superperiod of 4 has the distinct advantage of being a sub-multiple of the eightfold periodicity of the ISR. With S = 4, interaction regions can be aligned with the four even-numbered interaction regions of the present ISR. Three of these have additional space along the inner wall of the tunnel, and the fourth (I 6) is designed so that it can be enlarged. Also with S = 4, the region of maximum radius can be aligned with the extra passageways on the outer wall of the tunnel, thus facilitating personnel and equipment movement.

The argument for S = 4 with L in the range of 40 to 60 seems quite convincing. Nevertheless, the choice of L within this range still stirs up conflict between the desire for large L and large R. Each additional 10 m in straight section length (20% at L = 50 m) reduces the maximum beam momentum by 6%.

3. INTERSECTION REGIONS

The details of the perturbations required to bring these essentially "parallel" orbits into collision depend, of course, on the magnitude W and the plane of the separation. In the case of horizontal separation, some of the deflections required to bring the orbits together can be produced by omission of some bending magnets from the curved part, thus resulting in longer straight sections than in the case of vertical separation. For the examples below, a horizontal separation with W = 0.6 m has been chosen.

The simplest intersection is one with a crossing angle such that the outer orbit at one end of the long straight section is deflected into the inner orbit at the other end. The crossing angle for the example is 27 mrad (1.5 degrees) and requires the addition of 1.7 m of magnet to the outer orbit and the omission of the same amount from the inner orbit, reducing the magnet-free region from 44 m to 40.6 m.

A zero-angle intersection requires stronger deflections than in the simple case above, and at least two additional magnets per intersection which bracket the collinear region. These magnets consume a considerable fraction of the straight section length. They can, however, and therefore must, be interlaced with the matching and β-modulating quadrupoles so as to make dual use of this precious space.

The optimum scheme requires deflection of the beams towards each other by addition of M metres of magnet to the outer orbit, deletion of M metres of magnet from the inner orbit, and the insertion of M metres of magnet on the resulting cross-over to make the beams collinear. The beams drift towards each other for a distance Q between the additional magnet on the outer orbit and the new magnet at the confluence of the orbits. The system consumes 2M + Q of space at each end of the straight section. The relation between M, Q, R, and W, is: W = (3M + 2Q) M/R.

The system which consumes the least space is the one with no space for quadrupoles, namely with Q = 0, which for the example requires M = 4.9 m, and reduces the long straight section from 44 m to 24.4 m.

A more interesting system is one with M = 3 m, which leaves 7.5 m of space for quadrupoles near each end of the 17 m long collinear region. Figure 3 is a scale drawing of this zero-angle intersection system.
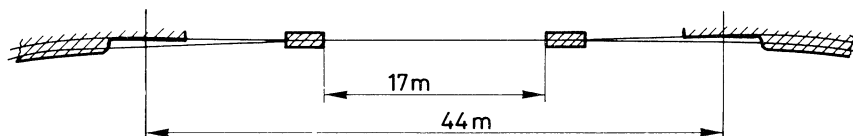
Fig. 3 Scale drawing of zero-angle intersection

Figure 4 shows the two rings with an exaggerated radial separation in a configuration having two small-angle regions, and two zero-angle interaction regions.
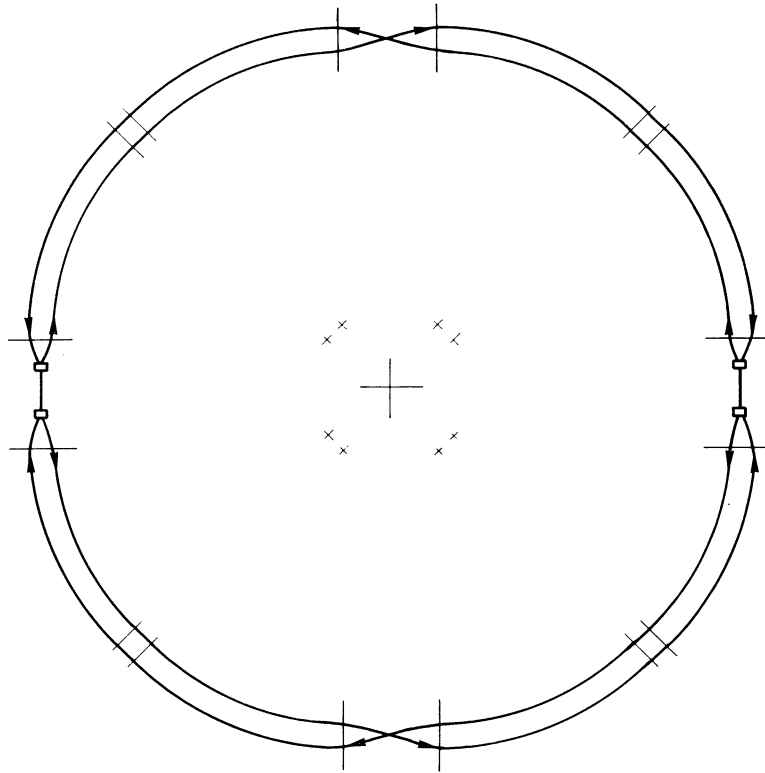
Fig. 4 Pair of intersecting rings with exaggerated radial separation

4. BEAM ENERGY

The momentum p is related to R and the magnetic field in the bending magnets B by:

$$p \text{ (GeV/c)} = \frac{R \text{ (m) } B \text{ (T) } F}{3.33} \quad ,$$

where F is the fraction of the curved section covered by bending magnets (E. Keil took this to be 2/3).

Present superconducting magnet technology suggests that a B of 5 tesla is practical; 5 T together with a filling factor of 2/3 yields the convenient relation that p (GeV/c) = R (m). Thus, the example chosen above has a momentum capability of 120 GeV/c. If the superconducting magnet technologies were to make fields as high as 8 tesla practical, the example would vault into the 200 GeV/c class.

5. CONCLUSIONS

The geometrical and practical constraints on placing a higher-energy superconducting storage ring in the existing ISR tunnel are analysed. One attractive solution is developed as an example and described by illustrations. Conservative estimates of the superconducting magnet technology lead to colliding beam energies four times that of the present ISR, within the confines of the present ISR facility.

REFERENCE

1) E. Keil, Machine geometries fitting into the ISR tunnel, CERN/ISR-TH/72-20 (1972).

II.3 MEASUREMENT OF THE LUMINOSITY FOR BEAMS CROSSING
AT SMALL ANGLES IN A LOW-β SECTION

H.G. Hereward and E. Keil

CERN, Geneva, Switzerland

1. INTRODUCTION

A very convenient method of measuring the luminosity in a storage ring has been proposed by Van der Meer[1]. It is widely used in the ISR. In connection with design studies for larger storage rings[2] in which the beams collide at small angles in low-β sections, the question arises whether the same method still gives the correct luminosity. It will be shown below that this is only true if a correction factor, which is calculated for a few typical cases, is included. It turns out that the correction factor is very close to unity under most conditions found in practice. The calculation below is done for vertical crossings of the beam. They can be applied to horizontal crossings by rotating the coordinate system and interchanging the words "horizontal" and "vertical" in the text.

2. ANALYTIC DERIVATION

The luminosity can be calculated in a straightforward manner if the shapes and intensities of the crossing beams are known. For small crossing angles α, such that $\sin \alpha = \alpha$ and $\cos \alpha = 1$, the expression is

$$\mathcal{L} = 2c \int \rho_1(x, y, s)\rho_2(x, y, s) \, dx \, dy \, ds \; . \tag{1}$$

Here, c is the velocity of light, and ρ_1 and ρ_2 are the (number) densities of the protons in the two beams. The integration goes over the whole interaction volume.

Van der Meer's method measures the luminosity Λ as a function of the horizontal beam displacement a which for vertical crossing is given by

$$\Lambda(a) = 2c \int \rho_1(x - a, y, s)\rho_2(x, y, s) \, dx \, dy \, ds \; . \tag{2}$$

If we integrate $\Lambda(a)$ over a and divide it by $\Lambda(0)$, we obtain an effective width a_{eff}

$$a_{eff} = \frac{\int \Lambda(a) \, da}{\Lambda(0)} = \frac{\int \Lambda(a) \, da}{\mathcal{L}} \; . \tag{3}$$

It is sufficient experimentally to observe a quantity which is proportional to the luminosity, e.g. a beam-beam counting rate in a given detector. Clearly, $\Lambda(0)$ is equal to the luminosity defined in Eq. (1). The merit of this definition of a_{eff} is that -- in the case of the ISR -- it can be inserted into the luminosity formula

$$\mathcal{L} = \frac{2c \; \lambda_1 \lambda_2}{a_{eff} \; \alpha} \tag{4}$$

and yields the correct luminosity. In Eq. (4), λ_1 and λ_2 are the line (number) densities in the two beams, and α is the crossing angle. When the transverse beam profiles vary within the length of the intersection region, Eq. (4) cannot be expected to be accurate.

In order to simplify the definition of a_{eff}, we introduce the integrated distribution functions σ_i:

$$\sigma_i(y, s) = \int \rho_i(x, y, s)\, dx \qquad (5)$$

and write explicitly

$$\int \Lambda(a)\, da = 2c \int \rho_1(x - a, y, s)\rho_2(x, y, s)\, dx\, dy\, ds\, da \ . \qquad (6)$$

Since a appears only inside ρ_1, we may perform this integration and find

$$\int \Lambda(a)\, da = 2c \int \sigma_1(y, s)\rho_2(x, y, s)\, dx\, dy\, ds \ . \qquad (7)$$

Repeating the same operation on ρ_2 yields

$$\int \Lambda(a)\, da = 2c \int \sigma_1(y, s)\sigma_2(y, s)\, dy\, ds \ . \qquad (8)$$

We shall show below that a_{eff} is equal to the width w of hypothetical beams with the following properties:

i)   their density distributions $\rho_i^h(x, y, s)$ are uniform in x and have the same dependence on y and s as $\rho_i(x, y, s)$ and the same currents;

ii) the width w is adjusted such that these hypothetical beams have the same luminosity as the actual beams.

The first condition is satisfied by choosing ρ_i^h as follows:

$$\rho_i^h(x, y, s) = \begin{cases} \dfrac{1}{w} \int \rho_i(x, y, s)\, dx = \dfrac{\sigma_i(y, s)}{w} & \text{for } |x| < \dfrac{w}{2} \\[2ex] 0 & \text{for } |x| > \dfrac{w}{2} \ . \end{cases} \qquad (9)$$

The hypothetical luminosity is

$$\left. \begin{aligned} \mathcal{L}^h &= 2c \int \rho_1^h \rho_2^h \, dx\, dy\, ds \\[1ex] \mathcal{L}^h &= \frac{2c}{w} \int \sigma_1 \sigma_2 \, dy\, ds \ . \end{aligned} \right\} \qquad (10)$$

Imposing the condition $\mathcal{L}^h = \mathcal{L}$, yields for w

$$w = \frac{\int \sigma_1 \sigma_2 \, dy\, ds}{\int \rho_1 \rho_2 \, dx\, dy\, ds} \qquad (11)$$

which may be seen to agree with Eq. (3), by using Eqs. (1) and (8).

We have thus demonstrated that Van der Meer's method allows us to determine a parameter a_{eff} which is equal to the width of a hypothetical beam which has the same luminosity as the actual beam.

In order to find that luminosity, we still have to do the integral (1) for the hypothetical beams. This implies that we have eliminated the actual beam profile in the x-direction, but not yet those in the y- and s-directions. Since the latter are trivial in the case of the ISR, Van der Meer's method works there without further calculation.

3. SPECIFIC EXAMPLES

Below, we shall calculate the luminosity for a few specific beam profiles, and derive a correction factor which relates the actual luminosity to the simple formula (4).

3.1 Gaussian beams without dispersion

We assume for the hypothetical beams that β_y has a minimum β_0 at the crossing point, that the r.m.s. beam half-height is given by σ_0, that the vertical dispersion and its derivative vanish there, and that the density distribution is given by a Gaussian. The distribution functions are then defined as follows:

$$\left. \begin{array}{l} \sigma_1(y, s) = \dfrac{\lambda_1}{\sigma_0 \sqrt{2\pi(1 + s^2\beta_0^{-2})}} \exp\left[- \dfrac{y^2}{2\sigma_0^2(1 + s^2\beta_0^{-2})} \right] \\[4ex] \sigma_2(y', s') = \dfrac{\lambda_2}{\sigma_0 \sqrt{2\pi(1 + s'^2\beta_0^{-2})}} \exp\left[- \dfrac{y'^2}{2\sigma_0^2(1 + s'^2\beta_0^{-2})} \right] \end{array} \right\} \tag{12}$$

Here, the two coordinate systems (y, s) and (y', s') belong to the two beams and are related by

$$y' = y \cos \alpha + s \sin \alpha$$

$$s' = s \cos \alpha - y \sin \alpha .$$

Since we are only interested in the case with $\alpha \ll 1$, and also $y \ll s$, we may simplify the transformation and write

$$y' \approx y + s\alpha$$

$$s' \approx s .$$

The luminosity $\mathcal{L}^h$ becomes

$$\mathcal{L}^h = \frac{2c\lambda_1\lambda_2}{2w\sigma_0 \sqrt{\pi}} \int_{-\ell/2}^{+\ell/2} \frac{\exp\left[- \dfrac{s^2\alpha^2}{4\sigma_0^2(1 + s^2\beta_0^{-2})} \right] ds}{(1 + s^2\beta_0^{-2})^{\frac{1}{2}}} . \tag{13}$$

The length over which the luminosity is integrated is ℓ. Comparing this to the luminosity formula $\mathcal{L}^f$ (4) gives for the ratio

$$\frac{\mathcal{L}^h}{\mathcal{L}^f} = \frac{\alpha}{2\sigma_0 \sqrt{\pi}} \int_{-\ell/2}^{+\ell/2} \frac{\exp\left[- \dfrac{s^2\alpha^2}{4\sigma_0^2(1 + s^2\beta_0^{-2})} \right] ds}{(1 + s^2\beta_0^{-2})^{\frac{1}{2}}} . \tag{14}$$

The ratio (14) is the correction factor F which has to be applied to the simple formula (4) in order to find the actual luminosity. If we introduce two parameters ξ and η used previously[3] and given by

$$\xi = \frac{\ell}{2\beta_0} \quad , \qquad \eta = \frac{\alpha\beta_0}{\sigma_0} \quad , \tag{15}$$

we may write

$$F(\xi,\eta) = \frac{\eta}{2\sqrt{\pi}} \int_{-\xi}^{+\xi} \frac{\exp\left[-\frac{\eta^2}{4}\frac{u^2}{1+u^2}\right] du}{(1+u^2)^{\frac{1}{2}}} \quad , \tag{16}$$

where ξ expresses the length of the intersection region in units of β_0, and η is the ratio between the crossing angle α and the r.m.s. beam half-divergence.

The correction factor F has been evaluated numerically for several values of ξ and η and is shown in Table 1.

Table 1

Correction factor $F(\xi,\eta)$

ξ \ η	4.0	5.0	6.0	8.0	10.0	12.0	14.0	16.0	18.0	20.0	25.0	30.0
0.1	0.222	0.276	0.328	0.428	0.520	0.603	0.677	0.742	0.797	0.843	0.923	0.967
0.2	0.426	0.518	0.602	0.741	0.843	0.912	0.955	0.980	0.993	0.999	1.003	1.002
0.3	0.599	0.708	0.796	0.914	0.973	0.998	1.006	1.007	1.006	1.005	1.003	1.002
0.4	0.737	0.843	0.916	0.990	1.011	1.013	1.010	1.008	1.006	1.005	1.003	1.002
0.5	0.842	0.933	0.985	1.019	1.019	1.014	1.011	1.008	1.006	1.005	1.003	1.002
0.6	0.920	0.991	1.022	1.029	1.021	1.014	1.011	1.008	1.006	1.005	1.003	1.002
0.8	1.021	1.053	1.053	1.034	1.021	1.015	1.011	1.008	1.006	1.005	1.003	1.002
1.0	1.078	1.079	1.062	1.035	1.021	1.015	1.011	1.008	1.006	1.005	1.003	1.002
1.5	1.144	1.101	1.068	1.035	1.021	1.015	1.011	1.008	1.006	1.005	1.003	1.002
2.0	1.172	1.108	1.069	1.035	1.021	1.015	1.011	1.008	1.006	1.005	1.003	1.002
2.5	1.188	1.111	1.069	1.035	1.021	1.015	1.011	1.008	1.006	1.005	1.003	1.002
3.0	1.200	1.113	1.069	1.035	1.021	1.015	1.011	1.008	1.006	1.005	1.003	1.002
4.0	1.215	1.115	1.069	1.035	1.021	1.015	1.011	1.008	1.006	1.005	1.003	1.002
5.0	1.226	1.117	1.070	1.035	1.021	1.015	1.011	1.008	1.006	1.005	1.003	1.002
6.0	1.235	1.118	1.070	1.035	1.021	1.015	1.011	1.008	1.006	1.005	1.003	1.002
8.0	1.247	1.120	1.070	1.035	1.021	1.015	1.011	1.008	1.006	1.005	1.003	1.002
10.0	1.257	1.121	1.070	1.035	1.021	1.015	1.011	1.008	1.006	1.005	1.003	1.002
12.0	1.265	1.122	1.070	1.035	1.021	1.015	1.011	1.008	1.006	1.005	1.003	1.002
14.0	1.271	1.123	1.070	1.035	1.021	1.015	1.011	1.008	1.006	1.005	1.003	1.002
16.0	1.277	1.124	1.070	1.035	1.021	1.015	1.011	1.008	1.006	1.005	1.003	1.002
18.0	1.282	1.124	1.070	1.035	1.021	1.015	1.011	1.008	1.006	1.005	1.003	1.002
20.0	1.286	1.125	1.070	1.035	1.021	1.015	1.011	1.008	1.006	1.005	1.003	1.002
25.0	1.295	1.126	1.070	1.035	1.021	1.015	1.011	1.008	1.006	1.005	1.003	1.002
30.0	1.303	1.127	1.070	1.035	1.021	1.015	1.011	1.008	1.006	1.005	1.003	1.002

3.2 Gaussian beams with dispersion

We assume that the beam profile comes from two contributions, betatron oscillations and momentum spread, and that both have Gaussian distributions with r.m.s. radius σ and τ, respectively. The over-all profile is then given by the convolution of the two distributions and becomes

$$\sigma_i(y, s) = \frac{\lambda_i}{\left[2\pi(\sigma^2 + \tau^2)\right]^{\frac{1}{2}}} \exp\left[-\frac{y^2}{2(\sigma^2 + \tau^2)}\right] \quad . \tag{17}$$

We further assume that β_y has a minimum β_0 at the crossing point, and that the vertical dispersion there is τ_0, and its derivative τ_0'. Then σ and τ depend on s in the following way:

$$\sigma(s) = \sigma_0 \left(1 + \frac{s^2}{\beta_0^2}\right)^{\frac{1}{2}}$$

$$\tau(s) = \tau_0 + \tau_0' \, s \; .$$

(18)

Note again that it is not necessary to know the horizontal beam profile and its variation due to betatron oscillations and momentum spread. Using Eqs. (10), (17), and (18), the luminosity of the hypothetical beams becomes

$$\mathcal{L}^h = \frac{2c}{w} \int \frac{\lambda_1 \lambda_2}{2\pi(\sigma^2 + \tau^2)} \; \exp\left[-\frac{y^2}{2(\sigma^2 + \tau^2)} - \frac{(y + s\alpha)^2}{2(\sigma^2 + \tau^2)}\right] dy \; ds$$

$$\mathcal{L}^h = \frac{4c}{w} \int \frac{\lambda_1 \lambda_2}{\sqrt{\pi(\sigma^2 + \tau^2)}} \; \exp\left[-\frac{s^2\alpha^2}{4(\sigma^2 + \tau^2)}\right] ds \; .$$

(19)

Dividing this by the luminosity formula (4) yields for the correction factor F

$$F\left(\xi, \; \eta, \; \frac{\tau_0}{\sigma_0}, \; \frac{\tau_0' \beta_0}{\sigma_0}\right) = \frac{\eta}{2\sqrt{\pi}} \int_{-\xi}^{+\xi} \frac{\exp\left[-\frac{\eta^2}{4} \frac{u^2}{\left[1 + u^2 + \left(\frac{\tau_0 + \tau_0' \beta_0 u}{\sigma_0}\right)^2\right]}\right] du}{\left[1 + u^2 + \left(\frac{\tau_0 + \tau_0' \beta_0 u}{\sigma_0}\right)^2\right]^{\frac{1}{2}}} \; .$$

(20)

Two special cases give simpler solutions:

i) $\tau_0 = 0$

When the vertical dispersion vanishes at the crossing point, we have

$$F\left(\xi, \; \eta, \; 0, \; \frac{\tau_0' \beta_0}{\sigma_0}\right) = \frac{\eta}{2\sqrt{\pi}} \int_{-\xi}^{+\xi} \frac{\exp\left[-\frac{\eta^2}{4} \frac{u^2}{1 + \left(1 + \frac{\tau_0' \beta_0}{\sigma_0}\right)^2 u^2}\right] du}{\left[1 + \left(1 + \frac{\tau_0' \beta_0}{\sigma_0}\right)^2 u^2\right]^{\frac{1}{2}}} \; .$$

(21)

By a change of variables this can be shown to yield

$$F\left(\xi, \; \eta, \; 0, \; \frac{\tau_0' \beta_0}{\sigma_0}\right) = F\left\{\xi\left[1 + \left(\frac{\tau_0' \beta_0}{\sigma_0}\right)^2\right]^{\frac{1}{2}}, \; \frac{\eta}{\left[1 + \left(\frac{\tau_0' \beta_0}{\sigma_0}\right)^2\right]^{\frac{1}{2}}}\right\}$$

(22)

where $F(\xi, \eta)$ has been defined previously.

ii) $\tau_0' = 0$

When the derivative of the vertical dispersion vanishes at the crossing point we find

$$F\left[\xi,\ \eta,\ (\tau_0/\sigma_0),\ 0\right] = \frac{\eta}{2\sqrt{\pi}} \int_{-\xi}^{+\xi} \frac{\exp\left[-\frac{\eta^2}{4}\ \frac{u^2}{1 + (\tau_0^2/\sigma_0^2) + u^2}\right] du}{\left[1 + (\tau_0^2/\sigma_0^2) + u^2\right]^{\frac{1}{2}}} \ . \tag{23}$$

By a change of variables this can be shown to give

$$F\left[\xi,\ \eta,\ (\tau_0/\sigma_0),\ 0\right] = F\left\{\frac{\xi}{\left[1 + (\tau_0^2/\sigma_0^2)\right]^{\frac{1}{2}}},\ \eta\right\} . \tag{24}$$

4. DISCUSSION

An inspection of Table 1 shows that for the distribution functions (12) and $\xi > \frac{1}{2}$ and $\eta \geq 10$ the correction factor differs from unity by less than $2\frac{1}{2}\%$. Different distribution functions -- in y and s only! -- will have different correction factors, which can also be evaluated numerically.

However, it can be shown for any distribution that at large enough ξ the correction factor F can be expanded into a power series in η as follows:

$$F = 1 + \frac{2}{\eta^2} + \frac{c_4}{\eta^4} + \ldots\ , \tag{25}$$

where the coefficients c_4, ... depend on the details of the distribution functions. Hence, if $2/\eta^2 \ll 1$, the higher-order terms in η must have a very small effect on the correction factor.

The intersection region where Van der Meer's scheme is least likely to work is the high-luminosity intersection[2]. It has the following characteristics:

$$\beta_0 = 5\ m$$

$$\sigma_0 = 0.3\ mm$$

$$\alpha = 0.86\ mrad$$

$$\ell = 20\ m$$

$$\alpha_p = 0$$

$$\alpha'_p = 0.063$$

$$\Delta p/p = \pm 1.8 \times 10^{-3}\ .$$

Converting these parameters into those necessary for calculating F, yields

$$\xi = 2$$

$$\eta = 14.3$$

$$\tau'_0 = 1.13 \times 10^{-4}$$

$$\tau'_0\ \beta_0/\sigma_0 = 1.89\ .$$

We find that the correction factor becomes $F(4.28, 6.69) \approx 1.06$.

A determination of the luminosity to an accuracy of a few percent requires the following quantities to be known well enough:

- the circulating currents I_1 and I_2
- the effective width a_{eff}
- the crossing angle α
- the correction factor F.

Measuring a crossing angle of about 1 mrad to 1% accuracy requires measuring the beam positions to 100 μm at 10 m distance. Thus the crossing angle may well be the most inaccurate ingredient in the luminosity measurement.

This difficulty can be avoided by calibrating the luminosity monitors while the beams cross at a much larger angle than usual. This makes the measurement of the crossing angle easier and brings the correction factor F even closer to unity.

5. CONCLUSIONS

We have shown that Van der Meer's method of measuring the effective beam width by displacing the two crossing beams with respect to each other and using that width in a simple luminosity formula can be used in high-luminosity insertions with small β-values and crossing angles, provided a correction factor F is applied. This correction factor has been evaluated for a few typical cases. It turns out that it differs from unity by only a few percent if the crossing angle is large compared to the r.m.s. beam divergence.

REFERENCES

1) S. Van der Meer, CERN/ISR-PO/68-31 (1968).

2) K. Johnsen, E. Keil, B.W. Montague and B.W. Zotter, private communication (1974).

3) E. Keil, CERN/ISR-TH/72-33 (1972).

II.4 MEASUREMENT OF THE LUMINOSITY AT THE SUPER-ISR

G. Matthiae
CERN, Geneva, Switzerland

Several methods have been considered for measuring the luminosity at a proton-proton storage ring. Some of them have been found to be of practical use at the ISR and will probably be adequate also at the Super-ISR.

The different methods can be classified as follows:

1) The machine luminosity is obtained by measuring the reaction rate of a process for which the cross-section is known. Cross-sections can only be calculated for electromagnetic interactions, and therefore the number of useful processes is limited to the following ones:

   a) Coulomb scattering,
   b) Coulomb excitation,
   c) electron pair production.

2) A simultaneous measurement of the total interaction rate and of the elastic scattering rate at small angles makes it possible, by using the optical theorem, to obtain the total cross-section and then the luminosity.

3) The luminosity can be determined by measuring directly the relevant beam parameters by means of:

   a) the Van der Meer method,
   b) the measurement of the beam profile from beam-gas interactions.

At the Super-ISR there will be different types of interaction regions (low-β, general-purpose, and high-β regions). Most of the methods listed above may be used only in one type of insertion. The merits and limitations of each method will now be discussed in some detail.

1. MEASUREMENT OF PROCESSES FOR WHICH THE CROSS-SECTION IS KNOWN

1.1 Coulomb scattering

Elastic scattering in the Coulomb region ($-t \approx 10^{-3}$ GeV^2) could be measured only in a special high-β insertion. The elastic scattering rate per unit solid angle is given by

$$\frac{\Delta R_{el}(\theta)}{\Delta\Omega} = L \frac{d\sigma(\theta)}{d\Omega} = L|f_c(\theta) + f_{si}(\theta)|^2 \ ,$$

where f_c is known, while the strong interaction amplitude f_{si} depends on the values of the total cross-section σ_t, of the real part, and of the slope b. By fitting the observed angular distribution to the differential cross-section $d\sigma/d\Omega$, we obtain the luminosity L. A beam-beam monitor placed in the intersection region can then be calibrated in an absolute way.

1.2 Coulomb excitation

The observation of Coulomb scattering being quite difficult, we are tempted to consider other electromagnetic processes[1]. The simplest one is perhaps the inelastic two-body reaction with production of the $\Delta(1236)$:

$$p + p \rightarrow p + \Delta^+ .$$

The contribution to this process of the one-photon exchange diagram is

$$\frac{d\sigma}{dt} = 16\pi\alpha \left(\frac{M}{M^2 - m_p^2}\right)^3 \Gamma_\gamma \frac{|t - t_{min}|}{t^2} ,$$

where m_p and M are the proton and Δ mass, respectively, and Γ_γ is the radiative decay width of the Δ, derived from photoproduction. This cross-section rises rapidly from $-t_{min} = (M^2 - m_p^2)^2/4s$ up to a maximum at $t = 2t_{min}$, and then falls roughly as $1/|t|$. At the Super-ISR (p = 400 GeV/c), the cross-section, integrated up to $-t = 10^{-2}$ GeV^2, which is the value of the momentum transfer where the proton form factor will start to cut, is about 7 µb. For a low-β insertion (L = 10^{33} cm^{-2} sec^{-1}) the corresponding total rate is about 2×10^3 events per second. The strong interactions' contribution should be small. In fact at the maximum PS energy, the production cross-section is about 60 µb and decreases with energy roughly as s^{-2}. In addition the t-distribution is very different.

The proton accompanying the Δ is produced at too small an angle to be detected, and therefore the only practical way to observe this process is to detect the neutron and π^+ from Δ decay. As a consequence there will be a problem in selecting beam-beam from beam-gas events. In addition, the experimental mass resolution must be good enough to allow the selection of the Δ signal over the continuum.

This scheme appears to be feasible. The main limitation is probably the accuracy of the cross-section formula.

1.3 Electron pair production

The production of e^+e^- pairs via the two-photon exchange diagram has been suggested by V.M. Budnev et al.[2] as a possible scheme for measuring the luminosity. The cross-section for this process increases logarithmically with energy as

$$\sigma \approx \frac{\alpha^4}{m_e^2} \left(\log \frac{p}{m_p}\right)^2 \log \frac{p}{m_e} ,$$

where p is the beam momentum and m_e is the electron mass. Numerical values are of the order of 0.1 mb at the ISR, and of the order of 1 mb at the Super-ISR. While the cross-section is high, the kinematics is not favourable. In fact, low values of the e^+e^- effective mass are strongly preferred. Transverse momenta are typically of the order of the electron mass. The proton scattering angle is of the order of $m_e/p \simeq 1$ µrad, too small to be observed. Typical values of the electron energies are of $(m_e/m_p) p \sim 200$ MeV. We are then bound to detect rather low energy electrons emitted at small angles. Therefore this scheme does not seem to be useful.

2. MEASUREMENT OF THE TOTAL RATE AND OF THE ELASTIC RATE

This method is based on the simultaneous measurement of the total interaction rate R_{tot} and of the elastic scattering rate $R_{el}(\theta)$ at small angles. The total rate is related to the total cross-section by the relation $R_{tot} = L\sigma_{tot}$. If the real part and the Coulomb contribution are negligible, the following expression holds:

$$\frac{\Delta R_{el}(\theta)}{\Delta\Omega} = L \frac{p^2\sigma_{tot}^2}{16\pi^2} e^{-bp^2\theta^2} \ .$$

By combining the two independent measurements one gets

$$\sigma_{tot} = \frac{16\pi^2}{p^2} \frac{\Delta R_{el}(\theta)/\Delta\Omega}{R_{tot}} e^{bp^2\theta^2} \ .$$

This method was used at the ISR by the CERN-Roma-Pisa-Stony Brook Group[3] with the following numerical values of the extrapolation factors, as determined by the experimental conditions:

i) $e^{bp^2\theta^2} \simeq 1.1-1.4;$

ii) the observed "total" interaction rate was 95% to 98% of R_{tot}.

The total cross-section could be determined with an accuracy of about ±1%, and then the machine luminosity would also be determined with the same precision.

This measurement can be performed at the Super-ISR with the same extrapolation factors and thus with the same accuracy in a general-purpose intersection region ($\beta \approx 50$ m) which has 100 m free space on both sides of the crossing point. With a circular vacuum pipe of 3 cm radius, the minimum observed angle would be 0.3 mrad, corresponding to $-t \approx 10^{-2}$ GeV^2. This minimum value of the momentum transfer is the same as the one reached in the ISR experiment. Elastic scattering events can be observed by means of drift chambers placed 100 m from the crossing point. The total interaction rate can be measured by a rather standard system of counters.

3. DIRECT MEASUREMENT OF BEAM PARAMETERS

3.1 The Van der Meer method

This method has been extremely successful at the ISR, and it is hoped to be able to use it again at the Super-ISR. The method consists in displacing the beams in the direction perpendicular to the plane where the two beams cross. While in the high-β and general-purpose insertions this method seems to be applicable, some problem may arise in the high-luminosity, low-β insertion, where the beam angular spread is not much smaller than the crossing angle, and the beam profile in the direction normal to the crossing plane changes considerably along the diamond. However, according to the calculations of Hereward and Keil (Part B, II.3) the corrections needed to allow for these effects would be of a few percent only.

3.2 Direct measurements of the beam profile

The measurement of the profile of the beams along the normal to the crossing plane, obtained by observing secondaries produced in beam-gas interactions, would in principle

allow us to determine the machine luminosity. This method, however, can hardly provide a reasonably accurate value of the luminosity because of the poor spatial resolution.

Another possibility for determining the beam profile is to observe the light emitted by atoms excited in beam-gas collisions[4]. The accuracy of this measurement is essentially determined by the quality of the optical system and could, in principle, be rather good.

These two methods might not be able to provide a sufficiently accurate determination of the beam profile; however, they could be of great value for measuring directly the actual value of the displacement of the beams during the Van der Meer scan. In this respect, the method based on the observation of the light seems quite attractive because of its better resolution.

4. CONCLUSIONS

Apart from the Van der Meer method, other methods which appear suitable and could provide useful independent checks are:

 i) the observation of Coulomb scattering,
 ii) the measurement of the total rate and of the elastic rate.

These methods could provide a measurement of the luminosity with an accuracy of about $\pm 1\%$. Also the Coulomb production method is of some interest but could hardly reach an accuracy of better than 10 or 20%.

Any method for measuring the luminosity will provide the absolute calibration of a monitor system which will have to be stable and simple, with good beam-beam versus beam-gas discrimination, and free from geometrical effects due to the size and position of the diamond. A simple and efficient system consists of two telescopes placed downstream of the crossing region. Each telescope could be made of two planes of scintillation counters having circular shapes. The optimum size of the counters can be inferred by scaling from the ISR. At the ISR a system of counters of the Pisa-Stony Brook Group, covering the angular range from 15 to 120 mrad, detects about 85% of the total observed rate, i.e. about 80% of the total interaction rate. The average production angle of the secondaries is proportional to the quantity $(\langle p_T \rangle /p)\langle n \rangle$ which changes by a factor of about 10 from the ISR to the Super-ISR. Therefore at the Super-ISR a monitor covering the angular range from 2 to 15 mrad will lose all elastic and single diffraction dissociation events but still have a high effective cross-section of the order of 60% of σ_{tot}. The counters could be disks of 20 cm radius placed around the standard pipe of 3 cm radius at about 15 m from the crossing point. Such a monitor would be suitable in any insertion region.

* * *

REFERENCES

1) B. Gobbi and J.L. Rosen, A scheme for absolute calibration of Isabelle luminosity, *in* BNL 17522 (1972), p. 127.

2) V.M. Budnev et al., Phys. Letters 39B, 526 (1972).

3) CERN-Pisa-Rome-Stony Brook Collaboration, Phys. Letters B (1976) (to be published).

4) E. Jones et al., CERN/ISR-VA/73-57 (1973).

II.5 PRODUCTION OF LEPTON PAIRS
IN PROTON-PROTON COLLISIONS AT VERY HIGH ENERGIES

N. Cabibbo

Department of Theoretical Physics,

University of Rome, Italy

1. THE PROCESSES

A pp colliding beam device (SISR) would allow the study of lepton pair production, through an intermediate photon, or through the weak interaction, either of the normal type (mediated by $W^{\pm}$), or through neutral currents (Z^0 meson). Here we will only discuss inclusive processes of the type

$$p + p \rightarrow X + (\gamma \text{ or } Z) \tag{1}$$
$$\hookrightarrow \mu^+ \mu^-$$
$$e^+ e^-$$

$$p + p \rightarrow X + W^+ \tag{2}$$
$$\hookrightarrow \mu^+ \nu_\mu$$
$$e^+ \nu_e$$

$$p + p \rightarrow X + W^- \tag{3}$$
$$\hookrightarrow \mu^- \bar{\nu}_\mu$$
$$e^- \bar{\nu}_e$$

X is in all cases a set of unobserved particles.

2. THEIR PHYSICAL INTEREST

Among the many reasons for the great interest of pp colliding beam devices is the fact that they allow the study of lepton pairs of very high invariant mass. If Q_μ denotes the total four-momentum of the pair, the kinematical limit for $Q^2 = (\ell_1 + \ell_2)^2$ is $Q^2 < 4E^2$, E being the energy of each beam in the centre-of-mass system (Fig. 1).

Given sufficient luminosity, the SISR would then allow the study of a mass region, $Q^2 \gtrsim (40 \text{ GeV})^2$, which is not available to other methods and, at the same time, is of great physical interest.
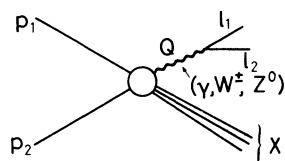

Fig. 1 Diagram for lepton pair production in pp collisions; ℓ_1, ℓ_2 is the lepton pair (e^+e^-, $e^+\nu_e$, etc.)

The following processes would be in competition with the SISR:

a) e^+e^- collisions: This is in principle a cleaner channel (limited to γ or Z^0 intermediate states). Machines with an energy up to 17 GeV per beam are now being proposed. The practical upper limit to the energy of this kind of device is about 20-25 GeV per beam.

b) pp collisions with conventional accelerators: In this case the limit is

$$Q^2 < 2M_p E_{beam} ,$$
(4)

i.e. $Q^2 < (40 \text{ GeV})^2$ for an 800 GeV machine.

c) A process of related interest is that of deep inelastic ep or μp scattering where the momentum transfer is space-like. For a conventional accelerator, the kinematical limit for $|Q^2|$ is the same as in Eq. (4), while higher $|Q^2|$ could be available in ep colliding beam devices:

$$|Q^2| < 4E_e E_p .$$
(5)

Although this process is of considerable interest, it does not allow the direct study of the $W^{\pm}$ or Z meson.

3. $W^{\pm}$ AND Z PRODUCTION

We recall that in the now popular Weinberg-Salam model one finds:

$$M_{W^{\pm}} = \frac{37.5}{\sin \theta_W} ,$$

$$M_Z = \frac{M_W}{\cos \theta_W} ,$$
(6)

where θ_W is Weinberg's mixing angle. An analysis of the recent Gargamelle results on neutral currents suggests

$$0.3 \lesssim \sin^2 \theta_W \lesssim 0.4 ,$$
(7)

so that

$$59 \text{ GeV} \lesssim M_{W^{\pm}} \lesssim 68.5 \text{ GeV} ,$$

$$76.5 \text{ GeV} \lesssim M_Z \lesssim 82 \text{ GeV} .$$
(8)

If the model is correct, direct Z or $W^{\pm}$ production is within the range of an experiment at the SISR, but cannot take place in any other competing device. A check of Eq. (6) would give a critical test of the model.

More generally, even neglecting the enhancement of weak effects due to the vicinity of the Z or $W^{\pm}$ poles, in the "Fermi" theory (point-like coupling of weak currents) one finds:

$$\frac{\text{Weak amplitude}}{\text{Electromagnetic amplitude}} = \frac{G/e^2}{Q^2} \approx 1 \text{ at } Q^2 = (40 \text{ GeV})^2 .$$
(9)

This means that in this range of invariant mass, the large weak interaction effects should appear even in process (1), which, at lower Q^2, is dominated by photon exchange.

Furthermore, at even higher Q^2 $[Q^2 \approx (200\text{-}300 \text{ GeV})^2]$ we are in a region where the naïve Fermi interaction reaches its unitarity limit, and it would be interesting to see how nature chooses to solve this problem, if it does not solve it in the way proposed in gauge theories[*].

Before discussing in more detail the possible identification of weak interaction effects, let us turn briefly to photon exchange.

4. PROBLEMS WITH ONE-PHOTON EXCHANGE

These problems fall into two classes:

i) properties of the hadronic vertex for emission of a virtual photon;
ii) properties of the photon propagator.

Present views on the first class of problems indicate two distinct kinematical regions (see Appendix on Kinematics):

A low Q_T region where a substantial fraction of the events should appear. According to present parton model ideas[1], this should be due to the annihilation of a quark in one of the protons with an antiquark in the other (Fig. 2).
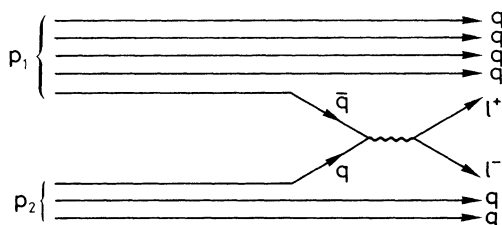
Fig. 2 Parton picture of process (1). Each proton is seen as three quarks plus a number of $q\bar{q}$ pairs (0, 1, 2, ...). For simplicity, only one pair of $q\bar{q}$ is shown in p_1, none in p_2. The surviving q and $q\bar{q}$ pairs rearrange themselves to give the final hadrons X.

This model leads to well-defined predictions. If the quark has an energy $x_1 E$, and the antiquark an energy $x_2 E$, one has (see the Appendix for definition of scaling variables)

$$t = x_1 x_2 \ , \qquad Q^2 = x_1 x_2 s$$

$$\xi = x_2 - x_1 \ ,$$

(10)

and the scaling form for the differential cross-section

$$\frac{d^2\sigma}{dx_1 dx_2} = \frac{4\pi\alpha^2}{2Q^2} \sum_\ell Q_\ell^2 q_\ell(x_1) q_{\bar{\ell}}(x_2) \ ,$$

(11)

---

[*] This point is emphasized by T.D. Lee in his report: High-energy electromagnetic and weak interaction processes, _in_ BNL 17522 (1972), p. 80.

where the sum is over different kinds of quarks (ℓ = p, n, λ), Q_ℓ is the charge ($\frac{2}{3}$ or $-\frac{1}{3}$) of each quark, and $q_\ell(x)$ $[q_{\bar{\ell}}(x)]$ represents the probability of finding a quark [antiquark] of type ℓ with a fraction x of the proton energy.

These functions are measured in deep inelastic ep and νp scattering. As an example, Fig. 3 shows a comparison of neutrino data from Gargamelle with a model[2] for quark and antiquark distributions. An extensive investigation of lepton pair production in pp collisions has been recently carried out within this model[3].
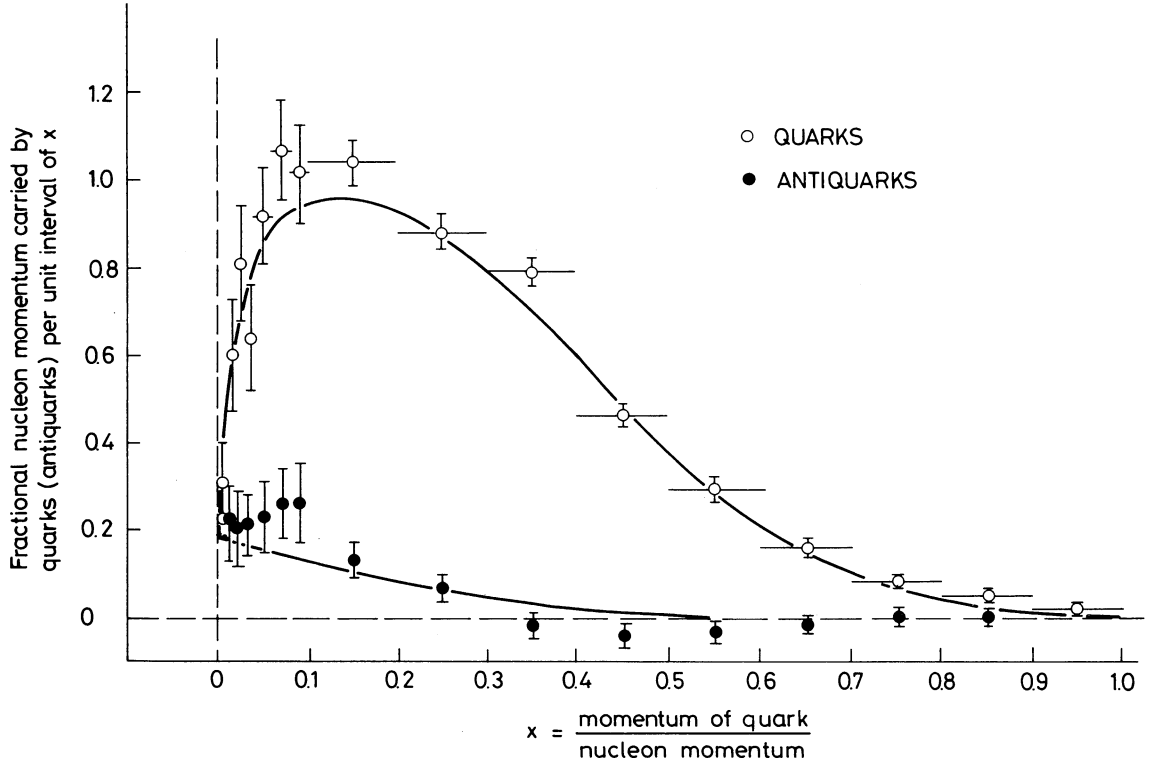
Fig. 3 Distribution of the fraction of the nucleon momentum carried by quarks and antiquarks as a function of x.

If we denote by ψ the lepton angle in the dilepton rest frame, the cos ψ distribution is predicted to be of the type 1 + cos^2 ψ, as a consequence of the spin $\frac{1}{2}$ nature of partons.

At higher Q_T there is no prediction from the parton model, and one might expect a $(Q_T)^{-n}$ behaviour similar to that observed in hadron production at high transverse momentum.

The problem of one-photon exchange is also interesting at lower Q^2. One might be led to doubt naïve predictions such as Eq. (11), given our poor understanding of quark confinement. The observation of deviations from this form would be rich in physical implications and could supply useful hints on alternative descriptions of this process.

5. WEAK INTERACTIONS IN THE PARTON MODEL

Detailed predictions for weak interactions [similar to Eq. (11)] follow from the parton model. At a qualitative level they amount to a predominance of events at low Q_T for weak processes as for e.m. ones. When averaging over this region (i.e. over Q and Q_T, see Appendix), the interference of weak (Z exchange) and e.m. amplitudes gives rise to a new term in the distribution

$$\frac{d\sigma}{d(\cos \psi)} \sim 1 + \cos^2 \psi + b \sin \psi \ .$$

Here the $\cos \psi$ term gives an asymmetry between the ℓ^+ and ℓ^-. For positive b the ℓ^+ is emitted preferentially along the direction of the total momentum of the pair, i.e. forward, the ℓ^- backwards. This means that in the c.m. of the reaction the ℓ^+ will have on the average more energy than the ℓ^-.

6. PREDICTIONS FOR WEAK INTERACTIONS INDEPENDENT OF HADRON MODELS

Relations between weak and electromagnetic contributions to processes (1), (2), and (3) can be obtained by general principles such as CVC, chiral invariance, etc. Such relations would still depend upon *weak interaction* parameters such as the Weinberg mixing angle.

7. CONCLUSIONS

The study of lepton production touches on many of the interesting problems in present-day physics:

1) Hadron structure: scaling, parton models, quark confinement, etc.

2) Weak interactions: existence of $W^\pm$ and Z, neutral current effects.

3) Electromagnetism: structure of the photon propagator.

Theoretical ideas, useful as a conceptual frame, are available on all these points.

The central problem is the availability of enough luminosity, a problem discussed, for specific experiments, in the contribution by L. Camilleri (Part B, paper II.6).

The only criterion for estimating luminosity requirements is given by our present theoretical expectations. However, our experience is that these can lead both to gross overestimates or gross underestimates. On the one hand this indicates the need for a safety factor; on the other hand any deviation from theoretical expectations would teach us something of value.

REFERENCES

1) S.D. Drell and T.M. Yan, Phys. Rev. Letters 25, 316 (1970).

2) G. Altarelli, N. Cabibbo, L. Maiani and R. Petronzio, Nuclear Phys. B69, 531 (1974); and Phys. Letters 48B, 435 (1974).

3) G. Altarelli, N. Cabibbo, L. Maiani and R. Petronzio, Nuclear Phys. B92, 413 (1975).

APPENDIX ON KINEMATICS

With reference to Fig. 1, we define the following variables:

$$(P_1 + P_2)_\mu = P_\mu$$

$$(P_1 - P_2)_\mu = D_\mu \qquad \qquad (A.1)$$

$$(\ell_1 + \ell_2)_\mu = Q_\mu .$$

In terms of these one defines scalars:

$$s = (P, P) = 4E^2$$

$$D^2 = (D, D) = 4(E^2 - M_p^2) \approx s \qquad \qquad (A.2)$$

$$Q^2 = (Q, Q)$$

and scaling (dimensionless) variables,

$$\tau = Q^2/s$$

$$\xi = 2(QD)/s \qquad \qquad (A.3)$$

$$\zeta = 2(QP)/s .$$

A convenient set of experimental variables is given by Fig. A1, where we define a production plane and a decay plane; ϕ is the angle between the two. Quantities $(\theta, \vec{Q})$ in the production plane are in the c.m. of the reaction, while quantities in the decay plane $(\ell_{1,2}, \psi)$ are in the c.m. of the lepton pair. The interest of these variables[*] is that in a current-current interaction the differential cross-section is a polynomial of second degree in the sine or cosine of ϕ and ψ, different terms corresponding to different physical effects.
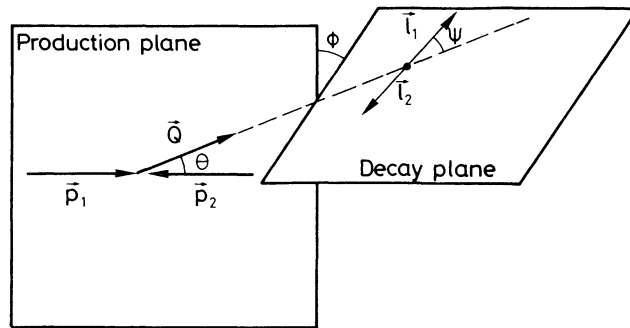
Fig. A1 A convenient set of variables to study the production of lepton pairs in pp collisions. The variables in the decay plane are defined in the centre-of-mass system of the lepton pair.

[*] This set is built by analogy to that used in K_{e4} decays (N. Cabibbo and A. Maksymovicz, Phys. Rev. 137, B438 (1965).

One finds, for example, that 1γ exchange leads to a distribution containing only 1, $\cos^2 \psi$, $\cos^2 \phi$, $\cos^2 \phi \cos^2 \psi$, which correspond to the four possible structure functions. Interference of weak and electromagnetic effects gives rise to terms which are linear in $\sin \phi$ or $\cos \phi$.

Higher-order processes -- a possible source of background -- give rise to higher powers in ($\cos \psi$, $\sin \psi$, $\cos \phi$, $\sin \phi$). These provide a way of identifying these processes.

The distribution in θ on the other hand, depends on the dynamics of the strong interaction. Present views suggest $Q_T = |\vec{Q}| \sin \theta$ as a variable of more physical significance than θ itself.

II.6 LEPTON PRODUCTION AT THE SISR

L. Camilleri

CERN, Geneva, Switzerland

1. INTRODUCTION

The Super-ISR (SISR) with a luminosity of 10^{33} cm^{-2} sec^{-1} and a centre-of-mass energy of 800 GeV would be particularly well suited for the study of charged lepton production via both the electromagnetic and weak interactions.

Two processes could be investigated:

$$p + p \to \ell^+ + \ell^- + \text{anything}$$

and

$$p + p \to \ell^\pm + \nu(\bar{\nu}) + \text{anything}$$

The $\ell^+\ell^-$ or lepton pair reaction would presumably be mediated by a continuum of virtual photons. In addition, enhancements could be present, due to the decay into a lepton pair of heavy particles such as vector mesons, ψ's, the Z^0 of neutral currents, or the neutral intermediate vector boson W^0.

The $\ell^\pm$ reaction, on the other hand, would be a consequence of the weak interaction. Here the interest lies in the fact that, at the SISR, the centre-of-mass energy of the pp system is 800 GeV, allowing the formation of $(\ell\nu)$ systems of mass well in excess of 300 GeV, the energy at which the weak cross-section violates the unitarity limit. The SISR would then allow, for the first time, the study of physical phenomena near this limit.

2. APPARATUS

The apparatus to be used must have the following properties:

  i) the ability to measure the lepton charge in order to observe any differences between positive and negative lepton production;

 ii) the ability to measure the energy or momentum of the charged leptons;

iii) a large solid angle to make full use of the high luminosity and to measure angular distributions;

 iv) low enough backgrounds to allow triggering on a single lepton.

Requirements (i) and (ii) clearly indicate the need for a magnet. Electron identification would in addition require lead-glass or argon calorimeters and Čerenkov counters or transition radiation detectors. On the other hand, muons can very simply be identified by requiring the particle to penetrate a large amount of material. In fact this material could be the magnet itself if an iron-core magnet is used. It was therefore decided to limit the present study to muons. It was further decided to concentrate on the 90° region where the lower flux of secondaries into the apparatus allows triggering on a single muon.

A possible experimental set-up is shown in Fig. 1. It is azimuthally symmetric and covers the angular region
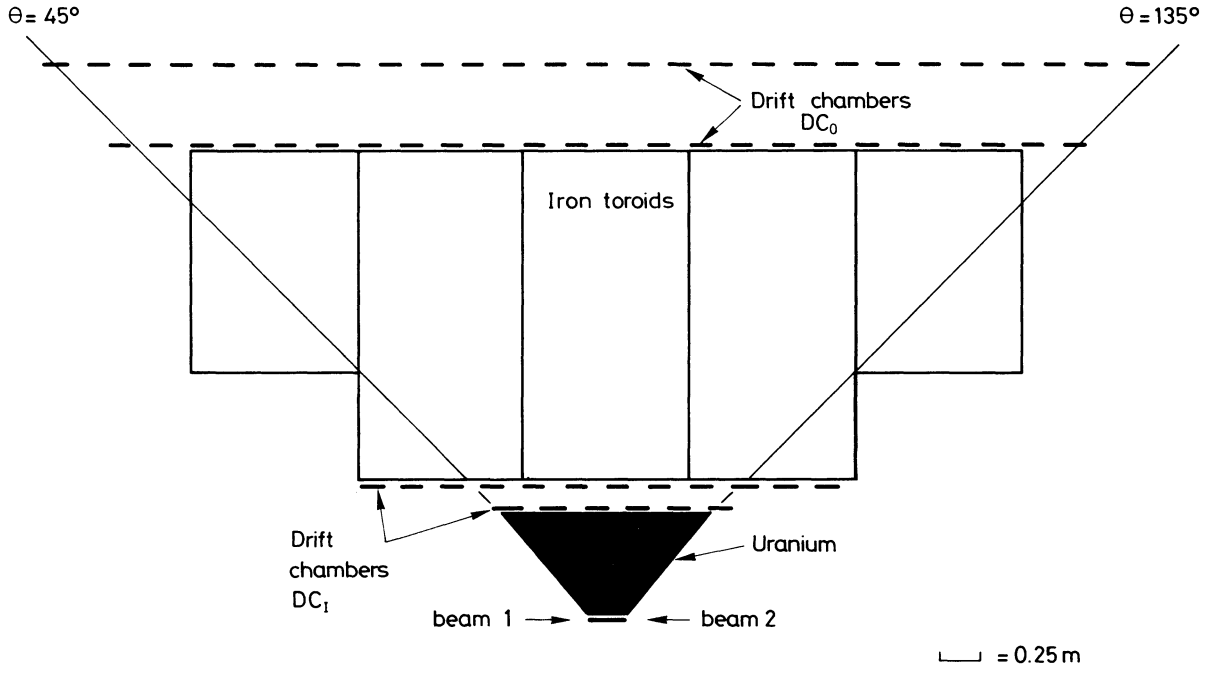
$$\theta = 90° \pm 45° \ , \quad \Delta\phi = 2\pi \ .$$

Fig. 1 Possible experimental set-up for the study of muon pairs and single muons at the SISR

It consists of the following:

a) 60 cm of uranium ($\sim$ 7 interaction lengths) to absorb strongly interacting particles before they can decay into muons. This shield is also used to limit the rates in the subsequent drift chambers.

b) DC_I, a set of cylindrical drift chambers to measure the production angle of the muons.

c) Iron toroids, 2 m thick ($\sim$ 15 interaction lengths) with an azimuthal field of 17 kG. These toroids can be modular.

d) DC_0, a set of plane drift chambers to measure the direction of the outgoing muons.

The momentum resolution of the spectrometer is given by

$$\frac{\Delta p}{p} = \frac{\Delta \theta}{\theta_B} , \quad \text{with} \quad \Delta \theta = \sqrt{\Delta \theta_{IO}^2 + \Delta \theta_{ms}^2} ,$$

where

θ_B = bending angle

$\Delta \theta_{ms}$ = multiple scattering in the iron

$\Delta \theta_{IO}$ = measurement error

= 0.76 mrad, using a space resolution ε = ±0.1 mm

in each of the drift chambers and lever arms of 20 cm and 50 cm in DC_I and DC_0 respectively.

Then, for p < 70 GeV/c $\Delta p/p$ = constant = ±16% (dominated by multiple scattering);

for p > 70 GeV/c $\Delta p/p$ is dominated by the measurement error and increases up to ±25% at p = 300 GeV/c.

For two muons emitted with an azimuthal separation of 180°, the mass resolution is dominated by the resolution in the momentum measurement and is given by

$$\frac{\Delta M}{M} \sim \frac{1}{2} \sqrt{\frac{\Delta p_1^2}{p_1^2} + \frac{\Delta p_1^2}{p_1^2}}$$

$$\sim \pm 11\% \quad \text{for } p_1, p_2 < 70 \text{ GeV/c .}$$

3. EVENT RATES AND BACKGROUND

3.1 Muon pairs

The expected rate was estimated using the parton-antiparton annihilation model[1-3]. Several experiments have observed single lepton production at Serpukhov[4], FNAL[5-7] and at the CERN ISR[8]. The level at which the signal is observed seems to be higher than predicted by the parton model, indicating that the estimated event rate for the SISR is probably on the conservative side. The model gives

$$\frac{d\sigma}{dQ^2 d\xi} = \frac{4\pi\alpha^2}{3Q^4} \frac{1}{\lambda} \left\{ \sum_i \frac{e_i^2}{(x_A + x_B)} \left[x_A f_i^A(x_A) x_B f_{\bar{i}}^B(x_B) + x_A f_{\bar{i}}^A(x_A) x_B f_i^B(x_B) \right] \right\} , \tag{1}$$

where

ξ = $2p_L/\sqrt{s}$; p_L = longitudinal momentum of pair

Q = mass of pair

λ = colour = 3

$f_i^A(x_A)$ = probability of finding a parton of type i and charge e_i carrying a fraction x_A of the momentum of hadron A

f_i's = polynomial fits to curves[9] making use of all available experimental information and yielding a small antiparton content in the proton.

The decay of the dimuon system is taken to be isotropic in its centre of mass, although a $(1 + \cos^2 \theta)$ decay distribution only lowers the expected number of events by 20%. The predicted dimuon rate, observable in the apparatus described above and assuming λ, the colour, to be 3, is given by curve c of Fig. 2, as a function of the dimuon mass. It is estimated that at least 10,000 pairs of mass greater than 15 GeV/c^2 would be observed for a 500 hours run.

The background to this process comes from the decay of both members of $\pi^\pm$, $K^\pm$ pairs before interaction in the uranium. Estimates of these correlated π and K pairs were obtained under the following assumptions:

i) $N(\pi^+) = N(\pi^-) = N(K^+) = N(K^-) = N(\pi^0)$;

ii) these single-particle production rates could be described by the fit to the high p_T single π^0 data obtained at the ISR[10],

$$A p_T^{-8.24} e^{-26.1 p_T/\sqrt{s}} ; \tag{2}$$

iii) the production of π and K pairs is larger than for uncorrelated π's and K's, and the enhancement factor R is a function of x_T ($= 2p_T/\sqrt{s}$) only, rather than a function of p_T
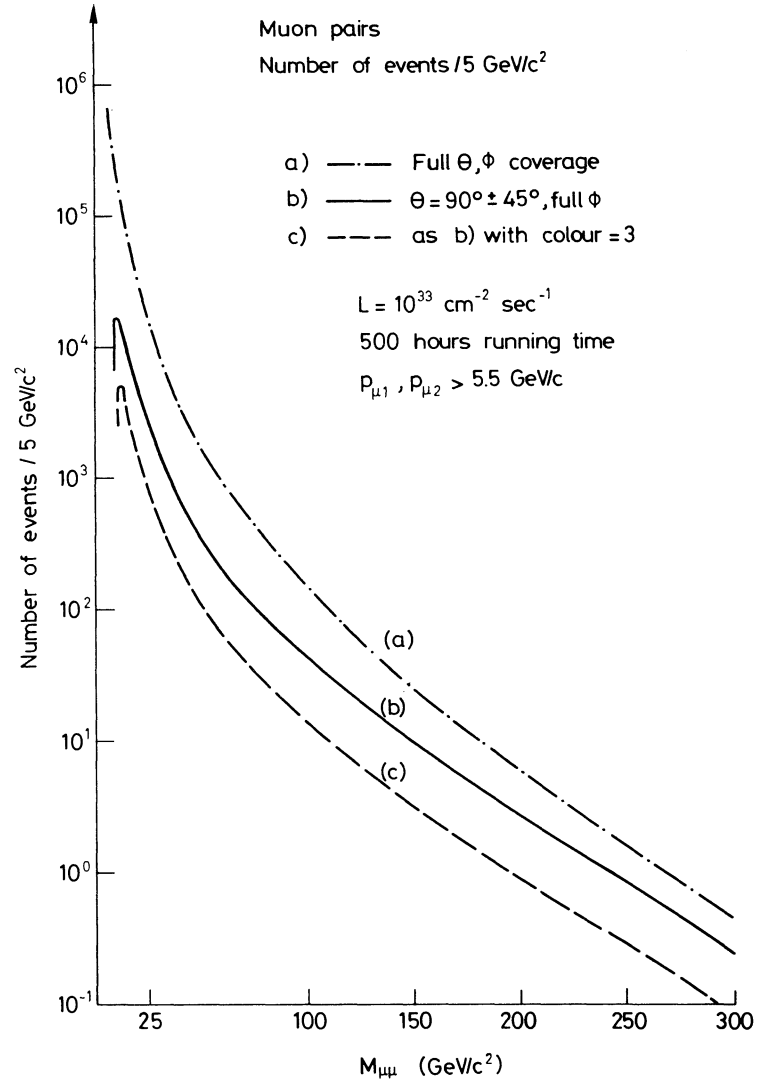
Fig. 2 Rates of muon pairs estimated using the parton-antiparton annihilation model referred to in the text

and $\sqrt{s}$. Then R can be obtained from $\pi^0\pi^0$ correlation data also obtained at the ISR[11]. For a typical pair produced with

$$p_{T1} = p_{T2} = 50 \text{ GeV/c} \quad , \quad x_{T1} = x_{T2} = 0.125 \quad ,$$

and R (0.125, 0.125) = 500. Even with this large enhancement factor, this background is several orders of magnitude below the expected muon pair rate.

In addition to measuring the cross-section with which the pairs are produced, the following quantities would be studied:

a) p_T, p_L and angular distributions of the pair.

b) Coplanarity of the two muons with the two beams. Non-coplanarity of the pair with the two beams could simply be due to the production of the pair with a large transverse momentum. More interestingly it could result from the muons being the decay products of two pair-produced heavy leptons or charmed particles.

3.2 Single muons

The production of $\mu\nu$ pairs is related to the production of $\mu\mu$ pairs by CVC. Then

$$\frac{d\sigma}{dm_{\mu\nu}} = \frac{d\sigma}{dm_{\mu\mu}} \frac{G^2}{(4\pi\alpha)^2} Q^4 K \;, \tag{3}$$

where

$Q = m_{\mu\nu} = m_{\mu\mu}$

$G = 10^{-5}/m_p^2$

K = 6 and is a factor arising from counting which pairs of partons can annihilate and with which helicities.

An estimate of the event rate was obtained from the above and again using the parton model for $d\sigma/dm_{\mu\mu}$. Note that all that is detected is a single muon. It is therefore imperative to investigate the possible sources of background giving rise to single muons. They come from two sources:

i) Decays of $\pi^\pm$, $K^\pm$ produced at large p_T. This contribution was estimated again assuming equal numbers of π^+, π^-, K^+, K^-, π^0 and the fit of Eq. (2).

ii) Single muons from $\mu^+\mu^-$ pairs where one of the muons is detected and the second one either stops in the uranium or misses the apparatus. This contribution was estimated from Eq. (1) and will in any case be exactly calculable from the $\mu^+\mu^-$ experiment.

An approximation of the mass of the ($\mu\nu$) system giving rise to the single muon is obtained from $2p_\mu$. The event rate obtained using Eq. (3) and the contributions due to the two backgrounds discussed above are shown in Fig. 3 as a function of $m_{\mu\nu}$ (or $2p_\mu$ for the backgrounds) for a 500-hour run. The following features of this plot must be noted:

a) the continuum of $\mu\nu$ pairs is relatively flat across the mass range;

b) beyond $m_{\mu\nu}$ = 65 GeV/c^2 both backgrounds are negligible;

c) measurable rates are obtained for masses as high as 500 GeV/c^2.

The triggering rate, arising mostly from muons due to π and K decays, is found to be less than 10/second, which is quite tolerable. Off line most of these background events are of course rejected by imposing a minimum mass cut. As was mentioned earlier, the signal dominates over the background above 65 GeV/c^2. In fact, this minimum mass cut must be chosen well above 65 GeV/c^2 in order to avoid background events spilling over into the good event sample, owing to poor momentum resolution. Imposing the cut at 100 GeV/c^2 would imply cutting 3 standard deviations in resolution above 65 GeV/c^2. This should be adequate.

The number of detected events above 100 GeV/c^2 is estimated to be 5600. The physics to be done with these is as follows:

1) An approximate effective mass of the ($\mu\nu$) system can be computed using $m_{\mu\nu} \sim 2p_\mu$. Enhancements in the mass plot could be looked for. These would arise from heavy particles such as the intermediate vector boson, decaying according to

$$W^\pm \rightarrow \mu^\pm \nu(\bar{\nu}) \;.$$
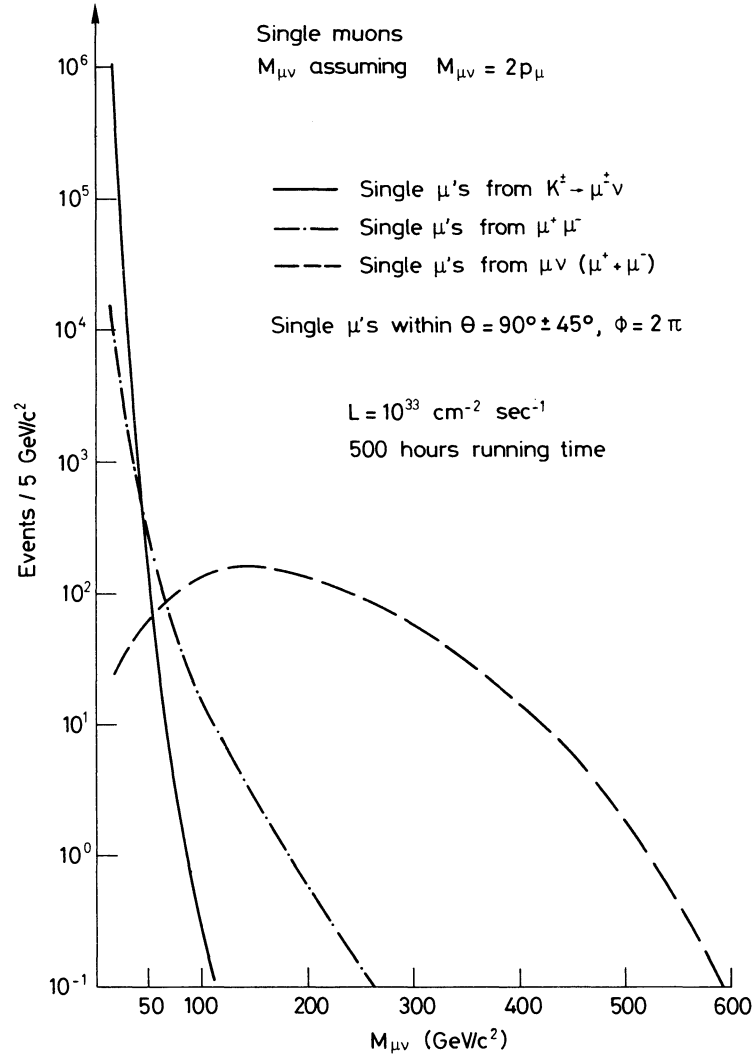
Fig. 3 Rates of single muons from ($\mu\nu$) pairs estimated from
CVC and the parton model

If a $W^{\pm}$ of mass M_W does exist and decays to $\mu\nu$ with a branching ratio B, then its production cross-section can be related to $d\sigma/dm_{\mu\nu}$ by

$$\sigma_W = \frac{3\sqrt{2}\ \pi^2\ B}{M_W\ G} \frac{d\sigma}{dm_{\mu\nu}}\bigg|_{M_W} . \tag{4}$$

Given this equation, and with B = 0.12, W's down to 25 GeV/c^2 could be detected before being overwhelmed by muons from K and π decays. As an example, for M_W = 100 GeV/c^2, 10^5 events are expected within the acceptance of the apparatus in the same 500-hour run. These events would be spread over a 30 GeV/c^2 mass interval due to resolution, but would be easily detectable since the contribution from the continuum in the same mass interval is less than 1000 events.

2) Observing events with single μ's of p_T > 50 GeV/c must be an indication of something new happening, such as a further flattening of the single-hadron inclusive distribution.

3) Taking partons to be quarks, negative muons come from $\bar{p}n$ quark annihilations whereas positive muons come from $p\bar{n}$. But in the proton

$$N(n) \sim \tfrac{1}{2} N(p) \quad \text{and} \quad N(\bar{n}) \sim N(\bar{p}) .$$

So we expect $\mu^+/\mu^- = 2$. Does it?

4) From helicity and angular momentum arguments $\langle p(\mu^+) \rangle$ should be less than $\langle p(\mu^-) \rangle$.

5) Finally, certainly the most intriguing question is, What happens to $d\sigma/dm_{\mu\nu}$ as $m_{\mu\nu}$ gets larger than 300 GeV/c^2, the value at which the weak cross-section reaches the unitarity limit? According to the above estimates, 1000 events with $m_{\mu\nu} > 300$ GeV/c^2 are expected. This should allow a thorough investigation of this interesting mass region.

4. SPECIAL REQUIREMENTS ON THE SISR

No special requirements are imposed on the SISR by this type of physics. Obviously the experiment requires the highest possible luminosity and would therefore use a low-β intersection region. Since part of the experiment is to detect a single particle, backgrounds have to be carefully suppressed. If the solution to place several intersection regions in a single long building is adopted, the set-up will have to be extensively shielded from other interaction regions.

5. CONCLUSIONS

The SISR is an instrument that would allow the observation of muon pairs of high invariant mass and of single muons arising from ($\mu\nu$) systems, also of large mass. A large solid-angle experimental configuration stressing the 90° region has been discussed. With it, it was found that the above two processes could be studied, essentially uncontaminated by background in the high mass region. It is estimated that measurable event rates would be obtained up to $m_{\mu^+\mu^-} = 150$ GeV/c^2 and $m_{\mu\nu} = 500$ GeV/c^2. The observation of ($\mu\nu$) systems of mass greater than 300 GeV/c^2 would allow, for the first time, the study of the effects of the unitarity limit on a cross-section. It is therefore concluded that, at least as far as lepton physics is concerned, the building of the SISR would be a very worth-while endeavour.

REFERENCES

1) S.D. Drell and T.M. Yan, Phys. Rev. Letters 25, 316 (1970).

2) J. Kuti and V.F. Weisskopf, Phys. Rev. D 4, 3418 (1971).

3) S.M. Berman, J.D. Bjorken and J.B. Kogut, Phys. Rev. D 4, 3388 (1971).

4) G.B. Bondarenko et al., presented by V. Lebedev, Proc. 16th Internat. Conf. on High-Energy Physics, Batavia, 1972 (eds. J.D. Jackson and A. Roberts)(National Accelerator Laboratory, Batavia, Ill., 1973), Vol. 2, p. 328.
   V. Abramov et al., Contribution No. 785 to Session A3 of the 17th Internat. Conf. on High-Energy Physics, London, 1974.

5) J.P. Boymond et al., Phys. Rev. Letters 33, 115 (1974).

6) J.A. Appel et al., Phys. Rev. Letters 33, 722 (1974).

7) D. Bintinger et al., Contribution No. 576 to Session A3 of the 17th Internat. Conf. on High-Energy Physics, London, 1974.

8) F.W. Büsser et al., CERN-Columbia-Rockefeller-Saclay Collaboration, Phys. Letters 53B, 212 (1974).

9) G. Altarelli et al., CERN preprint TH.1727 (1973).

10) F.W. Büsser et al., Phys. Letters 46B, 471 (1973).

11) F.W. Büsser et al., Phys. Letters 51B, 311 (1974).

II.7 PARTICLE PRODUCTION AT HIGH TRANSVERSE MOMENTA

L. Di Lella

CERN, Geneva, Switzerland

1. <u>INTRODUCTION</u>

A well-known aspect of proton-proton collisions at very high energies, first discovered at the CERN ISR, is the flattening of the cross-sections for inclusive hadron production with increasing transverse momentum[1-3]. Secondary pions with transverse momenta as high as 10 GeV/c have been observed at a total centre-of-mass energy $\sqrt{s}$ = 53 GeV, whereas extra-polations from pre-ISR data predicted unmeasurably small cross-sections for p_T > 4 GeV/c.

High transverse momentum secondary particles are a very useful tool for obtaining information about the structure of the system under study, down to small distances. In fact most of the theoretical models used to interpret the experimental results in this field describe the proton as consisting of hard, point-like constituents. Very definite predic-tions about the structure of high transverse momentum events are given by these models, such as the presence of "jets" of hadrons in the hemisphere opposite to that containing the high transverse momentum secondary particle. However, it is difficult with present machines to obtain good statistics at p_T > 4 GeV/c, a value which is probably not high enough to allow definite conclusions on this subject.

It is, of course, difficult to predict the magnitude of the cross-section for inclusive hadron production at centre-of-mass energies $\sqrt{s}$ = 800 GeV. Most of the theoretical models give the form $A p_T^{-n} F(x_T, \theta^*)$ for the invariant cross-section, where $x_T = 2p_T/\sqrt{s}$ and θ^* is the centre-of-mass angle. This form was used to fit ISR data on π^0 production at 90°, for values of $\sqrt{s}$ between 23 and 62 GeV, and x_T < 0.3 [1]. The result was

$$E \frac{d^3\sigma}{dp^3} = \frac{1.5 \times 10^{-26}}{p_T^8} \exp(-13 x_T) \text{ cm}^2/\text{GeV}^2 . \tag{1}$$

We shall therefore use Eq. (1) to extrapolate the pion production cross-section beyond the ISR energy range. The invariant cross-section for pion production as a function of p_T, at $\sqrt{s}$ = 53, 200, and 800 GeV, is shown in Fig. 1. The curve labelled BBK represents the prediction of a model[4] based on electromagnetic scattering of the proton constituents, for $\sqrt{s}$ = 800 GeV. While this contribution is reduced by a factor α^2 with respect to the purely hadronic cross-section, it varies with p_T as p_T^{-4} and becomes larger than the hadronic term around p_T = 36 GeV.

From Eq. (1) it is possible to calculate the expected pion rate $dN_\pi/d\Omega$. For a luminosity $L = 10^{33}$ cm^{-2} sec^{-1}, we find the following rates for p_T > 30 GeV/c:

$$dN_\pi/d\Omega = 0.17 \text{ events/sr·hour at } \sqrt{s} = 200 \text{ GeV}$$
$$dN_\pi/d\Omega = 4.3 \text{ events/sr·hour at } \sqrt{s} = 800 \text{ GeV} .$$

Furthermore, at $\sqrt{s}$ = 800 GeV, there are 0.4 events/sr·hour with p_T > 40 GeV/c.

Since experimental set-ups with a solid angle coverage of 1 sr around 90° are feasible, it appears from the event rates given above that secondary pions with transverse momenta as high as 40 GeV/c can be observed, thus providing us with a way of studying the proton with a resolution of 1/200 of its radius.
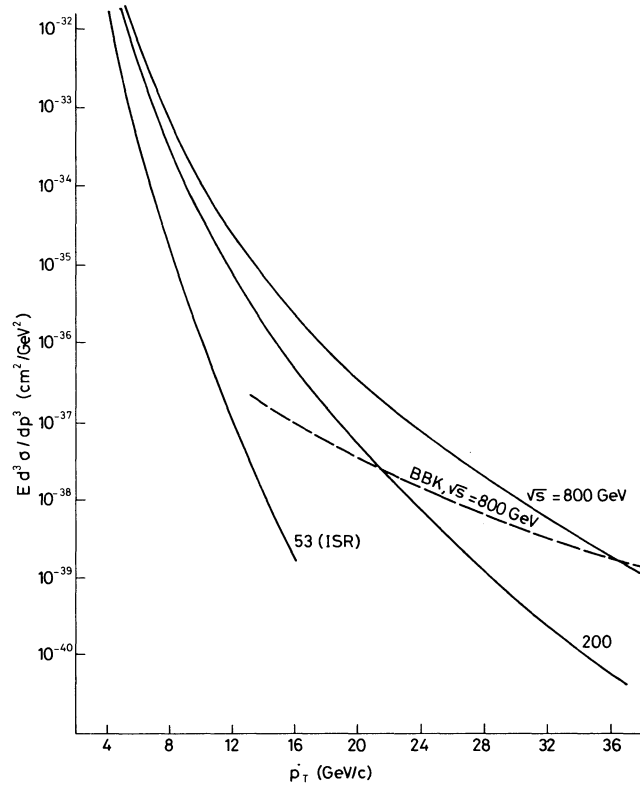
Fig. 1   Invariant cross-section for inclusive π^0
production versus p_T, at $\sqrt{s}$ = 53, 200,
and 800 GeV. The curve labelled BBK is
a theoretical prediction from Ref. 4.

There is also hope of seeing the effect of electromagnetic scattering of the point-like constituents of the protons, by observing a further flattening of the cross-section at $p_T > 35$ GeV/c.

2. DETECTION OF NEUTRAL PIONS

Neutral pions can easily be detected by their decay into two photons, using arrays of total absorption lead-glass Čerenkov counters. Since the longitudinal dimension of an electro-magnetic shower increases only very slowly with photon energy, it is possible to use counters only slightly thicker than those used at the ISR (55 versus 42 cm), and still have an accurate measurement of the π^0 energy. Furthermore, it is possible to select high p_T events in the trigger, by setting a suitable threshold on these counters.

A typical set-up to study the reaction $p + p \to \pi^0$ + anything, around 90°, is shown in Fig. 2. It is very similar to the apparatus used at the ISR for the same purpose[1]. It consists of an array of 288 lead-glass blocks, subtending a solid angle of 2.2 sr, and a system of MWPCs and scintillation counters for charged particle identification. Thin lead plates, 1.5 mm thick, are placed between adjacent chamber modules to convert the photons.

With a luminosity of 10^{33} cm^{-2} sec^{-1}, this apparatus would detect π^0's at p_T = 40 GeV/c, at a rate of 0.2/hour × GeV for $\sqrt{s}$ = 800 GeV.
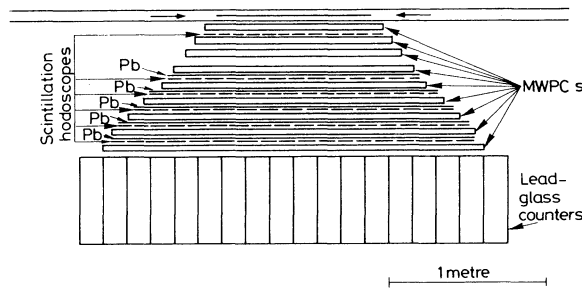
Fig. 2 Apparatus to study high transverse momen-
tum neutral pions

The number of inelastic interactions is $\sim 6 \times 10^7$/sec (assuming σ_{inel} = 60 mb), at
$L = 10^{33}$ cm^{-2} sec^{-1}. Each interaction produces an average of approximately one particle
within the solid angle of the apparatus. The energy deposited in the lead-glass array by
these particles is generally much less than 500 MeV; furthermore, the probability to overlap
in space with the π^0 is less than 10%. There is therefore no problem of pile-up in the study
of inclusive π^0 production.

However, a problem does exist in the study of particle correlations. Here, owing to
the relatively long sensitive time of the MWPCs ($\sim$ 100 nsec), approximately six interaction
vertices are observed. Most of them can immediately be rejected by scintillation counter
tagging. For a resolving time of $\sim$ 10 nsec, 60% of the events would still be accompanied
by another interaction vertex. In these cases, it becomes necessary to determine the vertex
of the high p_T π^0, by measuring the directions of the photons. This is achieved with the
lead plate/wire chamber sandwiches described above.

It should be pointed out that the apparatus of Fig. 2 can be built to cover up to 2π in
azimuth, thus making it possible to study π^0-charged particles and π^0-π^0 correlations. If
"jets" do indeed exist, and if their multiplicities increase less rapidly than p_T, the opening
angle of "jets" will then decrease with increasing p_T, thus making their identification easier.

3. DETECTION OF CHARGED PARTICLES

The detection of charged particles requires magnetic analysis and particle identification
by means of threshold gas Čerenkov counters. As a consequence, there is a loss in acceptance
with respect to π^0's.

A magnetic spectrometer for studying large-angle particle production is shown in Fig. 3.
It uses a superconducting dipole, 2.5 m long, with a useful diameter of 1.5 m and a uniform
magnetic field B = 2 T.

Particle trajectories are measured with MWPCs. Counter hodoscopes provide a trigger
sensitive to high p_T charged secondaries, by making coincidences only between the counters
which correspond to a bending angle smaller than a given one.

The solid angle subtended by this apparatus is 0.06 sr. The rate of pions above
p_T = 30 GeV/c is 0.26 events/hour at $\sqrt{s}$ = 800 GeV, based on Eq. (1). For 30 GeV/c particles,
the bending angle is 50 mrad. The momentum resolution is $\Delta p/p$ = (0.1 p)%, where p is in GeV/c,
for a 2 mm wire spacing in the chambers.
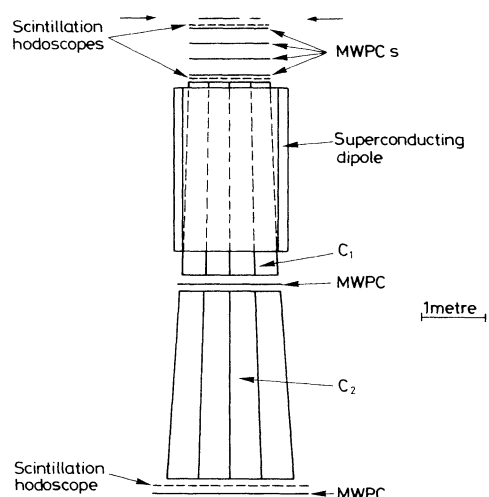
Fig. 3 Apparatus to study high transverse momen-
tum charged particles

Particle identification is achieved with two Čerenkov counters, C_1 and C_2, which must be subdivided into independent cells to reduce the probability that two particles may go through the same cell. It is possible to operate the two counters in the interval of p_T values between 15 and 25 GeV/c, so that the coincidence C_1C_2 identifies π's, while $C_1\bar{C}_2$ identifies only K's. At momenta below 15 GeV/c this problem is, of course, easier.

4. A MAGNETIC DETECTOR WITH LARGE ACCEPTANCE

Figures 4a and 4b show a magnetic detector for studying particle correlations in high transverse momentum events with full azimuthal coverage and a ±45° wide acceptance in θ around θ = 90°. This apparatus is similar to the solenoid at present being constructed for experiment

Fig. 4 A large acceptance spectrometer to study high transverse momentum events: a) top view;
b) view along the magnetic field direction.

R108 at the ISR[5]. However, some modifications are necessary, because of the much higher interaction rate expected at the SISR ($\sim 6 \times 10^7$ inelastic interactions/second, to be compared to $< 10^6$ at the ISR). The main modification is the use of MWPCs instead of drift chambers. The use of drift chambers in the SISR solenoid would result in ~ 180 charged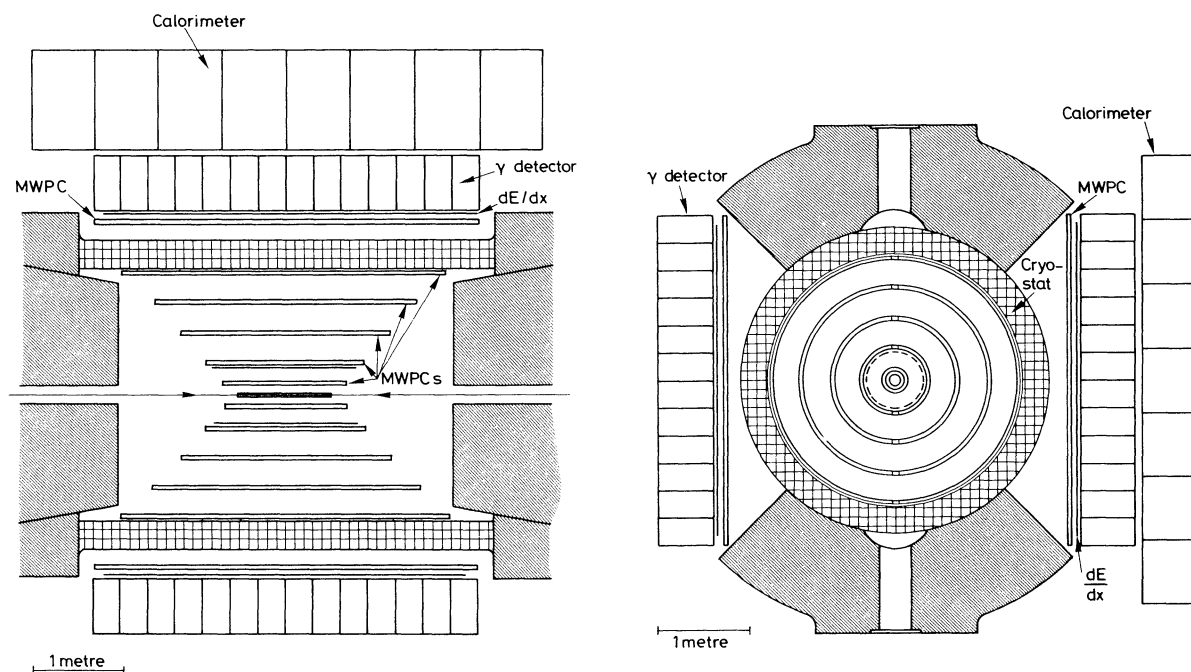 particle tracks being recorded for each trigger. This prohibitive number can be reduced by a factor of ~ 10 by the use of MWPCs, at the expense of a loss of a factor of ~ 3 in space resolution. A momentum resolution $\Delta p/p = (0.5 \, p)\%$ (p in GeV/c) can still be achieved with a radius R = 1.9 m and a field B = 1.5 T, or by any choice of these two parameters such that $BR^2 = 5.4$ T m^2. At R = 1.9 m, the length of the solenoid becomes ~ 4 m to achieve a 90° acceptance in θ. Thus the magnetic field volume is ~ 18 times that of the solenoid for the ISR.

Lead-glass counters and hadron calorimeters are located outside the field volume, to provide a trigger on high p_T π^0's and hadrons, as shown in Figs. 4a and 4b.

5. CONCLUSIONS

The study of particle production at high transverse momenta is experimentally a relatively simple matter at the SISR, even at total interaction rates as high as 10^8 sec^{-1}.

Reasonable extrapolations to $\sqrt{s} = 800$ GeV from the ISR results suggest that the detection of secondary particles with transverse momenta as high as 40 GeV/c can be achieved. The study of these events will provide information on the structure of the proton at distances as small as 5×10^{-16} cm. As an example, three types of experimental set-ups have been discussed. They represent an obvious extrapolation to the SISR of set-ups already used or to be used at the ISR. They would all use a low-β intersection region, where the highest luminosity is available.

It may happen that, as was the case with the ISR, the yield of high transverse momentum particles is larger than anticipated. In this connection, it is worth while pointing out that the apparatus described in Section 2 can operate just as well up to π^0 momenta of 400 GeV/c. Thus this set-up can study particles emerging at 90° and carrying as much as half of the available centre-of-mass energy, should they be provided by nature in measurable quantities.

REFERENCES

1) F.W. Büsser et al., Phys. Letters 46B, 471 (1973).

2) B. Alper et al., Phys. Letters 44B, 521 (1973).

3) M. Banner et al., Phys. Letters 44B, 537 (1973).

4) S.M. Berman et al., Phys. Rev. D 4, 3388 (1971).

5) CERN-Columbia-Oxford-Rockefeller Collaboration, Proposal for a continuation with increased sensitivity of the search for $e^{\pm}$, e^+e^- pairs, high transverse momentum $\pi^{\pm 0}$ and multiple pion correlations in collisions with high transverse momentum, CERN/ISRC/73-13 (1973).

II.8 ELASTIC SCATTERING AND TOTAL CROSS-SECTION
IN A 400+400 GeV PROTON STORAGE RING

A.N. Diddens

CERN, Geneva, Switzerland

1. INTRODUCTION

One of the questions of interest in the field of strong interaction physics is the asymptotic behaviour as a function of energy of the total and the elastic cross-section, the ratio of the real and the imaginary parts of the scattering amplitudes, and the angular distribution of the elastic cross-section.

This report investigates the constraints that experiments in this field impose on a super ISR.

2. ANGULAR DISTRIBUTION EXPECTED

The differential cross-section for proton-proton scattering in the forward direction can be written as

$$\frac{1}{\pi}\frac{d\sigma}{dt} = \left| \frac{2\alpha}{t} e^{i\alpha\phi} + \frac{\sigma_{tot}}{4\pi} (i + \rho) e^{-\frac{1}{2}bt} \right|^2 \tag{1}$$

$$= \left(\frac{2\alpha}{t}\right)^2 + \left(\frac{\sigma_{tot}}{4\pi}\right)^2 (1 + \rho^2) e^{-bt} + \text{interference term.} \tag{2}$$

The Coulomb amplitude $2\alpha/t$ dominates at small four-momentum transfer squared, $t = p^2\theta^2$ (p is the incident momentum, 400 GeV/c in the case under study, and θ the scattering angle; $\alpha \approx 1/137$); the phase $\alpha\phi$ is small and negligible. The strong interaction part is described by three parameters: the total cross-section σ_{tot}, the ratio ρ of the real and imaginary parts of the scattering amplitude, and the slope b.

The interference term is proportional to ρ, and the angular distribution is most sensitive to this term in the region where the two amplitudes are equal:

$$\frac{2\alpha}{t} = \frac{\sigma_{tot}}{4\pi} , \tag{3}$$

that is at

$$t_c = \frac{0.074}{\sigma_{tot} \text{ [mb]}} \text{GeV}^2 , \tag{4}$$

thus in practice at $t_c \approx 1.5 \times 10^{-3}$ GeV² since σ_{tot} is around 50 mb. Since the Coulomb amplitude is known, measurements in the region $t \le \frac{1}{2}t_c$ can be used to derive the luminosity. The parameter b is determined in the region $t \ge 3t_c$ and so is the total cross-section, for which, however, the luminosity has to be known, either by the Coulomb method or by another one. Some additional features in the angular distribution at the present ISR energies have been a break in the parameter b at $t \approx 0.1$ GeV² and a dip at $t = 1$ GeV². For a 400+400 GeV/c SISR, the angles at which these various phenomena appear are listed in Table 1 ($\sigma_{tot} \approx 50$ mb assumed).

Table 1

t (GeV^2)	θ (mrad)	Interest
$\frac{1}{2}t_c$	0.07	Luminosity
t_c	0.1	ρ
$3t_c$	0.17	b and σ_{tot}
0.1	0.8	Break in b
1	2.5	Dip

3. MACHINE PARAMETERS

The design-normalized beam emittance of the 400+400 GeV/c SISR is

$$E = 30\pi\ 10^{-6}\ \text{rad·m} \tag{5}$$

in both the horizontal and vertical planes. Since

$$E = 4\pi\beta\gamma R_0\theta_0 \ , \tag{6}$$

it follows that the product of the mean beam radius R_0 and beam divergence θ_0 is

$$R_0\theta_0 = 18\ \mu\text{rad·mm} \ . \tag{7}$$

Does this value allow some or all of the experiments above to be performed? What constraints does this set for the optical arrangement in the interaction region? This latter question is quantitatively characterized by the value of the amplitude function

$$\beta_0 = \frac{R_0}{\theta_0} \ . \tag{8}$$

The luminosity is proportional to $\beta_0^{-\frac{1}{2}}$. In the small-angle region the cross-sections to be measured are large, however, and considerations of luminosity therefore do not play an important role. At large momentum transfers the situation is different of course, and a low-β section should be used if possible, as is the case for other experiments that measure low cross-sections.

4. REQUIREMENTS ON β_0

4.1 Coulomb scattering

To start with the most demanding of the experiments: Is it possible to determine the machine luminosity via Coulomb scattering?

4.1.1 Let us assume initially that a technique similar to that at the present ISR will be used. Thus a detector is placed on each side of the interaction region, detecting scatterings in, for instance, the vertical plane; the scattering angle is determined as being

the angle between the line connecting two opposite detector elements and the nominal beam line; collinearity is the only test for rejecting non-elastic background. An expression of the type

$$\frac{A}{\theta^4} + \frac{B}{\theta^2} + C\ e^{-bp^2\theta^2}\ , \tag{9}$$

integrated over the acceptance of a detector element and over the θ range due to source dimensions and the beam divergence, fitted to the data, will allow the luminosity to be determined from the parameter A. The real scattering angle θ_0 is related to θ by:

$$\theta^2 = \theta_0^2 + \sum_i (\varepsilon_{i,V}^2 + \varepsilon_{i,H}^2)\ , \tag{10}$$

where the subscripts H and V stand for horizontal and vertical, and ε_i are the various contributions outlined above.

From practical experiences at the present ISR a reasonable requirement is

$$\frac{\varepsilon_{i,H\ or\ V}}{\theta_0} \leq 0.1\ , \tag{11}$$

thus leading to several corrections, each of which is of the order of 1%. Then in the Coulomb region all ε_i should be $\leq$ 7 µrad.

For the detector elements this is quite possible: 1 mm scintillation hodoscope elements, at 150 m distance from the intersect, or a proportional chamber would fulfil the requirements. Equations (7) and (8) determine R_0 = 2.5 mm and $\beta_0 \approx$ 370 m. The convolution of the two beams will make the interaction region have a radius of R = $R_0/\sqrt{2}$ = 2 mm which is, for a detector at 150 m, about a factor of 2 too large for requirement (11). However, by applying beam-shaving techniques and thus reducing the beam emittance (5) such a factor of 2 could be gained. The collinearity requirement will then also have been scaled inversely proportional to the energy from the present ISR to the new machine energy and thus have the same effectiveness.

In conclusion, with a β_0 of about 350 or 400 m horizontally and vertically the experiment seems feasible with detectors placed 150 m from the intersect. These conditions strongly resemble the conditions at 31+31 GeV/c at the present ISR where also some beam shaving is needed to perform the same experiment. It might be recalled that at 15+15 GeV/c these experiments have already been performed in the standard ISR environment without scraping.

4.1.2 Instead of copying the present techniques, we could argue that with two drift chambers with 0.1 mm resolution and 20 m separation, each scattered particle could be determined with the required 7 µrad precision. Although the information content of the event is thus somewhat richer, so that the requirement on the beam divergence could be relaxed a little, it is still the scattering angle relative to the initial beam particle that has to be determined. Thus not much can be gained on β_0. In addition, the collinearity test would deteriorate, which is also undesirable if we want to avoid the complication of momentum measurement of the outgoing particles.

A high-β section would probably not be without magnetic elements over a length of the order of 100 m. Since these elements act on both the primary and scattered beam in the same proportion, the arguments given above do not change appreciably. Detailed calculations by Keil and Montague confirm this.

4.2 Determination of ρ

Since the angles are $\sqrt{2}$ bigger, β_0 could be about a factor of 2 smaller, thus about 200 m.

4.3 Measurement of σ_{tot} and b

Three quarters of the elastic scattering is confined to the region $|t| \leq 0.1$ GeV^2. Thus a typical t-value in this range is t = 0.02 GeV^2, corresponding to a scattering angle of 300 μrad. Requirement (11) then sets the beam divergence to $\theta_0 \leq 30$ μrad, which leads to $\beta_0 \approx 25$ m. Thus measurements of this type could be performed in an intermediate-β section.

4.4 Large-t region

Around t = 1 GeV^2 a pronounced dip has been found. Since the depth of such a dip gives important information on the presence of other amplitudes than the main one, such a dip should be investigated with good resolution. Setting

$$\frac{\Delta t}{t} = 2\frac{\Delta\theta}{\theta} = 0.02$$

leads to $\Delta\theta = 25$ μrad at $\theta = 2.5$ mrad. Thus again the beam divergence should be ≤ 25 μrad, leading to $\beta_0 \approx 25$ m, and this experiment also could be done in an intermediate-β section.

At larger values of t the cross-section drops to such small values that a low-β section is clearly needed.

5. CONCLUSIONS

It seems feasible to perform measurements in the region of Coulomb scattering if amplitude functions $\beta_0 \approx 350$ to 400 m can be made both horizontally and vertically. In the diffractive region a standard intermediate-β section would suffice.

II.9 MULTIPLE PRODUCTION STUDIES AT THE SISR

P. Darriulat and J.C. Sens

CERN, Geneva, Switzerland

1. INTRODUCTION

The dominant process at SISR energies is multiple production. An understanding of its characteristic features is a basic requirement for any theory of strong interactions. At the SISR, the notions of scaling, short-range order, coherent excitation of high masses, well established at ISR energies, can be re-examined under very different, and in several ways more favourable, kinematic conditions. "Multiperipheral" and "diffractive" aspects of the collision mechanism are likely to separate more clearly as the width of the rapidity plot increases from eight units at the ISR to thirteen units at the SISR. At the ISR these features have emerged in *inclusive* measurements, indicating that significant conclusions can be drawn with only a partial knowledge of the variables. This point is of vital importance in the design of apparatus for the SISR, where the average charged multiplicity is around twenty.

In the following we consider first an extrapolation of present single particle ISR data to 400+400 GeV, in order to be able to predict rates at the SISR without recourse to any models. Then a four-arm spectrometer is considered in which the momentum, angle and type of up to four particles can be measured. It is assumed that sufficient angle-measuring detectors can always be added in order to label the events by their over-all multiplicity and to obtain angular distributions for given sets of variables in the four spectrometers.

The apparatus is intended to be used for the measurement of single-particle spectra in the "fragmentation" and "central" regions of the collisions; for studies of single and double diffraction dissociation ("fission" of protons by protons), with effective mass reconstruction on a subset of events; for the measurement of the mass spectrum and of the spin/parity properties of the system excited in collisions in which both incident protons lose only a small amount of energy (double Pomeron exchange); and for the study of cluster production in collisions in which the incident protons lose almost all of their energy ("fusion"). The apparatus would also be suitable for searches for stable, charged, new particles of high mass.

2. PARAMETRIZATION OF INCLUSIVE PION SPECTRA AT ISR ENERGIES

A compilation of data on inclusive π^+ production at ISR energies is shown in Fig. 1, taken from Albrow et al.[1]. The data have been obtained with spectrometers at 90°, at intermediate angles (80-300 mrad), and at small angles (35-180 mrad), for transverse momenta < 2.5 GeV/c. The data are displayed as contours of equal invariant cross-section in the x, p_T plane. Each contour resembles an ellipse, with major axis increasing exponentially to 1 as the minor axis a (= p_T for x = 0) is increased. A possible parametrization is thus:

$$\frac{p_T^2}{a^2} + \frac{x^2}{(1 - e^{-qa})^2} = 1 \ . \tag{1}$$

A reasonable fit (Fig. 1, solid lines) is obtained with q = 1.1. At 90° the different contours are connected by the relation

$$\sigma_{inv} = A\ e^{-bp_T} + B\ e^{-cp_T}\ ,\tag{2}$$

with p_T = a. The values A = 150, B = 6.0, b = 6.25, c = 3.7 fit the 90° π^+ data[2] to within 30% up to $p_T \approx 1.5$ GeV/c. Comparison of the data points at x $\neq$ 0 with the solid lines, calculated from Eqs. (1) and (2), indicates that the above parametrization represents the bulk of the ISR data ($\sigma_{inv} \gtrsim 10$ μb/GeV^2, say) reasonably well. For $\sigma_{inv} \gtrsim 10$ mb/GeV^2 its validity cannot be verified at present, for lack of ISR data at $p_T \lesssim 0.2$ GeV/c.

3. EXTRAPOLATION ISR → 400+400 GeV

The data of Fig. 1 have been taken at energies between $\sqrt{s}$ = 23 and 63 GeV. There is good evidence that the data scale, with the possible exception of the points at 90° in which

$$p + p \longrightarrow \pi^+ + X\ (ISR);\ \ E\frac{d^3\sigma}{dp^3}\ \ (mb.GeV^{-2})$$

Δ BRITISH-SCANDINAVIAN
∇ SACLAY-STRASBOURG
□ BOLOGNA-CERN
○ CERN-HOLLAND-LANCASTER-MANCHESTER

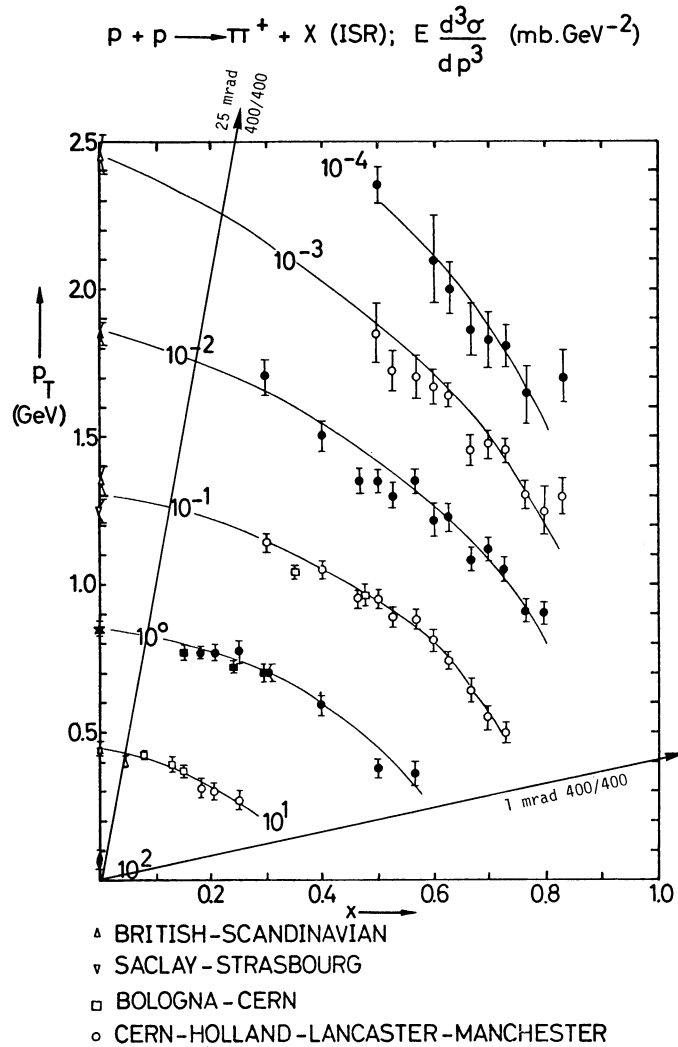Fig. 1 Contours of constant invariant cross-section at the ISR for the reaction pp → π^+ + X

a slight (< 10%) rise with energy has been observed. Figure 2 shows the same data, as well as those for other particles, in terms of rapidity. Scaling implies that with increasing energy the "plateau" extends to larger laboratory rapidity (giving rise to multiplicities increasing as $\Delta y \approx \Delta \ln s$) without any increase in height. Non-scaling in the central region implies an increase in height in the "flat" part of the cross-section as the y-range expands with energy. For the present purpose it will be assumed that scaling continues to hold up to $\sqrt{s}$ = 800 GeV.

If scaling holds, then the contours of constant σ_{inv} are again given by Fig. 1. Lines corresponding to θ = 1 mrad and θ = 25 mrad at 400+400 GeV indicate that most of the measured ISR range in x and p_T lies in a cone θ < 25 mrad at the SISR. The region of flat invariant cross-sections, between 17° and 90° at the ISR (15+15 GeV) extends from $\sim$ 10 mrad to 90° at the SISR (400+400 GeV). The entire fragmentation region at the SISR is thus confined to angles θ < 1°.
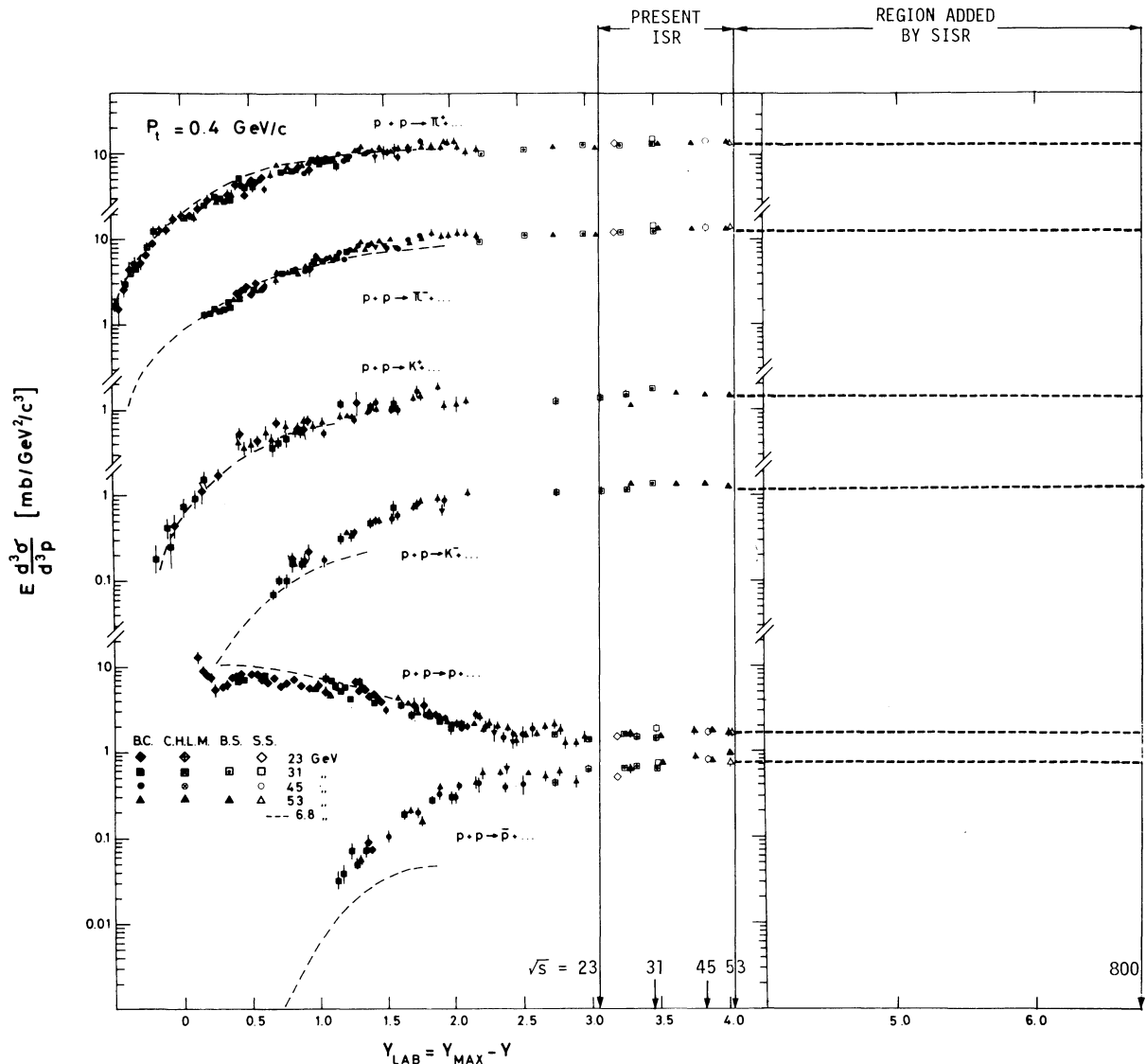

Fig. 2 The rapidity distribution for different particle types at the ISR at p_T = 0.4 GeV/c and extrapolation to $\sqrt{s}$ = 800 assuming scaling

Figures 3 and 4 show the dependence of rate on momentum for π^+ at θ = 5 and 25 mrad respectively, for 15.4+15.4 and 400+400 GeV. There are strong differences between the ISR and SISR. At 5 mrad the SISR rate at $x \approx$ 0.1-0.2 is a factor of 10 higher (for the same luminosity) than the ISR rate. At 25 mrad the difference at x = 0.2 is a factor of 1000. The x-dependence at the SISR is very much steeper and more rapidly varying with angle than at the ISR. This is further illustrated in Fig. 5 in which the non-invariant cross-sections have been integrated over momenta.

For the purpose of designing detection equipment, the following conclusions are relevant:

i) Magnetic analysis must extend down to θ < 1 mrad.

ii) From the contours of Fig. 1 it is easily deduced that for σ_{inv} = const., $\theta \approx$ 1/p. Hence a magnetic device with field inversely proportional to angle, as seen from the inter-section, is indicated.

iii) In the range 5-10 mrad there are 100 times as many particles at the SISR than at the ISR for the same luminosity. This represents rates (all particles) of up to $\sim 10^5$ particles per cm^2 of detection equipment at $\sim$ 50 m and L = 10^5 mb^{-1} sec^{-1}. For the range 5-25 mrad the SISR/ISR ratio is $\sim$ 16.

iv) At angles $\sim 90°$ the SISR and ISR cross-sections have the same dependence on momentum. Hence present 90° ISR apparatus can be used unmodified at the SISR.

Fig. 3 Differential cross-section as a func-
tion of x for π^+ production at θ =
= 5 mrad at the ISR (15.4+15.4) and
at the SISR (400+400). The SISR
curve is obtained, assuming scaling,
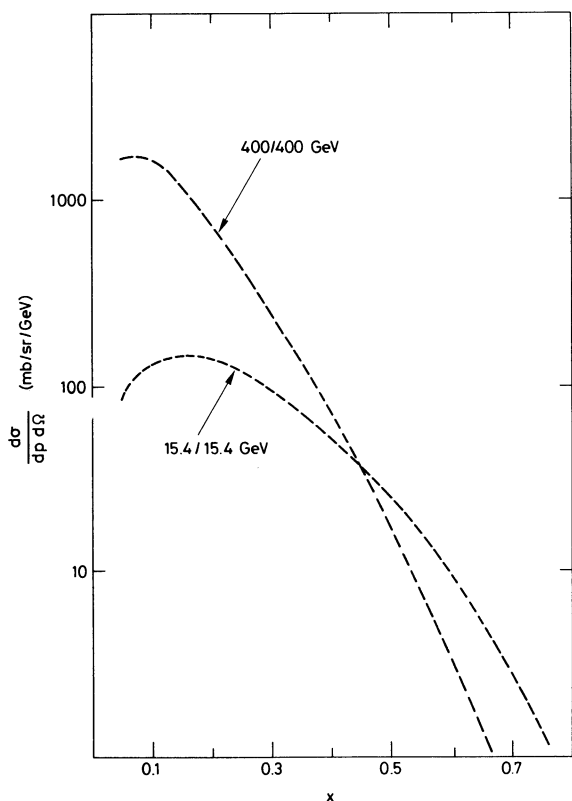from a parametrization of ISR data.

Fig. 4 Differential cross-section as a func-
tion of x for π^+ production at θ =
= 25 mrad at the ISR (15.4+15.4) and
at the SISR (400+400). The SISR
curve is obtained, assuming scaling,
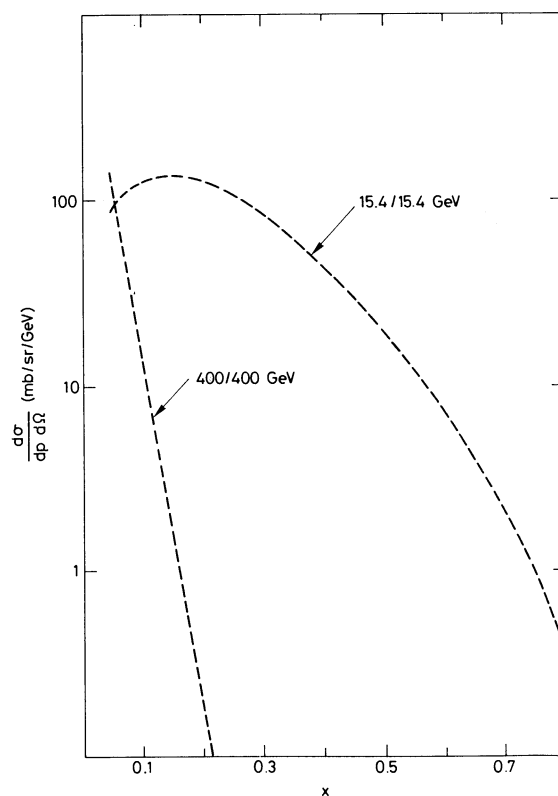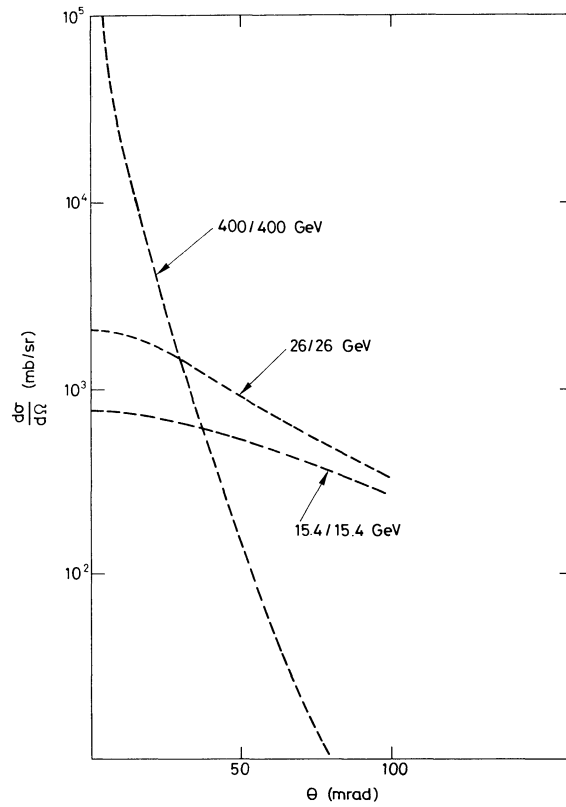from a parametrization of ISR data.

Fig. 5 Angular distributions for π^+ produc-
tion at 15.4+15.4, 26+26, and
400+400 GeV

4. PROTONS AT 400+400 GeV

The π^+ contours of Fig. 1 are representative of the other types of particles emerging from the collision as well, with the exception of protons. The possibility for a proton of being a leading as well as a produced particle significantly modifies the x and p_T dependence of the proton inclusive spectra. Figure 6 shows the contours of equal σ_{inv} at ISR energies. Elastic protons have been excluded from the plots. The proton contours show much less dependence on x than the pion contours. The peaks near x = 1 correspond to high mass diffractive excitation. The shapes of the distribution do not lend themselves to a simple parametrization. We have therefore estimated the proton rates at the SISR from Fig. 6 directly, using the solid lines eye-fitted through the points. There is excellent evidence that the data scale in the ISR region (not below). This is illustrated, for example, in Fig. 7, taken from Ref. 1. Assuming scaling to hold up to $\sqrt{s}$ = 800 GeV, the x-dependence of the rate at various angles can be obtained, as indicated in Fig. 8.

The conclusions are the following.

i)   At 5 mrad and 400+400 GeV the π^+ and p rates differ by less than a factor of 2 in the range 0.1 < x < 0.4; at x > 0.8 the p/π^+ ratio is > 100. Hence for p > 300 GeV a magnetic measurement specifies both type and momentum.

ii) Studies of diffraction dissociation require high resolution magnetic devices at angles < 5 mrad.

$$p + p \longrightarrow p + X \text{ (ISR)}; \quad E \frac{d^3\sigma}{dp^3} \text{ (mb.GeV}^{-2})$$

A BRITISH-SCANDINAVIAN
v SACLAY-STRASBOURG
□ BOLOGNA-CERN
o CERN-HOLLAND-LANCASTER-MANCHESTER
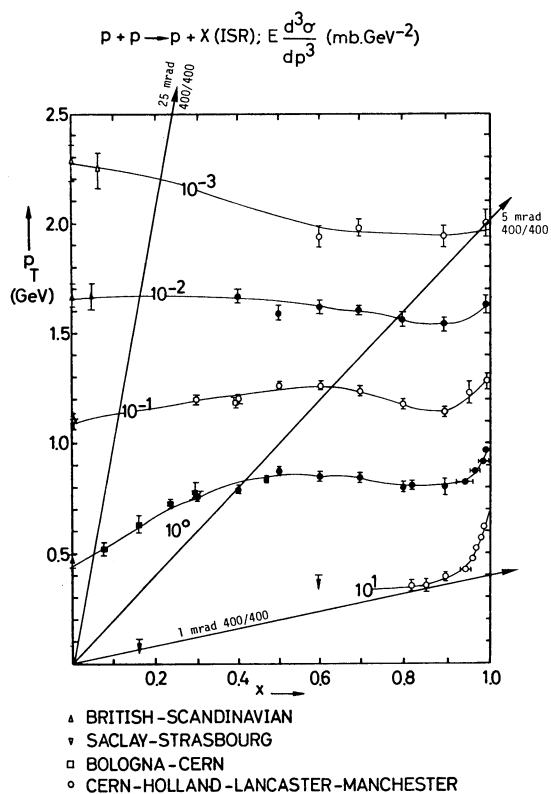
Fig. 6   Contours of constant invariant
cross-section at the ISR for
the reaction pp → p + X
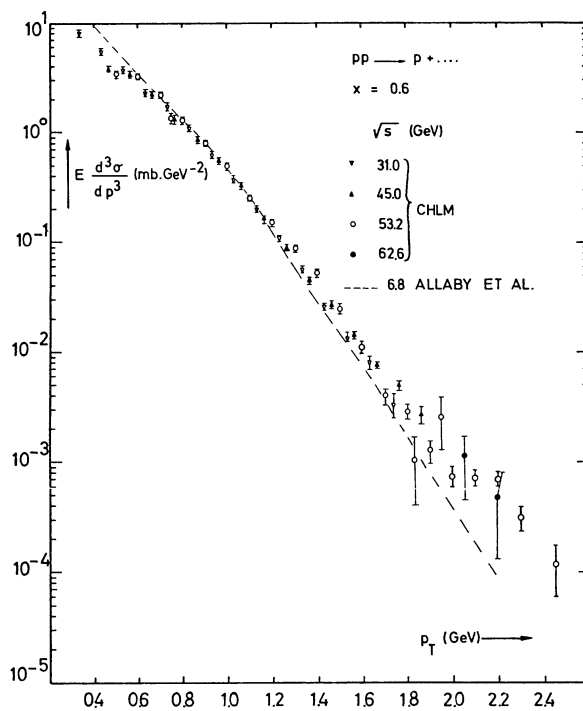

Fig. 7   Evidence for scaling in the ISR ener-
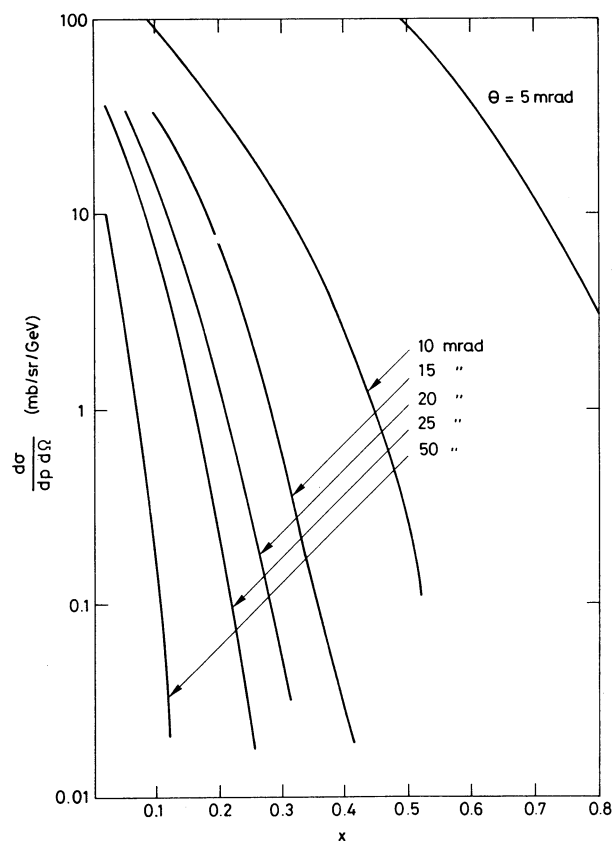gy range for the reaction pp → p + X

Fig. 8   Estimate of the x-dependence of the
non-invariant cross-sections for the
production of protons at various
angles for 400+400 GeV beam energy
as extrapolated from ISR data

5. CORRELATIONS AT 400+400 GeV

The study of correlations, i.e. clustering of secondary particles in phase space, can roughly be divided into three categories: i) correlations in general inelastic collisions; ii) correlations associated with diffraction excitation; iii) correlations associated with deep inelastic events, in which at least one particle of large transverse momentum is produced. In the following we are concerned only with the first two categories.

Data obtained so far at FNAL and at the ISR on correlations in general inelastic collisions lead to the following conclusions, relevant to the SISR:

1) Strong two-particle short-range correlations have been observed in *inclusive* charged-charged, charged-γ, charged-π^+, charged-p, charged-K^-, charged-π^-, $\pi^+\pi^-$, and $\pi^-\pi^-$ data with maxima which are different for the different combinations but independent of energy. In Fig. 9 the maximum value of

$$R(y_1, y_2) = \frac{\rho(y_1, y_2)}{\rho(y_1)\,\rho(y_2)} - 1$$

is shown versus energy for some of the combinations.

2) In *semi-inclusive* two-particle correlation data, with identified charges, in which two-particle distributions are examined for a fixed number of particles in the collision, there is no $\pi^-\pi^-$ correlation in the central region[3], while in $\pi^+\pi^-$ there are correlations suggestive of ρ and ω production and/or of diffraction excitation. Charge-charge correlation data at the ISR show short-range correlations, also in semi-inclusive distributions.

The lessons to be learned from these observations are that i) the SISR experiments on two-particle correlations should be designed in such a way as to measure from the start the charges of the two particles; ii) semi-inclusive distributions are more informative than inclusive ones, i.e. angle detectors must keep track of the multiplicity per event, over-all or in limited regions of phase space; iii) magnetic analysis is highly desirable in order to distinguish diffractive from non-diffractive correlations and to obtain effective masses from the data.
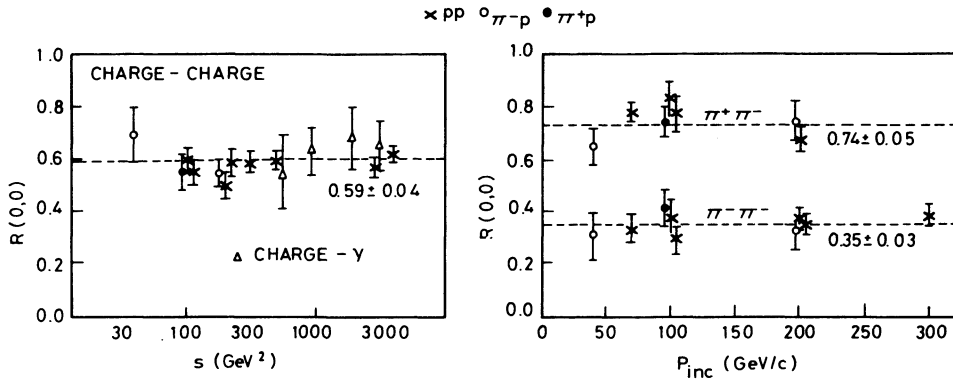

Fig. 9   The correlation coefficient $R(y_1, y_2)$ at $y_1 = y_2 = 0$ plotted as a function of reaction energies

The interest of studying diffractive dissociation at the SISR lies in the fact that states of very high mass can be coherently excited in the collision. In fact the criterion for coherence is that[4]

$$\Delta x = 1 - x < \frac{1}{2} \frac{m_\pi}{m_p} \approx \left(\frac{1}{4}\right)^2 .$$

Since also

$$\Delta x = \frac{M^2}{s} ,$$

we have that

$$M_{max} \sim \frac{\sqrt{s}}{4} = 200 \text{ GeV} , \tag{3}$$

at 400+400 GeV, compared to $\sim$ 15 GeV at the top ISR energy. Excitation up to 200 GeV is most easily seen by observing scaling in (σ_{inv} versus x) in pp $\rightarrow$ pX between ISR and SISR energies. This requires $\sim$ 1% resolution in momentum at 400 GeV and 1 mrad. The secondaries ejected from the high-mass system form clusters on the rapidity plot with centres determined by the magnitude of the mass excited and the shape and particle composition determined by the dynamics. Such clusters have been observed at ISR energies; their centres appear to be located approximately at $y = \ln \sqrt{s}/M$ and their edges at $\ln \sqrt{s}$ and $\ln \sqrt{s}/M^2$.

Extrapolation to the SISR then leads to the picture of Fig. 10. For a given mass M the cluster moves towards smaller angles, with no change in width. For example, the secondaries of a 5.6 GeV mass, spanning the entire hemisphere at the ISR (15+15 GeV), at the SISR cover an angular interval of 4.7° around the downstream direction. At M = 10 GeV the limits
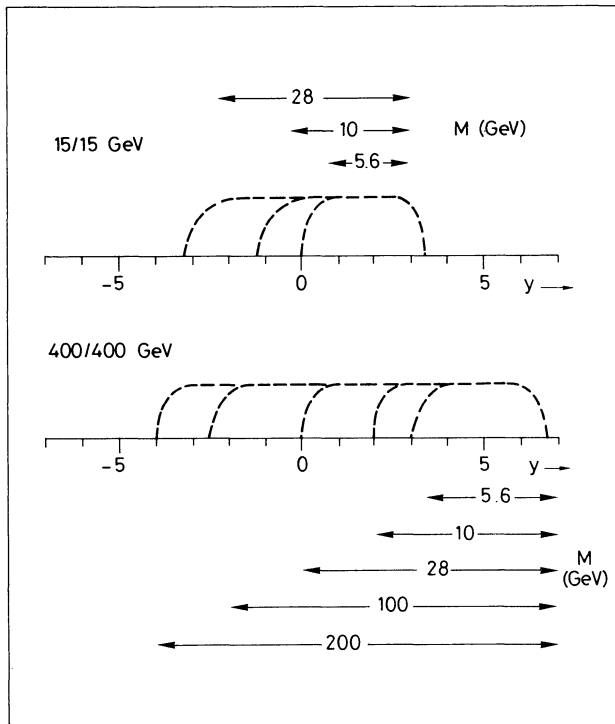
Fig. 10 Rapidity distributions associated with diffractive excitation at the ISR and at the SISR

are 147° and 14°, respectively. Data at FNAL and the ISR indicate that the multiplicities of these clusters do not depend on energy. The average density of tracks at small angles is therefore a factor of $\sim$ 20 higher than at the ISR.

A question of concern is the precision required in experiments on diffraction excitation at the SISR. A scale is provided by the contributions of diffraction to the rise in σ_{tot} through the SISR energy range (100+100 → 400+400 GeV). If the proton data would appear to scale at the SISR, then diffraction excitation contributes to a rise in σ_{tot} by virtue of Eq. (3), i.e. the linear increase of mass range excited with energy, by an amount given by

$$\sigma(s) = \frac{A}{\alpha'} \ln \frac{B - 2\alpha' \ln m_p^2/s}{B - 2\alpha' \ln M_{max}^2/s} \, , \qquad (4)$$

where A, B, and α' are constants, independent of s and known from ISR data on elastic and inelastic protons. Evaluating Eq. (4), using Eq. (3), leads to

$$\Delta\sigma_{tot} \sim 1.5 \text{ mb at the ISR (11+11 → 26+26 GeV)};$$

$$\Delta\sigma_{tot} \sim 1.5 \text{ mb at the SISR (100+100 → 400+400 GeV)} \, .$$

Hence the larger mass range covered by the SISR does not enlarge the rise of σ_{tot}. Therefore the accuracy in measuring the spectra and the luminosity must be similar to or better than what is currently reached at the ISR.

6. TOROIDAL MAGNETS AT SMALL ANGLES

The requirements implied by the extrapolations ISR → SISR above, can be met by an ensemble of four magnetic devices, two at small angles and two covering the larger angles over part of the solid angle. In this section the small-angle devices will be discussed briefly.

We consider two identical four-coil toroidal devices placed as closely as possible to the downstream arms of the "general-purpose" intersection, with azimuthally symmetric fields, varying inversely with the distance from the vacuum pipes. Their dimensions and electrical characteristics are fixed by the requirement of a 1-2% momentum measurement on a 1 mrad/400 GeV particle with two pairs of wire chambers (two before, two behind the toroid) for which we assume a position accuracy of dx = 0.3 mm. The resolution in momentum is then

$$\frac{dp}{p} = 10^{-3} \frac{p\sqrt{2}}{BL\ell} \, , \qquad (5)$$

where L = length of toroid (m),
  ℓ = spacing between chambers in each pair (m),
  B = field (T),
  p = momentum (GeV/c).

With a field of the form

$$B = \frac{0.02}{R \text{ (m)}} \text{ (T)} \, , \qquad (6)$$

a combination of parameters such as (see Figs. 11 and 12) L = 15 m, ℓ = 5 m, entrance at 28 m, satisfies the requirements on accuracy. The return coils are placed such that angles up to 25 mrad (i.e. the entire non-central region) are covered. Since we are interested only in processes with large cross-sections, say $\sigma_{inv} > 1$ µb/GeV², we have (Figs. 1 and 6)

$$\theta = 1 \text{ mrad} , \quad p_{max} = 400 \text{ GeV} , \quad \frac{dp}{p} = 1.3\%$$

$$\theta = 25 \text{ mrad} , \quad p_{max} = 80 \text{ GeV} , \quad \frac{dp}{p} = 6.7\% .$$
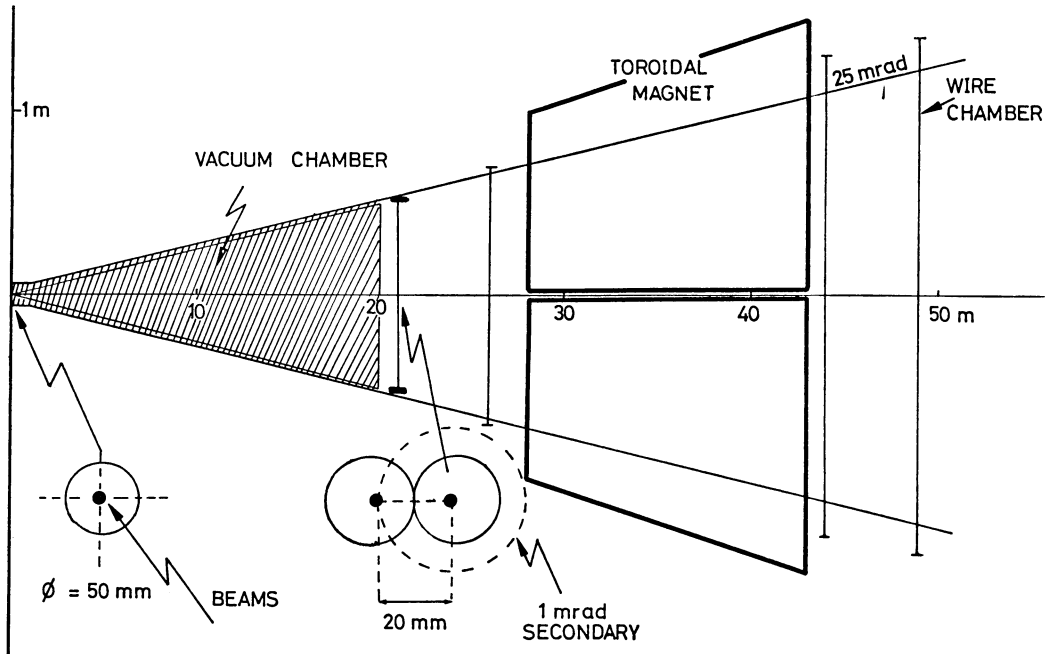
Fig. 11   Layout of a small-angle toroidal magnet set up for the SISR
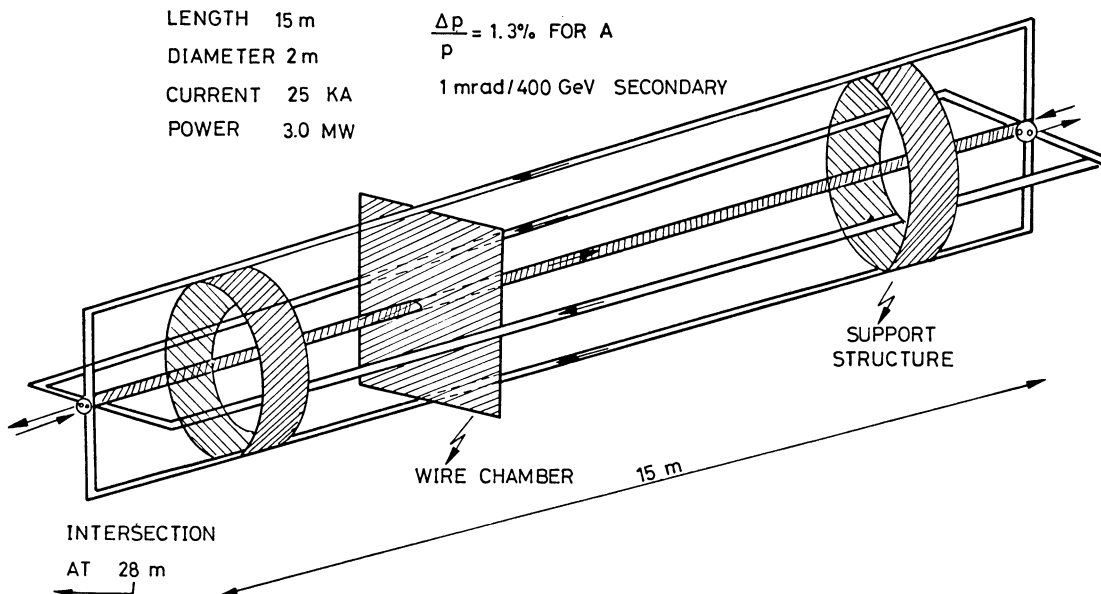
Fig. 12   Detail of the small-angle toroidal magnet for the SISR

This shows that, although not optimum, a field of the form $B \sim 1/\theta$ matches the physics requirements (highest accuracy at high momentum and low p_T, moderate accuracy elsewhere) sufficiently well. The diameter of the toroid is approximately 2 m.

The field of Eq. (6) requires 10^5 A turns. The power required is

$$P = \frac{3 \times 10^3}{nA} \text{ MW} ,$$ (7)

where n = number of coils, A = cross-sectional area per coil (mm^2). (It has been assumed that the return path has area = 10A.) For a current density of 100 A/mm^2 (i.e. maximum possible for "normal" cooling equipment) we have

$$P = 3 \text{ MW}$$

for a current-carrying area nA = 1000 mm^2.

It is a matter of detailed design how to distribute the current-carrying area around the downstream vacuum pipe. The main parameters are the crossing angle of the "general-purpose" intersection and the size of the vacuum chamber. One of the possible ways is sketched in Fig. 13. For a crossing angle of 1 mrad and a vacuum pipe of 2 cm diameter, and choosing four 20 $\times$ 20 mm^2 coils (current + water), one obtains azimuthal acceptances

$$\theta = 1 \text{ mrad} \qquad \Delta\phi = 0.40 \times 2\pi$$

$$\theta = 2 \text{ mrad} \qquad \Delta\phi = 0.77 \times 2\pi$$

$$\theta = 25 \text{ mrad} \qquad \Delta\phi = 0.98 \times 2\pi$$
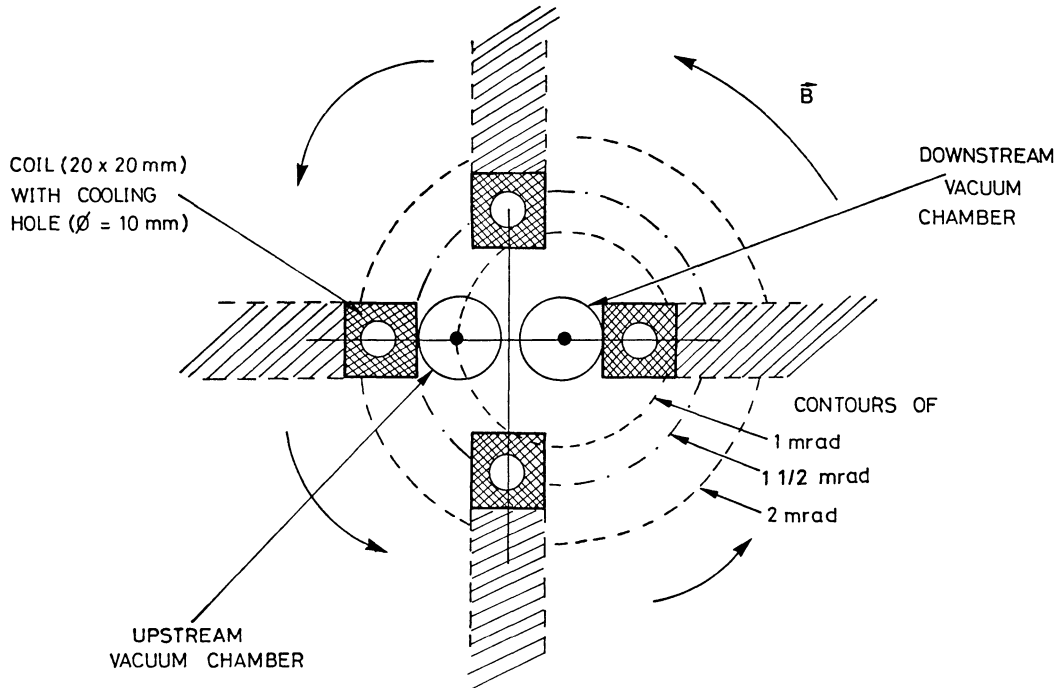
Fig. 13 Detail (entrance side) of the coil layout of the small-angle toroidal magnet for the SISR assuming a 1 mrad crossing angle.

in the configuration of Fig. 13. If the crossing angle were 10 mrad instead, the upstream beam would pass through the field of the toroid and hence require shielding or compensation. For a cylindrical iron shield, a wall thickness of well under 1 cm provides adequate screening of the upstream beam from the toroid field. Figure 14 illustrates the layout for a 10 mrad crossing angle.

Obviously a definitive design study should consider the toroid and the vacuum chamber as one unit.

From Fig. 8, and allowing for the reduction in acceptance due to the return coils, we obtain for the rate of inclusive events per mrad in θ and per GeV/c, for $L = 10^{31}$ cm^{-2} sec^{-1} in the case of a 1 mrad crossing angle:

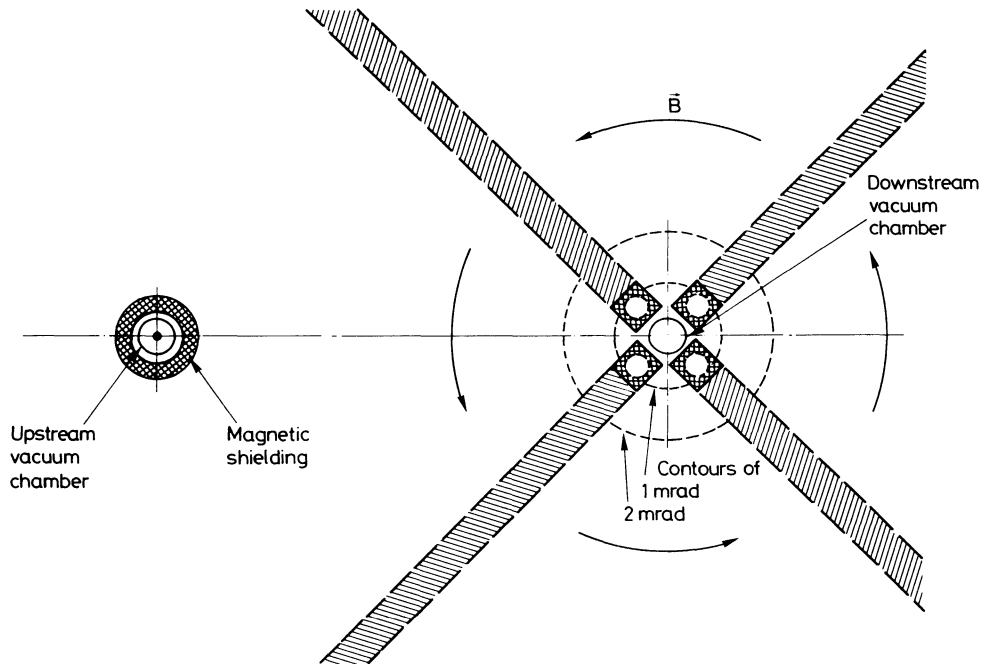| θ (mrad) \ p (GeV/c)	20	80	120	200	320
1	-	-	-	-	80
5	-	2×10^2	90	30	-
10	10^2	20	7	0.2	-
20	45	1	7×10^{-2}	-	-
25	30	0.3	8×10^{-3}	-	-

Fig. 14   Detail (entrance side) of the coil layout of the small-angle toroidal magnet for a crossing angle of 10 mrad

For a crossing angle of 10 mrad, similar figures are obtained.

As to particle identification by means of Čerenkov counters placed behind the toroid, it has been noted above that for p > 300 GeV virtually all particles are protons. Below 300 GeV, the need for identification of all or some of the tracks emerging at < 1° will depend on the experiment that is being performed. In examining the over-all properties of clusters, particle identification may be irrelevant, while for the reconstruction of particular final states identification will be indispensable. Furthermore, several investigations have been undertaken with the aim of obtaining increased light output from Čerenkov devices, resulting in a drastic shortening of the required path length in the gas. Shorter devices are obviously more easily built in a honeycomb structure as would be desirable in view of the high multiplicity in the toroid. For these reasons no detailed design has been attempted. One may anticipate that a space of approximately 5 m behind the last spark chamber would be sufficient for particle identification.

7. THE CENTRAL DETECTOR

As previously noticed, and in contrast with the forward cones, the situation at large angles is independent of s (of course within the validity of a straight extrapolation from the ISR data). Namely, we expect to produce of the order of two charged particles per unit of rapidity and per inelastic collision with a transverse momentum dependence as exp $(-6 \, p_T)$. As a first approximation we can therefore use the same types of central detectors as we have at the present ISR.

Recent progress in our understanding of high-energy collisions, however, suggests some minor conceptual modifications in the design. Let us recall it briefly.

The strong two-body correlation observed in the ISR range extends over ±1 unit of rapidity. It almost corresponds, in size and in shape, to groupings of particles similar to those which would be generated by some of the low resonances (ρ, ω, ϕ, etc.). These clusters, however, overlap so much that it is usually not possible to tell, event by event, from which cluster each particle originates. For this reason, while a 4π detector permits us to have at once an over-all view of the event, it does not give more information on the structure of the two-particle correlation functions than a pair of small solid-angle spectrometers would provide.

While we would advocate in an exploratory experiment the use of a 4π detector (streamer chamber or wire chambers) to obtain a general picture of the situation at large s, it would seem that progress is more easily achieved with a two-arm spectrometer providing momentum measurement and particle identification.

Let θ_{min} be the minimum production angle which can be reached by each spectrometer. Each one then spans a range from θ_{min} to $\pi - \theta_{min}$. We first remark that the exact location of the middle point (here $\pi/2$) of this angular range is irrelevant since we will in any case explore only a small part of the very long rapidity plateau. Concerning the angle between the arms, we would like to be able to reach up to $\sim$ 4 units of rapidity difference, which permits not only the study of the internal cluster structure but of correlations between neighbouring clusters as well. Also, in order to explore clusters with non-negligible (say up to 2 GeV/c) transverse momenta, it is necessary to be able to position the spectrometers either at opposite sides or at the same side of the beams at will.

The solid angle of each spectrometer can be as small as compatible with the production rate. With a luminosity $L = 10^{31}$, the single average rate is of the order of 10^3 particles per second and per centisteradian and the coincidence rate is of the order of 2 per second.

The above considerations suggest a design of the type sketched in Fig. 15. Figure 16 shows how a spectrometer of the type at present used by the British-Scandinavian Collaboration could fit in with such a design. Each spectrometer has a solid angle of 2×10^{-2} sr and provides p, π, K separation up to 6 GeV/c. With a 1 mrad crossing angle the diamond extends over about 1 m and is viewed with good efficiency. In the space above the beam plane we have added a large array of lead-glass Čerenkov detectors to permit observation of clusters or resonances with π^0's among their decay products.

LARGE ANGLE SPECTROMETERS
SCHEMATIC GEOMETRY
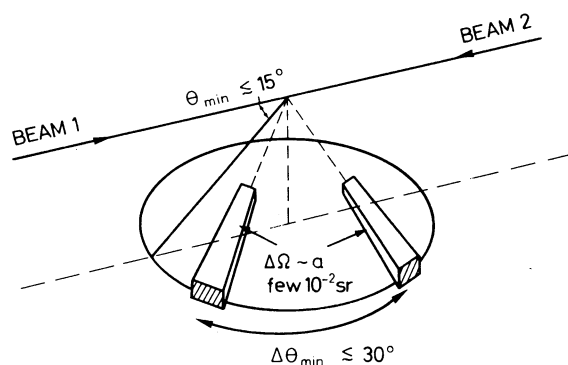
Fig. 15 Schematic geometry of a possible
large-angle spectrometers set up

SIDE VIEW
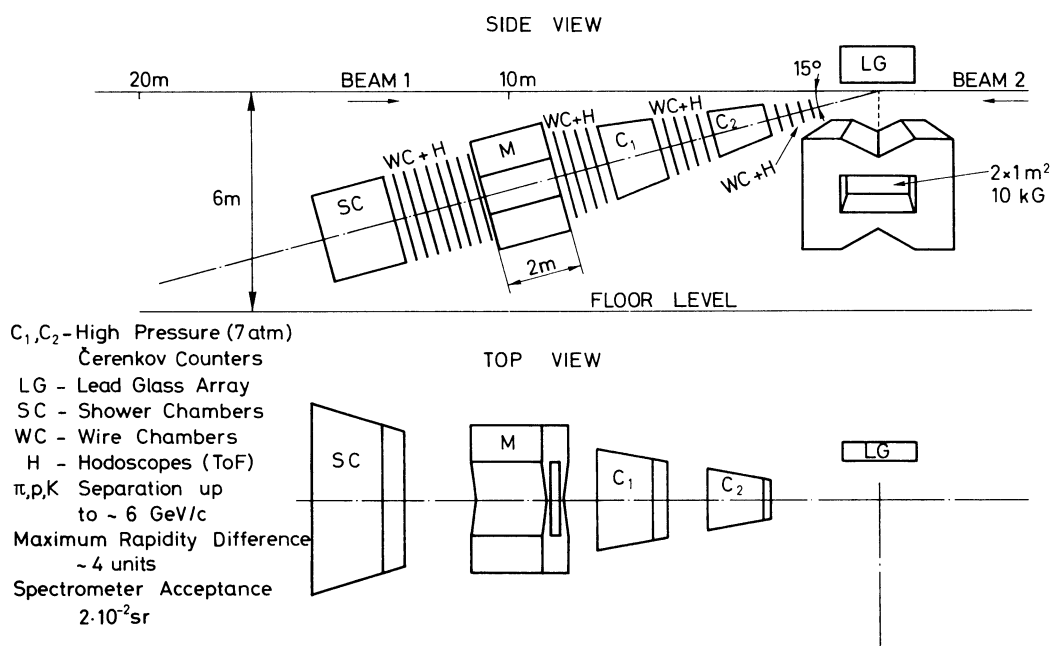
Fig. 16 Possible layout for a large-angle experiment including a
spectrometer of the type currently used at the ISR by the
British-Scandinavian Collaboration and a lead-glass array

8. CONCLUSIONS

It can be concluded that a general-purpose interaction, with crossing angle in the 1 to 10 mrad range, and length no less than ∿ 50 m along each downstream arm, is adequate for the study of multiple production processes in the SISR energy range.

Extrapolation from ISR data indicates that a set of four spectrometers, operated individually as well as linked together, is necessary to make a sufficiently extensive exploration of the one- and two-particle inclusive and semi-inclusive processes that make up most of the total cross-section at SISR energies.

Two of these spectrometers are to be located in the range 1-25 mrad. Azimuthally symmetric fields, strong near the vacuum pipes and weaker elsewhere, are best suited to the kinematics. It is highly desirable to design such devices together with the machine itself. The other two spectrometers, at large angles, can be of conventional design.

The system described is also suitable for the detection of new, stable, and charged particles, in particular in the mass range of 50 GeV and above.

A discussion with M.G. Albrow concerning the parametrization of ISR data is gratefully acknowledged.

* * *

REFERENCES

1) M.G. Albrow et al., Nuclear Phys. B73, 40 (1974).

2) B. Alper et al., Contribution No. 227 to the 17th Internat. Conf. on High-Energy Physics, London, 1974.

3) W. Ko et al., Contribution No. 437 to the 17th Internat. Conf. on High-Energy Physics, London, 1974.

4) M.L. Good and W.O. Walker, Phys. Rev. 120, 1857 (1960).

II.10 THE FEASIBILITY OF ANTIPROTONS IN THE ISR

K. Hübner, K. Johnsen and G. Kantardjian
CERN, Geneva, Switzerland

1. INTRODUCTION

The filling of the CERN Intersecting Storage Rings (ISR) with antiprotons was considered as early as 1962 [1]. The idea was to collect the antiprotons generated in a target by the ejected Proton Synchrotron (PS) beam.

O'Neill[2] had proposed to use antiprotons originating from antihyperon decay, and Van der Meer studied the feasibility of this scheme[3]. The antihyperons were supposed to be produced by an ejected PS beam impinging onto a target placed very close to the ISR aperture. Antihyperons would decay in the ISR aperture and some of the resulting antiprotons would continue to circulate in the ring.

In a preliminary study the numbers were updated, with the assumption that a 200 GeV/c proton beam from the CERN Super Proton Synchrotron (SPS) would be the primary beam[4], and the results of a more detailed investigation were published later[5] (the latter report will in what follows be referred to as "the previous report").

In the present report we update the numbers further, in particular assuming that we use a 400 GeV primary beam. We shall, however, also make use of the knowledge we have recently gained in various other respects, for instance on antiproton yield, instability problems, etc.

The present report has also the additional aim of probing some of the practical problems in order to see what hardware modifications and construction would be required and approximately what this would cost. In this way it should be possible to weigh cost and effort (and possible disturbance to other programs) against the richness and usefulness of a $p\bar{p}$ experimental program.

In one respect the present report is more limited than the previous one[5] as we concentrate only on filling the ring from an antiproton-producing target. The method using antihyperon decay we consider to be adequately covered by the earlier reports[2,3,5]. Possible methods involving cooling of the antiprotons[6] are considered to be outside the scope of this report.

2. PERFORMANCE

Trapping and stacking is performed as described in the previous report. From there we get, for the number of antiprotons in the stack, the formula

$$N_{\bar{p}} = \lambda_p \left(\eta_{ta} \frac{d^2N}{d\Omega dp} \frac{1}{r^2} \right) \left[\frac{\Delta p}{p} p \, 2R\pi \left(\frac{E}{\pi} \right)^2 \right] (\eta_t \eta_s) \pi \, , \tag{1}$$

where

λ_p is the line density in an SPS bunch

η_{ta} is the target efficiency

$d^2N/d\Omega dp$ is the yield per interacting proton

r   is the radius of beam spot

$\Delta p/p$ is the momentum bite of the stack

p   is the momentum at central orbit

$2R\pi$ is the circumference of the ISR

$(E/\pi)^2$ is the product of the transverse acceptances

η_t is the trapping efficiency in the ISR

η_s is the stacking efficiency in the ISR.

2.1 Parameters related to the SPS

Only one SPS parameter appears explicitly in expression (1), i.e. the line density λ_p, which should be made as high as possible. For this reason it was proposed in the previous report to eject the PS pulse at the end of acceleration without further manipulations and to trap the beam in the SPS in those 200 MHz buckets which happen to overlap with the 20 individual PS bunches[7]. Thus only a few SPS buckets would be filled and the bunch train would occupy only $1/11$ of the SPS circumference, forming there 20 groups of about 4 bunches with gaps of about 17 empty buckets between them. However, this mode of operation involves very high instantaneous beam loading and was not included in the design of the SPS RF system. Though possible in principle, it requires important additions and modifications to the SPS RF system, which would involve considerable cost.

Since the objective is to study the feasibility of an antiproton scheme which is based as much as possible on existing equipment, a solution should be found which makes the beam loading acceptable to the present SPS RF system with little or no modification. The proposal is to fill all the buckets uniformly on $3/11$ of the SPS circumference. The uniform filling avoids longitudinal modulation reflecting PS bunch structure and creating the 9.5 MHz side-bands around the 200 MHz. Distribution over a larger fraction of the circumference reduces the smaller side-bands from the SPS revolution frequency. In the following we concentrate on this scheme where a maximum of performance can be obtained with acceptable modifications to the low-level RF system of the SPS.

The proposed scheme assumes that the beam is ejected in three turns from the PS at 10 GeV/c during acceleration. The beam occupying $3/11$ of the SPS circumference after injection is left coasting until it is debunched. Subsequently, it is trapped adiabatically by the SPS RF system at 200 MHz. We assume that the momentum spread of the injected beam is adjusted such that the beam is stable in the presence of the coupling impedance $|Z/n| = 600\ \Omega$ of the SPS during the debunching process. This impedance comes mainly from the accelerating structure, which has a response time such that it does not see the bunch structure, but it does see the $3/11$ versus $8/11$ structure on the circulating beam. This means that the momentum spread, determined by the stability criterion expression[8], is arrived at by averaging the current over the filled bunch train. With a PS current of 0.75 A (i.e. 1×10^{13} protons per pulse), the average current for stability calculations is 0.25 A, and stability is reached when the momentum spread (HWHH) is

$$\frac{\delta p}{m_0 c} = 7.4 \times 10^{-3}$$

Assuming a parabolic distribution, we get a full width of the debunched beam of

$$\frac{\Delta p}{m_0 c} = 2\sqrt{2} \; 7.4 \times 10^{-3} = 2.1 \times 10^{-2} \; ,$$

and a bunch area, after adiabatic trapping, of

$$A_{SPS} = 0.132 \text{ rad} \; .$$

At top energy of the SPS and with the RF at its maximum value (i.e. 3.6 MV) and flat top, the length of such a bunch becomes 0.84 nsec.

Assuming 50% trapping efficiency in the SPS we find that each bunch carries

$$N_b = 0.4 \times 10^{10} \text{ protons} \; ,$$

and the line density averaged over one bunch becomes

$$\lambda_p = 1.58 \times 10^{10} \text{ m}^{-1} \; .$$

A few comments should be made. There may be high-frequency coupling impedances not covered by the above analysis. The theory for these is not very well advanced and the property of the SPS in this respect not yet very well known. However, assuming that such impedances in the SPS are not much different from the ones in the ISR, we can conclude from ISR experience that we should be safe.

It should also be mentioned that ways may be found in the future to reduce the 600 Ω coupling impedance or to suppress the instability by other means. This will improve on the line density, but not very much; λ_p is inversely proportional to the square root of the momentum spread after debunching. The stability criterion[8] shows that the necessary momentum spread is proportional to the square root of the coupling impedance. Therefore, λ_p becomes inversely proportional to only the fourth root of assumed coupling impedance.

Lastly, it should be noted that, since the circumference of the ISR is only one half of the length of the bunch train, only about 630 of the 1260 bunches can be injected in the ISR. The rest, still containing $\frac{1}{2} \times 0.5 \times 10^{13}$ particles, can be disposed of otherwise. Thus, in principle, the physics program of the SPS does not need to be interrupted during a fill of the ISR with antiprotons.

2.2 Parameters related to the p̄-producing target

All parameters related to the target are within the first bracket of Eq. (1), and we shall analyse each of them in some detail.

2.2.1 *Antiproton production*

Data on antiproton production from 400 GeV protons are not directly available. However, in order to estimate such a yield we used some results obtained in single-particle production experiments at the ISR.

In a first step we collected data on the measured differential cross-sections expressed in the Lorentz-invariant form:

$$E \frac{d^3\sigma}{dp^3} = \frac{E}{p^2} \frac{d^2\sigma}{dpd\Omega} = f(p_T, x)$$

where E, p, and p_T are the energy and the longitudinal and transverse momenta of the detected antiproton. The Feynman x-variable is defined as

$$x = \frac{2p^*}{\sqrt{s}} ,$$

where p^* is the longitudinal momentum of the antiproton in the centre-of-mass system, and s is the square of the total energy in the centre-of-mass system.

The data were extracted from several reports[9-14] for values of x between 0 and 0.4 and for values of p_T between 0 and 0.35 GeV/c.

Then all the values of the invariant cross-section $f(p_T, x)$ were extrapolated to $f(0, x)$ which gave a distribution of the invariant cross-section as a function of the variable x for the antiprotons produced in the forward direction. Hence we plotted the yield of antiprotons as

$$\frac{d^2N}{dpd\Omega} = f(0, x) \frac{p^2}{E} \frac{1}{\sigma_{tot}} ,$$

with p^2/E = 28 GeV/c^2 and the total cross-section $\sigma_{tot} \sim$ 40 mb.

Measurements of the antiproton production carried out with 200 and 300 GeV protons at FNAL with a beryllium[15] or an aluminium[16] target fit approximately the above distribution.

The value of x for antiprotons of 28 GeV/c generated by 400 GeV/c protons is

$$x = \frac{2p^*}{\sqrt{s}} = 53 \times 10^{-3}$$

where the square of the total c.m. energy s = 752 GeV^2, and the longitudinal momentum of the 28 GeV/c antiproton in the c.m. system, p^* = 0.72 GeV/c.

Finally, with this value of x, the yield of antiprotons is

$$\frac{d^2N}{dpd\Omega} = 0.84 \text{ sr}^{-1} \text{ (GeV/c)}^{-1} \text{ per interacting proton.}$$

A similar computation[17] for primary protons of 200 GeV/c gives a yield of 0.45 sr^{-1} (GeV/c)$^{-1}$ per interacting proton.

2.2.2 *Target efficiency*

Expression (1) shows that the number of captured antiprotons is inversely proportional to the beam spot area at the target, which implies that a small beam spot is imperative. In our case the radius can be made as small as 0.5 mm by using available quadrupole lenses to focus the primary beam[18]. Consideration of nuclear collisions in the target show that the optimum target length equals the collision length. The yield is reduced by a factor 1/e if this condition is fulfilled. Since the non-zero target length destroys the perfect match between target and beam, a target material of short collision length has to be used. Tungsten with a collision length of 5.6 cm was chosen. Knowing length ℓ and radius r of the target, the geometrical efficiency η_g can be worked out. The general formula is

$$\eta_g = \left\{ 1 - \frac{2}{\pi} \left[\arctg y - \frac{1}{y} \ln (1 + y^2) \right] \right\}^2 .$$

If the beam is matched to the middle of the target

$$y = \frac{E}{\pi} \frac{\ell}{2r^2} .$$

For our parameters $y = 1.1$; $\eta_g = 0.85$.

The ratio $\eta_{ta}(r)/r^2$ is not yet at a maximum for $r = 0.5$ mm. Thus, further lowering the radius of the beam spot would still be beneficial if ways of doing this can be found. This geometrical target efficiency did not appear in the previous report as the assumed spot radius was 1 mm implying a geometrical efficiency close to 1.

The total target efficiency becomes

$$\eta_{ta} = \frac{0.85}{e} = 0.31 .$$

Beam broadening by multiple scattering can be neglected for the primary as well as for the secondary beam.

2.3 Parameters related to the ISR

The rest of the parameters are related to the ISR and most of them can be listed without much comment:

$$\Delta p/p = 0.02$$

$$p = 28 \text{ GeV/c}$$

$$R = 150 \text{ m}$$

$$(E/\pi)^2 = 10^{-10} \text{ rad}^2 \text{ m}^2$$

$$\eta_t = 0.35$$

$$\eta_s = 0.5 .$$

The last two parameters were analysed in some detail in Ref. 5. We have chosen the trapping efficiency resulting from the basic sinusoidal RF system. Theoretically some improvement is possible by adding higher harmonic cavities. However, the RF handling will pose some very serious technical problems[19]. It will be very difficult to detect the feeble bunches for the phase-lock system which has to centre the RF buckets on them with an accuracy of about 10 mrad, and which has to keep track of them during stacking. In fact, some new development will be needed on the low-level part of the RF system to meet these requirements. For such reasons we feel we should not assume the highest theoretical efficiency but use the value quoted.

2.4 Resulting antiproton current and luminosity

We have now all the elements to evaluate $N_{\bar{p}}$ from Eq. (1). We recall them here:

$$\lambda_p = 1.58 \times 10^{10} \text{ m}^{-1}$$

$$\eta_{ta} = 0.31$$

$$d^2N/d\Omega dp = 0.84 \ sr^{-1} \ (GeV/c)^{-1}$$

$$r \qquad = 0.5 \ mm$$

$$\Delta p/p \qquad = 0.02$$

$$2\pi R \qquad = 940 \ m$$

$$(E/\pi)^2 \quad = 10^{-10} \ rad^2 \ m^2$$

$$n_t \qquad = 0.35$$

$$n_s \qquad = 0.5$$

This gives

$$N_{\bar{p}} = 4.76 \times 10^8 \ ,$$

which corresponds to an antiproton current of 24 μA.

For a proton current of 30 A in the other ring and an effective beam height of 13 mm determined by the antiproton inflector, the luminosity becomes

$$L = 5.5 \times 10^{24} \ cm^{-2} \ sec^{-1} \ .$$

This number is close to the one worked out in Ref. 5. A comparison of the parameters shows that the higher yield, the smaller beam spot, and the fact that we can now assume a 30 A proton beam compensate for the loss of a factor of 8.5 in SPS line density.

If one uses a primary beam of 200 GeV/c the luminosity is a quarter of the luminosity quoted above.

In the ISR there is at present a low-β insertion that could improve the $p\bar{p}$ luminosity by a factor of about 2 in this crossing. Similarly, if the ISR later becomes equipped with a superconducting low-β section, the improvement factor may be as high as 5 or 6. In evaluating the usefulness of these insertions for $p\bar{p}$ physics it should be kept in mind that the low-β insertion is unsuited to small- and medium-angle experimentation.

Contamination by other particles is negligible. The biggest contribution comes from the muons generated by decaying pions. Their current is only 14% of the antiproton current and their lifetime corresponds to 185 turns.

If the existing ISR RF system is used, we need about 1100 SPS pulses to build a stack of antiprotons. It will take 110 minutes for an SPS cycle of 6 seconds. The current stacked per cycle is very low, only 22 nA, i.e. 4×10^5 antiprotons per pulse.

Since the incoming beam has a 200 MHz structure we might think of using a 200 MHz system in the ISR. It would reduce the number of stacking cycles and the stacking time by a factor of ∿ 20. The current stacked per cycle would be around 400 nA.

It is open to question whether such an investment is worth while just for a reduction of the stacking time. However, it may turn out that the RF beam-handling is eased with a 200 MHz system. We can work with larger currents and hence not be confused with the 400 bunches injected but not used, as is the case with the 9.5 MHz RF system.

Luminosity measurements may be very difficult with such low beam currents and large vertical beam dimensions. For instance, the Van der Meer method cannot be used with normal beam dimensions. However, this method may still be used with a scraped $\bar{p}$ beam for calibration of monitors.

If destructive luminosity measurements have to be frequently used, the reduction of the filling time that a 200 MHz RF system can give may become very desirable.

3. POSSIBLE LAYOUTS FOR THE TRANSFER LINE

The layout of the transfer line between the SPS and the ISR is determined mainly by:

  i) the position and orientation of the SPS and ISR beams;
 ii) the junction of the transfer tunnel with the existing buildings.

The SPS extraction system in the long straight section 6 deflects the protons into the TT60 beam line. Starting from the ejection point there are two alternatives for the location of the branching off[20]:

a) Branching off from the external SPS proton beam between the quadrupoles QTLF 610200 and QTLD 610300 and joining the PS-ISR transfer line TT1 near the ISR as shown in Fig. 1 *(scheme A)*. The TT1 transfer line feeds ring 2 of the ISR.

The *characteristics* of this line would be:

- total length between TT60 and TT1	660 m
- horizontal angle between TT60 and this line	+25 mrad
- horizontal angle of the first bend	+43°
- horizontal angle of the second bend	-52°
- difference in level of floor SPS and TT1	32 m
- vertical bending angles	58 mrad

This transfer line would consist of four sections:

   i) the branching off from TT60, including matching and the target (about 140 m);
  ii) the first horizontal bend of 43°;
 iii) the long distance transfer (about 320 m);
  iv) the second horizontal bend of 52° and injection in TT1.

The main difficulty in this scheme lies in the civil engineering work for opening the TT60 tunnel.

b) Branching off between QTSF 620200 and QTSD 620300, about 92 m downstream of the switchyard for the neutrino beam and injecting in Ring 1 of the ISR at the level of straight section 533 as shown in Fig. 2 *(scheme B)*.

The *characteristics* of the transfer line would then be:

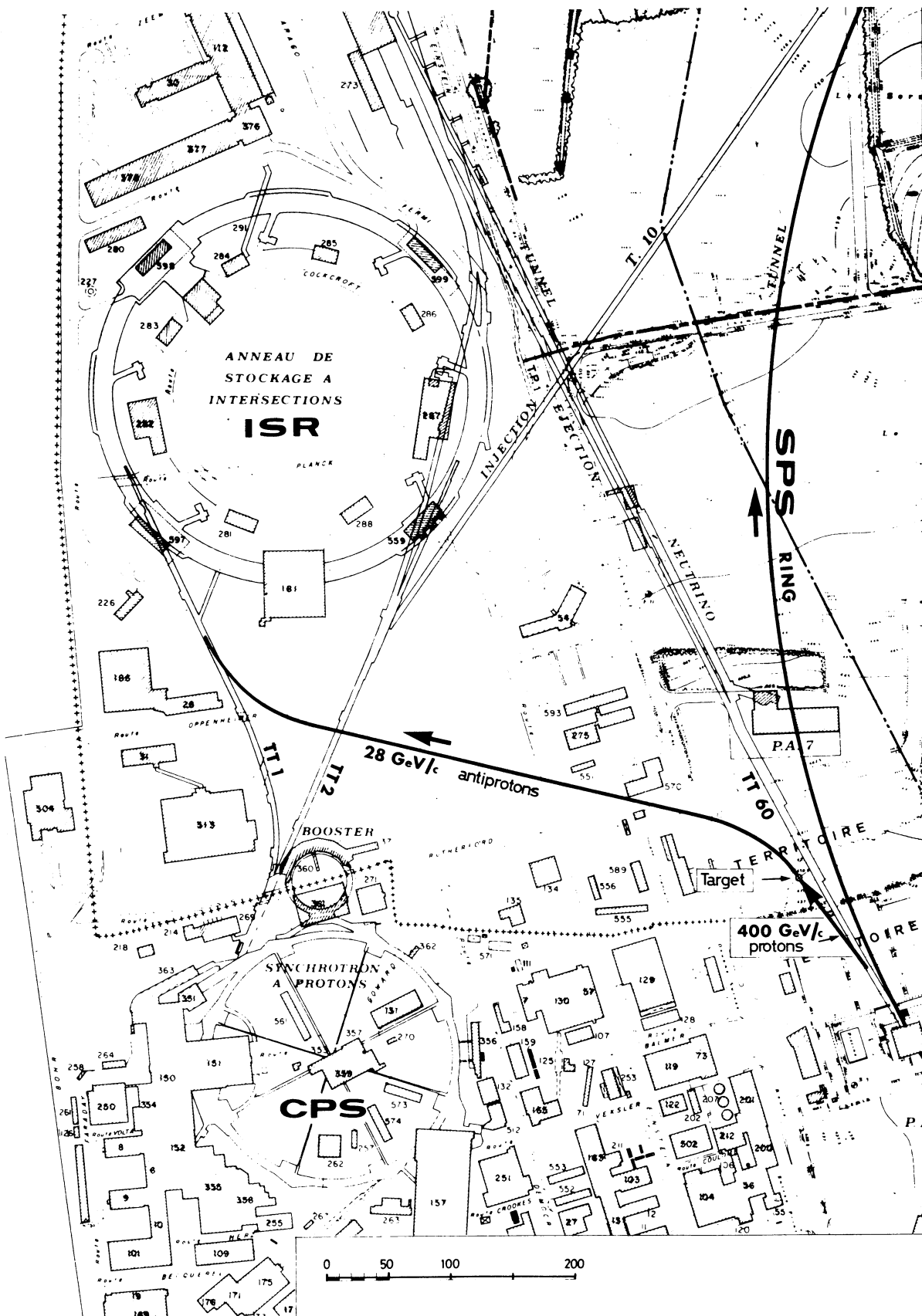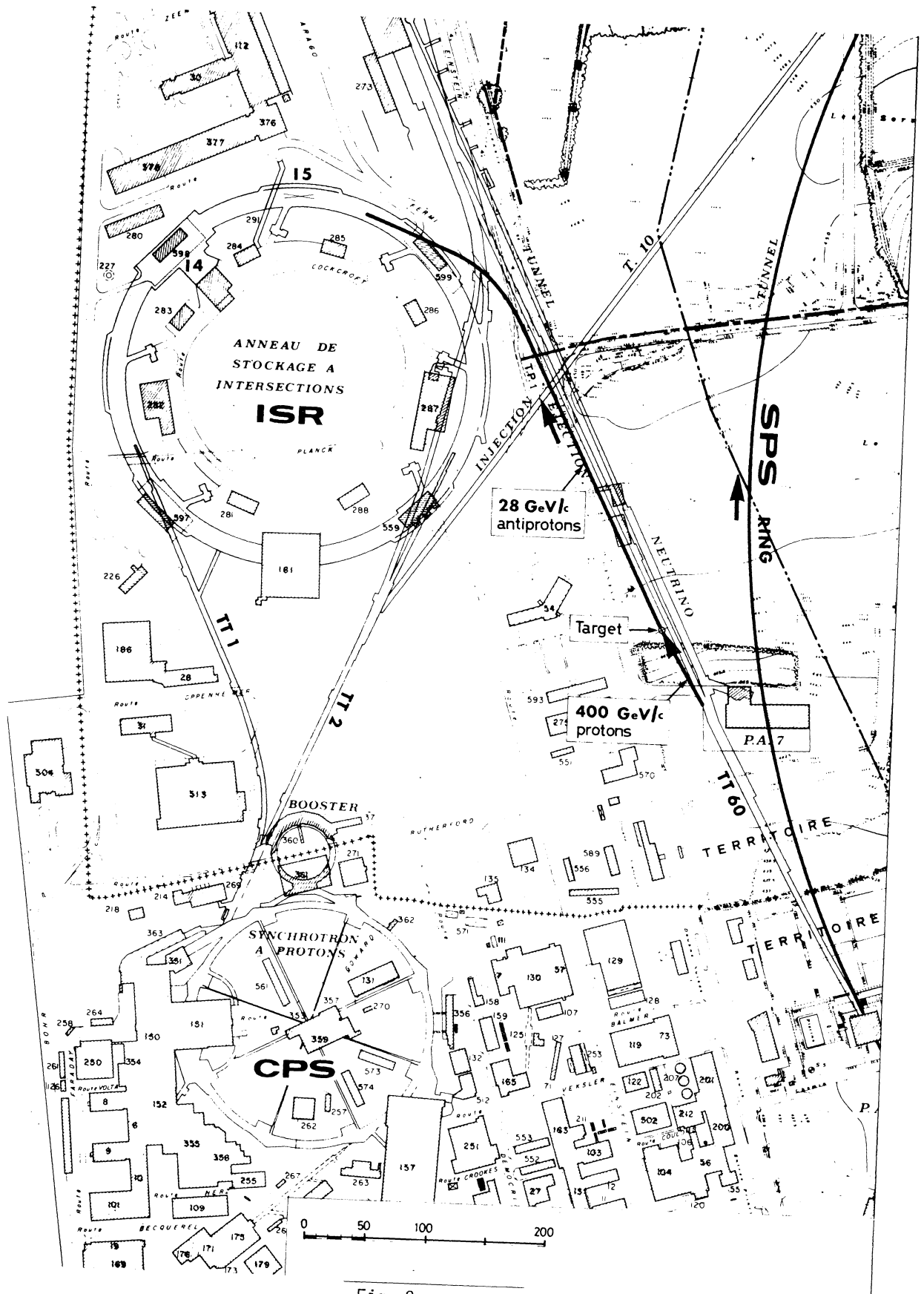|	
- total length between TT60 and ISR	560 m
- horizontal angle between TT60 and the line	+25 mrad
- horizontal angle of the first bend	-35 mrad
- horizontal angle of the second bend	+40°
- difference in level of floor TT60 and ISR	35 m
- vertical bending angles	67 mrad

Fig. 1   Scheme A

Fig. 2 Scheme B

The line would consist of four sections:

    i) the branching off from TT60, including the matching, the target, and the horizontal bend of 35 mrad (about 120 m);

    ii) the long straight part of the transfer (about 300 m);

    iii) the main horizontal bend of 40°;

    iv) the injection into the straight section 533 of the ISR.

The main work would then be opening a hole in octant 5 of the ISR.

4. BEAM TRANSPORT AND TARGETING

4.1 Primary 400 GeV/c proton beam[20]

The eight pulsed bending magnets required for the branching off from the proton beam to the West Area should be similar to the switching magnets foreseen for the neutrino beam. About ten standard SPS quadrupole magnets will focus and match the 400 GeV/c proton beam between the switchyard and the target.

Extraction with the layout of scheme B requires the replacement of quadrupoles QTSD 620100 and QTSF 620200, operating at 200 GeV/c, by long quadrupoles operating at 400 GeV/c.

4.2 The target

A pencil-like target of a diameter of 1 mm and a length of 5.6 cm made of tungsten is required. The thermal effects which occur in targets when irradiated by a fast SPS beam of 400 GeV/c with 10^{13} protons per pulse have been studied[21]. In these conditions the maximum temperature rise in a target of tungsten will exceed the melting point. An automatic replacement of the target after each SPS pulse corresponding to a repetition rate of 6 seconds should be designed.

It should be mentioned that in the ISABELLE design at BNL[22] a $p\bar{p}$ scheme is envisaged in which the target would be made of iridium and replaced after each pulse.

4.3 Antiproton beam transport

The antiproton beam emerging from the target is matched to the long distance transport channel. The characteristics of this transport channel could be very similar to the characteristics of the existing transfer lines TT1 and TT2 between the CPS and the ISR.

In this case a total of 62 quadrupoles (31 F + 31 D) is required for scheme A or a total of 48 quadrupoles (24 F + 24 D) is required for scheme B. The F and D quadrupoles are separately powered in series, with the exception of the first three quadrupoles at both ends which are powered separately for the required matchings. All the quadrupoles are operated d.c.

All the various horizontal and vertical bends along the transfer line could be achieved with a conventional magnet, 2.5 m long and operating at 1.4 T. The number of horizontal and vertical bending magnets would then be 48 and 4, respectively, for scheme A; 21 and 4 for scheme B.

5. THE INJECTION SYSTEM IN THE ISR

The antiprotons will be injected into the ISR by a fast kicker at the injection orbit ordinarily used for protons.

Scheme A makes use of the existing injection system of Ring 2. For scheme B it is intended to make use of the two existing spare kickers as well as their pulse-forming network[23]. A pair of injection septum magnets will have to be built,which could be copies of the existing ones.

In order to match the transverse acceptances of the beam transport system, it will be necessary to use the tuning quadrupoles scheme[24] in the ΔQ_V and $\Delta Q_H > 0$ mode. In this mode the relevant optic parameters[25] are at the kicker $\beta_V = 10.3$ m, $\beta_H = 42.9$ m, and at the septum $\beta_H = 17$ m, $\alpha_p = 1.68$ m. With the existing kickers[26] having a horizontal aperture = = 44 mm and a vertical aperture = 19 mm, we would then achieve a vertical acceptance $E_V = 8.8\pi \times 10^{-6}$ rad m and a horizontal acceptance $E_H = 11.3\pi \times 10^{-6}$ rad m. The product of the two acceptances is then $E_V \cdot E_H = 100\pi^2$ $(10^{-6}$ rad m$)^2$, a value which is used in the calculation of the antiproton current.

For scheme B, one Terwilliger quadrupole and one skew quadrupole with enlarged aperture will have to be built, as well as some vacuum components such as a sector valve and magnet vacuum chambers.

6. SUPPLIES AND BUILDINGS

6.1 Electricity - water cooling

As the TT2a transfer line is no longer in operation, the electricity power and the water-cooling capacities available should be enough for the proposed transfer line.

6.2 Auxiliary buildings

The space available in buildings BA6 and BA7 of Laboratory II[27] and in buildings A5 and A7 of the ISR should be enough to locate the power supplies of the beam transfer line.

7. TIME SCHEDULE AND COST ESTIMATES

7.1 Time schedule

The program for the *civil engineering work*[28] will depend very closely on the operation of the SPS and the ISR. Schemes A and B have also different requirements (see Table 1).

Table 1

Time schedule

Scheme	Tenders, etc.	Construction	Total
A	6 months	10 months including: - shutdown of 1 month for junction with TT1 - shutdown of 5.5 months for junction with TT60	16 months
B	6 months	10 months including: - shutdown of 4 months for junction with ISR - shutdown of 1.5 months for junction with TT60	16 months

The program for the *beam transfer system*[20] should be completed within a period of three to four years including the installation and tests.

It seems that all the other components including the ISR injection system for scheme B can be provided within the time required for the magnets of the beam transfer system.

Concerning the *ISR shutdown for scheme B*, two weeks for removing the equipment should precede the construction work of four months, and about five weeks of reinstallation work[29] should be added after the four months. Total shutdown for the ISR comes to about 24 weeks.

7.2 Cost estimates

The cost estimates of the two schemes are given in Table 2 which indicates the breakdown according to functional elements. (CERN staff cost is not included.)

Table 2

Cost estimates

Items	Scheme A (MSF)	Scheme B (MSF)
Civil engineering work[28]	6.21	4.63
Branch-off from SPS (incl. switching, 400 GeV transfer, and target)[20]	5.00	5.35
Injection system in the ISR	0.00	2.00
Bending magnets for 28 GeV/c transfer line	7.80	3.75
Quadrupoles for 28 GeV/c transfer line	2.48	1.92
Vacuum system for 28 GeV/c transfer line[30]	0.42	0.37
Power supplies for 28 GeV/c transfer line[31]	2.50	2.00
Supports for 28 GeV/c transfer line	0.67	0.43
Cooling for 28 GeV/c transfer line	0.40	0.30
ISR computer modifications[32]	0.20	0.20
Beam observation equipment	0.50	0.40
Cables - electricity supply in tunnel - modifications to the ISR[29]	0.52	0.65
Total (MSF)	26.70	22.00

8. CONCLUDING REMARKS

Optimists will find a few possibilities for raising the luminosity beyond the quoted figure, and a few such possibilities have been listed. Likewise, pessimists will find reasons for wanting a lower figure as a basis for the further considerations, and some of these reasons have also been mentioned in the report.

It is our feeling that, although we admit considerable uncertainties in both directions, a $p\bar{p}$ luminosity of 5×10^{24} cm^{-2} sec^{-1} is as realistic an estimate as can be made with present knowledge. We therefore recommend this figure to be used as a basis for the further analysis of a possible physics program, and the richness of this program should then be weighed against the quoted cost as well as the inconveniences caused to other programs.

* * *

REFERENCES

1) K. Johnsen, CERN-AR/Int. SG/62-11 (1962).

2) G.K. O'Neill, Princeton-Pennsylvania Accelerator Report PPAD 415 D (1961).

3) S. Van der Meer, CERN/ISR-PO/70-5 (1970).

4) K. Hübner et al., CERN/ISR-TH/72-16 (1972).

5) K. Hübner, CERN/ISR-TH/73-19 (1973).

6) G.I. Budker, Atomic Energy, Vol. 22, No. 5 (1967).
   Ya.S. Derbenev and A.N. Skrinskij, IYAF Preprint No. 255 (1968) [CERN Translation 69-18 (1969)].
   S. Van der Meer, CERN/ISR-PO/72-31 (1972).
   P. Bramham et al., Nuclear Instrum. Methods 125, 201 (1975).

7) D. Möhl, Spring Study on Accelerator Theory 1972, CERN/AMC-1, p. 249.

8) E. Keil and W. Schnell, CERN/ISR-TH/RF/69-48 (1969).

9) B. Alper et al., Phys. Letters 47B, 275 (1973).

10) P. Capiluppi et al., Nuclear Phys. B79, 189 (1974).

11) P. Capiluppi et al., Nuclear Phys. B70, 1 (1974).

12) A.M. Rossi et al., Nuclear Phys. B84, 269 (1975).

13) M.G. Albrow et al., Nuclear Phys. B56, 333 (1973).

14) U. Amaldi et al., Studies of particle production in the forward direction at the ISR (to be published).

15) W.F. Baker et al., NAL-Pub-74/13-Exp 7100.104 (1974).

16) B. Aubert et al., Fermilab. Conf. 75/31, Exp 7300.001 (1975).

17) J.C. Sens, Phenomenology of particles at high energies (Academic Press, Inc., New York, 1974), Chapter 2.

18) L. Evans, private communication (1975).

19) S. Hansen, private communication (1975).

20) B. de Raad, private communication (1975).

21) W. Kalbreier, W.C. Middelkoop and P. Sivers, CERN Lab. II/BT/74-1 (1974).

22) C. Baltay et al., Proc. 9th Internat. Conf. on High-Energy Accelerators, Stanford, 1974, p. 572.

23) H. O'Hanlon, private communication (1975).

24) J.P. Gourber and C. Wyss, CERN ISR-MA Memorandum, 4.11.1974.

25) C. Wyss, private communication (1975).

26) A. Knezovič and B. de Raad, CERN ISR-BT/71-24/Vol. III.

27) W.C. Middelkoop, private communication (1975).

28) Studies by B. Bianchi, CERN (1975).

29) C. Desmaris, H. Laeger and G. Leroy, private communications (1975).

30) G. Chapman, private communication (1975).

31) H.W. Isch, private communication (1975).

32) P. Wolstenholme, private communication (1975).

II.11 STUDY OF EXPERIMENTAL POSSIBILITIES OF p̄p COLLIDING BEAMS

U. Amaldi, P. Darriulat, E. Lohrmann and A. Minten

CERN, Geneva, Switzerland

1. INTRODUCTION

This note intends to discuss

i) some of the interesting physics which could be done with antiprotons stored in the ISR, and

ii) some investigations into the difficulties and prospects of doing experiments with antiprotons stored in the machine.

Apart from the obvious physics interest, this note was prompted by the investigation of the technical feasibility of storing antiprotons[1] and the prospect of having the SPS as a powerful injector of antiprotons. We shall base our considerations on the luminosity estimate of 10^{25}-10^{26} cm^{-2} sec^{-1} given by Hübner[2], and shall return to the question of luminosity later.

2. PHYSICS

With a luminosity of 10^{25}-10^{26} the following experiments appear feasible as far as counting rate is concerned:

i) Measurement of the total cross-section:
According to present-day expectations [see, for example, Bourrely and Fischer[3]], the p̄p cross-section is expected to have a minimum at about 300 GeV and then rise like the pp cross-section. In order to see this rise clearly, an accuracy of about 3% will be necessary. Total event rate $\sim$ 0.1-1/sec.

ii) Elastic scattering:
This is obviously connected with (i). Total event rate $\sim$ 0.1-1/sec.

iii) Inclusive particle distributions, multiplicity and multiplicity distribution; two-particle correlations.

iv) Study of annihilation events:
If we assume that at least the order of magnitude of the p̄p annihilation cross-section is given by the difference of p̄p and pp total cross-sections, we expect $\sigma_{annih} \approx$ 1 mb at 1500 GeV. This should be enough to see this process, e.g. in a streamer chamber. There may be a dramatic qualitative difference between annihilation and non-annihilation events at that energy, e.g. an increase of average multiplicity with c.m.s. energy like $\sqrt{E^*}$, leading to very high multiplicities. Estimated total event rate $\sim$ 0.5-5/minute.

3. BACKGROUND STUDIES

The luminosity of p̄p operation is down compared with pp by a factor of 10^4-10^5. The question is therefore whether one can detect p̄p events at all against a background of beam-gas events from the circulating high proton current in one ring. In order to study this, data were taken at the ISR with one beam only in the machine. This should imitate, as far as possible, the background conditions to be expected in a p̄p run. The vacuum conditions at these runs were fairly typical of normal operation. The proton beam current for most studies was about 3 A.

Results

1) With "minimum bias" trigger in the split-field magnet (SFM):

   A tape was written by the CERN-Hamburg-Orsay-Vienna (CHOV) Collaboration using as trigger the condition GEO1·GEO2, meaning a coincidence of the proportional chambers in two forward arms of the SFM detector. This trigger sees 60%-80% of the total cross-section.

   The trigger rate was 80/sec. Adding a timing requirement (16 nsec width) from two counters T1·T2, which see 50%-70% of the total cross-section, reduces the trigger rate by a factor of > 100.

   With the simple geometrical trigger GEO1·GEO2 with a rate of 80/sec, and requiring at least one track on either side of the interaction zone, the pattern recognition program MARC accepted 7.1% of these triggers. This sample was then passed through the geometry program NICOLE, which requires a reconstructable vertex. No event was found in a total observation time of 50 sec. The number of p̄p events to be expected in the same time is ∿ 20. So the ratio background/events is probably < 0.1.

2) Observations with the streamer chamber:

   The trigger used essentially the fast coincidence of two large (1.5 × 1.5 m²) arrays of scintillation counters in each arm, seeing 90% of the inelastic cross-section. With a trigger rate of 20/sec, 250 streamer chamber pictures were taken, corresponding to an equivalent observation time of 12 sec. None of these pictures showed an acceptable vertex in the interaction region. Again the conclusion is that the background is much smaller than the expected event rate.

Conclusion: It appears possible to suppress beam-gas background sufficiently, provided at least part of the event and the vertex are reconstructed with good accuracy. The trigger condition must be sharpened in order to come down to a trigger rate of less than a few per second. Observations in I 7 during these runs with a simple scintillator telescope indicate that this can very likely be achieved. Also a thinner vacuum chamber would help.

3) Special trigger at the SFM:

   A tape was written by the CHOV Collaboration using their special trigger for elastic events. This trigger, used at 11 GeV, sees about 3% of the elastic cross-section. The trigger rate was 0.4/sec. In a total observation time of 670 sec, 250 triggers occurred leading to 1 reconstructable event.

4) Small-angle scattering experiment in I 8:

   Observations were made with the experiment R802 set up to observe very small angle scattering. A run was made with one beam of 4.3 A at 15.5 GeV. In 300 seconds of observation time no elastic trigger was observed. For comparison, at a luminosity of 5×10^{29} cm⁻² sec⁻¹ we expect in the same time 6000 events, which translates to 0.6 events at $L = 5 \times 10^{25}$.

Conclusion: Observation of elastic p̄p scattering seems quite feasible. As far as counting rates go, it should be noted that, for example, the solid-angle acceptance of R802 could be improved by a factor of about 4, leading then to counting rates of about 0.5/min.

4. MONITORING

It is realized that measuring the luminosity will be a major problem. Two ways of attacking this problem are suggested here:

4.1 Self-calibration of the experiments

This method, which has been used and is continuing to be used, requires ideally both small-angle elastic scattering and total cross-section in an almost 4π solid angle apparatus to be done in the same intersection region. By the optical theorem the extrapolated elastic forward cross-section is

$$\left(\frac{d\sigma}{dt}\right)_0 = \frac{1}{16\pi}\,\sigma^2_{tot}\ ,$$

i.e. it depends on σ^2_{tot}, in contrast to the rate in a straightforward σ_{tot} measurement. The luminosity can therefore be eliminated between two such experiments.

4.2 Use of a thin carbon fibre for monitoring beam position, beam profile and intensity

This method was and is still used at the CEA and DESY storage rings. A carbon wire of about 4 µ diameter is swept through the beam once with a speed of about 80 cm/sec. The resulting bremsstrahlung is observed. The time-intensity correlation gives beam position, profile, and intensity. At the ISR, use of that method will widen the circulating beam by multiple scattering, and this constitutes the limitation of the method.

Example: Wire diameter = 4 µ, circulating beam = 10 µA (= 2×10^8 antiprotons), tolerable r.m.s. scattering angle of the antiprotons = 0.1 mrad. This limit on multiple scattering is reached after placing the wire in the beam for 120 sec, resulting in a total of 3×10^6 monitor counts. One could envisage, for example, 1000 sweeps with 3000 counts each, taken during the lifetime of the beam. While this is not extravagant, it may be sufficient.

Use of the method in the proton beam is limited by heating of the wire. The temperature rise is given by

$$\Delta T = \frac{0.34 \times 10^6}{C_p} \times \frac{I}{A} \times \Delta t\ ,$$

where I/A = current density (A/cm^2); Δt = time wire is in the beam (sec); $C_p \simeq 0.36$ cal/g between 20°C and 1000°C.

We see that the wire would have to be moved through a typical proton beam in less than 1 msec.

5. FINAL REMARKS

We believe that the physics interest and our studies of the experimental feasibility warrant further vigorous endeavours on behalf of a $p\bar{p}$ program. As a next step a cost estimate for the modifications to the ISR and the SPS, the tunnel, and the beam should be made[*], and the question of beam monitoring further studied.

---

[*] A cost estimate is in fact included in paper II.10 of this report.

It appears that luminosities in the range 10^{25} to 10^{26} permit the study of $p\bar{p}$ inter-actions with cross-sections larger than a few percent of the total cross-section. This includes a number of very significant experiments.

However, we would emphasize that the scope of the investigations and therefore the scientific return for the proposed investment increases significantly if a higher luminosity could be achieved. For example, the very important experiment on small-angle scattering, while feasible with a luminosity of 10^{25}-10^{26} (counting rate $\sim$ 0.5/min), would profit greatly from higher luminosity.

*   *   *

REFERENCES

1) K. Hübner, CERN/ISR-TH/73-19 (1973).

2) K. Hübner, CERN/ISRC/74-27 (1974).

3) C. Bourrely and J. Fischer, Nuclear Phys. B61, 513 (1973).

I.1 SOME REMARKS ABOUT LARGE STORAGE RINGS (LSR)
ep INTERACTION REGIONS: A PRELIMINARY REPORT

ep Working Group [*]

1. INTRODUCTION

Because it is feared at this time that it may be technically very difficult to maintain the stability of a tightly bunched proton beam, this note was originally motivated by some geometric considerations of how to bring an electron beam into interaction with an *unbunched* proton beam. In order to achieve optimum luminosity with an LSR proton current that is limited by stored energy and perhaps stability requirements to 7 A at 400 GeV, and an electron current limited by total RF power to 250 mA at 20 GeV, very small crossing angles, of the order of a few milliradians, are called for. Even if the long-range contribution to the beam-beam tune shift is reasonable, there still exists the problem of providing sufficient separation of the beams at the ends of the interaction regions (IR) whose length is limited by the need to maintain reasonable β values in the adjacent quads. One solution to this problem has been to pass the magnetically stiffer proton beam through holes in the iron yokes of the electron quads[1], another to separate the beams by Lamberston septa[2]. A third[3] and at first sight attractive method is to achieve overlap of the beams by means of a transverse magnetic field located in the centre or just on either side of the interaction point (IP). However, it can soon be recognized that the strength of any field is severely restricted, because manipulation of the electron beam produces a flood of synchrotron radiation that must not only be compensated by the RF system but can also play havoc inside the detector.

More than ever before in the design of storage rings, we are led from the interaction region to detector concepts, which in turn naturally lead to the kinematics of the reactions -- that is to the physics itself that is to be performed. Since this seems to be the wrong approach, the first section of this note will turn out to be a brief review of some physics and detector concepts, and at the end hopefully provide a conceivable solution and a list of requirements in plain language to help in the design of the interaction region geometry.

Most accelerators were planned to answer the burning physics questions of the day, but in most cases, by the time the machine was operating, these questions either had been answered or turned out to be the wrong ones to ask. However, aside from divine guidance, we have no choice but to impress on the design the prejudices current today and pray that the result will be sufficiently flexible to be useful. One exception to the foregoing pessimism seems to have been the almost universal experience that exploration of ever higher energy regions has been richly rewarding. Moreover in the case under discussion, the lepton-proton interaction, the questions appear to be so fundamental as to probably resist solution for a long time. In what follows, in the interest of brevity, gross simplifications will have to be made.

The spirit of this work is not so much to put forth a fixed proposal to be acted on tomorrow, as to choose a model configuration whose properties can be further studied in detail.

---

[*] The members of this Working Group are listed at the end of this report.

2. PHYSICS

The two main questions that ep rings[4] are expected to answer can be summed up in one sentence: "Do electromagnetic and weak interactions take place, within the proton, at points?" A third and also important subject, electro- or photoproduction, presents quite different geometric problems and possibly different luminosity requirements. This subject is beyond the scope of this work and will be treated in another report.

2.1 Deep inelastic ep scattering

$$e^- + p \rightarrow e^- + \text{anything (e.m.)} . \tag{1}$$

During recent years it has been found that in the deeply inelastic domain it appears as if electrons scatter from protons, not as from a fuzzy cloud of charge but from hard point-like constituents. These objects have been given the name partons. The reason for believing this is that in the formula that describes the scattering probability, the terms that describe the structure functions or form factors are functions, not of q^2 (the momentum transfer)[*] or ν (a variable related to energy transfer) separately, but of a single variable q^2/ν. This property has been given the name scaling. Electron-proton storage rings permit the extension of scattering experiments with enormous increases in the variables q^2 and ν and thereby permit us to ask the following equivalent questions.

A) At what point does scaling break down? That is, Do the partons themselves have a scale? a size? a structure? a form factor? Further, if scale invariance should be shown to break, the associated questions are:

B) Is this the result of the creation of new particles? modification of quantum electrodynamics? manifestations of the weak or as yet unknown force?

Interestingly enough, questions (A) can be examined simply by looking at the cross-section as a function of the scaling variable, while questions (B), which are model-dependent, require the measurement of multiplicities, momentum distributions, correlations, jets, etc.

The above remarks seem to imply that simple scaling is indeed experimentally valid. This is not quite true. In a recent review talk at the Palermo High-Energy Physics Conference, June 1975, Taylor[5] stated that slight deviations from simple scaling have already been observed both in ep scattering at SLAC and in the μp scattering data of Chen and collaborators[6] at FNAL.

2.2 Weak interactions

$$e^- + p \rightarrow \nu + \text{anything} \tag{2a}$$

$$e^- + p \rightarrow e^- + \text{anything (via neutral currents)} . \tag{2b}$$

The point-like Fermi interaction, with a coupling constant G, independent of energy, has now been successfully applied over many orders of magnitude in lepton energy (from $E_\beta = 10$ keV to $E_\nu = 200$ GeV)[7]. It is therefore natural to ask, At what energy does this concept break down? If the weak interaction is described by a field theory, then the

---

*) These variables are defined in the next section.

propagator of this field, the Intermediate Vector Boson (IVB), must mediate, in this case reduce, the cross-section at some energy. This should be seen in deviation from linearity[8] of the total cross-section with s (the square of the available centre of mass energy) at c.m. energies comparable to the IVB mass. Popular values for this mass based on gauge theories[9] range from 30 to 70 GeV. The proposed 20 GeV e^- × 400 GeV proton collision facility opens up centre-of-mass energies up to 180 GeV -- well above the presently supposed mass of the IVB, well above energies available with neutrino beams from accelerators of reasonable size on stationary targets, yet still below the unitarity limit set by the coupling constant itself. If it is intended to study the weak interaction with electrons, it is important that they are not drowned in a sea of electromagnetic interactions. This implies working at an s such that $(G^2s/\pi) \sim (4\pi\alpha^2/s)$ or an s $\sim$ 4000 GeV^2. This value is well inside the kinematic range of the facility. We will discuss methods of separating reaction (2b) from (1) later on, but it is important to notice that events belonging to reaction (2a) can be characterized by a *large transverse momentum imbalance* (including neutral momentum) and the *absence* of a recoil electron. An oversimplified program scenario might look like the following diagram:
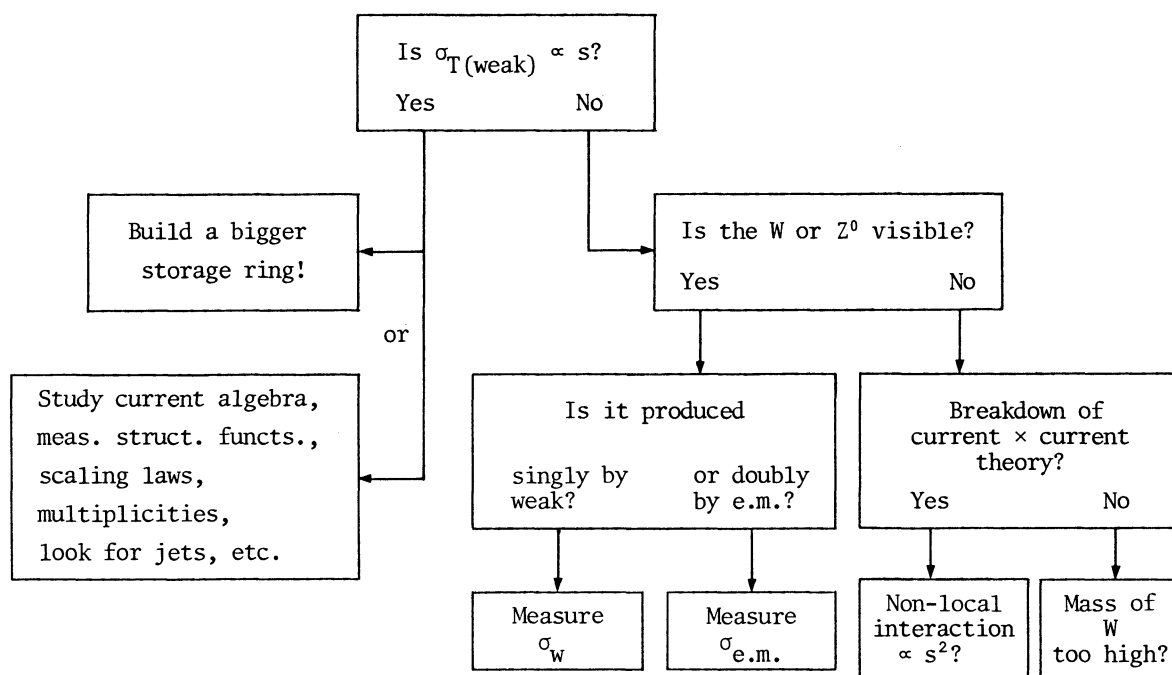
From the above discussion several requirements immediately become apparent:

i) the rings must operate up to an s such that the weak events dominate;

ii) it is essential that s be variable;

iii) there will exist stringent requirements on momentum determinations and detection efficiency.

If now, as stated above, high energy is good, "Is higher energy better?" The answer is, "Perhaps not at extreme values!" The reason comes from the fact that higher s is achieved by raising the proton ring energy, since the electron ring energy is RF power-limited to about 20 to 25 GeV. This means that the "interesting events" are kinematically folded more and more along the initial proton direction where they become harder to measure. This will be demonstrated in the next section. The essentials of any experiment include: i) rate, ii) kinematics, iii) normalization, iv) trigger efficiency, v) background, vi) detection, identification, and reconstruction efficiency. Some of these considerations may lead to contradictions in detector design. Again, the outlines presented in this note can at best be superficial. Moreover, there is always the risk of designing a detector to do the optimum job on the "expected" physics (scaling) and thereby missing the really interesting things that may be going on.

As of June 1975, Bjorken scaling has been shown to be valid (within comparatively large errors) up to the highest neutrino energies available at FNAL.

3. RATES AND KINEMATICS

In contrast to many experiments that are planned, the expected rates in this case are calculable provided scale invariance is assumed to hold in the enormously expanded kinematic range. This is true for both the electromagnetic and weak cases. We can also estimate the effects that the existence of the IVB would have, as well as details resulting from the Weinberg theory[9]. But before getting into a discussion of rates, we will define the kinematic variables that are usually used. For reference these will be written down in some detail (see the following diagram).
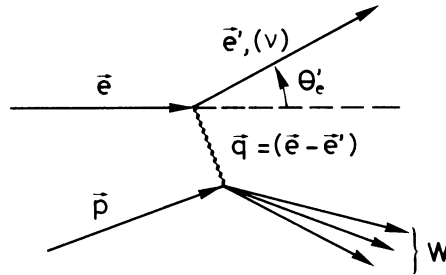
Let e, e', and p be the four-momenta of the particles shown. For masses m_p and m_e small compared to energies,

$$\vec{e} = (0, 0, E, E)$$

$$\vec{e}' = (E' \sin \theta_e', 0, E' \cos \theta_e', E')$$

$$\vec{p} = (0, 0, -E_p, E_p)$$

in which E_p = initial energy of the proton,

　　　　W = mass of state produced,

　　　　θ_e' = angle of final electron with respect to initial direction,

　　　E, E' = initial and final energies of the electron, respectively.

The invariant mass squared of the initial system (which is, of course, the mass squared of the final system also) is

$$s \equiv (\vec{e} + \vec{p})^2 = m_e^2 + m_p^2 + 2(E\,E_p - \vec{p}_e \cdot \vec{p}_p) = 2(E\,E_p + E\,E_p) = \boxed{4E\,E_p} \; . \tag{1}$$

The so-called (mass of the exchanged photon)^2 = Q^2, which is also equal to the negative of the (exchanged four-momentum)^2 between the electron and the proton, is $-q^2 \equiv -(\vec{e} - \vec{e}')^2$:

$$\boxed{Q^2 = 2E\,E'(1 - \cos\,\theta_e') = 4E\,E'\,\sin^2\frac{\theta_e'}{2}} \tag{2}$$

The energy transfer variable ν, which in the electron scattering on a stationary target was just the difference between the initial and final electron energies, is defined in the colliding beam case as

$$\nu \equiv \frac{\vec{p} \cdot \vec{q}}{m_p} \equiv \frac{p \cdot (\vec{e} - \vec{e}')}{m_p} = \frac{2E_p}{m_p}\left(E - E'\,\cos^2\frac{\theta_e'}{2}\right) = \frac{E_p}{m_p}\left[\frac{Q^2}{2E} + 2(E - E')\right], \tag{3}$$

which reduces to $(E - E')$ if $p = (0, 0, 0, m_p)$, i.e. if the proton had been at rest.

The mass squared of the finally produced excited state is $W^2 \equiv (\vec{p} + \vec{q})^2$:

$$W^2 = 4E_p(E - E') + Q^2\left(\frac{E_p}{E} - 1\right) + m_p^2 = 2m_p\nu - Q^2 + m_p^2 \; . \tag{4}$$

Note: The use of the symbol W should not be confused with the W boson.

We see that for a given s, the variables Q^2, ν, W^2 have certain limiting values. For example, the maximum for Q^2 occurs when $\theta_e' = 180°$ and the electron receives a momentum equal to that of the initial proton; so we have from relations (1) and (2)

$$Q^2_{max} = 4E\,E_p = s \; . \tag{5}$$

The maximum ν value occurs for maximum momentum transfer and when the mass of the final state W is the mass of the proton. Therefore from Eq. (4),

$$\nu_{max} = \frac{Q^2_{max}}{2m_p} = \frac{s}{2m_p} \; . \tag{6}$$

The heaviest final state W^2 occurs at ν_{max}, $Q^2 = 0$ or

$$W_{max} = \sqrt{\frac{2m_p s}{2m_p}} = \sqrt{s} \; . \tag{7}$$

For convenience, two-dimensional variables are often used. They are the Bjorken scaling variables

$$\boxed{x \equiv \frac{Q^2}{2m_p\nu}} \quad \text{and} \quad \boxed{y \equiv \frac{\nu}{\nu_{max}}} \; . \tag{8}$$

The relationships between kinematic variables are shown in Figs. 1, 2, and 3 for three ep facilities that have been discussed. These facilities are listed in Table 1.

Table 1

Kinematic limits for different ep storage rings proposals

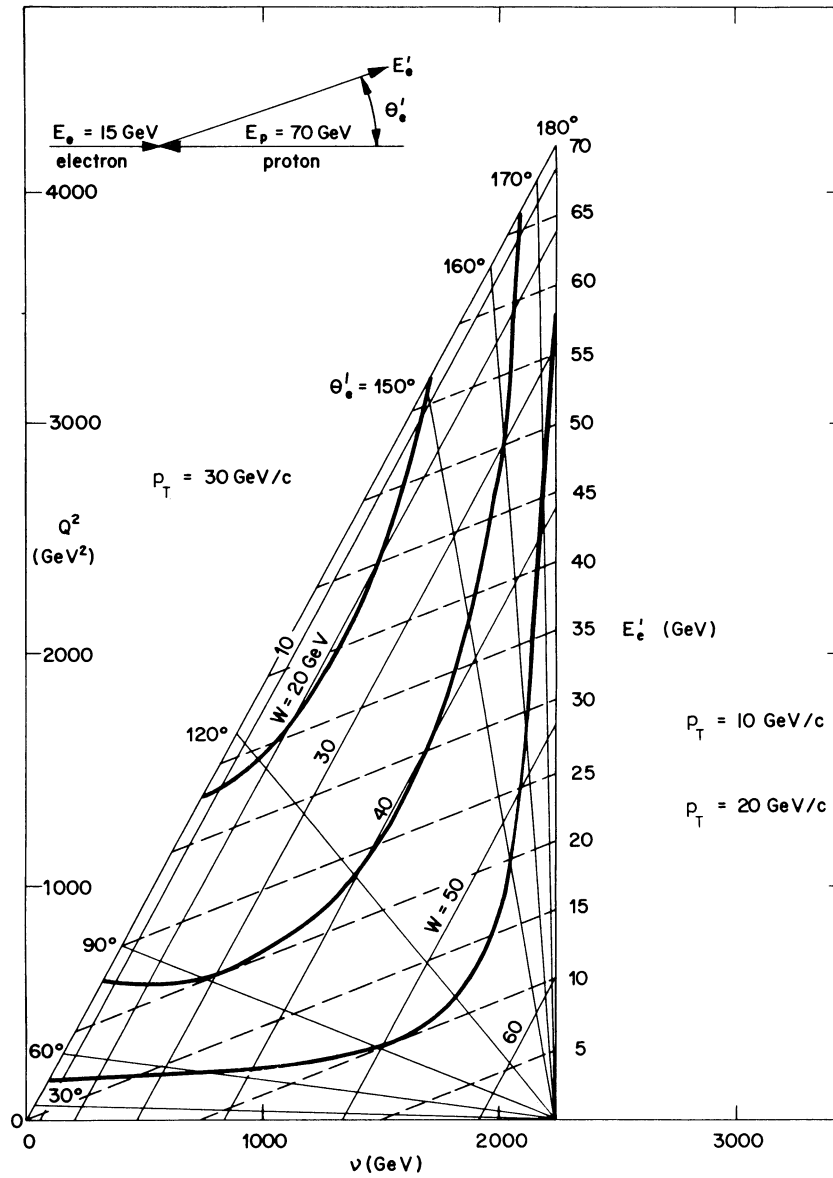| Energies in GeV e × p	Q^2_{max} (GeV^2)	W_{max} (GeV)	Proposal	Ref.
15 × 70	4,200	65	Original PEP at LBL/SLAC (April 1972)	10
20 × 400	32,000	180	LSR at CERN	11
30 × 2000	240,000	490	POPAE at FNAL	12

Fig. 1 Kinematics for the e-p option of the PEP proposal at SLAC (from Ref. 10)
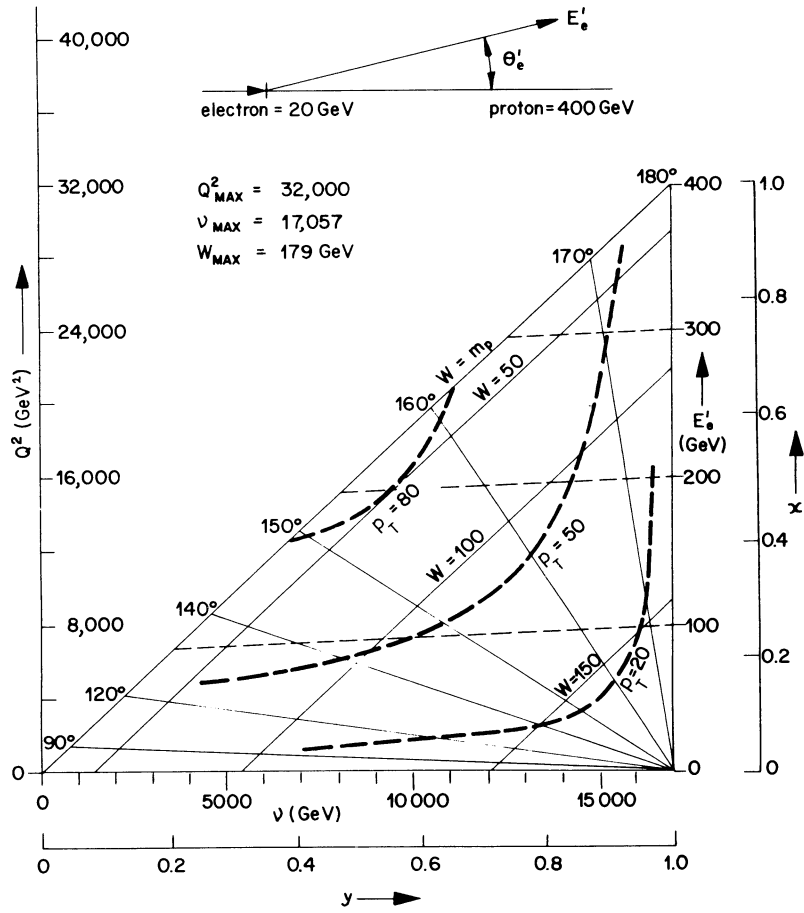
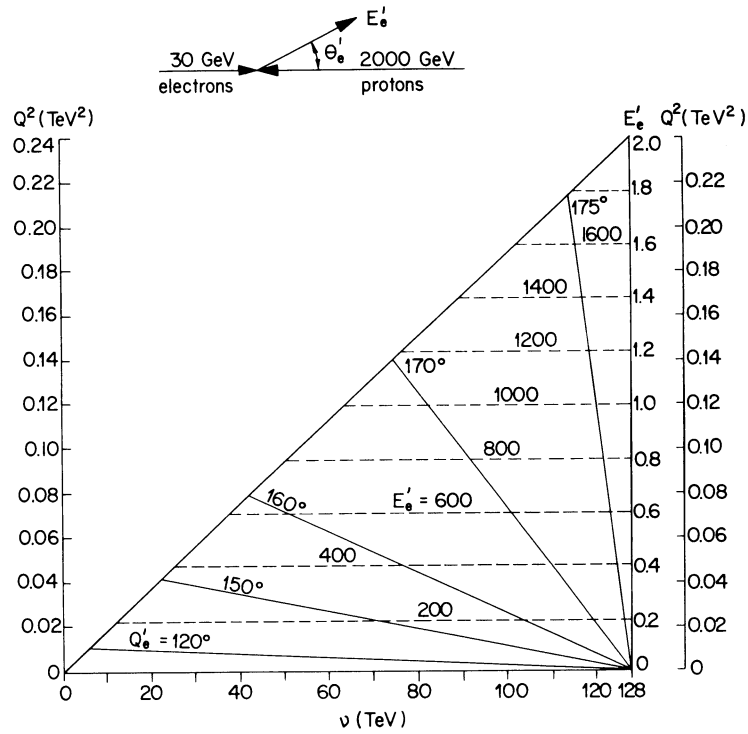Fig. 2 Kinematics for the CERN LSR ep proposal (from Ref. 11)

Fig. 3 Kinematics for the NAL POPAE ep proposal (from Ref. 12)

From these figures the reader will notice that the high Q^2, high ν parts of the available kinematic space occur for electron scattering angles $\theta'_e > 90°$; also, the higher the proton energy, the closer to the proton direction the electron will emerge.

The event rates for electromagnetic and weak interactions have been calculated by the authors[10-12] mentioned. Although they apply scaling with slightly different assumptions, the results suffice for our qualitative purposes. They are shown in Figs. 4, 5, and 6. A few comments follow:

1) At a luminosity of 10^{32} cm^{-2} sec^{-1} the rates are not unreasonable for "typical" experiments lasting the canonical "10 days". Breakdown in scaling, i.e. replacing $G^2/2\pi$ by $(G^2/2\pi)[m_B^2/(m_B^2 + q^2)]$, resulting in a factor of ~ 2 in the weak cross-section, would be quite measurable. However, a factor of 10 less in luminosity would make experiments very time consuming because cuts, inefficiencies, separations, etc., will all reduce the statistical accuracy achievable.

2) There are very few events per day with $x > 0.5$, $y > 0.5$, so the difficult region $\theta'_e > 160°$ is very sparsely populated. At a first glance this would prompt one to say, "Let us forget this region of the detector", but as we shall see later on, this would have serious consequences in event identification.
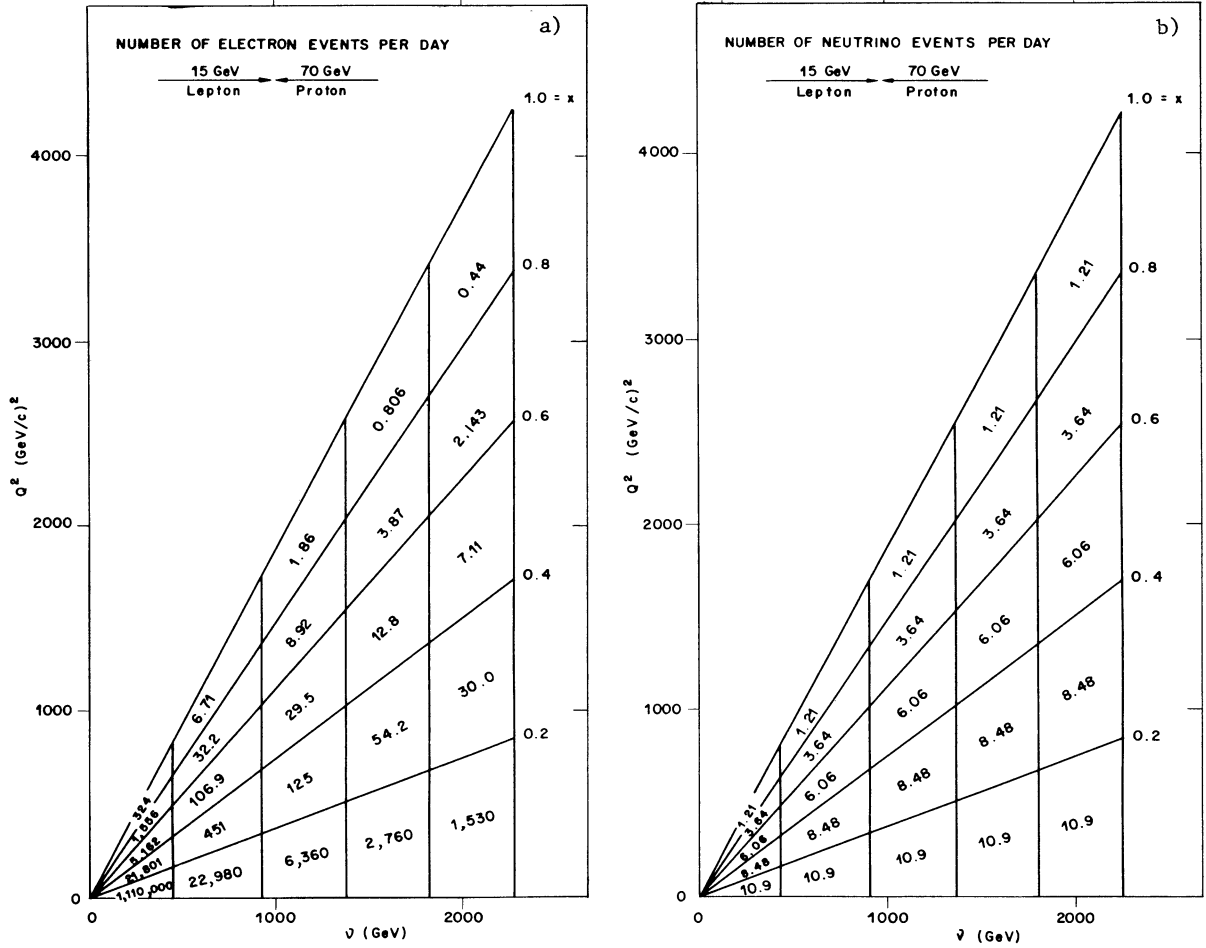

Fig. 4   Expected rates of events for the PEP e-p (from Ref. 10): for the reactions
a) $e^-p \rightarrow e^-X$;   b) $e^-p \rightarrow \nu X$.

3) How would one actually perform a scaling experiment? One way is to set the rings to a given s and measure the number of events in a given portion $\Delta x \Delta y$ of the kinematic diagram. This requires that x and y for a given event be measured with a resolution comparable to the bite size Δ in that variable. This in turn specifies the tolerable errors on energy and angle measurements of the scattered electron and/or recoil products. An analysis by Bartel et al.[13] indicates that in the interesting region x = y = 0.5, *resolutions of a few percent* for the hadron detector for weak interactions are required!

Another way of testing scale invariance (in ep inelastic scattering, for example) is to compare data at fixed Q^2/s and ν/s, but at differing s. This method, proposed by Strovink[14], has the advantage that we do not need to know the electron detector resolution functions which are strong functions of y *provided they are independent of s*. [This condition is met if the detector has fixed errors in $\Delta E'/E'$, and $\psi/\sin \psi$, where $\psi = (90° - \theta'_e)$.] In order to be fair, however, we must point out that another problem, also fraught with some difficulty, has thus been created, namely that of accurately measuring the luminosity as a function of the ring's energy.

4) How does one separate process (1) from process (2b), both of which look topologically identical? Electromagnetic events should dominate at low s and weak events at high s. This supposition alone should suffice, but we might have the case in which the e.m. cross-section scales, or is even enhanced[16] and the weak is suppressed by the existence of the neutral vector boson (NVB). The resulting confusion could be then disentangled at a ν and Q^2 where the two processes can interfere and different cross-sections should result if electrons are replaced by positrons[17]. Positrons are also needed to shed light on the recently discovered difference in ν and $\bar{\nu}$ effects[18]. Positron scattering is not altogether trivial, however, for the following reasons:
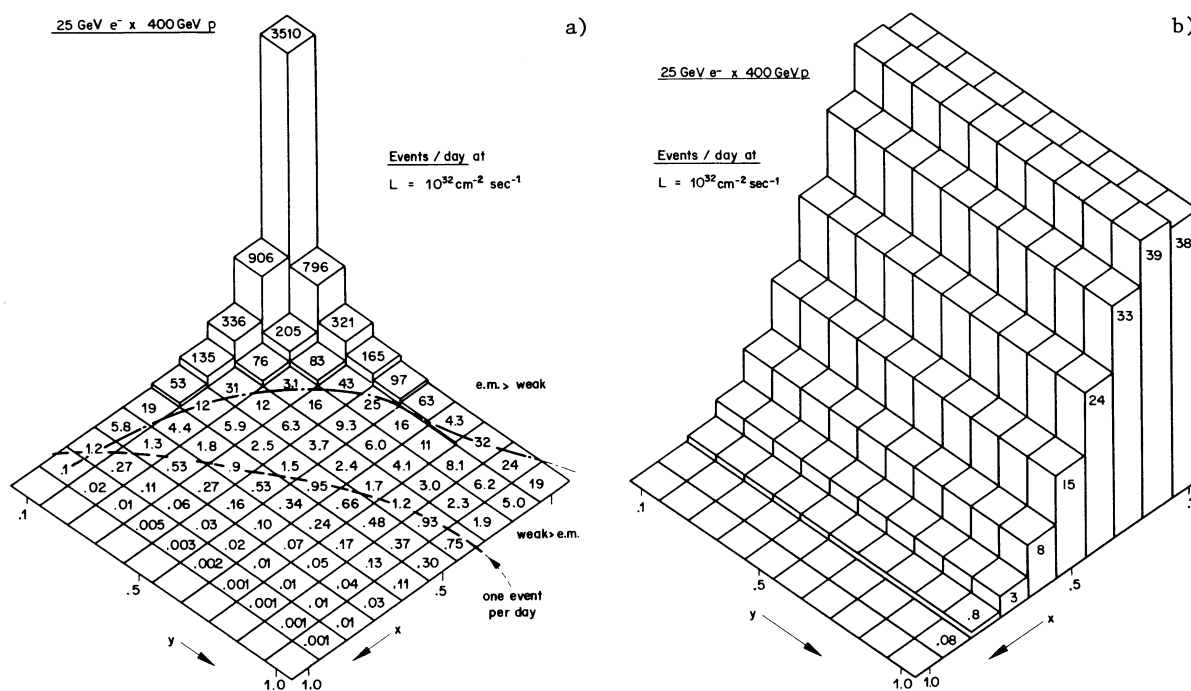
Fig. 5 Expected rates of events for the CERN (LSR)(from Ref. 11):
a) in the reaction $e^- p \rightarrow e^- X$; b) in the reaction $e^- p \rightarrow \nu X$.

a) The e^+ weak cross-section is down by a factor of 3 in the one-parton model.

b) The distribution of weak events in x, y for positrons is not the same as it was for electrons[11], requiring an accurate knowledge of the electron efficiency in the x, y plane.

c) Several bending magnets will need to be reversed in the interaction region and, if they happen to be common to the proton beam, changes in geometry will result.

NUMBER OF ELECTRON EVENTS PER 10 DAYS WITH SCALING

a) electrons
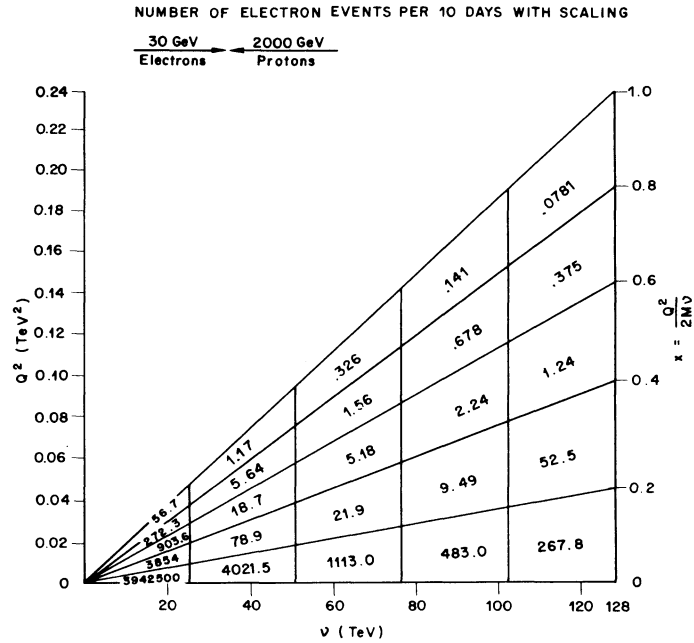
NUMBER OF NEUTRINO EVENTS PER 10 DAYS
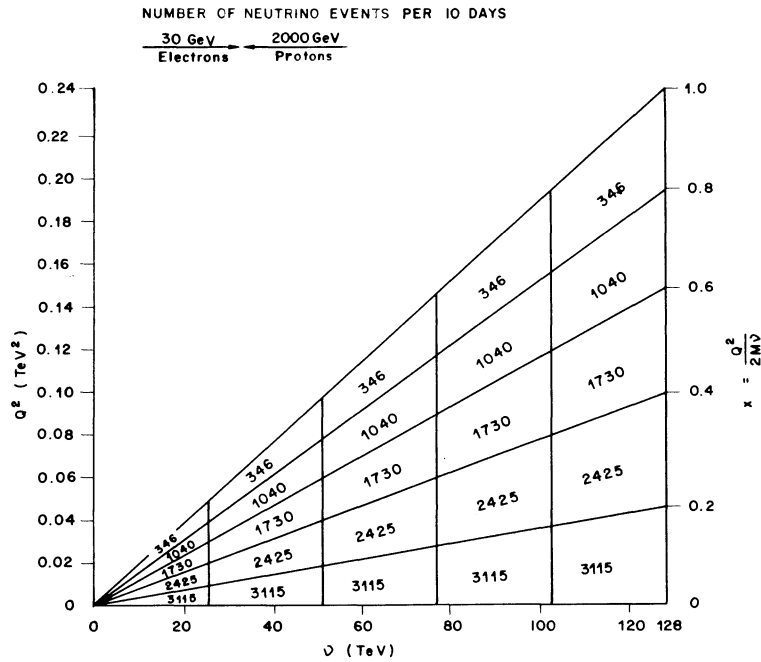
b) neutrinos

Fig. 6 Expected rates of events at NAL (from Ref. 12)

d) Systematic normalization errors of the luminosity monitor may occur.

e) It is more difficult to fill a ring with positrons since they need to be created first.

f) Last but not least, the e^+-e^- asymmetry may be the result of a two-photon exchange. A powerful technique for checking this and other points is to use specific helicity states of the electrons or positrons. These states can be produced by rotating the synchrotron radiation-induced transverse polarization vector to be longitudinal, using the g - 2 precession[19]. The angle the electron beam has to make with the bending plane of the ring is $\pi/\gamma(g - 2)$, which is 34 mrad for a 20 GeV beam. Extremely clever techniques (not yet developed) will have to be found to keep the vast amounts of resulting synchrotron radiation out of the detector.

It is not the purpose of this note to scare the reader out of thinking about these experiments, but rather to call attention to certain problems that should be kept in mind when designing interaction regions.

For instance, in connection with the last point mentioned above, in choosing the topologies of the two rings in the tunnel it will be necessary to reserve sufficient space ($\sim$ 100 m on either side of the intersection point) to allow for the vertical gymnastics of the proton beam that are subsequently required to keep the luminosity reasonable.

4. HADRON DETECTOR REQUIREMENTS

So far we have been concerned with the kinematics of the final lepton. Before going on to a discussion of the detector, we must ask, Where do the hadrons "W" of the interesting events go? One answer might be, If we do only scaling reactions (1) and (2b) we do not care (provided we do not misidentify the scattered electron with a π^0 decay, for example). The next answer is, Momentum is conserved so the reaction products recoil against the lepton -- But with what angular distribution? The answer to this last question is *very model-dependent*, and since we do not know *a priori* what model will be fashionable years from now, we can only make very general remarks. The two guesses listed below yield different results because they start from different input assumptions and different kinematic regions.
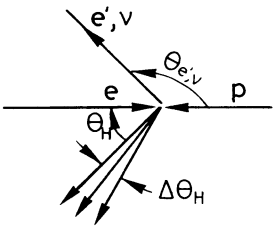
4.1 Weak interactions

Consider for the moment Figs. 1 and 2, the kinematics for 15 × 70 and 20 × 400 GeV. These figures contain lines of equal scattered electron energy and angle from which the transverse momentum carried by the lepton is easily calculated, $p_T = E'_e \sin \theta'_e$. From Figs. 2 and 5b in the region x $\sim$ 0.2 to 0.4 and y = 0.3 to 0.8, that is in a region well populated by weak interaction events, we can expect a p_T of 50 GeV/c! Applying the method of Richter[20], which assumes the heavy hadron state to decay with a total multiplicity, say $\langle n_{tot} \rangle \sim$ 15, and each hadron having 300 MeV/c with respect to the system's direction of flight, we estimate the angles given in Table 2.

Notice that if the electron direction is *not* measured, we obtain poor resolution in y at one end of the scale and poor resolution in x at the other end. Most important, however, is that it is necessary to catch the hadrons, *including the neutrals*, at small angles with respect to the proton, even for transverse momenta as high as 50 GeV/c! This fact is a consequence of the large initial proton-electron longitudinal momentum imbalance.

Table 2

Relationship between lepton and hadron angles

$\theta_{\nu,e}$ (deg.)	120	140	150	160	170	
$\langle\theta\rangle_{had}$ (deg.)	8	8.4	9	10.5	22	
$\langle\Delta\theta\rangle_{had}$ (deg.)	0.71	0.74	0.8	0.94	1.95	
E_{had} (GeV)	360	343	320	274	131	

Another model summarized by Manning[21] has been simulated via a Monte Carlo program. As a result of the assumptions made regarding the decay of the hadron state, it is shown that "proton fragments" and "boson fragments" are clearly separable by their angular distributions, which are shown in Fig. 7. For convenience, we reproduce excerpts from his paper:
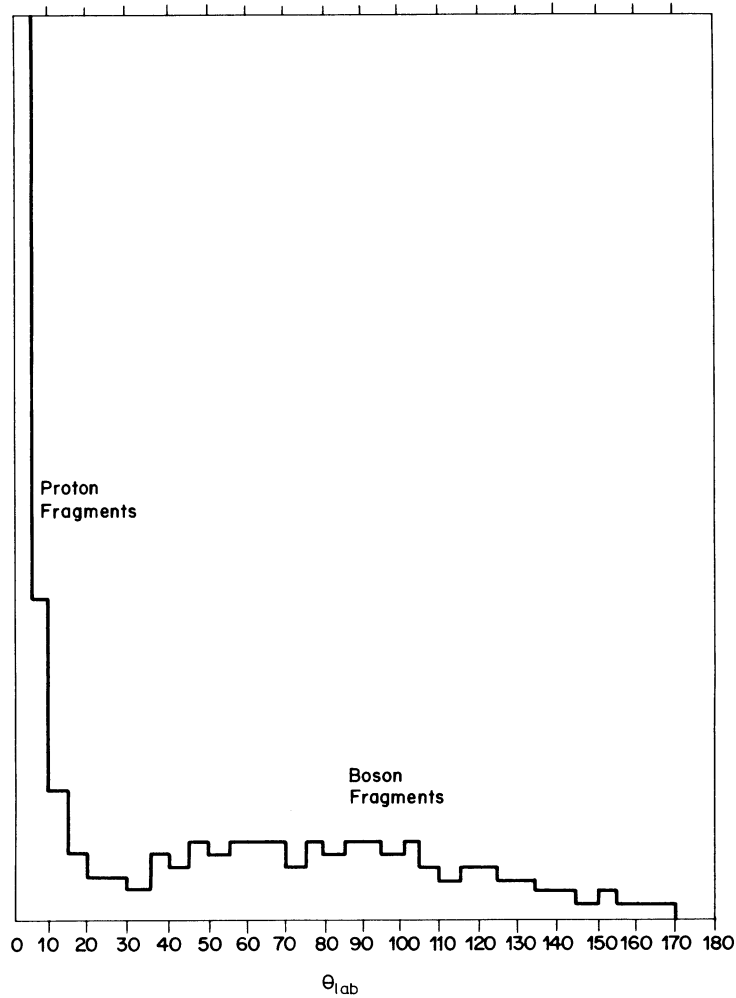

Fig. 7 Hadron angular distribution in the laboratory system for s = 5600 GeV^2 and M_W = 80 GeV in the region f (= weak inter. rate/e.m. inter. rate) = 0.01.

"The assumptions made were:

a) $s = 5600$ GeV^2, $E_p = 100$ GeV, $E_e = 14$ GeV.

b) $M_W = 80$ GeV.

c) Region studied, $f > 0.01$; f = weak rate/e.m. rate.

d) The hadron final state M_X is assumed to decay with forward-backward symmetry in its centre of mass with a transverse momentum distribution given by $dN/dp_T = p_T \, e^{-4.7 p_T^2}$. The average multiplicity is assumed to be $\langle n \rangle = 3(M_X/2)^{\frac{1}{2}}$ with a distribution chosen to fit available data from hadronic collisions. The momentum distribution of the hadrons is assumed to be $dN/dp = e^{-p/(M_X/n)}$.

To summarize, the conclusions from the Monte Carlo calculation are:

a) A 'typical event' has ~ 7 hadrons at large angles (W fragments) opposite the ν to balance the large p_T^ν and ~ 7 hadrons at small angles which carry very little p_T (proton fragments).

b) The events are coplanar and hence the hadrons fix the plane in which ν leaves.

c) One can fix value of x and y quite well providing one detects *all* of the W fragments."

One special case deserves mention. Suppose the intermediate vector boson (IVB) or neutral vector boson (NVB) is actually produced in the reactions

$$
\begin{array}{ccc}
e^- + p \to W^- + \text{hadrons}, & \quad & e^- + p \to Z^0 + \text{hadrons} \\
\quad \downarrow & & \quad \downarrow \\
\mu^- + \bar{\nu} & & \mu^+ + \mu^-
\end{array}
$$

then we are likely to see single or dimuon events with very large transverse momenta. This case deserves a special detector mentioned in Section 8.3.

4.2 Inelastic ep scattering

In this field the popular notion is that $(1 - x)$ of the proton behaves pretty much as a spectator and produces a hadron jet in the direction of the initial proton. This jet will need to be separated from the beam in some way. The x part of the hadron receives momentum transfer $\vec{Q}$ in the appropriate direction. Also in this case, the most easily identifiable transverse momentum events come from a region with medium to high x, medium y. If the collision is with a parton (let us say 1/3 the mass of the proton) then the angle this parton jet makes is estimated to be three times larger than that of the spectator jet (however small that may be).

Pictorially this was represented by Drickey and Hand[22] in the following way:
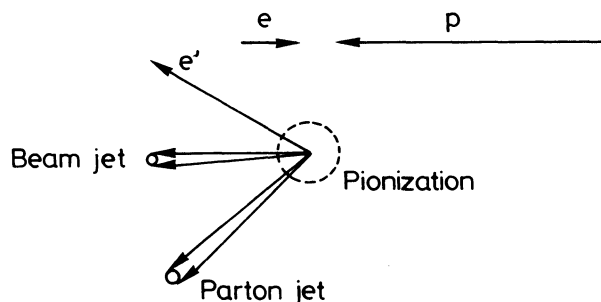
In summary we can take a leaf out of a paper by Drickey and Hand[23] in which they outline detector requirements for, of all things, a proton-proton facility of 1000 × 1000 GeV. It is reproduced below:

Requirements for the Detector

We have imposed the following constraints on the detector, based on what we feel will be necessary to interpret the observed high p_1 events:

a) A measurement is to be made of the energy transmitted in the direction of the incident beams ("beam pipe jet"). This allows a transformation into the centre-of-mass of the "elementary" collision without advance assumptions about the final states in such a collision. No detailed measurements of individual particles in the "beam pipe jets" are necessary, just the total energy and momentum not directly involved in the production of high transverse momenta.

b) Particle identification for hadrons (as a group), electrons, photons, and muons should be available.

c) A sign determination for charged particle momenta up to and beyond 100 GeV/c is made -- hence a magnetic field is required.

d) The detector must fit into a straight section of minimal length, since very long straight sections are extremely expensive.

e) A "split field" magnet causes the proton beams to collide in a collinear geometry and also serves to separate the neutral fragments in the beam pipe jets from the beams themselves.

f) The detector must have a large solid angle to permit the viewing of very rare processes and to give an unbiased view of the collisions themselves. Since high luminosities ($\approx 10^{32}$ or greater) will be used, backgrounds must be carefully considered. This again led to the use of a magnetic field in the wide-angle region.

Since this was taken from a paper dealing with proton-proton collisions, we are led to the interesting notion that except for the problems of synchrotron radiation and momentum imbalance, ep and pp detector considerations have a lot in common. In both cases the physics is the examination of high p_T reactions which also contain beam jets. However, we must add to the above list that electron detection efficiency should be very high.

5. COLLISION GEOMETRY

Let us now return to the problem raised in the introduction: how to get beams, that come out of and go into separate machines, to collide. In planning the interaction region we must then ask, How sharply must we, or can we, manipulate the electron beam?; that is, How serious is the synchrotron radiation problem?

The answer to the first part depends on our need to make the beams *overlap in a reasonable length*. Consider the following geometry[3]:
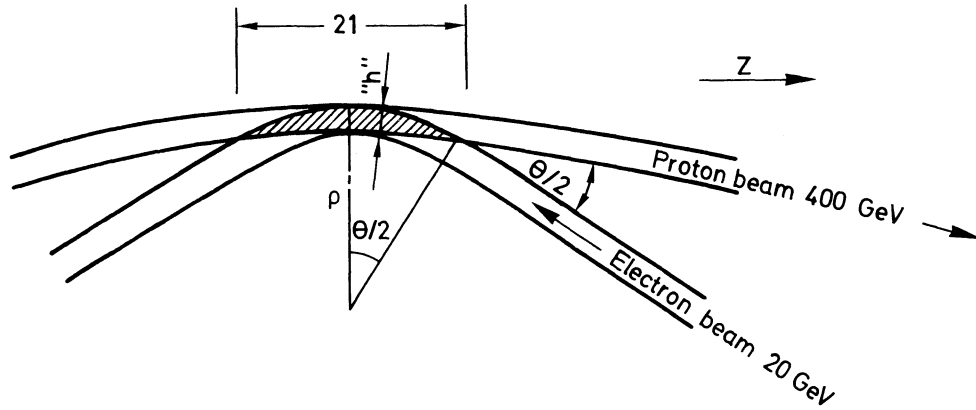
The effective "h" is set by beam emittances and the appropriate ring β-values. In order to provide the best luminosity without getting into long-range tune-shift difficulties, we use the rule of thumb that ℓ should be comparable to β^* (the value of β at the IP). Neglecting, for the moment, the variation of "h" with z, we have

$$\rho_{max} = \frac{\ell^2}{2h} \approx \frac{\beta^{*2}}{2h} .$$

Typical realizable values to achieve a luminosity of 10^{32} for $h_y = 2\sigma_y^*$ and β_y^* are around 0.02 cm and 30 cm, respectively (see Appendix A) so that the maximum permissible radius of curvature is 225 m, which in turn implies a minimum magnetic field of 3 kG for 20 GeV electrons. This yields a value of 1.3 mrad for $\theta/2$. This estimate is made for a vertical separation that takes advantage of the electron beam's natural aspect ratio. Note that the effective "diamond length" (2ℓ) of 60 cm is reasonable from the experimenters' point of view of localizing the source, but that the angle $\theta/2$ (which would have been the total crossing angle with the field turned off) has about the same *small* magnitude as would have been necessary to achieve the luminosity in a purely crossing geometry and is, in fact, only about four times the r.m.s. natural angle inside the beam envelope -- a situation intolerable from electron lifetime point of view. Clearly, in order to separate the beams further, we must increase the effective $\int B \, d\ell$ of the magnet. The consequences of increasing B, that is of decreasing ρ, are twofold. The first is to harden the X-ray spectrum -- something which, as we will see in the next section, is not desirable. The second is to lower the luminosity if the currents in the rings are already limited by other considerations. So we find, under these circumstances, that the maximum and minimum radii are about the same, and the necessary separation can only be achieved by extending the length of the field beyond the overlap region. Having some idea of the magnitude of B, we can go on to discuss synchrotron radiation properties. Various collision schemes are discussed in Section 7.1.

6. SYNCHROTRON RADIATION PROPERTIES

There are several problems connected with the fact that this radiation is generated. They are

i) the RF system must make up the additional losses;

ii) the surfaces that are struck by the radiation must be cooled;

iii) The large number of X-rays entering the detector region must be disposed of. Compton scattering, pair production, and π^0 production off the proton beam will produce a high-energy background in the same direction as electrons from high ν, high Q^2 events[24]. Pair production is perhaps the most serious background this experiment will encounter and requires a special geometry to reduce it.

iv) An additional vacuum problem may result, especially since some of the radiation is bound to enter the proton ring and there desorb gas, causing a pressure rise in a critical location.

In the following sections we will quantify these considerations in a general way. Conceivable solutions are treated later on.

6.1 Power

The power P radiated by a beam of current i (mA) and energy E (GeV) passing through a magnetic field of length ℓ (metres) with radius of curvature R (metres) is

$$P = \frac{dE}{dt} = \frac{88.46 \ i \ E^4}{R} \left(\frac{\ell}{2\pi R}\right) \ \text{(watts)} \ . \tag{8}$$

For the case in point we have

$$P = 88 \times 250 \times 20^4 \times \frac{1}{2\pi \times (225)^2}$$

$$= 11.1 \ \text{kW/m of magnetic field.}$$

At least one metre's worth of this will go into the proton pipe!

6.2 Power density

Synchrotron radiation energy is emitted with an angular spread normal to the plane of emission of about $\langle\theta\rangle_r \approx m/E \sim 0.5/20,000$. In the interaction region this angle is small compared to the r.m.s. betatron angles in the beam, $\langle\theta\rangle_\beta = \pm(\sigma^*/\beta^*)$.

If, as suggested in the previous section, the beams are brought into coincidence via a *vertical* bending, the width of the strip of vacuum chamber struck by the radiation is determined by the electron beam's *horizontal* properties.

For the usual absorber geometry shown below:
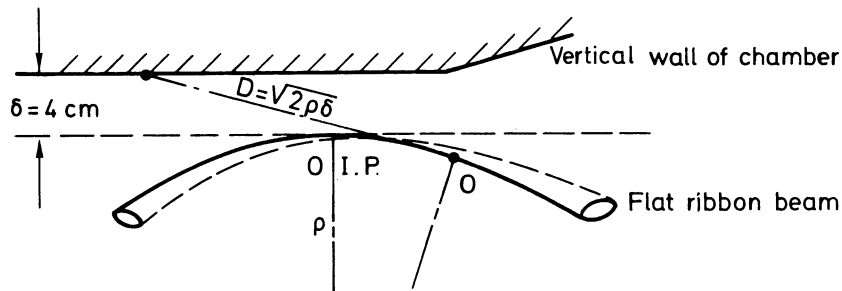
the distance D from the radiating particle to the absorber is

$$D = \sqrt{2\rho\delta} = \sqrt{2 \times 225 \times 0.04} \sim 4 \ \text{m} \ .$$

Actually, because of the low-β section optical properties, the radiation appears to come from the interaction point, so D is more like 2 m. The width w of the strip is then

$$w = D\ 2\ \langle\theta\rangle_{horiz} = 2\ D\ \frac{\sigma^*_H}{\beta^*_H} =$$

$$= 200 \times 2 \times \frac{0.03}{100} \sim 0.12\ cm\ ,$$

and the power density at a ring energy of 20 GeV is

$$\frac{11.1 \times 10^3}{100 \times 0.12} \sim 925\ W/cm^2\ .$$

This value is just below the maximum allowable density for water-cooled surfaces[25], but we will see later that this problem is somewhat mitigated in that the hard X-rays can penetrate the absorber wall if it is made of low-Z material. Note, however, that this geometry is ruled out for reasons of background in a detector. It is presented here only to alert the reader to the magnitude of the problem.

Most likely the power radiated will not scale simply as $1/E^4$, because if the electron ring is run at lower energy the RF power will become available to increase the beam current. For planning purposes this power might be considered a constant down to an operating energy of 15 GeV, by which time the electron current can rise to 800 mA, a current that is perhaps still storable in a multibunch machine. Whether the allowable proton beam-beam tune shift is then reached remains an interesting question.

6.3 Critical energy, spectral photon density

In order to calculate the number of photons and their spectrum, we use the functions that are so conveniently tabulated by Mack[26]. These functions are universally applicable because they employ the variable $r = \varepsilon/\varepsilon_c$ in which ε is the energy of the photon and ε_c is the so-called critical or characteristic energy:

$$\varepsilon_c\ (eV) = 2218\ \frac{E^3\ (GeV)}{R\ (m)}\ . \tag{9}$$

For the case in question, using the radius R of 225 m developed in the last section, we have, for various operating energies E, spectra that range into the hard X-ray region.

Table 3

Characteristic energy and wavelength of the synchrotron-radiation for various operating energies

E (GeV)	ε_c (kV)	λ_c (Å)
10	9.8	1.25
15	33	0.37
20	79	0.16
25	154	0.08

The number of photons of energy $\varepsilon = r\varepsilon_c$ radiated in an interval of 1 eV/sec/m of magnetic field is

$$\frac{d^2N}{dEdt} = \frac{1.5 \times 10^{14}}{2\pi} \times \frac{i \ (mA)}{E^2 \ (GeV)^2} \ \frac{g(r)}{r} \ .$$

The function $g(r)/r$ may be found in Appendix B. For 20 GeV operation, $i = 250$ mA, at $r = 1$, a flux of $\phi = 4.52 \times 10^{12}$ photons/eV/sec/m results. Figure 8 shows the complete spectrum, as well as that for other energies (assuming the same current).
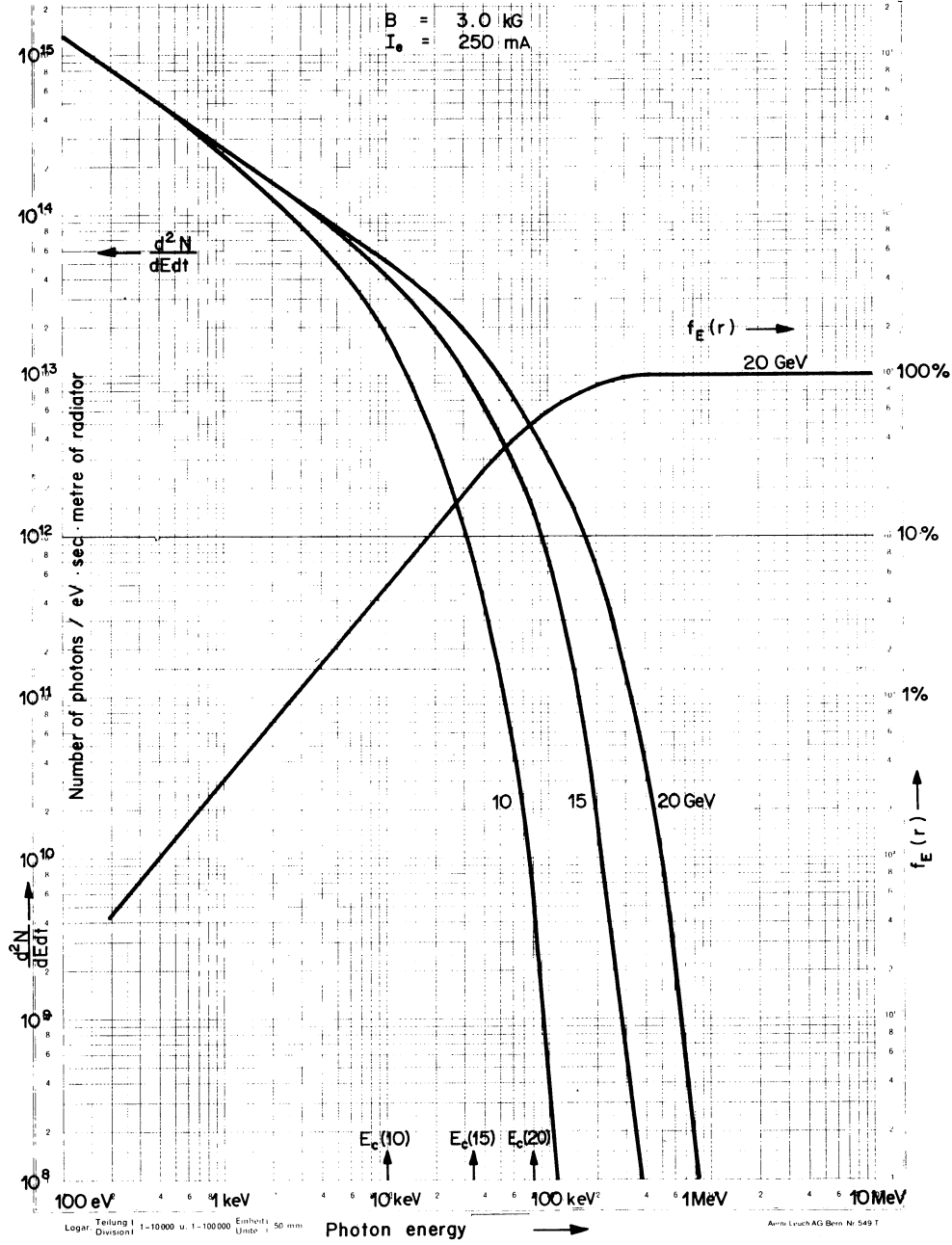

Fig. 8   Spectral photon density per metre, as a function of the photon energy and for several electron beam energies. The function f_e (defined in the text) is also shown for a 20 GeV beam.

Another interesting function is $\mathcal{F}_E(r)$. It is the fraction of total radiated power contained in radiation having less than a given r. In fact at r = 1, $\mathcal{F}_E(r)$ = 0.5, which means that half the power is carried by photons above the critical energy. Since the number spectrum falls so rapidly above r = 1 we can safely say that the upper half of the spectrum is carried in a band between ε_c and $3\varepsilon_c$. For 20 GeV operation then, photons of 80 to 240 keV are important; these have a mean absorption length of about 1 cm in aluminium. This depth considerably simplifies the water-cooling problem.

But let us make a remark about the number of photons -- a seemingly astronomic number. Please refer to Table 4 to get some feeling of the order of magnitudes involved.

Table 4

Data on synchrotron radiation: number of photons and power as a function of photon energy

(1) Energy range (keV)	(2) E_{mid} (keV)	(3) ΔE (keV)	(4) Photons per eV/sec	(5) Photons/sec	(6) Photons per circ. electron[*]	(7) Power[*] (kW)	(8) %	(9) Absorber thickness	
								(cm Al)	(cm Pb)
0.01-0.1	0.05	0.09	2×10^{15}	1.8×10^{17}	0.12	-	-		
0.1-1	0.5	0.9	4×10^{14}	3.6×10^{17}	0.23	-	-		
1-10	5	9	8×10^{13}	7.2×10^{17}	0.46	0.56	5	0.12	
10-40	30	30	1.8×10^{13}	5.4×10^{17}	0.35	2.22	20	0.11	0.14
40-100	70	60	6×10^{12}	3.6×10^{17}	0.23	3.89	35		1.8
100-200	150	100	1×10^{12}	1×10^{17}	0.06	2.78	25		1.3
200-400	300	200	1×10^{11}	2×10^{16}	0.016	1.67	15		8.6
400-800	600	400	2×10^{9}	8×10^{14}	0.5×10^{-3}				38
800	1200	1000	7×10^{5}	7×10^{11}	0.5×10^{-6}				53
		Total		2.28×10^{18}	1.46	11.1	100		

[*] All numbers per metre of radiator

From column 6 we see that about one photon per circulating electron is radiated per metre of field. A useful approximate way of finding this number is to divide the power (in eV/sec) by 1/3 the critical energy.

The bottom row appears to contain a relatively small number of photons but still corresponds to the equivalent of a 20 Ci source of ^{60}Co. Since the hardness of the X-ray spectrum goes with the radius of curvature, it now becomes evident that we cannot afford to increase the field much over the minimum value found in the last section. For instance, a factor of two raises our cobalt source to a million curies!

6.4 Absorber materials

What happens to all these X-rays when they strike material? This is best seen in Fig. 9 for various metals that are used as absorbers[27]. The very low energy photons are photo-absorbed, but those with energies in the range 100 keV to 1 MeV are likely to Compton scatter, a process calculable via the Klein-Nishima formula. While the higher-energy (1 MeV) ones
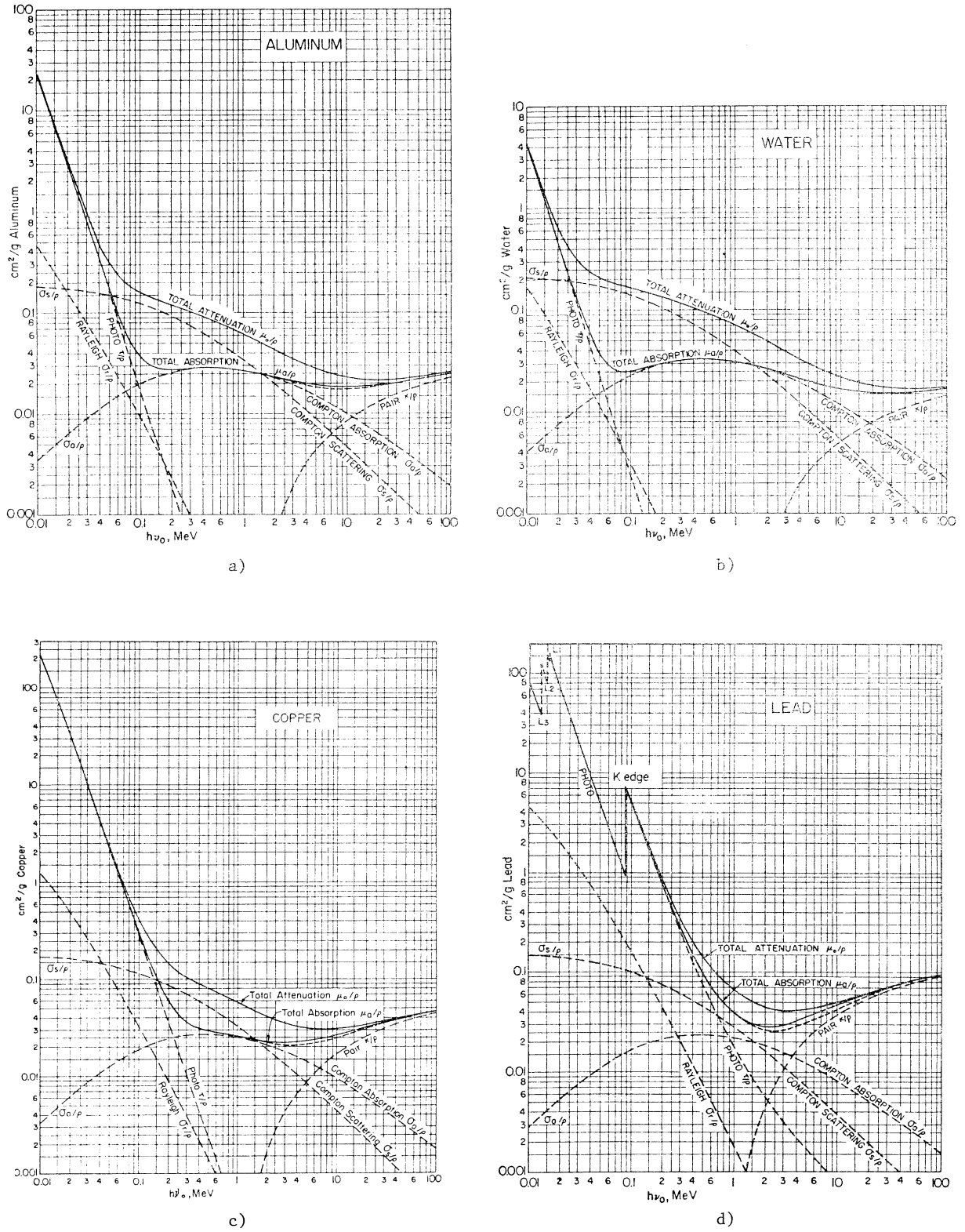
Fig. 9 Mass attenuation coefficients for photons in different materials. The dashed branch
on the μ_a/ρ curves shows the effect of excluding the annihilation photons. The
corresponding linear coefficients may be obtained by multiplying all curves by:
a) $\rho = 2.70$ g/cm^3 Al; c) $\rho = 8.92$ g/cm^3 Cu; d) $\rho = 11.35$ g/cm^3 Pb. (Taken from
Ref. 28.)

go mostly forward, the medium-energy (60 keV) ones unfortunately scatter more or less isotropically [see Fig. 10 [28)] requiring the absorber to have a re-entrant face. Fortunately, the Compton electrons carry their energy into the bulk of the material.

In column 9 of Table 4 we also estimate the absorber thickness required to attenuate the photon flux to some reasonable rate, say 10 kHz. Notice that the thickness of lead is determined by the highest-energy photons, even though there may not be many present.

Fig. 10 a) Dependence of the energy $h\nu'$ of the Compton-scattered photon on $h\nu_0$ and the photon scattering angle θ

b) Collision differential cross-section $d(_e\sigma)/d\Omega$ for the number of photons scattered per unit solid angle in the direction θ

Taken from Ref. 28.

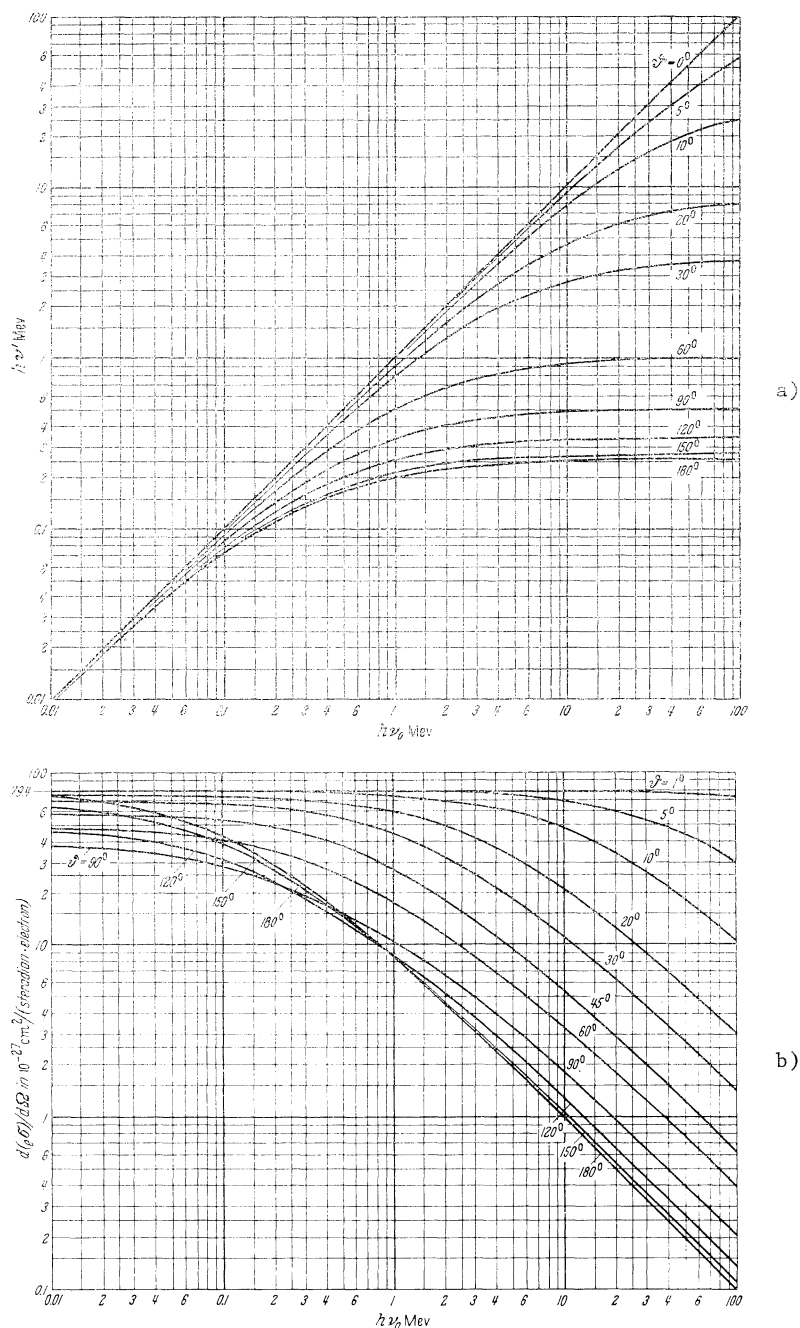## 6.5 Gas load

Electron-positron storage rings work at pressures of typically 10^{-9} to 5×10^{-8} Torr to provide a gas bremsstrahlung dominated lifetime of a few hours. Typical synchrotron radiation desorbed gas compositions[29] are 60% H_2, 25% CO_2, 6% CO with proportionately more hydrogen as the surfaces clean up under bombardment with time. Some considerable care is usually taken to keep synchrotron radiation out of the interaction regions.

The main contributions to the experimental trigger rate come from cosmic-ray accidentals with the trigger counter placed around the beam pipe and from electromagnetic showers initiated by particles that spill out of the beam uniformly around the ring by gas bremsstrahlung. Events actually due to gas collisions in the interaction region amount to no more than a few percent and are usually identified as not originating in the fiducial volume or having a large longitudinal momentum imbalance. The point is, the gas in the IR is not as important as that all around the ring.

Experience at the ISR indicates the following[30]. In the absence of proton loss due to non-linear resonance behaviour of the proton beam or electron-proton neutralization instabilities, the background for a large solid-angle experiment is dominated by the halo that is generated by beam-gas collisions occurring up to 10 m upstream of the IP. This pressure is of the order of 10^{-11} Torr in the ISR. One should also note that the threshold of a runaway pressure bump is a function of surface condition at that location but not of the ambient pressure.

Combining these experiences for an ep interaction region, we see that the proton halo dominates and that the relevant problem will be with the surfaces in the proton ring upstream of the IP that will be struck by radiation. A very rough estimate of the gas load might proceed as follows:

The number of gas molecules desorbed per metre of synchrotron radiator is

$$N_{molecules}/sec = \int_{threshold}^{\varepsilon_{max}} N_\gamma(\varepsilon)K(\varepsilon)D(\varepsilon') \, d\varepsilon \; ,$$

in which $N_\gamma(\varepsilon)$ is the number of photons radiated at energy ε,

$K(\varepsilon)$ is the electron photo coefficient for a photon of ε,

$D(\varepsilon')$ is the electron desorption coefficient in molecules/electron.

For the numerical example we will oversimplify by removing the dependences on ε and take N_γ from the previous section, assuming $K(\varepsilon) \sim 0.1$ and $D \sim 1 \times 10^{-6}$. We find $N_m =$ $= 2.2 \times 10^{18} \times 10^{-6} \times 0.1 = 2.2 \times 10^{11}$ molecules/sec/m or 6.3×10^{-9} Torr·ℓ/sec/m. In order to maintain a pressure of say 2×10^{-11} Torr in the region where the radiation strikes, a pumping speed of $S = 6.3 \times 10^{-9}/2 \times 10^{-11} = 300$ ℓ/sec/m is required -- a number not too hard to obtain from an integrated distributed ion pump. (This general statement will be considerably modified when we consider an actual geometry in the next section.)

The question now is, Is the figure for $D \sim 1 \times 10^{-6}$ realistic? Such figures have been achieved in the laboratory after a great deal of electron scrubbing[31] but have not been achieved in the field. The best figures for SPEAR I, June 1974[29], yield values of 6×10^{-5}; that is, almost two orders of magnitude higher. Also we are assuming that the outgassing rate is linearly proportional to the ring energy. Our optimism is based on the fact that

most electron rings have been repeatedly opened and the surfaces have never had a chance to get the same kind of treatment performed in the laboratory, but there is no reason not to propose ion bombardment[32] cleaning *in situ* as was recently tried successfully at DORIS[33]. Further, since we are considering only those few metres upstream of an interaction region, one might employ relatively heroic measures such as sublimating all over the walls to achieve *negative* desorption coefficients[34].

The conclusion we may draw from this section is that synchrotron radiation is a serious problem, but one that can be solved provided the radius of curvature is not decreased below that found in the discussion in previous sections. Further, more detailed questions regarding background are treated in Section 9. We are now in a position to return to the geometry problem.

7. INTERACTION REGION LAYOUT

7.1 General

A conceivable component arrangement is shown in Fig. 11. In order of appearance, starting at the IP and looking in the direction of the protons, this arrangement is as follows:

a) The vertically bending coincidence magnet whose function was explained previously.

b) The first proton septum magnet-calorimeter (S1) that bends protons and forward-going reaction debris in the horizontal plane. The magnet is sectioned in planes perpendicular to the beam to receive the scintillation planes of a hadron calorimeter. The field is limited to about 1 tesla.
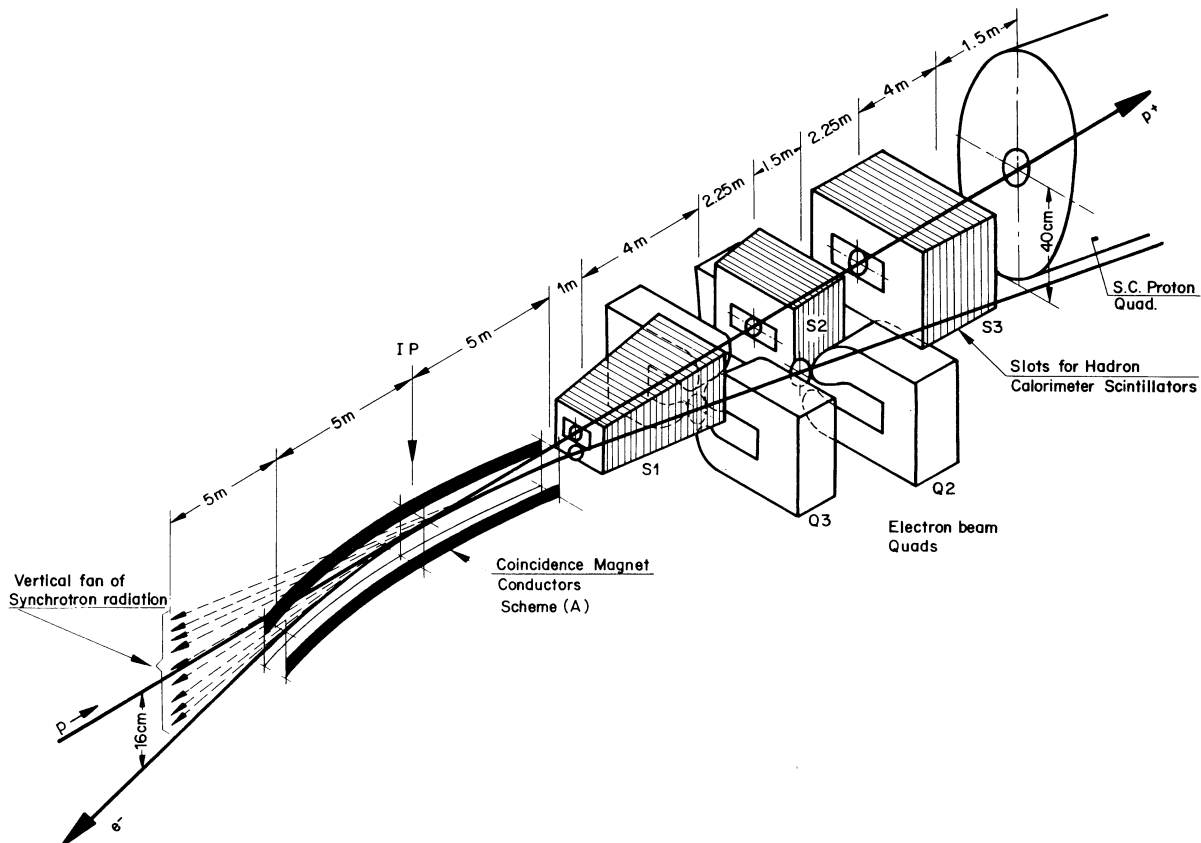

Fig. 11 Beam line components in one ep interaction region (vertical scale enlarged)

c) The final electron quad (Q3) focusing vertically to provide the low vertical β at the IP.

d) The second proton septum-calorimeter (S2) running at about 1.5 tesla.

e) The horizontal electron quad (Q2).

f) Another proton septum (S3) (if required) with field up to 1.8 tesla.

g) A calorimeter designed to measure the forward neutral component of the proton jet. A hole is provided to let the proton beam pass through.

h) The final superconducting proton beam quad. The entrance of this quad is some 22 m downstream, clears the electron beam completely, and is followed by the next proton quad and other components of the proton insertion. If item (f) is not required, this magnet could be moved forward to lower the vertical proton β.

The IR is (at the time of this writing) symmetric about the IP, so that one should imagine the same magnetic layout in the direction of the electrons also. It is important to note, however, that this is the direction in which the vertical fan of intense synchrotron radiation is travelling. From the previous discussion with respect to power deposition as well as background experience recently gained at SPEAR II, we must take care that the photons of this fan are not allowed to strike anything until far removed from the detectors around the IP. This is achieved by slotting all these components in a vertical plane containing the beam. A more detailed description of the magnetic components follows.

7.2 The coincidence magnet

In Section 5 we considered the case of zero crossing angle produced by a uniform horizontal field. To provide sufficient clearance between the beams, this field is shown in Fig. 11 to extend ±5 m on either side of the IP.

A particularly interesting modification of this scheme is to reverse this field at the IP; that is, make a so-called "split field" configuration. The resulting orbits are shown schematically in Fig. 12. The principal advantage, so derived, is that *variable* vertical crossing angles become possible. In fact, since the electron ring is above the proton ring on one side and below on the other, it is possible (at considerable expense of luminosity) to turn off the coincidence magnet altogether and therefore not commit, for all time, the overall design to what some experimenters might consider an untested or risky situation. Some vertical rearrangement of components is implied to compensate for changes in the orbit, but this should not produce fundamental difficulties. The introduction of a vertical crossing angle of only 1 mrad would reduce the luminosity by only about 25% and yet reduce the amount of synchrotron radiation which is emitted tangentially to the electron orbit and which would travel down the proton beam pipe. This angle also helps the photon-proton scattering problem[24]. This problem can also be ameliorated by introducing also a horizontal crossing angle of about 1 mrad [35] and/or tapering the fields at the ends of the magnet that face the IP. A few disadvantages also occur. The first of these is that electron tagging for photoproduction experiments is not easily accomplished because the "tagged" electrons now travel in the same direction as the radiation fan. Another is that the synchrotron radiation from both halves of the magnet is now emitted into the same sector, increasing power density problems at the absorber. Finally, the conductors now have coil ends near the IP. These questions deserve further study.
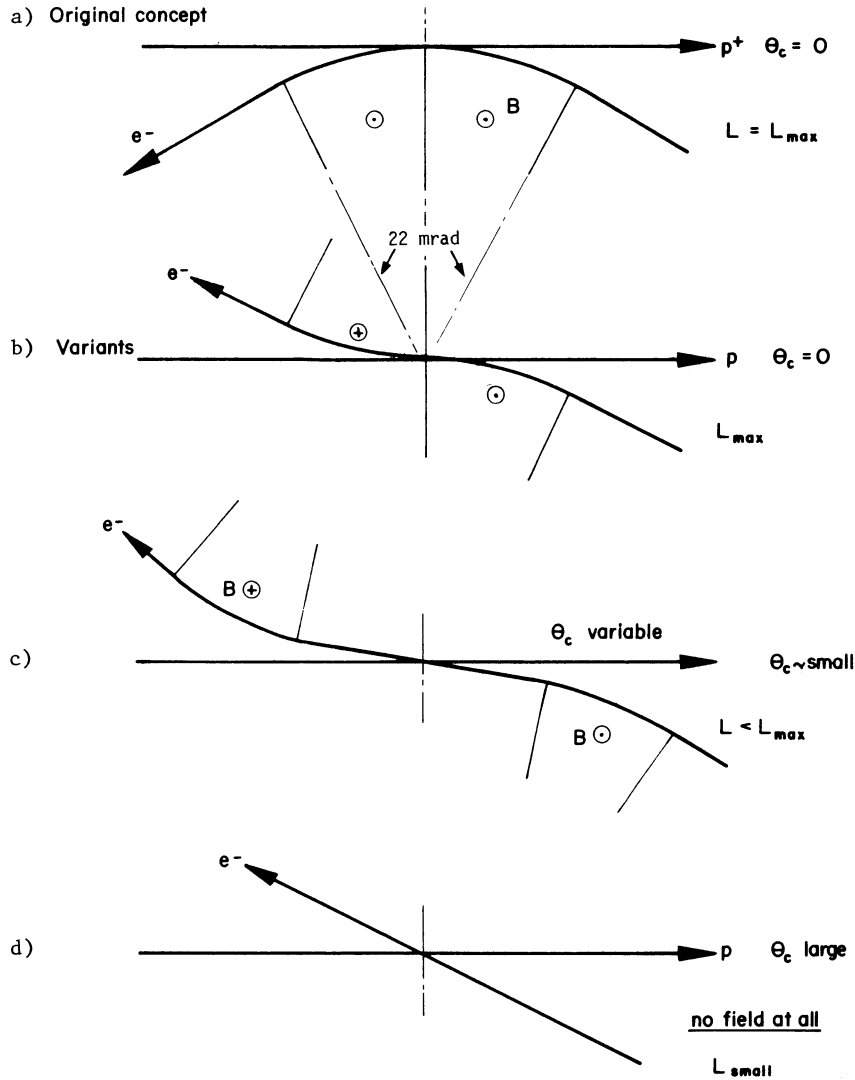
a) Original concept

b) Variants

c)

d)

Fig. 12 Orbits for the following field configurations at the intersection point:-
a) uniform horizontal field, b) "split" field with crossing angle = 0;
c) "split" field with small crossing angle; d) no field, and crossing angle
large.

A cross-section of the coincidence magnet is shown in Fig. 13. The conductors are arranged to form a Helmholtz coil and shaped to obscure as little of the aperture (20%) as possible. The amount of copper will be determined by cooling requirements. The conductors bend along the electron orbit so that, at the ends of the magnet, the proton beam has passed through the reversal region and some of its deflection has been compensated. A thin, perhaps corrugated, vacuum chamber, tall enough to let the radiation pass downstream unobstructed, surrounds the conductors. The conductors are fastened to the chamber, which is held from collapsing by tension bars located in the shadow of the conductors. An examination of the parameter list indicates that this is a difficult but not unreasonable magnet to construct. The most dangerous place as far as radiation from the Gaussian tails of the beam is concerned occurs where this radiation must pass the vertical inside corners of the conductors. Remembering that the effective source position is the interaction point itself, this place is 3 m

Direction of synchrotron radiation

Location of electron beam

$$B = \frac{16\mu i}{10\pi a}$$
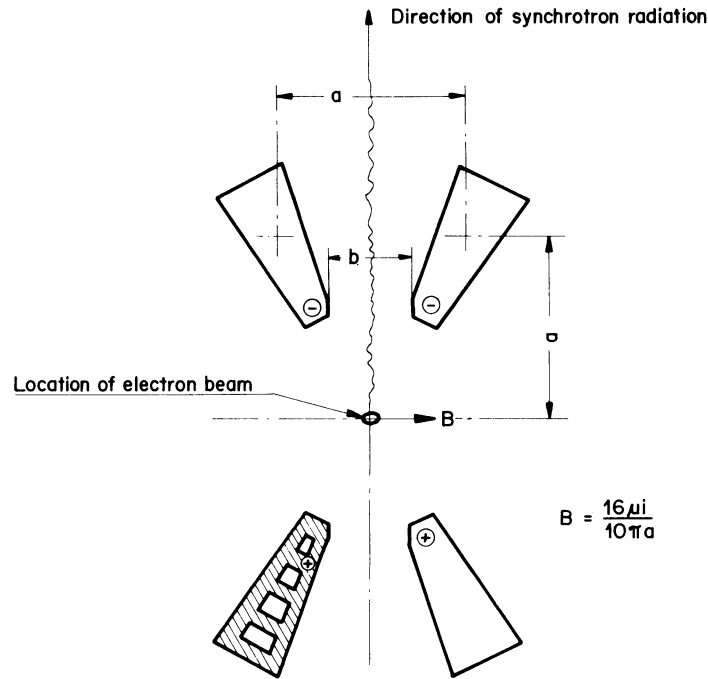
B	= 0.3 T	V_{10m}	=	9.26 V
a	= 0.0385 m	$P_{10\,m\,of\,conductor}$	=	166 kW
b	= 1.8 cm	F_{metre}	=	1600 N/m
I	= 18 kA	A_{holes}	=	68 mm²
A_{Cu}	= 3.11 cm²	ΔT_{water}	=	60°C
R_{10m}	= 5 × 10⁻⁴ Ω	Q_{10m}	=	4.0 ℓ/min

Fig. 13   Schematic cross-section of a coincidence magnet

downstream, at which point the beam has a horizontal effective width $\sigma = 1$ mm. The clearance provided is ±9 mm, i.e. 9 standard deviations. The fractional number of photons outside this aperture is 2×10^{-19}, a small number, but of course we have 10^{18} photons/sec to begin with. Whether or not the beam is in fact Gaussian at such a large number of deviations is of course a question, but a scraper far upstream can be used to mask the dangerous region. Orbit distortions become important at the millimetre level.

A field plot of a trial conductor (without water holes) was made using the program POISSON, and is shown in Fig. 14. The vertical gradient seen by the electrons was less than 20 G/cm. The effect of gradient fields on the protons must still be investigated in detail but is felt to be small at this time since this beam is 20 times stiffer. Unfortunately the gradient is vertically defocusing, and would move the IP about 26 cm, a problem that requires minor compensation by the last proton quads. Non-linear effects may be more serious.

7.3   The split proton septum magnet

A cross-section of this magnet at its entrance is shown in Fig. 15. A slot of 2 cm width is provided to let the radiation pass. Since only the downstream magnet needs to be split, the upstream magnet could have a solid septum, ensuring that the upstream electrons
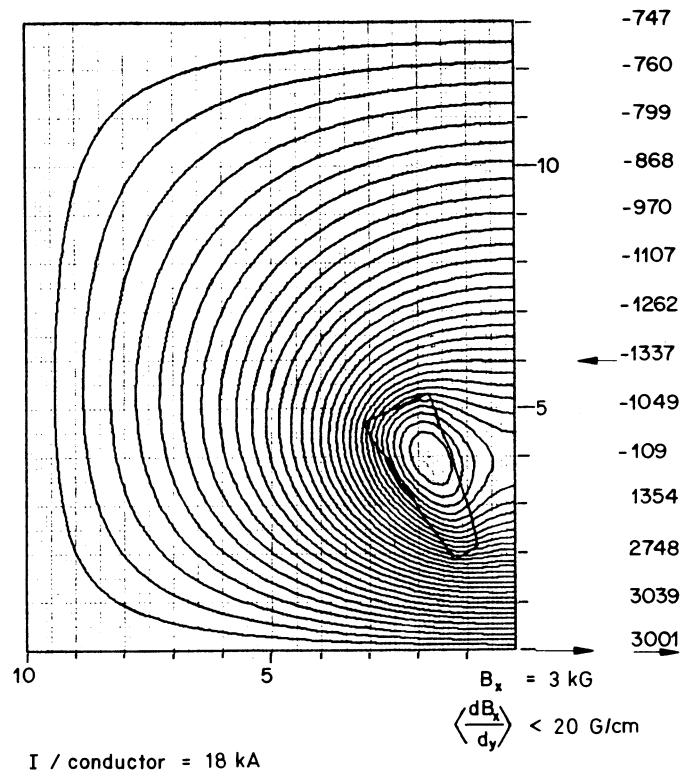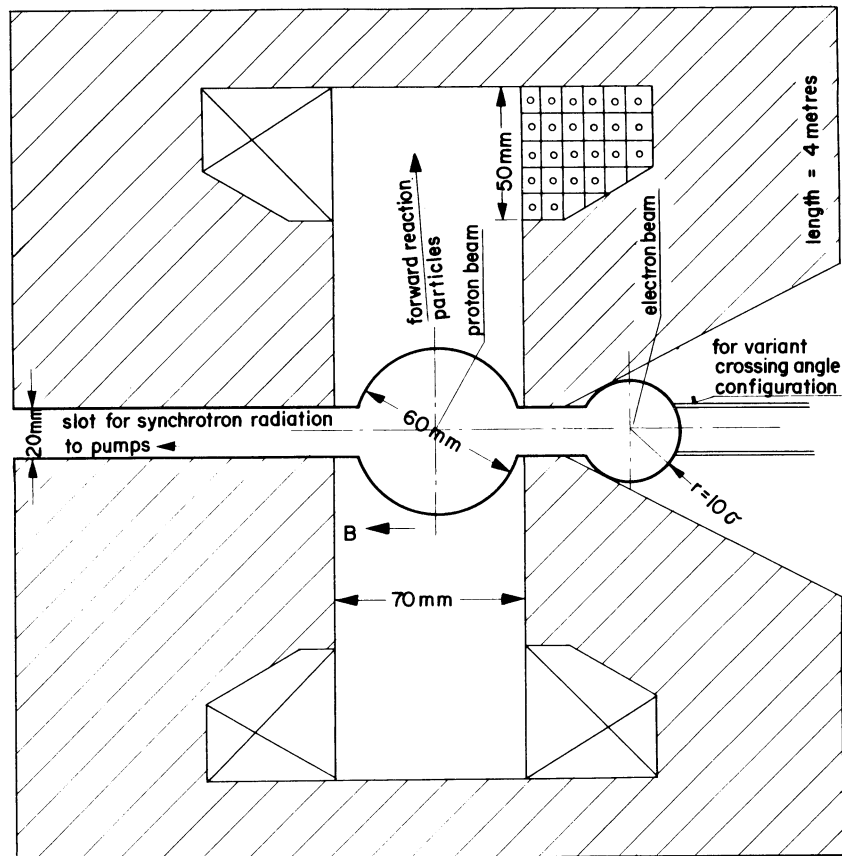
Fig. 14 Field plot of coincidence magnet

Fig. 15 Cross-section of split septum magnet (at entrance), with Z = 6 m

see truly no field. The slot is about 5 standard deviations wide, permitting all but 10^{-5} of the power to escape. *The slot is also used to pump the chambers along their length.* The coil is placed in an unorthodox region to permit reaction particles that are bent horizontally to enter the iron calorimeter without having to pass through the conductors. From the calorimeter point of view, it would be useful to have the outside dimensions of the magnet increase with distance from the IP. From the physics point of view, it would be best to have the walls of the vacuum chamber extend to fill the field volume completely. The reason they are shown as circular in Fig. 15 is to maintain, as much as possible, the electrical continuity of the chamber. Radio-frequency beam impedance considerations will determine the final design. In any case, the walls should present as few interaction lengths as possible. A field plot of one quadrant of the magnet is shown in Fig. 16. The object of the design is to obtain as high a field as possible for the protons and yet let the electrons pass in as low a field as possible. We find a main field of 10 kG can be reached, limited by flux compression in the lower inside yoke. No optimization has been made; the calculation was performed only to establish an existence proof. The field at the electron orbit is less than 100 G and the uniformity of the main field is quite acceptable. A longitudinal packing fraction of 90% should not impair the performance but would require about 10% more current than indicated. The resolution of such a calorimeter should be no worse than that achieved by Barish et al.[36]. The power parameters are modest. If, as is likely, the variant coincidence crossing scheme is adopted, turn the drawing upside down and imagine an extension of the electron chamber for the synchrotron radiation. The magnet cores will have to be retractable for baking the aluminium chamber. Since the chamber may not have posts, external tie bars will be required to keep it from collapsing.
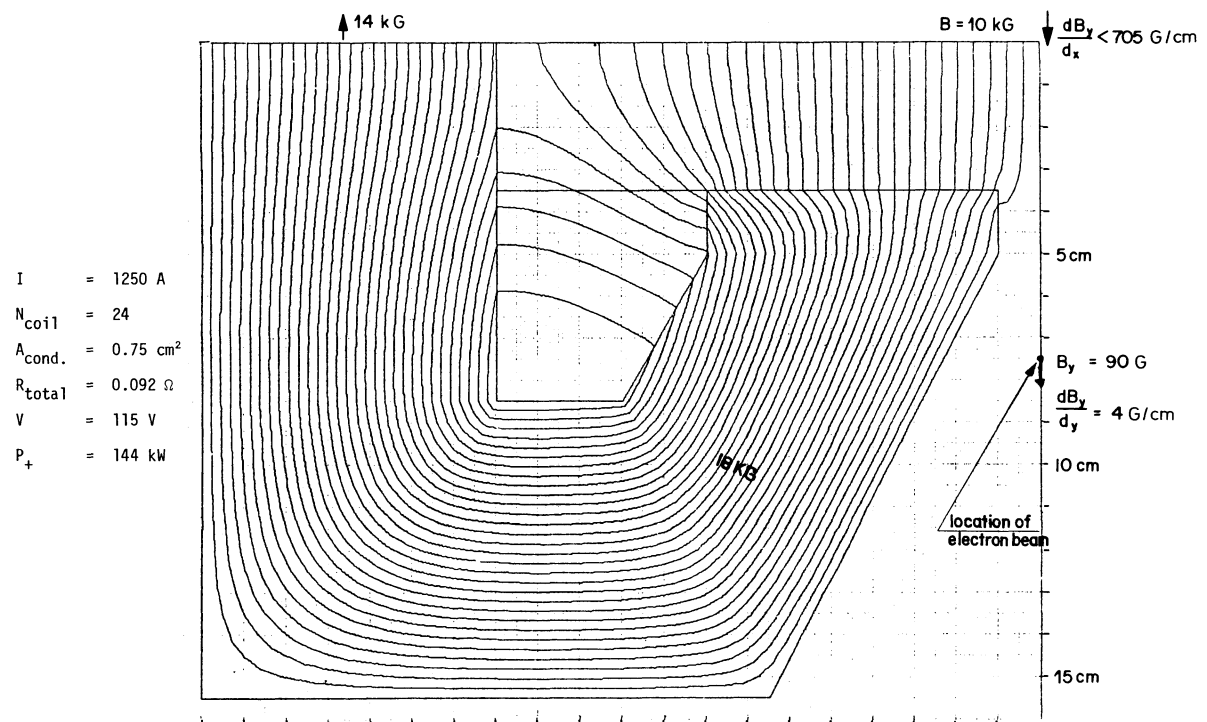

Fig. 16   Field plot of split septum S1 (one quadrant)

7.4 Electron beam quadrupoles

To let the radiation pass through the next element we adapt a Collins-type quadrupole[37,38]. The location of these lenses is set by the desire to keep the β functions below bout 360 m, a procedure adopted by most designers[39]. Fortunately, because the electron ring in this design will contain *many bunches* it is possible to keep the machine emittance small by focusing tightly in the lattice and still stay within the allowed beam-beam tune shift. The resultant machine aperture requirements are therefore quite modest. Experience, however, has shown that it is important not to pass through these lenses off axis and to keep the quadrupolar quality very high. For the latter reason we are generous with the aperture and make the lenses long enough to keep the fields on the poles at low values. This last point may also be important with respect to generation of synchrotron radiation from the lens fields themselves, radiation which would spray down the beam pipe into the detector.

Figure 17 shows a cross-section of the proposed quadrupole and Fig. 18 a field plot.

The further away from the IP the particles are, the more care we need to exercise over the stray fields they feel. Although no optimization has yet been made, the POISSON calculation indicates that fields and gradients suffered by the protons are quite tolerable in this type of design.
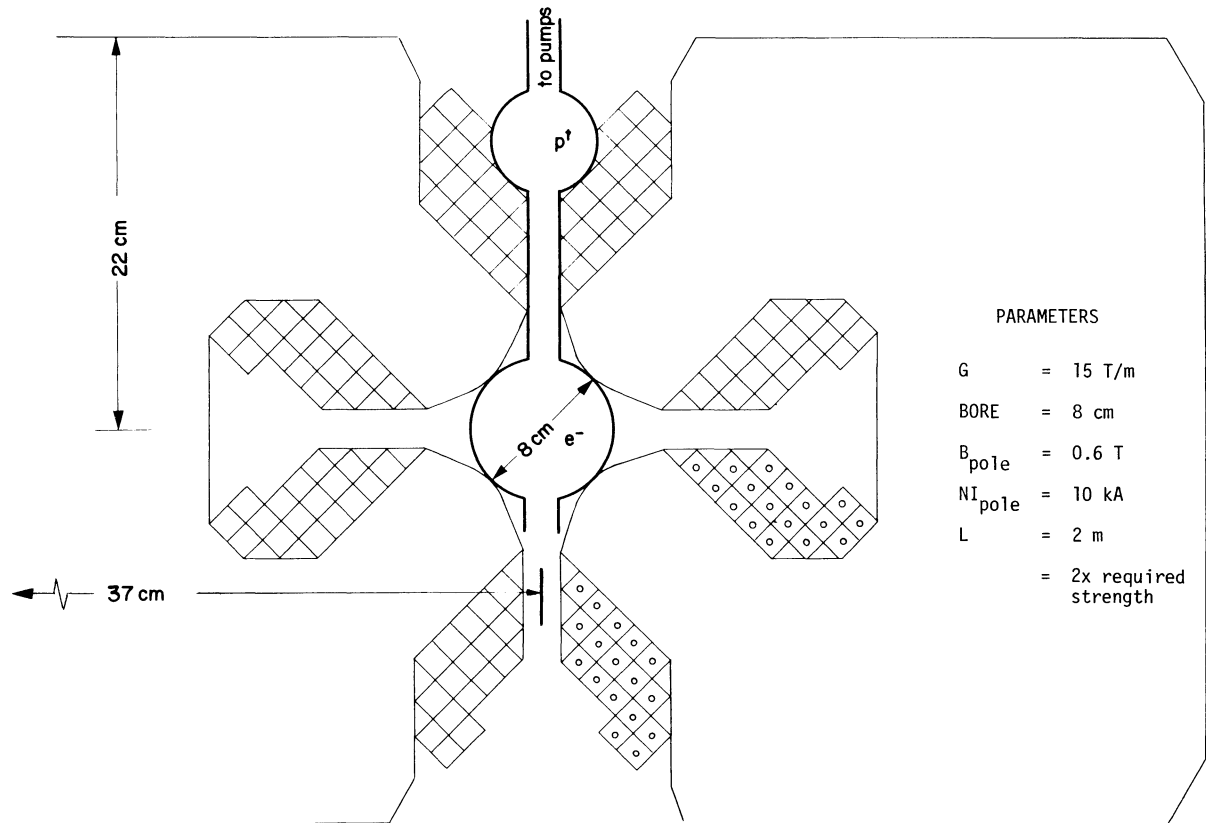

PARAMETERS

G	=	15 T/m
BORE	=	8 cm
B_{pole}	=	0.6 T
NI_{pole}	=	10 kA
L	=	2 m
	=	2x required strength

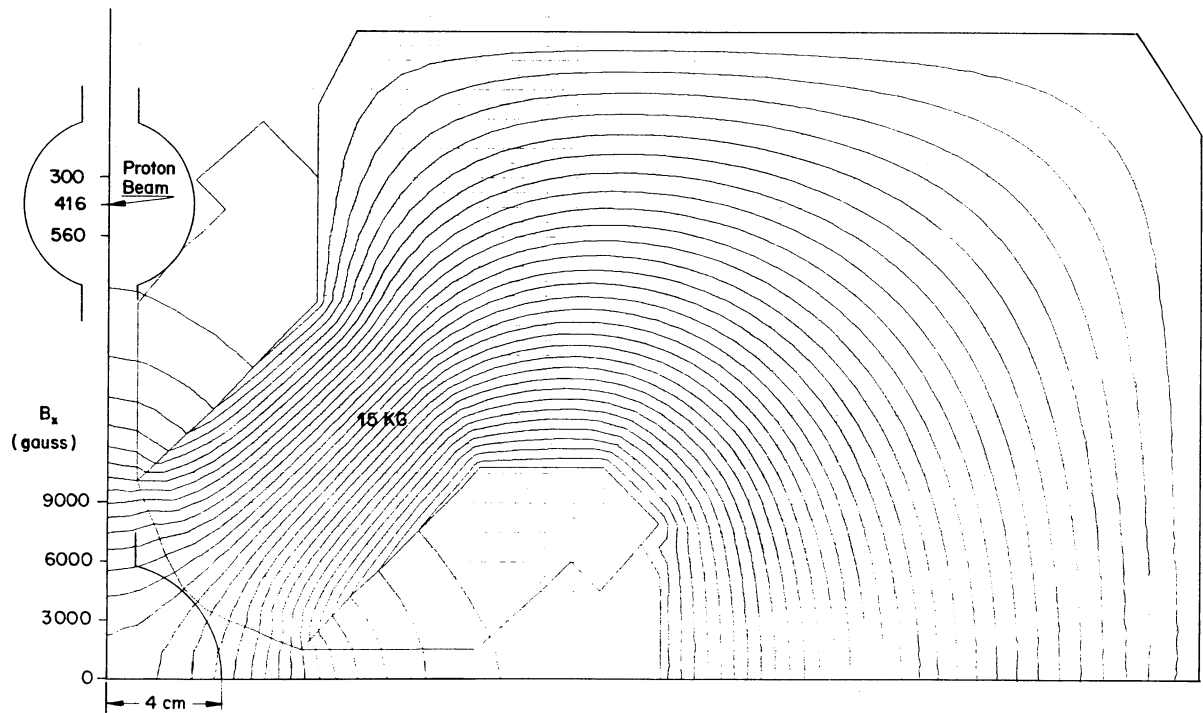Fig. 17   Cross-section of split quadrupole

Fig. 18 Field plot of split quadrupole

7.5 Further components

As shown in Fig. 11, more septum magnets and another electron quad follow. The designs of the septa are similar but, since the ep beam separations are larger at their location, they may run at higher fields. After the third septum, the proton beam has been horizontally displaced by 7 cm, permitting the installation of a calorimeter that samples the most forward *neutral* hadron component that has not entered the other calorimeters. The proton beam pipe diameter remains 6 cm. Without the last bending magnet the deflection is 4.8 cm. If the proton beam is tipped horizontally by 1 mrad at the IP as mentioned previously, another 2 cm are gained, but the slots of course should be along the electron axis. It is felt at this time that the superconducting proton quad will clear the electron beam. However, the fringing field that such a magnet is likely to throw about the landscape must not be seen by the electrons.

7.6 Absorber temperature rise

We are now in a position to re-examine the radiation absorber surfaces which must be located somewhere ahead of the superconducting quad entrance, probably 1 m ahead of the final neutral calorimeter to provide sufficient space to protect this device from hard photons (see Table 4, p. 179). The absorber itself is inside the vacuum chamber, which is split up to this point and pumped along its length via the auxiliary slot as shown in Figs. 15 and 17. The geometry is shown in Fig. 19 for the two coincidence schemes A and B. There is no way to avoid normal incidence of the radiation and still provide adequate water flow at the crotch of the chamber. Assuming the radiation comes from the IP with an angle of 0.33 mrad, the radiation width at the absorber is about 7 mm. Note: One had better not mis-steer the electron beam!
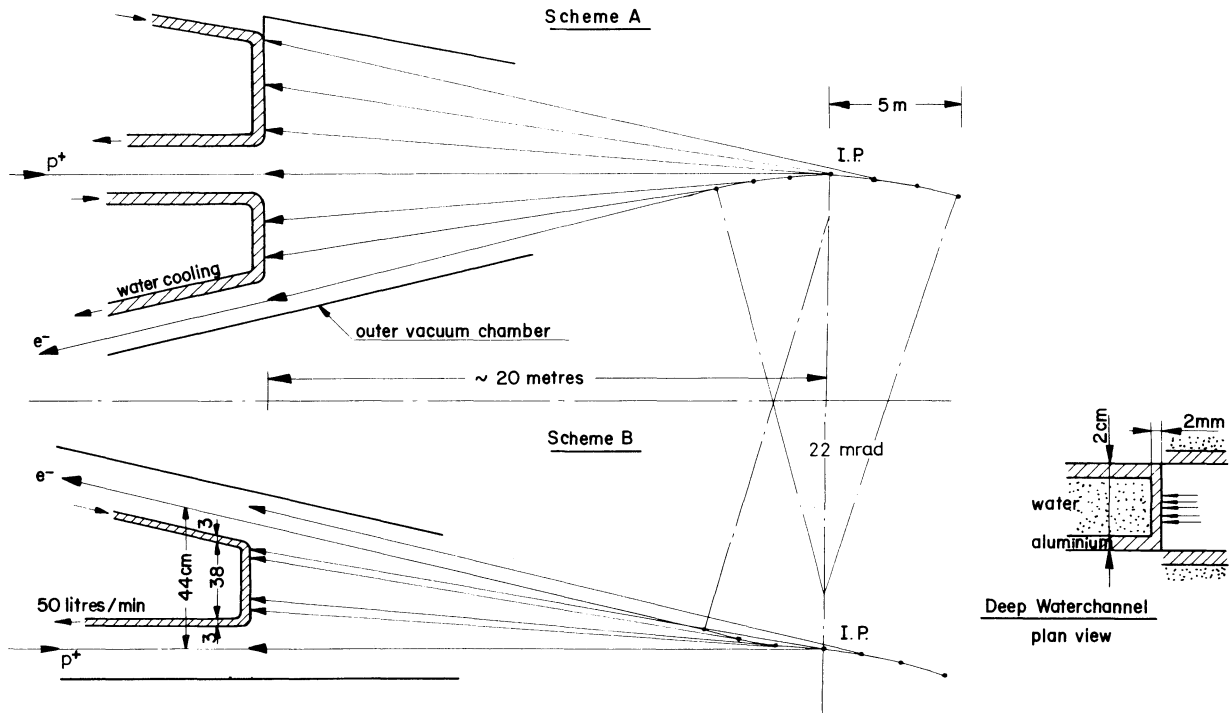
Fig. 19 Absorber geometries for schemes A and B (not to scale)

In the worst case (Scheme B) the incident flux density is then 3.6 kW/cm². Fortunately only a fraction is absorbed by the aluminium, the rest goes into the cooling water directly. In Table 5 we calculate the power absorbed for 2 mm and 4 mm aluminium walls and an electron energy of 20 GeV.

Taking the 2 mm case and assuming that all the power is deposited on the front surface implies a temperature rise of 60°C across the metal boundary. We believe this is still a safe situation *provided the water does not stop flowing*. It is hard to model. Another note of caution: If it is decided to lower the electron energy while at the same time raising

Table 5

Power absorbed for 2 mm and 4 mm wall thicknesses

Photon energy		Power		Absorpt. coeff. σ		$e^{-\sigma x}$		Power absorbed	
Range (keV)	Average (keV)	%	Density (kW/cm²)	(cm²/g)	(cm⁻¹)	x = 2 mm	x = 4 mm	2 mm (kW/cm²)	4 mm (kW/cm²)
1-10	5	5	0.18	100	0.0037	0	0	0.18	0.18
10-40	30	20	0.72	1	0.37	0.58	0.33	0.30	0.48
40-100	70	35	1.26	0.07	5.26	0.96	0.92	0.05	0.09
100-200	150	25	0.90	0.03	12.5	0.98	0.99	0.02	0.01
200-400	300	15	0.54	0.03	12.5	0.98	0.99	0.01	0.01
Total		100	3.60					0.56	0.77

the electron current to keep the total RF power consumed the same, then this favourable situation will not apply since more low-energy photons will be absorbed in the metal. Also one suspects that the main absorber side walls should also be cooled to catch the Compton back-scattered power.

8. THE MAIN DETECTOR

In order to discuss event reconstruction and background problems, a model detector configuration must be chosen. For this purpose we construct a version of the Willis Impacto-meter[40], use of which has been proposed for ep collisions by several authors[13,41]. The reasons for this choice are as follows.

For the very high energies considered in this work and the forward angles of the reaction products from "interesting events", a solenoidal spectrometer, whose field is parallel to the axis, is *not* well adapted. This is not to say that such a device would not be useful for analysing the pionization cloud in detail or looking at events at 90°, but these latter reactions come from a region of the kinematic diagram that is not in line with the physics interest covered in this note. Remembering that the electron beam must not feel the high fields that would be required for any useful kind of energy resolution, we may consider toroidal field configurations that have no field on the axis. Preliminary indications are that the development of such a magnet and its associated high resolution track chambers would be extremely costly -- nor is it clear that the very high multiplicities involved can be unscrambled. (A toroid in the forward direction may be appropriate at a later stage.) Further, since electron-hadron discrimination is required in any case, the physical size of the shower counter array is probably prohibitive. The same can also then be said for the hadron detectors that would have to be outside this field and that are essential for catching the neutral component. The special case of a toroidal magnetized muon detector is treated later on. The reader is also referred to many other magnetic configurations suggested at the PEP Summer Study 1974 (PEP-137).

Calorimeters, on the other hand, distinguish themselves by the fact that their fractional energy resolution *improves* with energy. They have very short response and memory times and are insensitive to soft radiation such as electrons and protons up to a few tens of MeV.

Cross-sections of a conceivable device are shown in Figs. 20 and 21. An attempt has been made to keep the apparatus as compact as possible so as to reduce the sheer volume of material and yet cover the solid angle. As it is, as can be seen from the "artist's conception" shown in Fig. 22, the device is by no means trivial. One advantage of a modular concept is, however, that some interesting studies could begin with partial coverage. Clearly no attempt at optimizing the engineering has been done. A brief description of various components, using today's technology, follows.

8.1 Calorimeters

8.1.1 Electron shower detectors

We consider two types of system that appear to be applicable in this case. They are lead-glass Čerenkov[42,43] and liquid-argon hodoscopic shower detector arrays[44,45]. Although sodium iodide crystals are capable of very high resolution, we believe their cost would be prohibitive, nor is their speed of response as good. Lead-scintillator sandwiches are cheaper
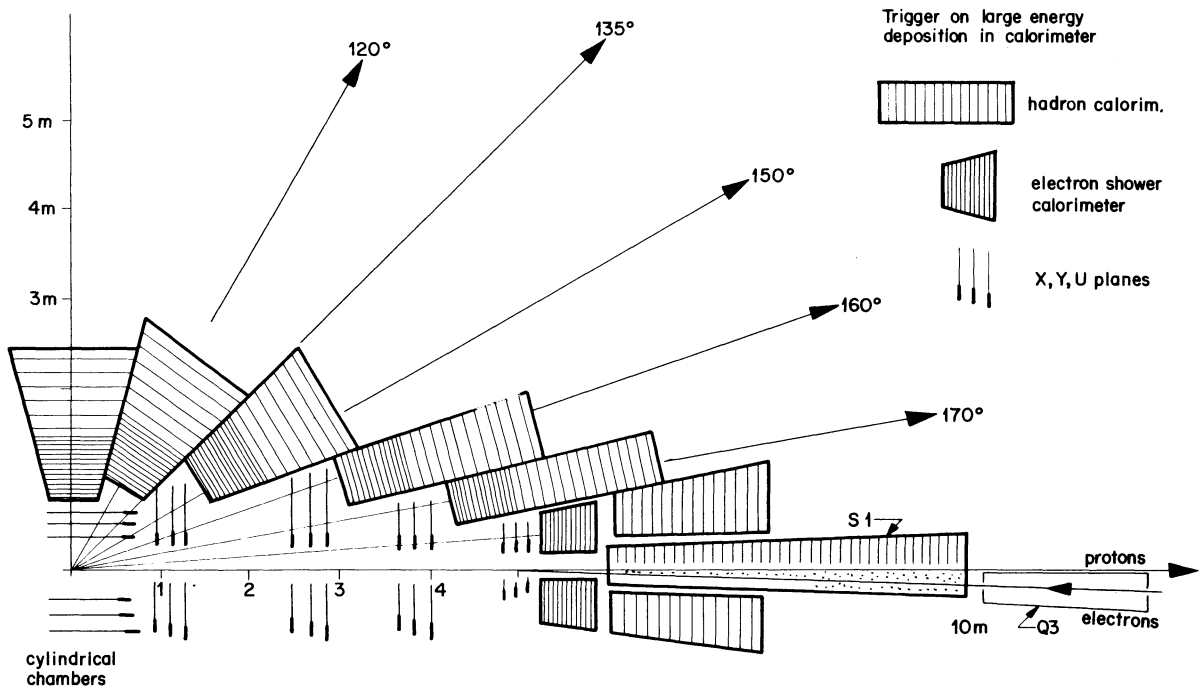
Fig. 20   Vertical mid-plane section of LSR ep calorimeter detector
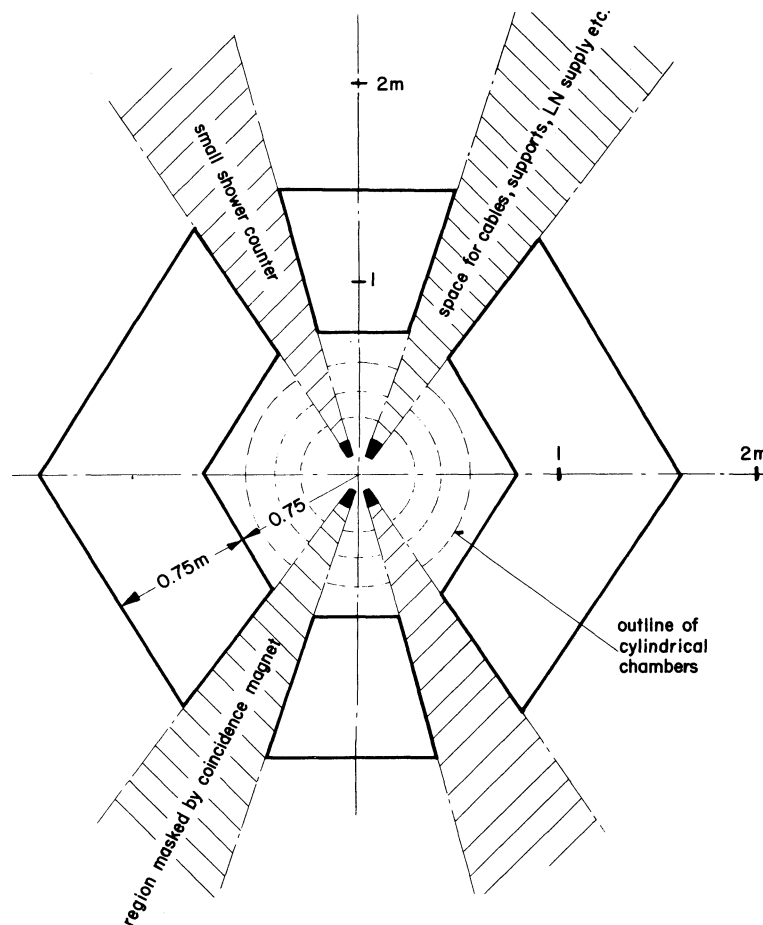
Fig. 21   Section through the detector 3.5 m downstream of the IP
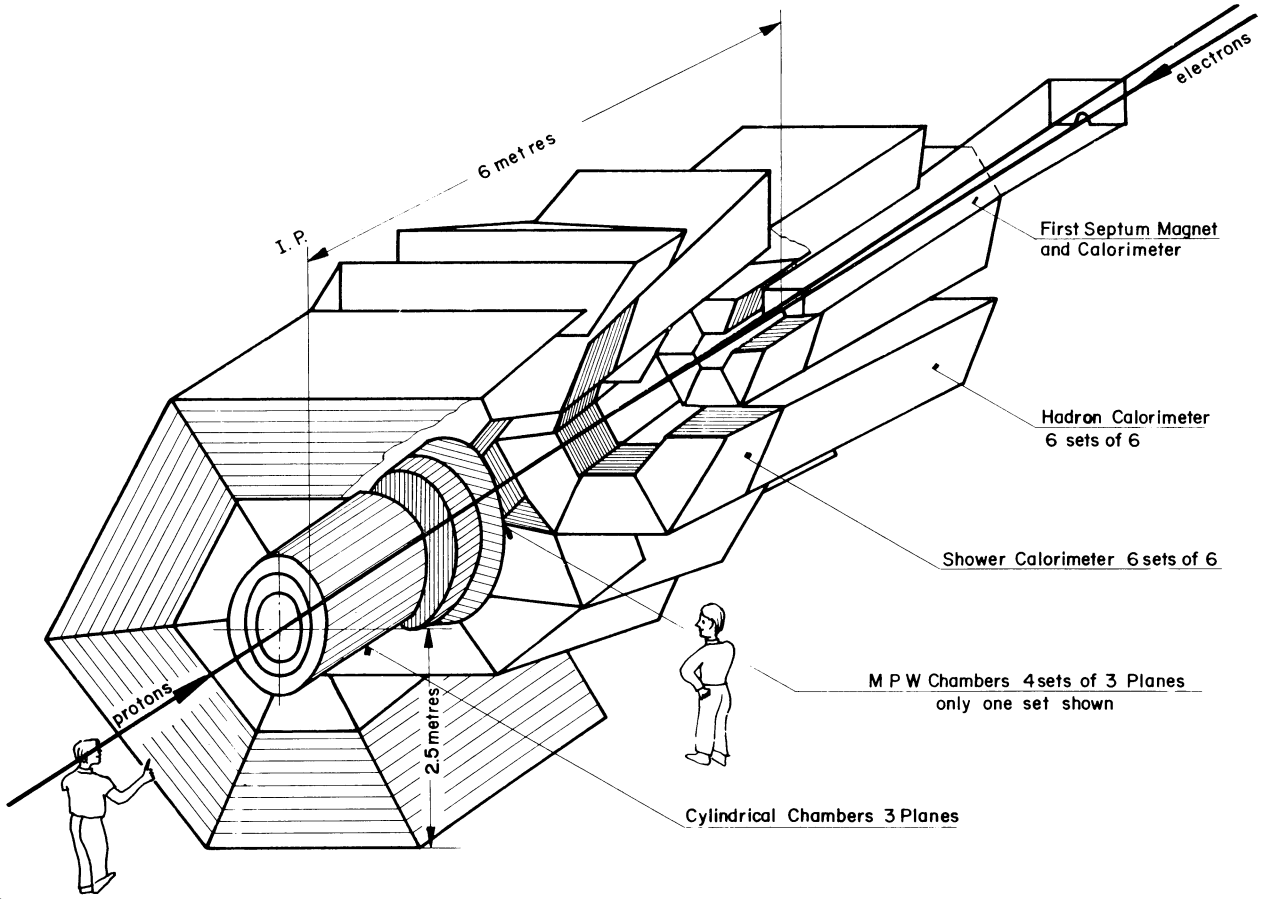
Fig. 22 Artist's view of the LSR ep detector

but their resolution for the electron shower is not as good and their light-piping in this geometry would be difficult.

Experience with lead-glass counters indicates that, with care, a large system is capable of good linearity and resolutions, FWHM = $[(10/\sqrt{E}) + 1]$% (E in GeV). Extrapolating this result, we note that a 100 GeV electron could be measured with about 2% -- quite well enough for our purposes. For an appreciation of the problems encountered and their solutions, the reader is referred to the references cited. The lead glass, in one case, was 35 + 10 cm deep which, together with end-view phototube, would fit into the 75 cm space shown in Fig. 20, although at higher energies a few more radiation lengths may be required to reduce energy leakage out the rear face.

Liquid-argon ionization chambers are also very well suited as far as resolution is concerned, as well as having an additional advantage with respect to cost in a very large installation. This saving may be partially offset by the complications of having to deal with cryogenic liquids and the associated engineering and materials problems. The perform-ance of an iron-plate unit, for instance, can be summarized by the expression

$$\frac{\Delta E}{E} \text{ FWHM} = \left(0.026 \frac{D}{E} + 3.6 \ e^{-0.035L} \right)^{\frac{1}{2}}$$

D = plate thickness, L = over-all length of the calorimeter,

valid for $1 < D < 10$ mm, $E > 2$ GeV, in which D and L are in mm and E in GeV. The first term represents the influence of sampling, the second a contribution due to energy leakage. Since this expression was arrived at by fitting Monte Carlo calculations, it represents the physics inherent in shower development and does not contain instrumental effects such as drifts, amplifier noise, etc., which may become dominant at much higher energies. Setting $D = 1.5$ mm, $L = 300$ mm $\sim 17X_0$ (that is 200 cells), we see that the first term still dominates by 4 to 1, and extrapolating to 100 GeV we find a FWHM of 2.2%. The over-all length of such a device with 2 mm argon spacing is about 70 cm. In this case the problem of standardizing the gain of a phototube array is replaced by tolerances on cell spacing and calibration of charge amplifiers, but these problems have been successfully solved. By breaking the collector plates into strips, fine spatial resolutions have been achieved in the ionization mode. Since each strip must have an amplifier, the width of the strip is set only by the greed of the experimenter and the size of his computer and pocket book. We believe it is too early to estimate which of the two systems will be more suited years from now, but either one is entirely satisfactory at this time.

8.1.2 Hadron calorimeters

While the development of an electron shower is usually described in terms of radiation length, the development of a hadron shower depends on *interaction* length, and by this fact it is possible to *partially* distinguish between these two types of radiation. A much studied device is the iron-plastic scintillator sandwich. Several of these devices have been tested[36,46], as has the argon calorimeter mentioned in the previous section. A discussion of the factors that go into determining the resolution can be found elsewhere[47]; however, one consideration should be singled out, namely that in the hadron case, the over-all resolution becomes fundamentally limited by fluctuations in the amount of energy deposited in the nucleus, energy which is not sampled by an ordinary calorimeter. A novel idea for recovering this energy is to replace the iron by uranium-238, in which case the lost binding energy can be recovered in the prompt electromagnetic emission from decay products following the break-up of this nucleus (see Fig. 23)[48]. This trick, of course, has several consequences, among them cost. We hope to show that the iron calorimeter may suffice.

Present-day indications are that a well-designed iron-argon calorimeter will yield a FWHM = $120/E^{\frac{1}{2}}$, which would give a 12% resolution for a 100 GeV hadron. The question in our application is, What is the hadron energy in this experiment? We have already indicated that we expect high multiplicities, so the average energy per hadron is perhaps 20 GeV and the resolution is clearly not good enough. However, this may be one of the few times in physics when one can cheat statistics. This is because the energies of the hadrons from a single event are correlated. Further, as indicated, the kinematically formed jets are so narrow that all the hadron energy is likely to end up in a single calorimeter. It does not therefore matter, in measuring p_T, whether the multiplication took place in the target nucleon or in the front face of the calorimeter. Table 2, p. 172, shows that we have anywhere between 150 and 300 GeV available, just barely giving the required resolution. One must remember, though, that this procedure of adding energies is valid only if statistical fluctuations dominate the resolution. Single-particle inclusive reaction studies will be hard to carry out, since one does not in this way measure the momentum of each particle. With uranium plates the resolution is expected to be a factor of 2 better (see Fig. 24)[48]. One could imagine using a large energy deposit ($E \geq 100$ GeV) as the trigger signature in these experiments.
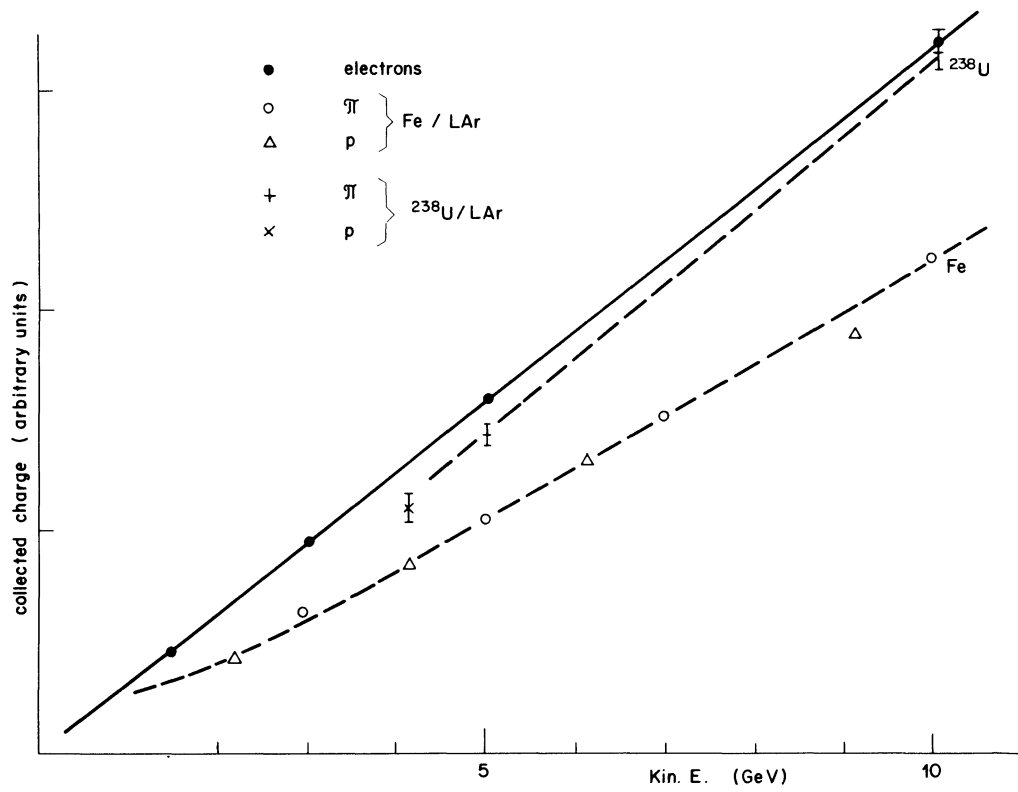
Fig. 23 The response of an iron plate and a uranium plate calorimeter as a function of the kinetic energy of the incident particle for electrons, pions and protons.
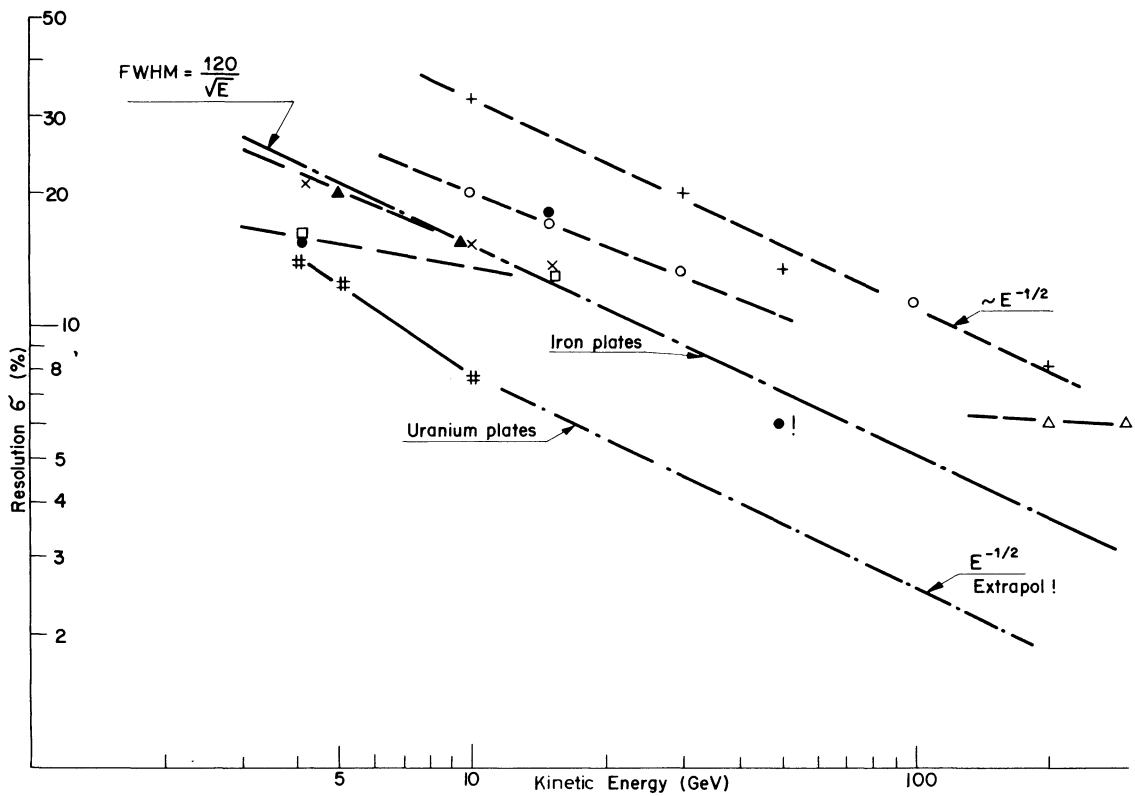
Fig. 24 Comparison of the calorimeter resolutions with uranium and iron plates, as a function of the kinetic energy of the incident particle.

Developments in this art in the next several years may permit the combination of electro-magnetic and shower detector into one container. As of now, we will plan for a hadron de-tector depth of 1 to 1.5 m.

8.2 Track chamber and scintillation hodoscope considerations

Several sets of wire planes are shown in Fig. 20. Their purpose is to permit recon-struction of charged particle tracks to their origin in order to eliminate "pipe" events and to aid in determining the multiplicity of an event. How close to the beam pipe they may be placed is unknown at this time, so it may be wise to plan on small, local, high-rate chambers as well.

The interaction volume is fractions of a (millimetre)^2 in cross-section and about one metre long. The nearest high-mass object to this volume is a coincidence magnet conductor which is about 1 cm away horizontally and 2 cm vertically. The chambers should be arranged so that each track has a substantial lever arm between two sets of planes and a third set of planes or more for discrimination. The worst case is for events with angles near the proton direc-tion. About 1 mm wire spacing is called for. The effect of the coincidence magnets' field on high-energy particles will be small since this field is weak and most particles will have small path length in it, but this effect must still be investigated and put into the other-wise simple reconstruction programs. The field will aid in determining the sign of a charged particle. The estimated opening angle of a hadron jet in the forward direction at p_T = 50 GeV/c is about 14 mrad. Taking the recent FNAL results[49] for the average charged multiplicity on hydrogen in neutrino reactions, $\langle n_c \rangle$ = 1.0 + 1.1 ln W^2, and extrapolating to our energy region, we would expect $\langle n_c \rangle$ = 11 at W = 120 GeV. (See kinematics, Fig. 2.) One millimetre spacing in a small-angle chamber at 4 m from the IP should be fine enough to resolve this multiplicity on the average, provided ambiguities from stray sparks do not overwhelm the reconstruction.

Given a duty cycle of $\sim$ 10% (depending on the amount of bunch-lengthening, electrons fill about 5% to 20% of an RF bucket to maintain quantum lifetime) we favour multiwire proportional chambers for their speed of response, short memory time, and single wire rate capability. With an RF frequency of 200 MHz the interbunch period is 5 nsec. It may be better to fill only every other bucket so as to better match a 10 nsec trigger resolution time, but this obtains at the expense of duty cycle. Consideration should be given to a ring RF frequency of 100 MHz. This frequency is probably also preferable to lower "higher mode losses" around the ring but is achieved at the expense of shunt impedance/metre of the accelerating structure.

A serious effort should be made to find ways of reducing chamber sensitivity to soft photons in the keV range. Perhaps those regions of the chambers immediately in front of the calorimeters could be "hardened" by thin absorbers without introducing much multiple scattering or energy loss. Also some care should be taken to avoid backscatter from the face of the calorimeters. A special set of counters should be placed in the shadow of the coincidence magnet conductors to identify high-energy electrons from *bona fide* events that will shower in the copper.

8.3 A muon detector

For the study of the reactions listed in Section 4.1.3, in which a single or dimuon emerges at high energy (as, for example, from the decay of a heavy boson), Lederman has pro-posed the so-called "magnetized iron ball detector"[50]. Variants of this device may also be

found in the literature[51]. In most of these proposals the iron absorber is placed very close to the interaction point so that muons from pion decay are suppressed. The consequence of this choice is to discard the inner detector. Since many tons of absorber surround either the IP or the detector, the muons from these probably *very rare* reactions can be measured in a relatively background-free environment. This subject is mentioned only to provide another guide as to dimensions required for the interaction area pits. However, we must remember that the cases discussed before dealt with incident protons or electrons of *equal* momentum, *not* with the large momentum imbalance involved in ep reactions.

9. BACKGROUND

Only a few of the most serious sources have been investigated at this time, and these are connected with synchrotron radiation interacting with the proton beam itself. This subject is treated in a separate note[24] and is summarized at the end of this section. However, we will list others, not necessarily in order of importance, that have been identified at SPEAR[52] and at the ISR to see how they affect machine design.

9.1 Electron-induced effects

9.1.1 Background from electrons which have been lost from stable orbits

The dominant process expected to contribute to electron beam lifetime is beam-gas bremsstrahlung. Beam-gas Coulomb scattering is important only for low-energy operation, and beam-beam bremsstrahlung has been calculated for the ep case[53] to be several hundred hours. In contrast to the PEP or EPIC design, this results from the fact that we propose to fill nearly all the buckets, a fact that also makes Tousheck lifetime problems negligible.

The mechanism of beam-gas bremsstrahlung loss is that a particle suffers a collision with the gas and loses enough energy for it to be excluded from the energy acceptance of the RF system. It will drift away from the bucket over *several orbital periods* until it strikes a physical aperture. The loss rate is given by

$$- \frac{dn}{ndx} = \frac{\rho}{X_0} \ln \frac{E}{\Delta E} = \frac{\ln (E/\Delta E)}{X_0} \frac{MP}{RT} , \tag{1}$$

where $\Delta E/E$ = energy acceptance = 5×10^{-3};

  X_0 = radiation length of the most dangerous gas species thought to be present, namely CO = 38.5 g/cm^2;

  M = molecular weight = 28 g/mole;

  P = *partial* pressure of CO.

Then,

$$- \frac{dn}{ndx} = 2.25 \times 10^{-14} \text{ P (in } 10^{-9} \text{ Torr)} \quad m^{-1} . \tag{2}$$

The number of particles circulating per second is

$$Nf = I/e . \tag{3}$$

At the design current of 250 mA this is 1.6×10^{18} particles/sec.

We must now estimate the average pressure at which the electron ring will operate, and for this we scale (Table 6) the PEP design figures[29]. The pressure figure quoted in their report is very likely conservative.

The reader will notice that the machines are really quite similar except for the circumference. If we assume the same linear pumping speed for the distributed pumps and scale linearly with radiated power, we would expect the figures *in italics*.

Combining the results of Eqs. (2) and (3) and the above obtained pressure yields a loss rate of 250 kHz per metre! The last bending magnet that would sweep the showers, caused by these losses, out of the beam direction, is located some 60 metres upstream of the IP. Since each electron carries 20 GeV, clearly we must place well-shielded aperture stops in the intervening region to dispose of this flux and to prevent, as much as possible, the electrons leaving the machine from striking the pole faces of the last quadrupoles or the conductors of the coincidence magnet. Perhaps the whole upstream aluminium pipe[*] should be surrounded by a lead sheath. A detailed examination of impact points requires knowledge of the specific lattice and is beyond the scope of this report. However, it is important to note that the magnitude of the effect is proportional to the *average pressure around the ring*. Fortunately, most of this background is very directional and travels opposite to our main physics interest, but "small-angle" luminosity monitors must deal with this problem. Further calculations may show that the conductors of the coincidence magnet should be pulled back somewhat.

Table 6

A comparison between PEP and LSR e-ring parameters

Parameter	Units	PEP design	LSR e-ring	Ratio LSR/PEP
Total circumference	m	2100	6150	2.9
Circum. in arcs	m	1386	4400	3.2
Radiated power	MW	5.2	6.9	1.33
Beam current	mA	2 × 100	250	1.25
Beam energy	GeV	15	20	1.33
Average linear pumping speed	ℓ/sec m	110	110	
Critical energy	keV	44	34	0.77
Fraction of pressure in CO equivalent		0.3	0.3	
Average total pressure	Torr	5×10^{-8}	2.2×10^{-8}	
Partial pressure in CO equivalent	Torr	1.6×10^{-8}	7.2×10^{-9}	

[*] Until now, we have assumed that the main part of the electron ring vacuum chamber will be made of aluminium. The advantages over stainless steel with respect to heat conductivity and lower desorption coefficients for synchrotron radiation have been proved at SPEAR. A continuation of this material into the IR, however, has consequences for the design of the proton vacuum chamber to which it is joined.

The lifetime associated with these losses is given by

$$\frac{1}{\tau} = -C \left(\frac{dn}{ndx}\right) \quad \text{or} \quad \tau = \frac{41 \text{ hours}}{P_{CO} \text{ (in } 10^{-9} \text{ Torr)}}$$

For $P_{CO} = 7.2 \times 10^{-9}$, $\boxed{\tau = 5 \text{ hours}}$

A lower pressure for CO is certainly important! If the discharge treatment at present being studied at the ISR[54], using oxygen to clean out carbon, is applicable to aluminium chambers, a great stride in electron-ring vacuum technology will have been taken.

9.1.2 *Background from direct gas bremsstrahlung interactions near and in the interaction region*

We now discuss electrons, initially stable in their orbits, suffering gas collisions upstream of the IP and losing some of their energy in the form of a photon. Two things happen: i) the electron will not be properly focused by the last quads and will hit something; ii) the photons will not be focused at all and hit something. The rate for this loss process is proportional to the pressure in and *upstream of the IP*. Since there are no bending magnets for about 60 m, little synchrotron radiation impinges on the walls and a much lower pressure in this selected region is, in principle, possible. The rates are lower than those of paragraph 9.1.1 but harder to combat.

9.1.3 *Direct nuclear electron-gas collisions near the IP*

Since the IP region itself will require a vacuum of the low 10^{-11} Torr order, for other reasons such as proton beam stability, this background will be small and is generally eliminated by reconstruction of the impact point.

9.2 Proton-induced effects

Loss rates as low as 10^{-6}/minute have now been observed for high current stacks in the ISR. This is equivalent to a lifetime of 2 years! but requires a few comments. 1) This phenomenally small loss rate obtains only if no part of the stack contains particles on non-linear resonances below eighth order[55]. In fact several hours after stack creation some particles may have diffused onto such resonances causing loss rates perhaps a factor of 10 higher, but these can be removed by a scraper and/or Q-shift manipulation. 2) All parts of the ring must have proper electron clearing plates to avoid the electron-proton neutralization instability[56,57]. As in the ISR, this also requires a vacuum in the LSR of the order of 10^{-11} Torr [58]. 3) As mentioned before, proton pressure stability requires that all surfaces seen by the proton beam have sufficiently low ion desorption coefficients.

For comparison with the electron case, a 10 ppm/min loss of a 7 A LSR proton beam yields a loss rate of 25 kHz/m of circumference. Again we would hope that suitable scrapers would be able to localize these losses far from the IR, but experience at the ISR has not yet yielded satisfactory results. This may be because high-energy protons are far harder to remove from a machine than electrons. Since the electron beam is bunched, some part of the 7 A proton contribution to background can be gated out.

9.2.1 *Proton-gas Coulomb scattering upstream of the IP*

Given that a pressure of the order of 10^{-11} Torr exists in the 0-30 m region upstream of the IP, it appears that the halo of beam particles causing background in ISR experiments is

caused by Coulomb gas and nuclear collisions. Rates are observed to be proportional to the *local* pressure. The most serious problem will be that faced by the downstream neutral hadron shower calorimeter. We suspect that this device cannot be included in the energy deposition trigger. Track chambers close to the ISR beam pipe seem to survive. More calculations must be made.

9.2.2 *Proton beam instability due to collision with a periodic electron beam*

This subject has received some attention[59] and we make two comments. First, the proton beam-beam tune shift in this design is of the order of 10^{-4}, small compared to that required to fulfil the decoherence condition studied in the computer model[60]. Secondly, it may be useful to design the proton and electron ring circumferences to operate the rings in an *asynchronous* mode. Single-particle intrabeam scattering effects are probably negligible.

9.3 Synchrotron radiation effects

From a background point of view, the introduction of the coincidence magnet is, at first sight, quite unthinkable, but the spirit of this work is not so much to propose the above design as the only solution to the crossing angle problem, but to examine the consequences of the idea. As mentioned above in some detail, the first line of defence has been i) to move the dump as far away from the detectors as possible (20 m from the IP); ii) to make the absorbers re-entrant to catch the Compton-scattered photons; iii) to rely on a trigger that is extremely "hardened" (energy deposition in the calorimeters, say 50-100 GeV); and, iv) to protect the chambers against soft radiation. Even with these precautions some effects appear to be unavoidable. Steps can be taken to minimize them.

9.3.1 *The interaction of synchrotron radiation with the proton beam[24]*

The mechanism is as follows. Synchrotron X-rays with a continuous spectrum from keV to MeV transform to energies from 1 MeV to 1 GeV in the rest frame of the proton. Four processes have been examined; their cross-sections are known:

i) Elastic proton Compton scattering: The photons scattered backward in the protons' rest frame can reach energies up to the 300 GeV range and possibly simulate back-scattered electrons from the processes that we are interested in.

ii) Pair production in the field of the proton: This case is harder to follow, but, in general, final pairs (1 to 10 MeV) from the high-energy X-rays (150 keV to 1 MeV) go forward in the lab and would not disturb the experiment other than to curl up in the coincidence magnet field. Pairs produced by photons in the 5 to 100 keV range, on the other hand, can go backwards in the lab (i.e. in the protons' direction). With their energies 1 MeV to 1 GeV and cross-section in the millibarn range, they will be impossible to keep out of the chambers.

iii) and iv) π^+ and π^0 production: These particles can also go into the backward hemisphere with energies up to a few hundred GeV. Strange particles are also possible.

The rates for these backgrounds[*] are listed in Table 7.

---

[*] For details of the energy and angle distributions of these backgrounds, the reader should consult Ref. 24. Most of the events have characteristics that make them identifiable and are not fatal to the experimental program considered in this work.

Table 7

Integrated rates due to various processes with photons

Process	Coincidence magnet of 3 kG	Taper to 500 G at ends of magnet
Compton	60/sec	5/sec
Pairs	4×10^5/sec	2×10^4/sec
Pions	10^3/sec	0.05/sec

Two countermeasures have been proposed to deal with this problem. The first is to introduce a horizontal crossing angle of about 1 mrad [35]. The fan of vertical synchrotron radiation will then miss the proton beam line except for the volume in which the two particle beams cross. A factor of about 3 can be gained this way. The real luminosity is reduced by only 25%. The second countermeasure is to additionally taper the field in the S-shaped magnet configuration (Fig. 12, variant b^1). The proton beam is then illuminated by photons of a much lower critical energy, and processes (i), (iii), and (iv) are much reduced kinematically, and (ii) is reduced because the flux is very much decreased. More calculations on this multiparameter problem are recommended but present indications are that a tolerable 25 kHz rate results.

9.3.2 *Interactions of synchrotron radiation with the gas in the IP*

The defence against synchrotron radiation effects is not to permit it to strike *anything* in or near the interaction region. The residual gas is unavoidable. The mechanism is that of Compton scattering of photons that have sufficient energy to penetrate the vacuum chamber wall and convert in the track chambers. For a pressure of 10^{-9} Torr of CO, 5 m length gives rise to a rate of 15 kHz. At 10^{-11} Torr this is negligible and provides another reason for good vacuum in the IR.

Before leaving the subject we must re-emphasize that most of the power generated in the coincidence magnet ends up inside the vacuum chamber in a critical location; that is, 20 m on the upstream proton side of the IP. This calls for special pumping measures. One would suspect that these surfaces, if not super-clean to begin with, will soon become so, but the adjacent surfaces might not be so lucky. Electron desorption laboratory tests of aluminium surfaces following ion-bombardment cleaning are very much indicated.

10. CONCLUSIONS

The above study is an attempt to bring together, for the benefit of the accelerator designer, various aspects and past speculations regarding ep physics interaction areas and apply them to the case of an unbunched 400 GeV LSR proton beam. We have tried to combine the suggestions of many authors, and in a few cases provide some critical examination of the problems encountered in order to see whether some of the most interesting physics experiments can in fact be performed. The conclusion in our minds at this time is: "Yes, but each topic listed requires much further work to study in detail the consequences of the model we have chosen". In particular, lower energy operation of either ring has not been examined. As an aid to machine design, a short form requirements list is appended.

REQUIREMENTS LIST (to do inelastic and weak ep interaction physics)

1. Energy e × p: at least 20 × 400 GeV.

2. Luminosity: at least 10^{32} cm^{-2} sec^{-1}.

3. Energy variability: $80 < E_p < 400$ GeV.

4. Resolutions in x, y: ±0.1 require ∿ 5% on E, p_{x1}

5. e^- detection inefficiency: for $e^- + p \to \nu + X$, ∿ 10^{-5}, $20 < E_e < 400$.

6. Solid angle: complete in kinematically available angles.

7. Neutral detection efficiency: important at all angles but particularly in the forward direction.

8. Longitudinal free space in IR for chambers: at least 4 m for wire chamber resolution.

9. e^+ beam: very desirable.

10. Luminosity monitor: should work equally well for e^+p and e^-p.

11. Vacuum in IR: $< 10^{-11}$ Torr.

12. Vacuum in proton ring: $< 10^{11}$ Torr.

13. Average partial pressure of CO equivalent, in e^- ring: $< 5 \times 10^{-9}$.

14. Partial pressure of CO equivalent in e^- ring upstream of IP: $< 5 \times 10^{-10}$.

15. Longitudinal polarization of e^+ or e^- beams: very desirable, but may require considerable extra length for both proton and electron insertions.

16. Muon identifier: desirable.

17. Sign of particles: magnetic field for charge separation is desirable.

18. Number of intersection regions: at least two; if possible two more of geometry more suitable for photoproduction experiments.

19. Add your own comments.

REFERENCES

1) R.W. Chasman, Proc. Seminar on ep and ee Storage Rings, DESY, 1973 (DESY report 73-66), p. 353.

2) M. Tigner, Proc. Seminar on ep and ee Storage Rings, DESY, 1973 (DESY report 73-66), p. 514.
   Report SS-73/234, *in* Proc. NAL 1973 Summer Study (NAL, Batavia, Ill., 1974), Vol. 2, p. 1.

3) B.W. Montague, CERN-ISR-DI/72-44 (1972).

4) C. Pellegrini et al., Proc. 8th Internat. Conf. on High-Energy Accelerators, CERN, 1971 (CERN, Geneva, 1971), p. 153.
   Particle physics with positron-electron-proton colliding beams, report SLAC 146/LBL-750 (1972).

5) R. Taylor, Proc. EPS Internat. Conf. on High-Energy Physics, Palermo, 1975 (to be published), p. 377.

6) D.J. Fox et al., Phys. Rev. Letters $\underline{33}$, 1504 (1974).

7) D. Cline, A. Mann and C. Rubbia, Physics Today $\underline{28}$, 23 (1975).

8) J.D. Bjorken and E.A. Paschos, Phys. Rev. $\underline{185}$, 1975 (1969).

9) S. Weinberg, Phys. Rev. Letters 19, 1264 (1967); Phys. Rev. Letters $\underline{27}$, 1688 (1971).

10) Particle physics with positron-electron-proton colliding beams, report SLAC 146/LBL-750 (1972).
    B. Richter, Proc. Seminar on ep and ee Storage Rings, DESY, 1973 (DESY report 73-66), p. 322.

11) B. Wiik, private communication. A 25 × 400 GeV facility was suggested (see this report, Part C, paper 3.

12) Report SS-73/234, *in* Proc. NAL 1973 Summer Study (NAL, Batavia, Ill., 1974), Vol. 2, p.1.

13) W. Bartel et al., Proc. Seminar on ep and ee Storage Rings, DESY, 1973 (DESY report 73-66), p. 269.

14) M. Strovink, report SS-73/213, *in* Proc. NAL 1973 Summer Study (NAL, Batavia, Ill., 1974), Vol. 2, p. 109.

15) M. Strovink, report SS-73/214, *in* Proc. NAL 1973 Summer Study (NAL, Batavia, Ill., 1974), Vol. 2, p. 113.

16) M.L. Stevenson, report SS-73/204, *in* Proc. NAL 1973 Summer Study (NAL, Batavia, Ill., 1974), Vol. 2, p. 49.

17) C.H. Llewellyn Smith, Proc. Seminar on ep and ee Storage Rings, DESY, 1973 (DESY report 73-66), p. 105.

18) A. Benvenuti et al., Phys. Rev. Letters $\underline{34}$, 597 (1975).

19) N. Christ, F.J. Farley and H.G. Hereward, Nuclear Instrum. Methods $\underline{115}$, 227 (1974).
    R. Schwitters and B. Richter, SLAC PEP Note 87 (1974).
    See also PEP Notes 167, 168, 169 (1974).

20) B. Richter, Proc. Seminar on ep and ee Storage Rings, DESY, 1973 (DESY report 73-66), p. 314.

21) G. Manning, Proc. Seminar on ep and ee Storage Rings, DESY, 1973 (DESY report 73-66), p. 181.

22) D. Drickey and L. Hand, report SS-73/242, *in* Proc. NAL 1973 Summer Study (NAL, Batavia, Ill., 1974), Vol. 2, p. 71.

23) D. Drickey and L. Hand, report SS-73/207, *in* Proc. NAL 1973 Summer Study (NAL, Batavia, Ill., 1974), Vol. 2, p. 175.

24) H. Hoffmann, report CERN-ISR-LTD/75-53 (1975).

25) J. Jurow, reports SLAC-TN-64-71 (1964), SLAC-TN-63-66 (1963), SPEAR-41, SLAC PEP Note 88 (1974).

26) R.A. Mack, Cambridge Electron Accelerator report CEAL-1027 (1966).

27) R.D. Evans, American Institute of Physics Handbook (McGraw-Hill, New York, 1972), 3rd edition, Chapter 8, pp. 190-218.

28) R.D. Evans, Handbuch der Physik (Springer Verlag, Berlin, 1958), Vol. 34, pp. 218-298.

29) D. Bostic et al., Proc. 1975 National Accelerator Conference, Washington, 1975 (SLAC PUB 1547), p. 1540.

30) H. Hoffmann, private communication.

31) M. Bernardini and L. Malter, J. Vacuum Sci. Technol. 2, 130 (1965);
G. Fischer and R. Mack, J. Vacuum Sci. Technol. 2, 123 (1965);
E. Garwin et al., Proc. 4th Internat. Vacuum Congress, Manchester, 1968 (Inst. of Phys. and The Physical Soc., London, 1969), p. 131.

32) A.G. Mathewson, Vacuum 24, 505 (1974), and references therein.

33) J. Kouptsidis and M. Schwartz, private communication, and DESY internal report H3-75/1 (1975).

34) For a definition of negative desorption coefficient, see R.S. Calder, Vacuum 24, 437 (1974), and references therein.

35) J. Allaby, private communication.

36) B.C. Barish et al., Nuclear Instrum. Methods 116, 413 (1974).

37) See, for example, the design of R. Kilpatrick, Proc. Internat. Symposium on Magnet Technology, SLAC, 1965 (AEC, Washington, DC, 1965), p. 262.

38) A. Asner, Proc. Internat. Symposium on Magnet Technology, SLAC, 1965 (AEC, Washington, DC, 1965), p. 218.

39) P. Morton and J. Rees, SLAC PEP Note 7 (1971).

40) W.J. Willis, BNL Report CRISP 72-15 (1972).

41) J. Marx, BNL Report CRISP 72-16 (1972);
Rutherford Lab. EPIC report RL-74-124 (1974), pp. 42 and 53.

42) See, for example, a large system developed for an ISR experiment:
J.S. Beale et al., Nuclear Instrum. Methods 117, 501 (1974) and references therein.

43) J. Appel et al., FERMILAB PUB 75/41 (1975).

44) W.J. Willis and V. Radeka, Nuclear Instrum. Methods 120, 221 (1974).

45) J. Engler et al., Nuclear Instrum. Methods 120, 157 (1974).

46) V. Böhmer et al., Nuclear Instrum. Methods 122, 313 (1974).

47) W.J. Willis, BNL report CRISP 72-45 (1972).

48) C. Fabjan, private communication.

49) F.A. Nezrick, Neutrino interactions on protons at Fermilab energies in the 15' HBC, Particle Physics Seminar, CERN, Geneva, June 1975.

50) L.M. Lederman, BNL report CRISP 74-1 (1974).

51) For example, U. Camerini et al. (PEP-159), Proceedings of the 1974 PEP Summer Study
   (PEP-137), p. 309;
   W.A. Wenzel (PEP-162), *ibid.*, p. 332.

52) H. Lynch, R.F. Schwitters and W. Toner, SLAC PEP Note 176 (1975).

53) H. Brück, CERN-ISR-AS/75-19 (1975).

54) A.G. Mathewson, private communication.

55) W. Schnell, CERN-ISR-DI/75-10 (1975).

56) H.G. Hereward, CERN 71-15 (1971).

57) O. Gröbner, CERN-ISR-AS/74-67 (1974).

58) D. Blechschmidt, CERN-ISR-VA/75-29 (1975).

59) Working Group on coasting beam phenomena, CERN-ISR-AS/74-68 (1974).

60) E. Keil and A.M. Sessler, CERN-ISR-AS/74-60 (1974).

Parameters for the ep option of the LSR (June 1975)

Parameter	Symbol	Unit	Electrons	Protons[*]
Beam energy	E_0	GeV	20	400
Energy in the centre of mass	$\sqrt{s}$	GeV	178	
Circumference	L_0	m	6150	6132
Average radius of lattice	$\bar{R}$	m	721	718
Bending radius	ρ	m	515	339
Bending field	B_0	T	0.13	3.9
Revolution frequency	f_0	kHz	48.8	48.9
RF frequency	f_{RF}	MHz	200	-
Harmonic number	h		4100	-
Energy loss per turn	U_0	MeV	27.5	-
Beam current	I	A	0.25	7
Radiated power	P_r	MW	6.9	-
Total RF power	P_{RF}	MW	10	-
Damping rate for energy osc.	α_ε	sec^{-1}	66	-
Damping rate for betatron osc.	$\alpha_x \approx \alpha_y$	sec^{-1}	≈ 33	-
Min. RF voltage (peak)	V_{RF}	MV	35	-
Min. phase osc. frequency	f_s	kHz	≈ 1.7	-
Energy spread	$\Delta E/E_0$	%	0.077 r.m.s.	0.52 full
r.m.s. bunch length	δ_{z_0}	cm	3	-
Q-value without insertions	$Q_x \approx Q_y$		≈ 24	≈ 24
r.m.s. betatron ampl./$\sqrt{\beta_x}$	$\delta_x/\sqrt{\beta_x}$	$\sqrt{m}$	3×10^{-4}	1.33×10^{-4}
Momentum compaction factor	α		1.7×10^{-3}	1.7×10^{-3}
Horiz. ampl. funct. in IR	β_x^*	m	1	5
Vert. ampl. funct. in IR	β_y^*	m	0.3	1
Off-momentum funct. in IR	α_p^*	m	0	0
r.m.s. beam width in IR	δ_x^*	m	3×10^{-4}	3×10^{-4}
r.m.s. beam height in IR	δ_y^*	m	1.3×10^{-4}	1.3×10^{-4}
Number of bunches	M		4100/2050	Unbunched
Horiz. crossing angle	$\bar{\alpha}_x$	rad	$\approx 1.5 \times 10^{-3}$	
Vert. crossing angle	$\bar{\alpha}_y$		Variable	
Max. luminosity	L		$\approx 0.7 \times 10^{32} \, cm^{-2} \, sec^{-1}$	
Beam-beam Q-shift, M = 4100	ΔQ		≈ 0.014	$\approx 0.8 \times 10^{-4}$
" " " " , M = 2050	ΔQ		≈ 0.014	$\approx 1.6 \times 10^{-4}$
Distance to first quad.	D_Q	m	±10	±22
Polarization time	τ_p	h	2	-

[*] The parameters listed refer to luminosity operation where the protons are not bunched; during injection, the RF frequency for protons is 200 MHz.

APPENDIX B

r	$\dfrac{g(r)}{r}$	f(E) in %
10^{-9}	1×10^{6}	-
10^{-6}	1×10^{4}	-
10^{-4}	4.6×10^{2}	-
10^{-3}	99.1	0.01
10^{-2}	20.7	0.2
0.1	3.81	4.1
0.2	2.10	9.5
0.4	1.05	20.8
0.6	0.644	31.6
0.8	0.432	41.4
1.0	0.303	50.0
1.5	0.139	66.9
2.0	0.070	78.5
3.0	0.0199	91.1
4.0	6.14×10^{-3}	96.4
6.0	6.5×10^{-4}	99.4
8.0	7×10^{-5}	99.9
10.0	1×10^{-5}	99.99
15.0	5×10^{-8}	100
20.0	3×10^{-10}	100
25.0	2×10^{-12}	100

I.2 INTERACTIONS OF THE SYNCHROTRON RADIATION WITH THE PROTON BEAM IN THE LSR ep INTERACTION REGIONS

H.F. Hoffmann

CERN, Geneva, Switzerland

1. INTRODUCTION

In the LSR ep option[1] (20 GeV electrons, 400 GeV protons), it is proposed to use a "coincidence" magnet[2] to bend the electron beam vertically through the proton beam in order to achieve a luminosity of $10^{32}/cm^2$ sec with a short overlap area. Originally, a continuous bending magnet of 0.3 T was envisaged.

The synchrotron radiation emitted in that magnet has a critical energy of 70 keV and leads to a luminosity "photon-proton" of $\sim 2 \times 10^{32}/cm^2$ sec.

This report considers the effects arising from this "background" luminosity but does not deal with other types of background induced by the synchrotron radiation such as pressure rises in the vacuum vessel of the proton beam, photons scattered into the detectors from the residual gas, etc., all of which are treated in the original report of the LSR ep Working Group[*].

The photon-proton interactions possible are governed by the photon energy in the rest frame of the proton, namely

$$k_0 = 2\gamma_{proton} k_i$$

(k_0 and k_i being the photon energies in the rest frame of the proton and in the lab respectively, $\gamma_{proton} \sim 426$ in this case). Thus in the rest frame of the proton, the photon energies range between several keV and one GeV and the following processes occur: Compton scattering (~ 40 events/sec); pair production ($\sim 0.5 \times 10^6$ events/sec); photoproduction of π^0 and π^+ ($\sim 10^3$ events/sec); and double-pion production and η, K, Λ, Σ production ($\ll 1$ event/sec). Compton-scattered photons, π^0, π^+, η, K, Λ, and Σ, are produced mainly within a few milliradians of the outgoing proton beam with momenta up to ~ 250 GeV in the lab. The pair-electrons, however, are visible in a solid angle of 4π sr with energies of several hundred keV up to several GeV near the outgoing proton beam.

In order to reduce these background rates, a magnet was evolved in the discussions of the ep Working Group, with a magnetic field tapered to 0.05 T towards the overlap of the beams (critical photon energy, 12 keV). In addition, a horizontal crossing angle of ~ 1 mrad was introduced.

The magnet was considered to be either continuous or a "split-field" magnet with field regions of opposite sign leading to a cross-over of the electron beam. The beam layout is shown in Fig. 1.

---

*) This Working Group is composed of D. Blechschmidt, G.E. Fischer, A. Hofmann, H.F. Hoffmann and B.W. Montague. The physics consultants are J. Allaby, L. Di Lella, W. Willis (CERN), and B. Wiik (DESY).
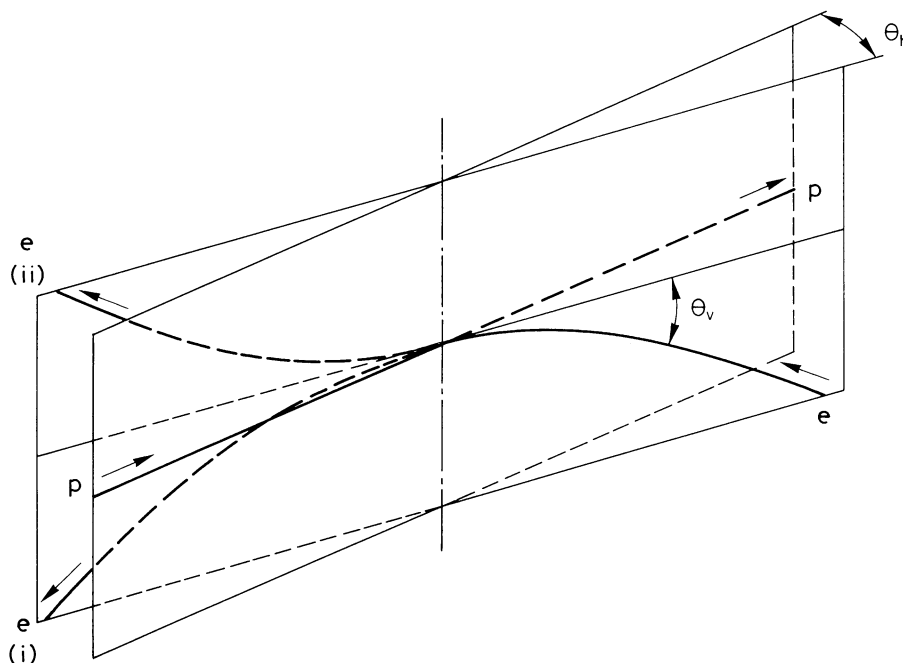
Fig. 1 Layout of the beams in the interaction area: θ_h is the horizontal crossing angle (θ_h = 1 mrad); θ_v is the vertical angle of the electron beam versus the proton beam before and after the coincidence magnet ($\theta_v \sim 20$ mrad). Both the continuous (i) and the split-field (ii) case are demonstrated.

By means of these modifications the luminosity "photon-proton" was reduced to $\sim 0.3 \times 10^{32}/cm^2$ sec and the rates to 6 events/sec Compton scattering, 2×10^4 events/sec pair production, 0.05 events/sec pion production, and the rest negligible.

It should be kept in mind that this background is time-correlated with the electron bunches and has the same time-structure as the real ep events. Accidental coincidences, however, between a real ep event and a background γp event are rare, since the RF frequency foreseen is 200 MHz, the number of bunches 4100 (2050) and, together with the above-mentioned background rate of 2×10^4/sec, there is only 1 (2) background event(s) per 10^4 bunches.

The features of the background event also allow a fairly easy discrimination: very low initial multiplicity, missing initial lepton, restricted angular range, and mostly a missing proton in the case of pair production.

In the following, these problems are treated in some detail. As only over-all aspects are interesting in such a study, simple approximations of cross-sections were used, and in the case of the pair production an approximation to the proper three-body kinematics.

2. LUMINOSITY OF THE SYNCHROTRON RADIATION AGAINST THE PROTON BEAM $L_{\gamma p}$

The synchrotron radiation "beam" is almost identical in geometry to the electron beam because of the emission angle of the photon $\delta_{em} \sim m_e$/energy of the electron = 2.6×10^{-5}, which is much smaller than the r.m.s. angle of the electrons in the beam. In either type of intersection mentioned, cross-over or continuous, a pessimistic estimate gives an effective length of 1.4 m electron beam producing synchrotron radiation in a 0.05 T field (which

traverses the proton beam). On the average, one photon per four circulating electrons and per metre of magnetic field is produced, resulting in a luminosity

$$L_{\gamma p} \sim 0.3 \times L_{ep} = 0.3 \times 10^{32}/cm^2 \ sec \ .$$

For comparison, the corresponding value in the original design with a 0.3 tesla magnet was

$$L_{\gamma p} > 2 \times L_{ep} = 2 \times 10^{32}/cm^2 \ sec \ .$$

(For details, see Table 1).

Table 1

Data on synchrotron radiation

Synchrotron radiation photon energy	Average photon energy	Photon energy k_0 (rest frame of p)	No. of photons (0.3 T) a)	No. of photons (0.05 T) a)	$L_{\gamma p}$ (0.3 T) b)	$L_{\gamma p}$ (0.05 T) b)	σ_{tot} (Compton)	σ_{tot} (pair)	σ_{tot}^+ (π^0)
eV	eV	keV			$10^{32}/cm^2$ sec	$10^{32}/cm^2$ sec	10^{-30} cm^2	10^{-27} cm^2	10^{-30} cm^2
1-10	5	4.3	0.054	0.017	8×10^{-2}	0.02	0.2	0	0
10-100	50	43	0.12	0.036	0.17	0.05	0.2	0	0
100-1000	500	430	0.23	0.073	0.32	0.1	0.2	0	0
$(1-10) \times 10^3$	5×10^3	4.3×10^3	0.46	0.099	0.64	0.14	0.2	0.9	0
(10-40) "	30×10^3	25.6×10^3	0.35	0.013	0.49	0.02	0.2	3.5	0
(40-100) "	70×10^3	60×10^3	0.23	7×10^{-4}	0.32	1×10^{-3}	0.18	5.2	0
(100-200) "	150×10^3	128×10^3	0.06	7×10^{-6}	0.08	1×10^{-5}	0.16	6.4	~ 50
(200-400) "	300×10^3	256×10^3	0.016	3×10^{-11}	0.02	4×10^{-11}	1.3	7.7	400
(400-800) "	600×10^3	512×10^3	5×10^{-3}	-	7×10^{-3}	-	1.3	9.0	200
(> 800) "	$\sim 1.2 \times 10^6$	1.02×10^6	5×10^{-6}	-	7×10^{-6}	-	~ 1	10.3	200
			Total: 1.53 photons	Total: 0.24 photons	Total: 2.1×10^{32} cm^2 sec	Total: 0.33×10^{32} cm^2 sec			

a) Number of synchrotron radiation photons emitted per circulating electron and length of magnetic field.

b) Luminosity of synchrotron radiation against high-energy protons as function of photon energy (normalized to an ep luminosity of $10^{32}/cm^2$ sec).

3. POSSIBLE INTERACTIONS OF THE SYNCHROTRON RADIATION WITH THE PROTON BEAM

Transforming the four-momentum vector of the photon into the rest frame of the proton (centre-of-mass frame in brackets) gives the following:

Energy: $\quad k_0 = \gamma_p k_i (1 + \beta_p) \sim 2\gamma_p k_i \quad [k_{cm} = \gamma_{cm} k_i (1 + \beta_{cm})]$

Momentum: $k_{01} = -\gamma_p k_{i1} (1 + \beta_p) \quad\quad [k_{cm_1} = \gamma_{cm} k_i (1 + \beta_{cm})]$

$\quad\quad\quad k_{02} \sim 10^{-3} k_{i1} \quad$ for a small ($\sim$ 1 mrad) crossing angle

$\quad\quad\quad k_{03} \sim 10^{-3} k_{i1} \quad\quad\quad$ " $\quad$ " $\quad\quad\quad$ " $\quad\quad\quad$ "

$\quad\quad\quad (k_{cm2} \sim k_{cm3} \sim 10^{-3} k_{i1} \quad$ " $\quad\quad$ " $\quad\quad\quad$ " $\quad\quad$ ")

index i: initial state in the laboratory

" 0: initial state in the rest frame of the proton

" cm: initial state in the centre-of-mass frame

$\gamma_p = E_p/m_p \ ; \quad \beta_p = E_p/p_p \ ,$

$[\gamma_{cm} = (1 - \beta_{cm}^2)^{-\frac{1}{2}} \ , \quad \beta_{cm} = (p_p - k_{i1})/(E_p + k_i) \quad$ for $p_{p1} = p_p] \ ; \quad p_{p2} = p_{p3} = 0.$

The incident proton energy is taken to be 400 GeV throughout. Therefore the photon momentum k_{01} is raised by about a factor of $\sim 10^3$, and hence the other components of the incident photon momentum can be neglected in the present case of small crossing angles between the ep beams. Thus the following interactions are possible:

$$\gamma p \rightarrow \gamma p \text{ (Compton or elastic scattering)}$$

$$\gamma p \rightarrow e^+ e^- p \text{ (pair production)}$$

$$\gamma p \rightarrow \pi^+ n \text{ or } \pi^0 p \text{ (photoproduction of pions) .}$$

Photoproduction of η, $K^+\Lambda$, $K^+\Sigma$ (threshold photon energies k_0 of 710 MeV, 910 MeV, or 1046 MeV, respectively) does not need to be considered with the lower bending field, but could occur in the old scheme with very small rates. Also the photoproduction of pions is out of the range of the considerable luminosities achieved with the tapered magnet.

Table 1 gives a summary of the synchrotron radiation yield for various photon energies, and the corresponding luminosities and total cross-sections for the mentioned processes as a function of the photon energy.

The corresponding total rates integrated over all energies are:

$$N_{\text{Compton}} = 6/\text{sec} \qquad (40/\text{sec})$$

$$N_{\text{pair}} = 2 \times 10^4/\text{sec} \qquad (4.5 \times 10^5/\text{sec})$$

$$N_{\pi^+\pi^0} = 0.05/\text{sec} \qquad (10^3/\text{sec})$$

(in brackets: with a 0.3 T magnet).

The common feature of all these processes as compared to ep events is the missing lepton and, for pair production, mostly also the missing proton, which remains in the beam. The Compton scattering and pion production are considered in detail, since the total energy deposited in the detectors is ~ 400 GeV. Thus these events are somewhat similar to the type of real ep events, where also the lepton is "missing" in the final state:

$$ep \rightarrow \nu + \text{anything .}$$

The difference in total energy between ep and γp reactions is only 20 GeV or 5%. No foreseeable detector can measure the total energy of all ep events with sufficient precision to discriminate against this background. Useful features for discrimination are then only the low initial multiplicity and the kinematics of the γp events.

In the following the various reactions are treated in some detail.

3.1 Compton scattering

Even with the very low rate of only 6 events/sec this reaction is sufficiently interesting to be investigated, since it yields photons up to more than 200 GeV near the direction of the proton beam.

The scattering angle θ of the protons in the laboratory ($\theta = 0$ in the direction of the proton beam) is given by

$$\tan \theta = (1/\gamma_p) \cot (\theta_0/2)$$

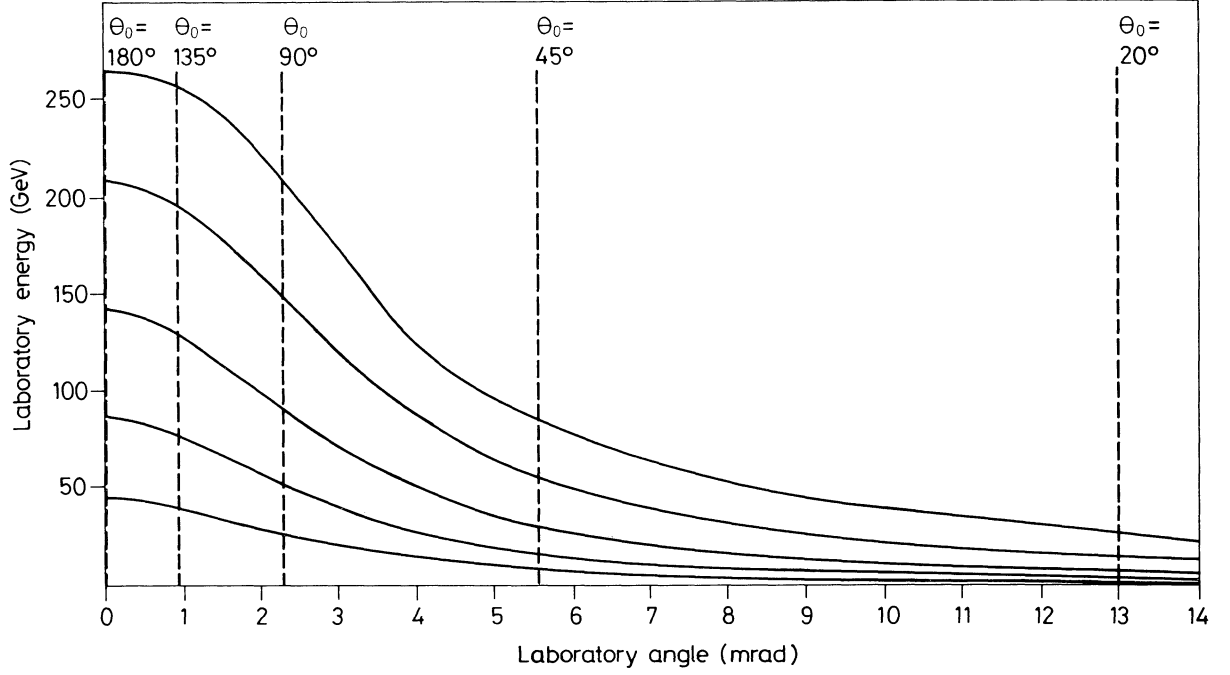(θ_0 measured in the rest frame of the proton in the direction of the γ-ray).

Fig. 2   Compton scattering of the synchrotron radiation against the proton beam: lab. energy
of the scattered photon versus scattering angle in the lab. θ_0 is the scattering
angle in the rest frame of the proton, k_i the energy of the synchrotron radiation
photons in the lab.

The final energy of the photon in the laboratory, after scattering, is

$$k_f(\theta_0, k_0) = \frac{\gamma_p k_0 (1 - \beta_p \cos \theta_0)}{k_0/m_p (1 - \cos \theta_0) + 1} \qquad (k_0 \sim 2\gamma_p k_i)$$

which has a maximum for $\theta_0 = 180°$:

$$k_f \sim 4\gamma_p^2 k_i \ .$$

The differential cross-section in the rest frame of the proton is the Klein-Nishina
cross-section up to $k_0 < 100$ MeV [3]. At higher photon energies, data are available from
small electron synchrotrons[4-6]; 93% of the total cross-section falls within $0 < \theta < 10$ mrad
laboratory angle and 14% within $0 < \theta < 1$ mrad.   In Fig. 2 the final photon energy is plotted
versus the scattering angle θ in the laboratory for several incident photon energies.

3.2   Pair production

Pair production is a process with a large cross-section (several millibarns) and more
complicated kinematics because of the three-particle final state.

In the rest frame of the proton, pair production can be described in the following way,
which is sufficiently precise for this study:

$$\sigma_{tot}(k_0) = 1.8 \log k_0 - 2.22 \text{ mb} \quad \text{for } k_0 \geq 10 \text{ MeV} ,$$

and k_0 measured in MeV [7]. Below 10 MeV, experimental data have to be used. The angular distribution of the electrons around the direction of the incident γ-ray is in the relativistic case $(k_0 \gg 2 \, m_e)$ [8]:

$$\frac{d\sigma}{d\theta_0} = A \frac{\theta_0}{\left[\theta_0^2 + (m_e/k_0)^2\right]^2} \left[\log \left(1 + \frac{\theta_0^2 m_e^2}{k_0^2}\right) + B\right]$$

Then the differential cross-section can be written approximately as

$$\frac{d\sigma}{d\theta_0} = \sigma_{tot}(k_0) g(k_0) \frac{\theta_0}{\left[\theta_0^2 + (m_e/k_0)^2\right]^2} \; ;$$

$g(k_0)$ follows from:

$$\int_0^\pi (d\sigma/d\theta_0) \, d\theta_0 = \sigma_{tot}(k_0) \; .$$

Below 10 MeV photon energy the concentration in the forward direction is less marked.

The distribution of the available photon energy between the electrons is assumed to be such that the e^+ can take on any energy e_{e+} between m_e and k_0 with uniform probability, the e^- then taking the complementary part $e_{e-} = k_0 - e_{e+}$ with no energy transferred to the proton. The relation between the scattering angle θ in the laboratory ($\theta = 0$ in the direction of the proton beam) and the scattering angle θ_0 in the rest frame of the proton ($\theta_0 = 0$ in the direction of the incident photons) is

$$\tan \theta = \frac{\sin \theta_0}{\gamma_p \left(\dfrac{\beta_p}{\beta_e^0} - \cos \theta_0\right)} \; ,$$

where β_p is the proton velocity in the laboratory

β_e^0 is the electron velocity in the rest frame of the proton .

For $\beta_e^0 < \beta_p$ the angle θ is limited, $\theta < \theta_{max} < 90°$, and for each θ there are two angles θ_0 which fulfil the relation. For $\beta_e^0 > \beta_p$, electrons appear in the full range $0 \le \theta \le 180°$. So electrons with an energy in the rest frame of the proton of $\sim$ 5, 26, 60, 128, and 218 MeV have a θ_{max} of 1, 6, 17, 31, and 90 degrees, respectively. Above 218 MeV ($= \gamma_p \times m_e$) electrons cover the full θ-range from 0° to 180°.

The correlations between the laboratory angle and the momentum of the electrons and the corresponding part of the cross-section are listed in Table 2. The values were derived using the description of pair production given above.

As can be seen in Table 2, the advantage of the weaker magnetic field for the pair production process does not lie in the shift of the synchrotron radiation spectrum to lower energies but in the reduced number of photons, since the lower photon energies of several keV lead to higher energy electrons in the lab. because of the larger scattering angles in the rest frame of the proton.

Table 2

Event rate for pair production induced by synchrotron radiation

k_i laboratory energy of the incident photon in keV

e_f laboratory energy of the outgoing electron in MeV

$\Delta\sigma$ part of the total cross-section contributing to a certain bin

$\Delta N_{0.05\,T}$ corresponding rate in the case of 0.05 T magnetic field

$\Delta N_{0.3\,T}$ corresponding rate in the case of 0.3 T magnetic field

$\Delta\theta$ angular range in the laboratory (θ = 0 in the direction of the proton beam).

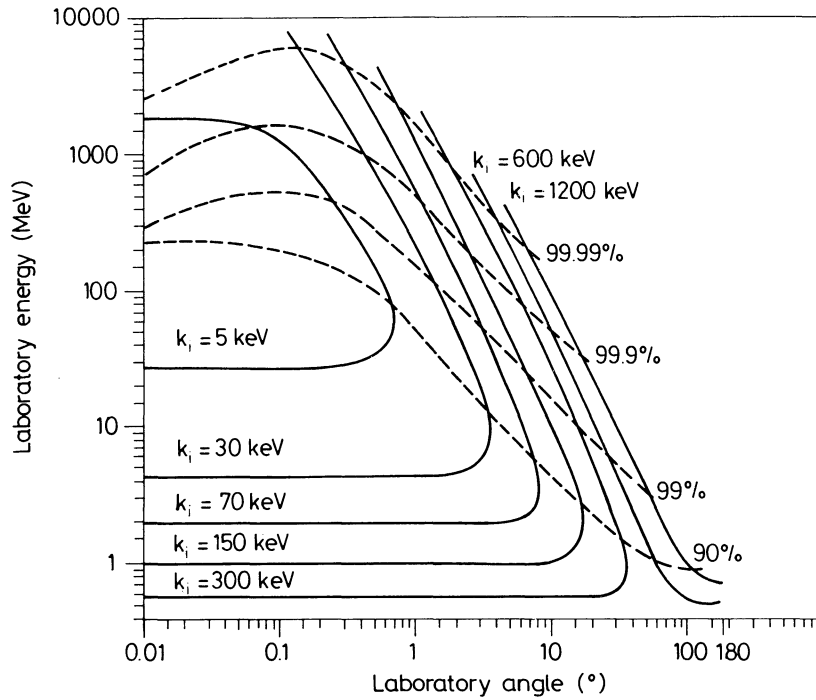| k_i (keV)	Parameter	$0 \le e_f \le 1$ (MeV)	$1 < e_f \le 10$ (MeV)	$10 < e_f \le 100$ (MeV)	$100 < e_f \le 2000$ (MeV)
5	$\Delta\theta$			$0 \le \theta \le 17$ mrad	$0 \le \theta \le 12$ mrad
	$\Delta\sigma$	–	–	0.8×10^{-27} cm²	0.05×10^{-27} cm²
	$\Delta N_{0.05\,T}$			11 kHz	0.7 kHz
	$\Delta N_{0.3\,T}$			51 kHz	3.2 kHz
30	$\Delta\theta$		$0° \le \theta \le 6°$	$0° \le \theta \le 4.3°$	
	$\Delta\sigma$	–	2.9×10^{-27} cm²	0.7×10^{-27} cm²	–
	$\Delta N_{0.05\,T}$		5.8 kHz	1.4 kHz	
	$\Delta N_{0.3\,T}$		1.4×10^5 Hz	34 kHz	
70	$\Delta\theta$		$0° \le \theta \le 17°$	$0° \le \theta \le 7°$	
	$\Delta\sigma$	–	5.0×10^{-27} cm²	0.14×10^{-27} cm²	–
	$\Delta N_{0.05\,T}$		0.5 kHz	14 kHz	
	$\Delta N_{0.3\,T}$		1.6×10^5 Hz	4.5 kHz	
150	$\Delta\theta$	$0° \le \theta \le 31°$	$0° \le \theta \le 31°$	$0° \le \theta \le 8°$	
	$\Delta\sigma$	3.3×10^{-27} cm²	3.2×10^{-27} cm²	0.1×10^{-27} cm²	–
	$\Delta N_{0.05\,T}$	3 Hz	3 Hz	0.1 Hz	
	$\Delta N_{0.3\,T}$	26.4 kHz	25.6 kHz	0.8 kHz	
300	$\Delta\theta$	$0° \le \theta \le 180°$	$0° \le \theta \le 180°$	$0° \le \theta \le 19°$	
	$\Delta\sigma$	6.3×10^{-27} cm²	1.5×10^{-27} cm²	0.1×10^{-27} cm²	–
	$\Delta N_{0.05\,T}$	$< 10^{-4}$ Hz	$< 10^{-4}$ Hz	$< 10^{-5}$ Hz	
	$\Delta N_{0.3\,T}$	12.6 kHz	3 kHz	200 Hz	
600	$\Delta\theta$	$0° \le \theta \le 180°$	$0° \le \theta \le 180°$	$0° \le \theta \le 19°$	
	$\Delta\sigma$	7.5×10^{-27} cm²	1.5×10^{-27} cm²	10^{-30} cm²	–
	$\Delta N_{0.05\,T}$	0	0	0	
	$\Delta N_{0.3\,T}$	5.2 kHz	1 kHz	1 Hz	
1200	$\Delta\theta$	$0° \le \theta \le 180°$	$0° \le \theta \le 180°$		
	$\Delta\sigma$	9.2×10^{-27} cm²	1.0×10^{-27} cm²	–	–
	$\Delta N_{0.05\,T}$	0	0		
	$\Delta N_{0.3\,T}$	6 Hz	1 Hz		
	Tot. 0.05 T	3 Hz	6.3 kHz	12.4 kHz	0.7 kHz
	Tot. 0.3 T	44 kHz	3.2×10^5 Hz	90.5 kHz	3.2 kHz

Fig. 3   Pair production by the synchrotron radiation against the proton beam: lab. energy
of the electron versus its lab. angle. A special case is shown where the electron
received half of the proton energy without energy transfer to the proton. The
percentages correspond to the amount of total cross-section up to the indicated
point. (Compare also Table 3 and 4.)

In order to demonstrate the pair production kinematics in a simple way, the symmetrical
case, where both electrons have the same energy, is plotted in Fig. 3, again disregarding
energy transfer to the proton. The percentages of total cross-section indicated are for the
unrealistic case that pair production only occurs symmetrically.

Having used the same parametrization of the differential cross-section for all photon
energies, these cross-section percentages also correspond to certain scattering angles of
the electrons in the rest frame of the proton. In Table 3 this correspondence is given with
the angles measured in units of m_e/k_0. Table 4 contains the angles in milliradians and the
total cross-sections for various photon energies.

The given description of the differential cross-section should be valid up to $10 \times m_e/k_0$
and still give a good estimate up to a $100 \times m_e/k_0$.

To summarize, one can say that at least a factor of 5 to 10 in rate can be gained by
introducing the weaker magnet for electrons in the energy range of 10 to 2000 MeV in the
laboratory. For the range of 0 to 10 MeV the gain is much higher.

The total rate of produced electron pairs is still high. But only one electron pair
is produced per 10^4 bunches passing through the proton beam [RF: 200 MHz, 4100 (2050) bunches].
A fraction of these electrons will be trapped in the coincidence magnet, giving rise to low-
energy γ-rays. The rest will appear in the surrounding detectors at fairly small angles to
the proton beam. The proton, in most cases, will remain in the beam, so that the process
can easily be separated.

Table 3

Correspondence between cross-section
percentages and electron scattering angles

Part of σ_{tot} (%)	Angle θ_0 (m_e/k_0)
50	1
90	3
99	10
99.9	30
99.99	100

Table 4

Angles and cross-sections
as a function of photon energy

k_i (keV)	m_e/k_0 (mrad)	σ_{tot} (mb)
5	119	0.8
30	20	3.6
70	9	5.1
150	4	6.5
300	2	/.8
600	1	9.0
1200	0.5	10.3

3.3 Photoproduction of pions

Pion photoproduction occurs for photon energies $k_0 > 145$ MeV (rest frame of the proton). Detailed data on differential cross-sections are available from close to threshold up to several GeV photon energy in the c.m. frame[4]. A pion produced at threshold with no momentum in the rest frame of the proton already has in the laboratory frame a momentum of ~ 60 GeV in the proton direction.

The relation between the pion laboratory angle and the scattering angle in the c.m. frame is

$$\tan \theta = \sin \theta_{cm}/\gamma_{cm} \ (- \cos \theta_{cm} + \beta_{cm}/\beta_{cm}^{\pi}) \ ,$$

where

θ is the angle in the lab. frame ($\theta = 0$ in the proton direction)

θ_{cm} is the angle in the c.m. frame ($\theta_{cm} = 0$ in the photon direction)

$\gamma_{cm} = 1/(1 - \beta_{cm}^2)^{\frac{1}{2}}$

$\beta_{cm} = (p_p - k_i)/(E_p + k_i)$

β_{cm}^{π} velocity of the pion in the c.m. frame.

As in the electron case, the pion angle θ is limited. It would reach 90° for photon energies in the lab. of ∿ 70 MeV. But even with a 0.3 T magnet, γ energies above 1 MeV are already very rare. Therefore in the case of synchrotron radiation the pion angle is confined to about 10 mrad. The pion energy can reach more than 200 GeV at very small angles for photon energies of about 1 MeV.

A description of the kinematics is given in Fig. 4. About 50% of the total cross-section lies above the line: θ_{cm} = 90°. Thus half of the pions produced have momenta in excess of 60 GeV in the laboratory.
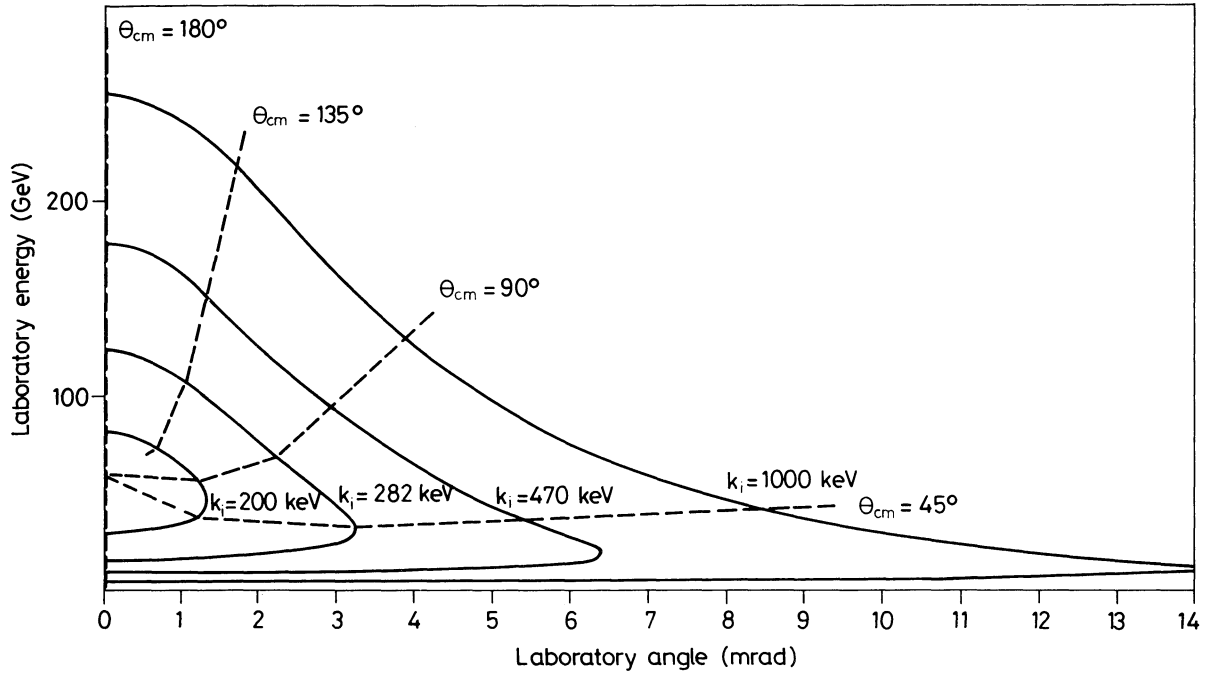
Fig. 4   Pion production by the synchrotron radiation against the proton beam: lab. energy of the pion versus its lab. angle. θ^{cm} is the production angle of the pion in the centre-of-mass frame.

4. CONCLUSION

The synchrotron radiation caused by a coincidence magnet on the intersection produces considerable background rates. If no care is taken, all the "physics" studied at low-energy electron synchrotrons (< 1.5 GeV end-point energy) can be observed also in the ep machine, in a strange Lorentz frame however. The produced particles (γ, π^0, π^+, etc.) can reach energies of several hundred GeV in the laboratory frame; the rates observed can be as high as several hundred kHz. By introducing a crossing angle and by weakening the magnetic field near the overlap of the electron and proton beams, the rates can be lowered to acceptable values (∿ 20 kHz in the case considered). The total rates for various processes and for the two geometries and magnetic fields studied are given in Table 5.

There is some physics interest in studying π^0 production and Compton scattering at ∿ 180° scattering angle, which is not possible in conventional small electron synchrotrons.

Table 5

Rates for processes induced by
synchrotron radiation in two configurations

Process	1 mrad crossing angle and 0.05 T magnet	Zero crossing angle and 0.3 T magnet
Compton scatt.: $\gamma p \rightarrow \gamma p$	6/sec	40/sec
Pair production: $\gamma p \rightarrow pe^+e^-$	2×10^4/sec	4.5×10^5/sec
Pion production: $\gamma p \rightarrow p\pi^0$ $\gamma p \rightarrow n\pi^+$	0.05/sec	10^3/sec

Acknowledgements

REFERENCES

1) LSR ep Working Group, Some remarks about LSR ep interactions, CERN ISR-GS/75-33 (1975).

2) B.W. Montague, ep interaction region with separating magnet (int. note 20.12.74).

3) J.D. Jackson, Classical electrodynamics (J. Wiley and Sons, Inc., New York, 1963).

4) Landolt Börnstein New Series; Group 1; Vol. 8: Photoproduction of elementary particles (Springer-Verlag, Berlin, 1973).

5) H. Fischer, Experimental data on photoproduction of pseudo-scalar mesons at intermediate energies, Bonn Univ. PI 1-122 (1970).

6) H. Genzel, M. Jung, K.R. Rausch, R. Wedemeyer and H.J. Weyer, Proton Compton effect in the first resonance region, Bonn Univ. PI 1-138 (1971).

7) T.M. Knasel, The total pair production cross-section in hydrogen and helium, DESY reports 70/2 and 70/3 (1970).

8) W. Heitler, The quantum theory of radiation (3rd edition)(Clarendon Press, Oxford, 1954).

I.3 SHOULD AN ELECTRON RING BE ADDED TO A pp COLLIDING BEAMS FACILITY AT CERN?

B.H. Wiik

DESY, Hamburg, Fed. Rep. Germany

At CERN a highly successful proton-proton colliding beams facility -- the ISR -- exists, and at present an upgrading of this facility is under discussion. Feasibility studies for large pp storage rings capable of reaching centre-of-mass energies of 800 GeV are also under way. In view of this, and considering the importance of lepton-hadron physics at high energies, it seems reasonable to investigate whether an electron ring should be added to the proton ring or not. Such an addition would allow us to study deep inelastic electron scattering, weak interactions, and photoproduction at extremely high energies. In this note we will estimate the rates for some standard experiments in each of these areas. To compute the rates the available c.m. energy and the luminosity must be known. Luminosities as high as 10^{32} cm^{-2} sec^{-1} have been estimated for electron-proton colliding rings and this number will be used, although it might well be too optimistic by an order of magnitude. For the available c.m. energy we will consider two options:

I) Add an e^- beam to an upgraded version of the ISR. Using superconducting bending magnets with B = 6 T the proton energy could be raised to about 140 GeV. The energy of the electron beam would be limited by the radius of the present ISR tunnel to about 12 GeV. With this accelerator a c.m. energy of 82 GeV can be reached, corresponding to q^2_{max} = = 6720 GeV^2.

II) Add an e^- beam to a super ISR. Here we assume 25 GeV e^- on 400 protons, or $\sqrt{s}$ = 200 GeV and q^2_{max} = 4 × 10^4 GeV^2.

In this note we will first discuss the large-q^2 processes and then photoproduction.
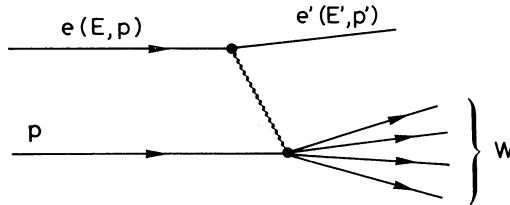
1. LARGE-q^2 REACTIONS

With ep colliding beams we can investigate the reactions

$$e^{\pm}p \rightarrow e^{\pm\prime}X \quad \text{(electromagnetic and weak)}$$

$$e^{\pm}p \rightarrow \bar{\nu}(\nu)X \quad \text{(weak)}.$$

The kinematical variables are defined as usual:

$$q^2 = -Q^2 = -(e - e')^2 = 4 EE' \sin^2 \theta/2$$

$$\nu = pQ/m_p = 2E_p/m_p (E - E' \cos^2 \theta/2)$$

$$W = 2m_p\nu + m_p^2 - q^2.$$

The available kinematical region for the two options are listed in Table 1 and plotted in Figs. 1 and 2.

Table 1

Available kinematical region

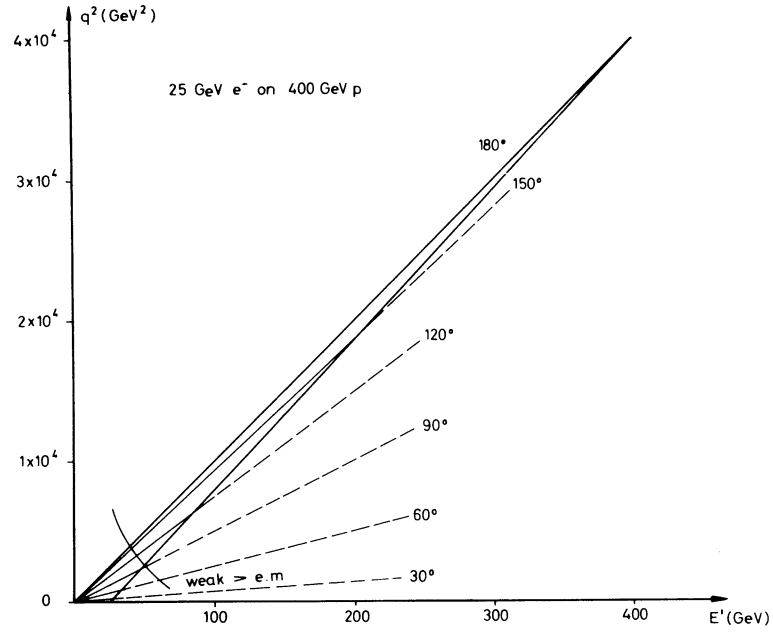| e + p (GeV)	$\sqrt{s}$ (GeV^2)	Q^2_{max} (GeV^2)	ν_{max} (GeV)	E$'$ (GeV)
12 + 140	82	6720	3580	140
25 + 400	200	4×10^4	21300	400

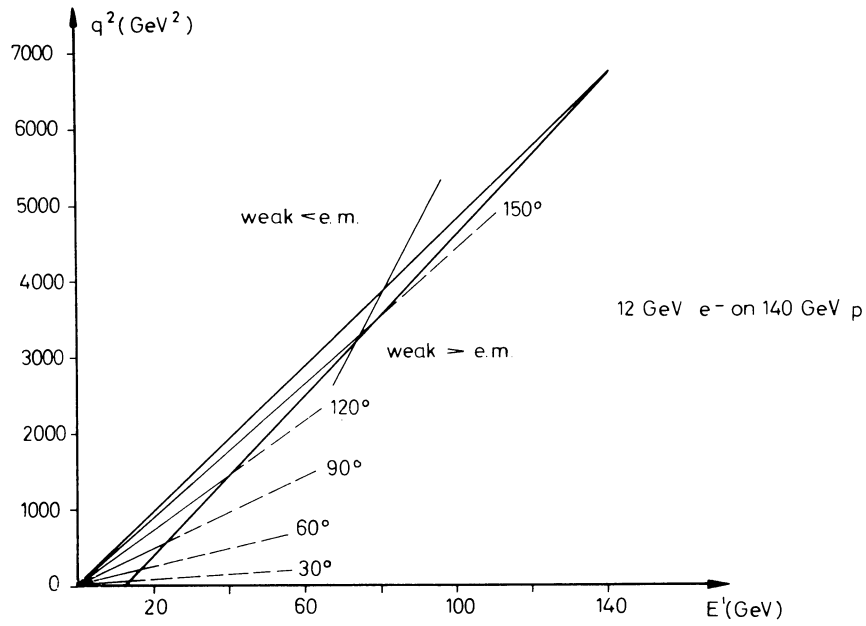Fig. 1 Available kinematical region for 25 GeV e$^-$ on 400 GeV p storage rings

Fig. 2 Available kinematical region for 12 GeV e$^-$ on 140 GeV p storage rings

A 5000 GeV muon or neutrino incident on a stationary proton corresponds to a c.m. energy of 96 GeV and Q^2_{max} = 9380 GeV^2. Hence the kinematical region covered by option (I) can also be reached with a conventional accelerator, whereas option (II), corresponding to an incident energy of 21300 GeV, seems out of reach by conventional means.

1.1 Rates

The reaction $e^{\pm}p \rightarrow e^{\pm}X$ can proceed either by one-photon exchange or by the exchange of Z^0 as indicated in the graphs below:
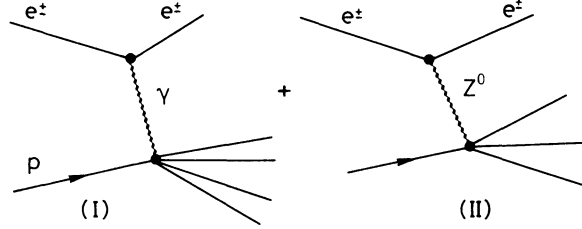
The relative magnitude of these graphs is roughly $0.3 \, GQ^2/4\pi\alpha$ -- hence at low values of Q^2 the one-photon exchange will dominate. By sufficiently high values of Q^2, however, the weak process might give the largest contribution. The transition takes place around $Q^2 \sim 12000$ GeV^2.

Hence it is obvious that option (II) will permit us to study both of these regions in detail, whereas basically only the electromagnetic region and the interference effects can be investigated with option (I). To see this we will evaluate the cross-section resulting from one-photon exchange only.

The one-photon cross-section can be written in terms of the two structure functions νW_2 and mW_1 as

$$\frac{d^2\sigma}{dxdy} = \frac{4\pi\alpha^2}{s} \frac{1}{x^2y^2} \left[\nu W_2 \left(1 - y \frac{m_p xy}{2\nu_{max}} \right) + m_p y^2 \, xW_1 \right] .$$

Here $x = q^2/2m_p\nu$ and $y = \nu/\nu_{max}$.

In the parton model with spin $\frac{1}{2}$ partons the structure functions are related as follows in the scaling limit:

$$\frac{\nu W_2}{x} = 2 \, m_p W_1 .$$

Inserting this result into the above formula and dropping the term $(m_p/2\nu_{max})xy$ we obtain

$$\frac{d^2\sigma}{dxdy} = \frac{4\pi\alpha^2}{s} \frac{\nu W_2}{x^2y^2} (1 - y + y^2/2) .$$

For $\nu W_2(x)$ a recent fit by Barger and Phillips[1] was used:

$$\nu W_2(x) = 4/9 \, u(x) + 1/9 \, d(x) + 4/3 \, c(x) ,$$

with

$$c(x) = 0.145 \, (1-x)^9$$

$$d(x) = \sqrt{x} \left[0.594 \, (1-x^2)^3 + 0.461 \, (1-x^2)^5 + 0.621 \, (1-x^2)^7 \right]$$

$$u(x) = \sqrt{x} \left[0.072 \, (1-x^2)^3 + 0.206 \, (1-x^2)^5 + 0.621 \, (1-x^2)^7 \right] .$$

The number of events per day in a bin of dx = dy = 0.1 was computed as a function of x and y (x,y ≥ 0.01) by integrating the cross-section over the bin. An average luminosity of 10^{32} cm^{-2} sec^{-1} was assumed. The results are plotted in Figs. 3 and 4 for the two options. Note the logarithmic scale. For option (II) (25 GeV e$^-$ on 400 GeV p) more than 300 events a day are produced with $Q^2 \geq 2000$ GeV^2; in the region $Q^2 \geq 10000$ GeV^2 we expect 8 events per day. With option (I) (12 GeV e$^-$ on 140 GeV p) 24 events a day with $Q^2 \geq 2000$ GeV^2 are produced.

The reaction e$^-$p → e$^-$X is ideally suited for an investigation of the interplay between the weak and the electromagnetic interactions. In this experiment only the scattered electron must be identified and measured in order to determine x and y. The rates in option (II) seem to be sufficiently large to permit the region around q^2 = 10000 -12000 GeV^2 (neutral current ≅ one photon) to be investigated in some detail.

The neutral weak interaction can be identified by its interference with the one-photon exchange. This interference will lead to a different cross-section for electrons and posi- trons; it will also make the cross-section dependent upon the helicity state of the lepton.

A rough estimate[2] of the e$^+$-e$^-$ asymmetry leads to

$$\frac{\sigma_+ - \sigma_-}{\sigma_+ + \sigma_-} = \left(\frac{10^{-4}\ Q^2}{m_p^2}\right)\left(\frac{m_Z^2}{Q^2 + m_Z^2}\right)\frac{4y}{3 + 1/x} \ .$$

For $Q^2 = 2000$ GeV^2 and $m_Z = 80$ GeV we expect asymmetries of the order of a few percent. That is, these effects might be marginal with option (I), but easy with option (II) where one might increase Q^2 and still retain a sufficiently large event rate.

Unfortunately the interpretation of the observed asymmetry is not unique; such an asymmetry might also be caused be the interference between one- and two-photon exchange.

A unique signature of the weak interaction is a dependence of the cross-section on the helicity of the electrons. Owing to the synchrotron radiation the electrons, at fixed energies, will be polarized normal to the flight direction. A bending magnet located before the inter- action region can be used to rotate the spin of the electrons to be parallel or antiparallel to the direction of flight. The expected asymmetry for such left- and right-handed electrons can be written[2] as

$$\frac{L - R}{L + R} = \left(\frac{10^{-4} \times Q^2}{m_p^2}\right)\frac{m_Z^2}{m_Z^2 + Q^2} \ ,$$

i.e. with $Q^2 = 2000$ GeV^2 and $m_Z = 80$ GeV we expect effects of the order of 10%.

The total cross-section for the weak interaction is given by[3] (assuming the appropriate helicity state for the lepton)

$$e^-p \to \nu X, \ \sigma = 0.83 \times 10^{-38}\ k_{max}\ cm^{-2} \ ,$$

$$e^+p \to \bar{\nu} X, \ \sigma = 0.28 \times 10^{-38}\ k_{max}\ cm^{-2} \ ,$$

where $k_{max} = s/2m_p$, the equivalent laboratory energy. The rates for L = 10^{32} cm^{-2} sec^{-1} are listed in Table 2.
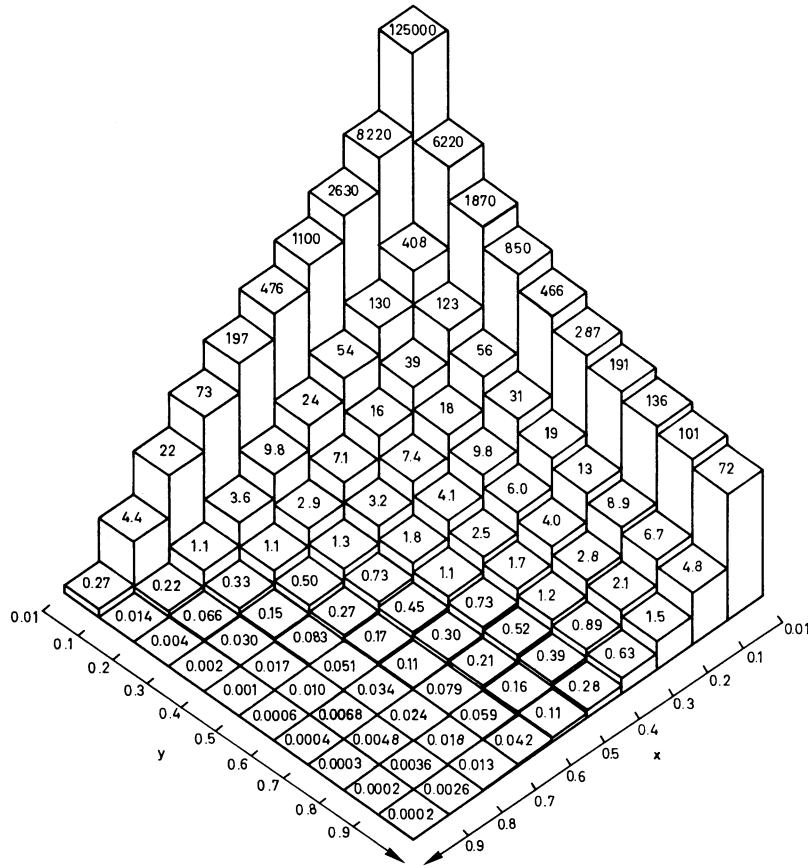
Fig. 3

Number of events per day as a function of x and y for the reaction $e^\pm p \to e^\pm X$ for the 25 GeV e^- on 400 GeV p option. The rates were evaluated using one-photon exchange and the assumptions described in the text.
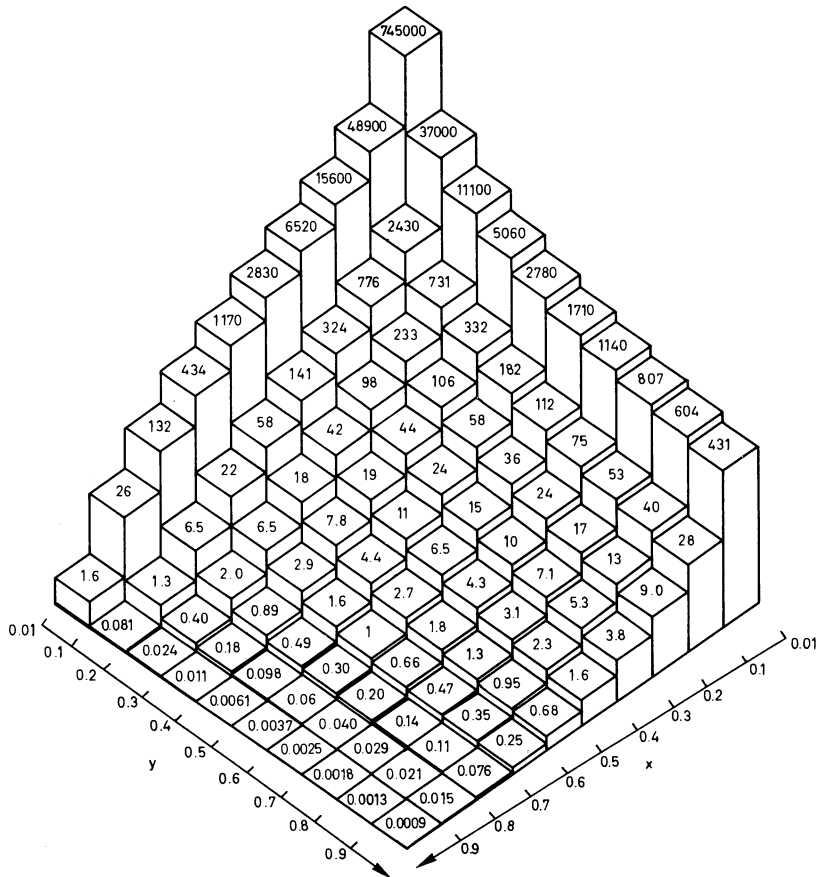

Fig. 4

Number of events per day as a function of x and y for the reaction $e^\pm p \to e^\pm X$ for the 12 GeV e^- on 140 GeV p option. The rates were evaluated using one-photon exchange and the assumptions described in the text.

Table 2

Number of events a day

Option	$e^-p \to \nu X$	$e^+p \to \bar{\nu} X$
12 GeV e^- × 140 GeV p	255	86
25 GeV e^- × 400 GeV p	1520	513

To see how these events are distributed as a function of x and y we evaluate the differential cross-section:

$$\frac{d^2\sigma(e^+p \to \bar{\nu}X)}{dxdy} = \frac{G^2s}{2\pi}\left[(1-y)^2 \times 2d(x) + (1-y + y^2/2) \times 4c(x) \right]$$

$$\frac{d^2\sigma(e^-p \to \nu X)}{dxdy} = \frac{G^2s}{2\pi}\left[2u(x) - (1-y + y^2/2) \times 4c(x) \right]$$

(assuming right-handed e^+ and left-handed e^-).

The number of events per day in a bin $dxdy = 10^{-2}$ is plotted for the various reactions as a function of x and y in Figs. 5 to 8.

It is clear that with a luminosity of 10^{32} cm^{-2} sec^{-1} a large fraction of the available kinematical area can be exploited. For example, in option (II) about 750 events a day with Q^2 larger than 5000 GeV^2 are expected -- a sufficiently high counting rate even to separate the various form factors. Note that the reaction ep $\to$ eX produces only about 60 events/day for $Q^2 > 5000$ GeV^2.

Hence this device allows us to explore a kinematical region not accessible by other means. For example, an intermediate vector boson with mass $m_W < 150$ GeV can be inferred from a measurement of the total cross-section as a function of Q^2. A problem with this experiment is that x and y must be determined from a measurement of the hadron shower.

2. PHOTOPRODUCTION

2.1 The beam

Electroproduction in the limit of $q^2 \to 0$ can be described as the radiation of an almost real photon followed by the interaction of the photon with the proton. Since the probability of radiating an almost real photon is known, the electron beam can be looked on as a source of a well-collimated bremsstrahlung beam with an end-point energy of 3580 GeV (12 GeV on 140 GeV) and 21300 GeV (25 GeV on 400 GeV), respectively. The intensity of the beam, i.e. the number of photons with energies between k and k + Δk per incident electron, is given by the Weizäcker-Williams approximation:

$$N(k)\ dk/k = \frac{\alpha}{2\pi}\left(\frac{E^2 + E'^2}{E^2}\right) \ln\frac{|q^2_{max}|}{|q^2|}\ dk/k .$$

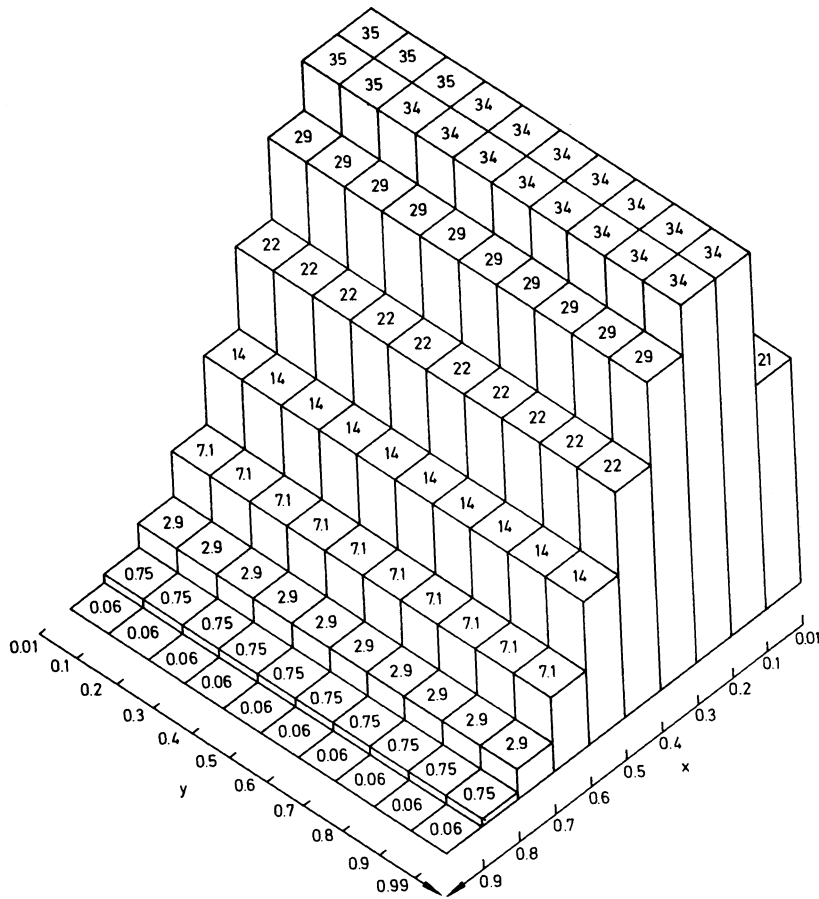Fig. 5

Number of events per day as a
function of x and y for the
reaction $e^-p \to \nu X$ at
$s = 40,000$ GeV^2

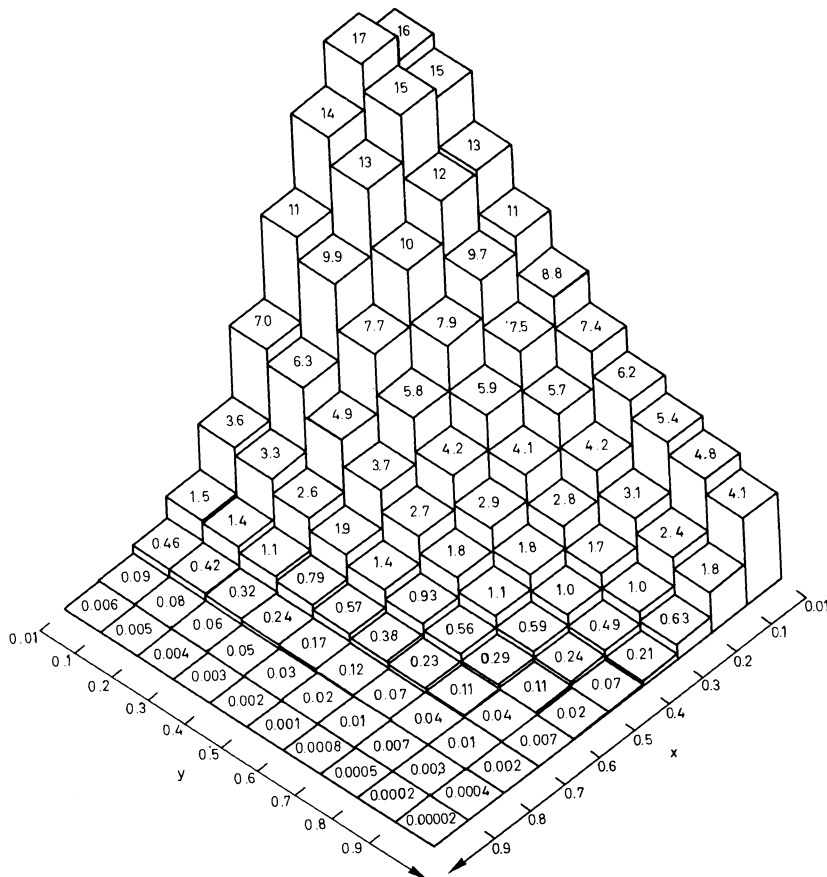
Fig. 6

Number of events per day as a
function of x and y for the
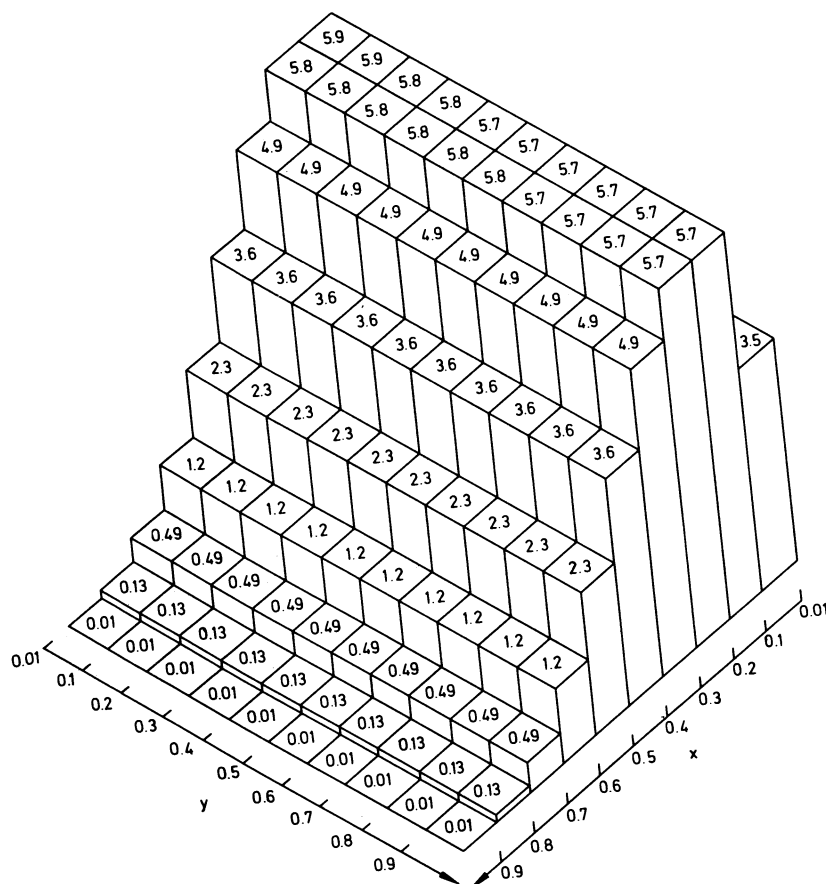reaction $e^+p \to \bar{\nu}X$ at
$s = 40,000$ GeV^2

Fig. 7

Number of events per day as a function of x and y for the reaction $e^- p \rightarrow \nu X$ at $s = 6{,}720$ GeV^2
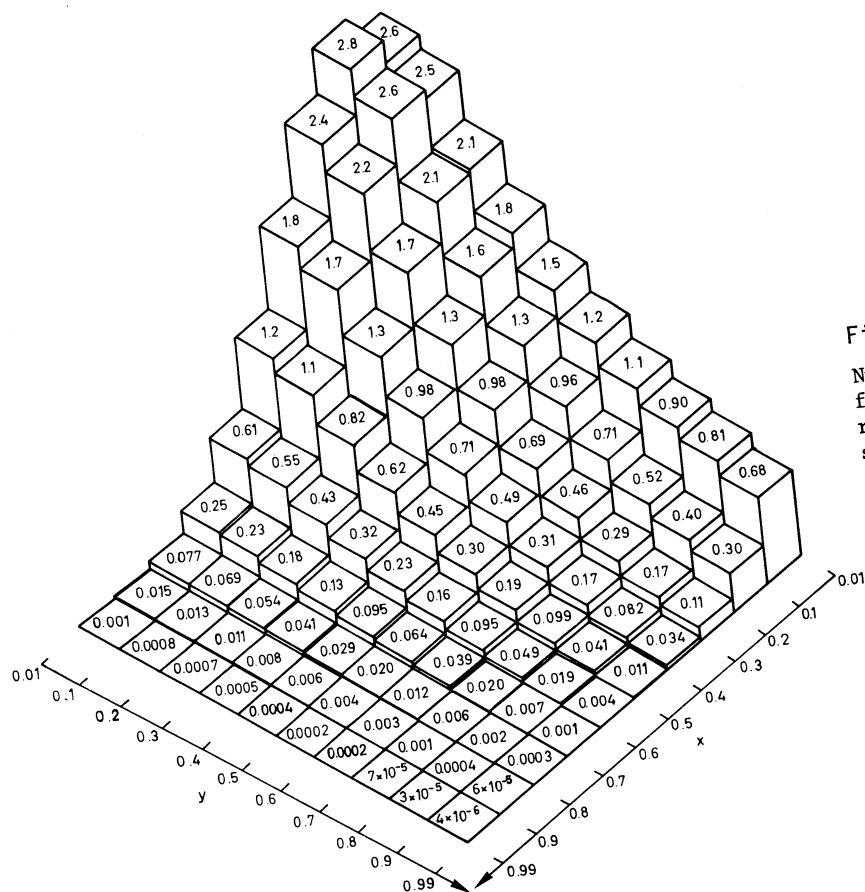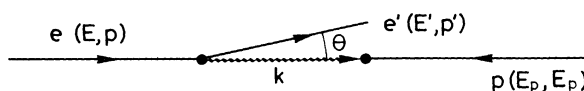

Fig. 8

Number of events per day as a function of x and y for the reaction $e^+ p \rightarrow \bar{\nu} X$ at $s = 6{,}720$ GeV^2

The nomenclature is defined in the figure:

where
$$k = E - E'$$
$$q^2 = -EE'\theta^2$$

The above formula gives the intensity for the case where the electron is being observed in the angular range between θ_{min} and θ_{max}. In general, θ_{min} will be determined by the minimum allowed distance between the counter and the beam as well as the length of the interaction region. We assume here $\theta_{min} = 5$ mrad, corresponding to a counter located 5 cm from the beam 10 m downstream from the interaction point.

In order to be able to neglect the longitudinal part of the cross-section, q^2_{max} and hence θ_{max} must be rather small. Here we assume $|q^2| \leq m_\pi^2$. Tagging the scattered electron offers important advantages. Firstly, by measuring the energy of the scattered electron the energy of the virtual photon is fixed, i.e. it is equivalent to having a monochromatic photon beam. Secondly, since the polarization vector of the photon must be normal to the scattering plane defined by the incident and the scattered electrons, a measurement of the direction of the scattered electron determines the polarization of the photon with respect to the production plane (defined by the incident proton and some outgoing hadron). Independently of the tagging, however, it is also possible to have a longitudinally polarized photon beam. As mentioned earlier, owing to the synchrotron radiation the electrons, at fixed energies, will be polarized normal to the flight direction. Using a bending magnet the polarization vector of the electron can be rotated to be parallel (antiparallel) to the flight direction. The corresponding polarization vector of the photon will then be either parallel or antiparallel to the direction of flight of the photon.

Although tagging the scattered electrons does offer important advantages, it reduces the effective luminosity considerably. Some experiments, such as measuring a cross-section between two rather widely spaced energies ν_1 and ν_2, can be done without tagging. In this case the number of events is measured for two different end-point energies ν_1 and ν_2 of the virtual bremsstrahlung spectrum. The difference between these rates, properly normalized, is then due to photons with energies between ν_1 and ν_2. In this case

$$q_{min} = \left(m_e^2/2\right)\left(\frac{E - E'}{EE'}\right) \quad \text{and} \quad q_{max} \sim m_\pi .$$

The properties of the photon beam for the two options are listed below.

Properties of the photon beam

I) 12 GeV electrons on 140 GeV protons:

$\nu_{max} = 3582$ GeV
Tagging counters: $\Delta\phi = 2\pi$, $5 \times 10^{-3} \leq \theta \leq (m_\pi^2/EE')^{\frac{1}{2}}$
$L_{\gamma p} \simeq 7 \times 10^{-3}$ $L_{ep} = 7 \times 10^{29}$ cm^{-2} sec^{-1}
for 600 GeV $< \nu <$ 3200 GeV

II) 25 GeV electrons on 400 GeV protons:

ν_{max} = 21300 GeV

Tagging $\Delta\phi$ = 2π, 5 $\times$ 10^{-3} $\leq$ θ $\leq$ $(m_\pi^2/EE')^{\frac{1}{2}}$

$L_{\gamma p}$ $\simeq$ 3 $\times$ 10^{-3} L_{ep} = 3 $\times$ 10^{29} cm^{-2} sec^{-1}

for $\cdot$ 2000 GeV $\leq$ ν $\leq$ 20000 GeV

If the tagging can be dispensed with, the effective luminosity L will increase substantially. In this case we expect roughly

$$L_{\gamma p} \simeq 0.1 \ L_{ep} = 10^{31} \ \text{cm}^{-2} \ \text{sec}^{-1}$$

for ν larger than several hundred GeV.

2.2 Physics

One of the most remarkable facts to emerge from the study of various photoproduction reactions is that a photon beam can be looked upon as a beam of strongly interacting bosons. That is, from a comparison between the results obtained in pp and γp collisions, we might hope to gain new information on the hadron dynamics. We should bear in mind that such high c.m. energies can be reached only in γp and pp (p$\bar{\text{p}}$) collisions. Furthermore, the polarization of the photon beam will be very useful in untangling the various reaction mechanisms. At these energies a search for some property unique to the photon (i.e. non-VDM) becomes important.

To acquire a feeling for the kind of experiments which can be carried out using such a beam, the next section lists some counting rates for typical experiments. Since we here assume a detection efficiency of one, these rates are certainly upper limits.

2.3 Expected rates

The rates will be evaluated for 25 GeV e$^-$ on 400 GeV p using a tagged photon beam. Tagging the electrons between 1 GeV and 23 GeV correponds to a photon beam with equivalent laboratory energies between 2000 GeV and 20000 GeV. The resulting luminosity is

$$L_{\gamma p} = 3 \times 10^{-3} \ L_{ep} = 3 \times 10^{29} \ \text{cm}^{-2} \ \text{sec}^{-1} \ .$$

For some of these reactions an untagged photon beam can also be used. In this case the intensity will increase by more than an order of magnitude.

2.3.1 $\sigma_{tot}(\gamma p)$

The total γp cross-section into hadrons is expected to be around 100 μb in this energy range. This corresponds to about 2.6 $\times$ 10^5 events a day for ν between 2000 and 20000 GeV, $\cdot$ permitting a detailed investigation of the total cross-section in this energy range.

2.3.2 Compton scattering

The forward Compton cross-section can be written as

$$\frac{d\sigma}{dt} = \sigma_{tot}^2/16\pi + \frac{\pi}{k^2} \ |\text{Re} \ f_1|^2 + \frac{\pi}{k^2} \ |\text{Re} \ f_2|^2 \ .$$

Neglecting $|\text{Re } f_1|$ and $|\text{Re } f_2|$ and assuming $\sigma_{tot} = 100$ μb, we find

$$\frac{d\sigma}{dt}\bigg|_{t=0} = 0.51 \text{ μb/GeV}^2 \ .$$

The t-dependence of $\gamma p \to \gamma p$ at 17 GeV was found to be well represented by $e^{-6.6t+1.1t^2}$ for values of t between 0.15 GeV^2 and 1.1 GeV^2. Assuming this t-dependence to hold true at high energies, we have

$$\frac{d\sigma}{dt} = 0.51 \text{ μb/GeV}^2 \ e^{-6.6t+1.1t^2} \ .$$

The total cross-section for Compton scattering is thus 0.08 μb, resulting in 2,000 events a day. The t-dependence of the rate is listed in Table 3.

Table 3

Compton events per day in bins of $\Delta t = 0.2 \text{ GeV}^2$

t	Events/day
0.1	1350
0.3	395
0.5	126
0.7	44
0.9	17
1.1	7
1.3	3.1
1.5	1.5

A measurement of the Compton process at high energies can provide a stringent test of the parton model. For example, this model predicts a breakdown of s-channel helicity conservation resulting in a positive asymmetry $A = (\sigma_T - \sigma_L)/(\sigma_T + \sigma_L)$. Furthermore, the t-dependence should be rather gentle (compared, say, to ρ-production). As can be seen from Table 3 the rates are sufficiently high to test both these features.

2.3.3 *Photoproduction of vector mesons*

Since the vector mesons have the same quantum numbers as the photon, we would expect on general grounds that the process $\gamma + p \to V + p$ is mainly diffractive at high energies. Therefore by measuring the photoproduction of vector mesons we can study the elastic scattering process $V + p \to V + p$. Furthermore, since the photon beam is linearly polarized, important quantities, such as natural to unnatural parity exchange, or the amount of helicity conservation, can be directly determined in these reactions. A measurement of φ photoproduction should determine the Pomeron trajectory directly, without any interference from lower trajectories.

The differential cross-sections for these reactions can be written for t not too large:

$$\rho \ : \ \frac{d\sigma}{dt} = 100 \ \mu b/GeV^2 \ e^{7t}$$

$$\omega \ : \ \frac{d\sigma}{dt} = 10 \ \mu b/GeV^2 \ e^{7t}$$

$$\phi \ : \ \frac{d\sigma}{dt} = 2 \ \mu b/GeV^2 \ e^{4.5t} \ .$$

The number of events per day is shown in Table 4 for all values of t and for $|t| \geq 1.0$:

Table 4

Event rates for photoproduction of vector mesons
using a tagged photon beam

Reaction	Total number of events per day	Number of events per day with $|t| \geq 1.0$
$\gamma + p \to \rho^0 + p$	3.7×10^5	335
$\gamma + p \to \omega + p$	3.7×10^4	34
$\gamma + p \to \phi + p$	1.1×10^4	127

Besides these exclusive channels a series of inclusive experiments can also be performed, double diffractive processes $\gamma + p \to \rho + N$ can be studied, a comparison with proton data would allow a test of factorization, new vector mesons can be searched for ($t_{min} = 0.1$ GeV^2 for $m_V = 100$ GeV), and so on.

3. CONCLUSION

It seems to me that the addition of an electron ring ($E \geq 25$ GeV) to a proton ring ($E > 400$ GeV) offers rather unique possibilities and should be seriously entertained. For example, here we start to approach the unitarity limit for the s-wave in the weak interactions. A 12 GeV electron beam on a 140 GeV proton beam is to my mind more on the border line, especially if the energy of FNAL and the SPS can be increased to 1 TeV or beyond.

I thank C.H. Llewellyn Smith and K.H. Mess for discussions and help with this note.

This note will be superceded shortly by a more complete treatment written in collaboration with C.H. Llewellyn Smith.

REFERENCES

1) V. Barger and R.J.V. Phillips, Nuclear Phys. B73, 269 (1974). (A different parametrization of $\nu W_2(x)$ was used in the original version of the paper. That version gave too large a cross-section.)

2) C.H. Llewellyn Smith, preprint CERN TH-1710 (1973).

3) B.C. Barish et al., CalTech report CALT 68-460 (1968).